A new method to assess the climate effect of mitigation strategies for road traffic
The fast chemistry-climate response model TransClim

Rieger, Vanessa

DOI
10.4233/uuid:cc96a7c7-1ec7-449a-84b0-2f9a342a5be5

Publication date
2018

Document Version
Final published version

Citation (APA)
Rieger, V. (2018). *A new method to assess the climate effect of mitigation strategies for road traffic: The fast chemistry-climate response model TransClim*. [Dissertation (TU Delft), Delft University of Technology]. https://doi.org/10.4233/uuid:cc96a7c7-1ec7-449a-84b0-2f9a342a5be5

Important note
To cite this publication, please use the final published version (if applicable).
Please check the document version above.

A new method to assess the climate effect of mitigation strategies for road traffic

The fast chemistry-climate response model TransClim

Vanessa S. Rieger

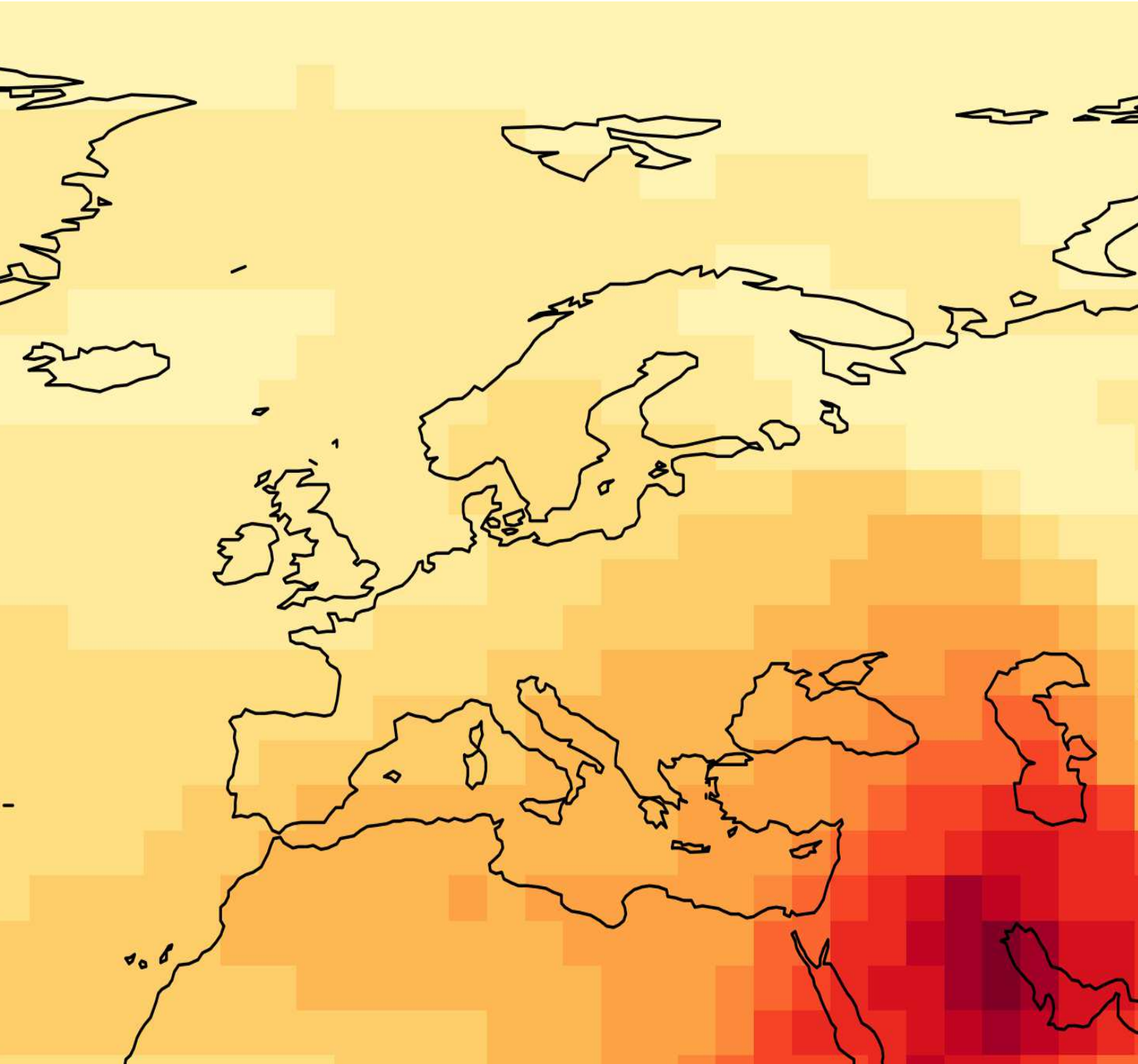

A new method to assess the climate effect of mitigation strategies for road traffic

The fast chemistry-climate response model TransClim

Dissertation

for the purpose of obtaining the degree of doctor
at Delft University of Technology
by the authority of the Rector Magnificus, prof.dr.ir. T.H.J.J. van der Hagen,
chair of the Board for Doctorates
to be defended publicly on
Friday 7 December 2018 at 10:00 o'clock

by

Vanessa Simone RIEGER

Master of Science in Physics, Ludwig-Maximilians-Universität München, Germany,
born in Munich, Germany

This dissertation has been approved by the promotor.

Composition of the doctoral committee:

Rector Magnificus	chairperson
Prof.dr. V. Grewe	Delft University of Technology, German Aerospace Center, promotor

Independent members:

Prof.dr. M. Dameris	German Aerospace Center (DLR)
Prof.dr. D.G. Simons	Delft University of Technology
Prof.dr.ir. H.W.J. Russchenberg	Delft University of Technology
Prof.dr. A.P. Siebesma	Delft University of Technology
Prof.dr. M.C. Krol	University Utrecht
Dr. P. van Velthoven	Royal Netherlands Meteorological Institute (KNMI)

An electronic version of this dissertation is available at
`https://elib.dlr.de/`.

Contents

Summary

Emissions of road traffic crucially influence Earth's climate. The vehicle fleet emits not only carbon dioxide (CO_2), but also nitrogen oxides (NO_x), volatile organic compounds (VOC) and carbon monoxide (CO). The latter species lead to a production of ozone (O_3) and a reduction of methane (CH_4) in the troposphere.

As the demand of mobility is expected to further increase in future, a reduction of the climate effect from road traffic emissions is indispensable. Therefore, it is essential to assess the climate impact of emission changes caused by technological trends and mitigation strategies for road traffic. Hereby, it is not only important to determine the *impact* but also the *contribution* of road traffic emissions on climate.

Several studies have already quantified the impact of road traffic emissions on climate. But climate simulations with complex chemistry climate models are still computational expensive hampering the assessment of many road traffic emission scenarios. Consequently, an efficient method for quantifying the climate impact and contribution of mitigation options is required.

Within the scope of this thesis, I developed a unique chemistry-climate response model called *TransClim* (Modelling the effect of surface *Trans*portation on *Clim*ate) which assesses the impact and the contribution of road traffic emission scenarios on O_3 and CH_4 concentration as well as their corresponding radiative forcings. I tested various algorithms to find an efficient approach. The following approach was chosen: Road traffic emissions are split into seven emission regions. Climate simulations are performed with the global chemistry climate model EMAC by varying the road traffic emissions of NO_x, VOC and CO in each emission region individually. These simulations deliver the input data for a look-up table (LUT) for each emission region. To determine, for example, the O_3 concentration of a particular emission scenario, the difference of O_3 to a reference simulation is computed by interpolating within each LUT. These O_3 changes of each emission region are added to the reference O_3 to obtain the new O_3 concentration. Comparing the results delivered by TransClim with simulations of the complex global chemistry climate model EMAC reveals very low deviations (0.02 – 6 %). Thus, TransClim reproduces the results calculated by EMAC very well.

To determine not only the impact but also the contribution of road traffic emissions to O_3, OH and CH_4 in TransClim, a so-called *tagging* method is applied. It attributes the concentrations of O_3 to emission sources such as road traffic. This tagging method also determines the contribution of the short-lived species OH and HO_2. However, the former version had certain shortcomings which I improved. It now applies not only to the troposphere but also to the stratosphere. Moreover, the sum over all contributions equals the total concentration. Additionally, I introduced a new tagging method which determines the contribution of road traffic emissions to CH_4.

Within the scope of this thesis, TransClim enabled to assess the climate effect of two scientific questions. First, the effect of three prospective mitigation options of German road traffic is quantified with TransClim. The future emission scenario including the strictest environmental regulations and emission controls leads to the strongest decrease of O_3 and CH_4 radiative forcing. Second, two scenarios have been constructed describing the cases that European vehicles use fuel blends containing a low and a high proportion of biofuels. Simulations with TransClim reveal that fuels with a low content of biofuels mainly reduce CH_4 while fuels with a high content of biofuels reduce tropospheric O_3.

Summing up, TransClim offers a new method to quickly assess the climate impact and the contribution of mitigation strategies for road traffic in a sufficiently accurate manner. As TransClim simulates about 6000 times faster than a complex chemistry climate model, it enables to quantify the effect of many emission scenarios in different regions.

Samenvatting

Emissies van wegverkeer hebben een cruciale invloed op het klimaat op aarde. Alle rijdende voertuigen stoten niet alleen koolstofdioxide (CO_2) uit, maar ook stikstofoxiden (NO_x), vluchtige organische componenten (VOC) en koolstofmonoxide (CO). Deze laatste stoffen leiden tot de productie van ozon (O_3) en een reductie van methaan (CH_4) in de troposfeer.

Terwijl de vraag naar mobiliteit in de toekomst naar verwachting verder zal stijgen, is een reductie van de klimaatimpact als gevolg van wegverkeer emissies noodzakelijk. Het is daarom van essentieel belang om de klimaatimpact van het veranderen van emissies, als gevolg van technologische trends en mitigatie strategieën (uitstoot beperkende maatregelen), te kunnen beoordelen. Het is hierbij belangrijk om niet alleen de *impact* maar ook de *bijdrage* van wegverkeer emissies op het klimaat te bepalen.

Verscheidene studies hebben de impact van wegverkeer emissies op het klimaat al gekwantificeerd. Klimaat simulaties met complexe chemische klimaat modellen vereisen echter nog steeds veel numerieke rekenkracht en verhinderen hierdoor het beoordelen van veel wegverkeer emissie scenario's. Daarom zijn efficiente methoden vereist, waarmee de klimaat impact en de bijdrage van verzachtende maatregelen kan worden gekwantificeerd.

In het kader van deze thesis, heb ik een uniek chemisch-klimaat respons model ontwikkeld genaamd *TransClim*. Het modelleert de impact van grond *Trans*port op het klimaat (in het Engels: *Clim*ate). TransClim beoordeelt de impact en de bijdrage van wegverkeer emissie scenario's op O_3 en CH_4 concentraties en tevens de corresponderende stralingsforceringen. Ik heb verschillende algoritmes getest om een efficiënte aanpak te vinden. Er is voor de volgende aanpak gekozen: Wegverkeer emissies worden opgesplitst in zeven emissie regio's. Klimaatsimulaties worden uitgevoerd met het globale chemische klimaat model EMAC door het, in elke van de zeven emissie regio's afzonderlijk, variëren van de wegverkeer emissies NO_x, VOC en CO. Deze simulaties leveren de input data voor een *Look-Up-Table* (LUT) voor elke emissie regio. Om bijvoorbeeld de ozon concentratie van een bepaald emissie scenario te bepalen, wordt het ozon verschil met een referentie simulatie bepaald door te interpoleren in iedere LUT. De ozon verschillen van alle emissie regio's worden opgeteld bij de referentie ozon concentratie om zo de nieuwe ozon concentratie te bepalen. Wanneer de resultaten geleverd door het TransClim model worden vergeleken met de resultaten van het complexe globale chemische klimaat model EMAC, zijn de afwijkingen zeer klein (0.02 – 6 %). TransClim reproduceert de resultaten van EMAC dus zeer goed.

Om niet alleen de impact, maar ook de bijdrage van wegverkeer emissies aan O_3, OH en CH_4, te bepalen met TransClim wordt een zogenaamde *label* methode toegepast. De methode schrijft O_3 concentraties toe aan bronnen zoals bijvoorbeeld

wegverkeer. Deze label methode bepaalt ook de bijdrage van stoffen met een korte levensduur zoals OH en HO_2. De vorige versie had echter bepaalde tekortkomingen die ik heb verbeterd. Nu is de methode niet alleen meer toepasbaar in de troposfeer maar ook in de stratosfeer. De som van alle bijdragen is nu bovendien gelijk aan de totale concentratie. Daarnaast heb ik een nieuwe label methode geïntroduceerd waarmee de bijdrage van wegverkeer emissies aan de CH_4 concentratie kan worden bepaald.

In het kader van deze thesis, heeft TransClim ons in staat gesteld om het klimaat effect te beoordelen van twee wetenschappelijke vragen. Allereerst is de impact van drie mitigatie strategieën van Duits wegverkeer gekwantificeerd met TransClim. Het toekomstige emissie scenario, inclusief de strengste klimaat maatregelen en emissie controle's, leiden tot de sterkste afname van O_3 en CH_4 gerelateerde stralingsforcering. Daarnaast zijn twee scenario's geconstrueerd waarin wordt beschreven dat het Europese wegverkeer brandstofmengsels gebruiken die voor een klein respectievelijk groot deel uit biobrandstoffen bestaan. TransClim simulaties laten zien dat brandstoffen met een klein deel biobrandstoffen voornamelijk zorgen voor een afname van CH_4 terwijl brandstoffen met een groot deel biobrandstoffen troposferische O_3 reduceren.

Samengevat biedt TransClim een nieuwe methode om snel de klimaat impact, en de bijdrage van mitigatie strategieën voor wegverkeer, op voldoende accurate wijze te beoordelen. Een TransClim simulatie is ongeveer 6000 keer sneller dan een complexe chemische klimaat model en kan hierom de effecten van veel emissie scenario's in verschillende regio's kwantificeren.

1

Introduction

Mobility is a basic need of human beings. Workplaces, residences and leisure activities are often spatial separated in today's society leading to a steady increase of mileage per person in the last decades. Additionally, our economical system crucially depends on the transport system. The globalisation requires a dense and efficient transportation network of goods. So far, 80 % of motor-driven passenger kilometres are covered by only 10 % of global population (Sims et al., 2014). But in future, the transport volume of the developing countries is expected to rise strongly. Overall, this leads to a growing demand of mobility.

However, our present-day concept of mobility is not sustainable. Although cars and heavy good vehicles become more and more efficient, the steady growing transport volume compensates the efficiency gain. Global transport needs about 28 % of energy consumption. Moreover, emissions from transport sector grow faster than any energy-consuming sector. Since 1970, greenhouse gas emissions from transport have even doubled. In total, all transportation modes (road traffic, railways, shipping and aviation) emit about one-fifth of the total anthropogenic CO_2 emissions. (Sausen et al., 2012; Sims et al., 2014)

These large amounts of emissions originating from the different transportation modes strongly influence Earth's climate. Four major effects on climate are identified (e.g. Sausen et al., 2012; Hendricks et al., 2017):

1. Transport emits directly greenhouse gases such as CO_2 and N_2O and thus contributes to global warming.

2. Transport also emits precursors which impact other greenhouse gases. NO_x, VOC and CO produce O_3 in the troposphere. They also impact OH which in turn influences the atmospheric lifetime of the greenhouse gases O_3 and CH_4.

3. Transport emits particulate matter (PM). These so called aerosol particles mainly consist of soot which comprises black carbon (BC) and organic carbon (OC). Transport further emits aerosol precursor gases such as NO_x and SO_2. They can directly and indirectly change clouds and the radiation.

4. Moreover, aviation directly induces additional clouds (i.e. contrails, contrail cirrus) which modify the radiation budget of the Earth.

Consequently, all four effects influence Earth's radiation budget and contribute to *climate change*. The anthropogenic global warming affects the Earth as well as humans and animals in many ways: amongst others, it leads to higher surface temperatures, rises sea levels and changes precipitation patterns (IPCC, 2013).

Numerous studies exist focussing on the climate impact of the different transport modes such as shipping (e.g. Lauer et al., 2007; Eyring et al., 2010; Righi et al., 2013), aviation (e.g. Lee et al., 2009; Frömming et al., 2012; Grewe et al., 2014) and road traffic (e.g. Niemeier et al., 2006; Hoor et al., 2009; Uherek et al., 2010; Righi et al., 2015; Mertens et al., 2018). Each transport mode affects the climate differently. Not only the composition of emissions varies, also the emissions are released in very different regions with different background concentrations. Road traffic emits in the polluted planetary boundary layer. Ships release their emissions in the rather clean maritime boundary layer and aviation emits in the upper troposphere and lower stratosphere region. As these regions possess a different chemical background, an emission in a polluted region may cause a very different impact than an emission in a pristine region (Hoor et al., 2009).

The strength of an external perturbation on Earth system is usually quantified as *radiative forcing*. It describes the net change in radiative fluxes of Earth's energy balance (in W m^{-2}) caused by this perturbation. CO_2 radiative forcing from road traffic emissions is the strongest and contributes to the total anthropogenic CO_2 radiative forcing by 8 %. Each of the transport modes aviation, shipping and railways contribute only by 1 – 2 %. The ratio of CO_2 radiative forcings distinguish from the ratio of CO_2 emissions. The transport modes shipping and railways started to emit CO_2 many decades earlier than road traffic and aviation. As CO_2 usually remains in the atmosphere for more than a century, shipping and railways have accumulated more CO_2 in the atmosphere than road traffic and aviation leading to different contributions to CO_2 forcings. Moreover, O_3 radiative forcing caused by road traffic is the largest (14 %), the sector aviation and shipping follow with 9 %. Summing up all radiative effects, the transport sector road traffic contributes the most to the total anthropogenic radiative forcing (14 %). Interestingly, the total impact of shipping to the anthropogenic RF is negative (-26 %) as the emitted aerosols cause a strong increase of maritime clouds cooling the Earth. (Sausen et al., 2012)

Summing up, compared to the other transport modes, emissions from road traffic contribute the most to global warming. About 74 % of all transport CO_2 emissions originate from road traffic (Sausen et al., 2012). They even increase by 2 – 3 % each year. In particular, the sector road traffic presents the largest growth rates among the other transport sectors (Sims et al., 2014).

Road traffic emits not only carbon dioxide (CO_2) but also nitrogen oxides (NO_x), volatile organic compounds (VOC), carbon monoxide (CO), sulphur dioxide (SO_2), nitrous oxide (N_2O) and particulate matter (PM). CO_2 and N_2O are greenhouse gases directly contributing to global warming. The emissions of road traffic also strongly influence the atmospheric chemistry: in general, NO_x, VOC and CO from road traffic emissions produce O_3 and destroy CH_4 in the troposphere (Hoor et al.,

2009). PM also directly and indirectly influences the climate.

Several studies exist investigating the climate impact of global road traffic emissions on the atmospheric chemistry (e.g. Niemeier et al., 2006; Fuglestvedt et al., 2008; Hoor et al., 2009; Uherek et al., 2010; Righi et al., 2015; Mertens et al., 2018). Overall, road traffic emissions increase tropospheric O_3. In particular in the Northern Hemisphere during summer, the surface O_3 concentration is increased by 5 – 15 % at mid-latitudes (Granier and Brasseur, 2003). Road traffic emissions further reduce CH_4 lifetime by about -(1.61±0.25) % (Hoor et al., 2009).

Also the impact of road traffic emissions on regional and local level have been investigated (e.g. Reis et al., 2000; Tagaris et al., 2015). Hendricks et al. (2017) focus on the climate impact of regional road traffic emissions. For German road traffic emissions, they find a total RF of about 12.76 mW m^{-2} which amounts to approximately 0.8 % of total anthropogenic RF. Hendricks et al. (2017) also deduce a corresponding surface temperature change of about 4.78 mK due to German road traffic emissions for the year 2008.

Emissions from road traffic influence not only Earth's climate, they also impact local air quality. Particulate matter, O_3 and NO_x harm human health and destroy plants (e.g. Finkelstein et al., 2004; Gan et al., 2010; Mills et al., 2007; Ainsworth et al., 2012). To improve the air quality, the World Health Organization sets certain thresholds for these species (WHO, 2006a).

Most studies use the perturbation method to determine the effect of road traffic emissions on O_3. This method compares two climate simulation: one simulation including all road traffic emissions and one simulation with a reduction of road traffic emissions. However, these methods do not account for the non-linearities of the tropospheric O_3 chemistry and thus can only determine the *impact* of road traffic emissions on climate. A change of road traffic emissions influence also the contributions of other emission sectors such as industry or shipping. Thus to determine the *contribution* of only road traffic emissions to O_3, Grewe et al. (2010) suggest to use a tagging method. It enables to determine the contribution to O_3 by following the reaction pathways of the road traffic emissions of NO_x, VOC and CO. Consequently, the perturbation method determines the impact while the tagging method calculates the contribution of road traffic emissions. In general, the contribution of road traffic emissions is larger than their impact (Grewe et al., 2010; Mertens et al., 2018). Tsati (2014) and Grewe et al. (2017) suggest a method to also attribute concentrations of short-lived species OH and HO_2 to emission sources such as road traffic. However, their method still presents certain short-comings: it is only applicable in the troposphere and the sum over all contributions does not deliver the total concentrations, i.e. the budget is not closed (deviations of more than 70 %). Moreover, there is so far no tagging method which determines the contribution of a certain emission sector to CH_4.

To reduce the climate effect of road traffic emissions, several mitigation options are proposed (e.g. Sims et al., 2014). Technical innovations or stringent policies of road traffic may reduce its climate effect. To completely assess these mitigation options, it is essential to evaluate the *impact* and the *contribution* of mitigation strategies on climate.

Usually, studies use complex chemistry climate models to evaluate the climate effect of road traffic emissions. However, climate simulations with complex chemistry climate models are still computational expensive. A climate simulation spanning over a the time period of 40 years may take up to 3 months on a high performance computer. This hampers the assessment of many road traffic emission scenarios. Consequently, an efficient method for quantifying the climate impact and contribution of mitigation options is required. Hereby, following questions arise:

- What is an efficient approach to assess the climate effect of many road traffic emission scenarios? Depending on the research question, the approach shall determine the climate effect within minutes to hours to ensure a fast applicability and an assessment of many emission scenarios. Furthermore, the computed climate effects shall only deviate by less than 10 % from the effects calculated by a complex climate model. Besides, how can the approach consider the non-linearity of the tropospheric O_3 chemistry?

- How is it possible to determine not only the impact but also the contribution of road traffic emissions? There is already a promising method for O_3. But which method enables to determine the contribution to OH and CH_4?

To answer these questions, I developed the chemistry-climate response model called *TransClim* (Modelling the effect of surface *Trans*portation on *Clim*ate). TransClim quantifies the impact and contribution of road traffic emissions on O_3 and CH_4 as well as their corresponding radiative forcings. It bases on a look-up table which contains pre-calculated relations of road traffic emissions and their climate effect. These relations are simulated with a complex chemistry climate model (EMAC). I tested various algorithms to find an efficient approach which combines the data points within the LUT to compute the climate effect of any emission scenario. As the O_3 chemistry in the troposphere is highly non-linear, it is challenging to find a suitable algorithm which correctly represents the O_3 concentration of a particular emission scenario. Consequently, the testing of various algorithm focuses on O_3 concentration.

To determine not only the impact but also the contribution, the *tagging* method according to Grewe et al. (2010, 2017) is applied. It attributes O_3 concentration to emission sources such road traffic. Within the scope of this thesis, I improved the tagging method of OH and HO_2. I extended the method on the stratosphere and closed the budget. Additionally, I introduced a new tagging method which determines the contribution of road traffic emissions to CH_4. These tagging methods are used in TransClim to quantify the contribution of road traffic emissions to the concentrations of O_3, OH and CH_4.

The thesis is structured a follows: After the basic background informations are presented in chapter 2, the global chemistry climate model EMAC, which is used for climate simulations, is explained in chapter 3. Chapter 4 describes the tagging method being applied to determine the contribution of road traffic emissions to O_3, OH and CH_4 concentrations. I further developed the tagging method to attribute OH and HO_2 to emission sources which is presented in section 4.4. Additionally, I also introduce a new method to determine the contribution to CH_4 in section

4.5. The development of TransClim as well as the model description are presented in chapter 5. The performance of TransClim is evaluated in section 5.6. The climate effect of two mitigation options are assessed with TransClim in chapter 6. The first example describes prospective mitigation options for German road traffic (section 6.1). The second example assesses the introduction of biofuels in Europe (section 6.2). Finally, chapter 7 concludes the presented work.

2

Background

The first part of this chapter is dedicated to emissions of road traffic (sect. 2.1). It describes which direct and indirect emissions are produced by road traffic. In particular, the production of exhaust emissions is described in more detail. Subsequently, sect. 2.2 explains the effect on the atmospheric composition imposed by exhaust emissions. It focusses on the chemical species ozone (O_3), hydroxyl radical (OH) and methane (CH_4). Each section describes the general processes of the atmospheric chemistry. Subsequently, it explains the effects caused by road traffic emissions on O_3, OH and CH_4. Furthermore, particulate matter emitted by road traffic imposes an important influence on the atmosphere. Although this work does not concentrate on particulate matter, their effect on atmosphere is described in sect. 2.3. Road traffic emissions also influence Earth's climate. Therefore, the definition of radiative forcing is introduced in sect. 2.4. Additionally, the radiative forcings caused by the different exhaust emissions of road traffic are discussed. But road traffic emissions affect not only the climate, they also influence the health of humans and animals as well as plants. Although these effects are not the focus of this thesis, they are important and thus briefly explained in sect. 2.5.

2.1. Emissions of road traffic

Passenger cars and heavy goods vehicles typically possess combustion engines. However, the combustion of fossil fuels delivers not only energy for the movement of vehicles, it also liberates pollutants into the atmosphere. Due to incomplete combustion in the engine, not only carbon dioxide (CO_2) and water vapour (H_2O) but also substances such as carbon monoxide (CO), volatile organic compounds (VOC, e.g. formaldehyde (HCHO), acetaldehyde (CH_3CHO), benzene (C_6H_6)), nitrogen oxides (NO_x = NO + NO_2), sulphur dioxide (SO_2) and particulate matter (PM) are emitted by road traffic. The following explanations are extracted from Breuer et al. (2015); Winkler et al. (2015) and Pucher et al. (2015).

A lack of oxygen during the combustion leads to an early interruption of the

reaction chains and to a formation of CO and VOC. Due to side reactions with nitrogen in the ambient air, nitrogen oxides are produced. Mainly NO and NO_2 but also small amounts of N_2O are generated. The production of NO_x during combustion is strongly temperature dependent and is described by the extended Zeldovich mechanism (Zeldovich, 1946). Sulphur contained in fuels is responsible for the emission of SO_2. Furthermore, fine particles with diameters of 1 – 1000 nm are emitted as well. They can be either solid, liquid or soluble. Mainly soot but also sulphates, ashes and particles from lubricating oil or from corrosion are emitted. Soot is produced locally by a strong lack of oxygen at high combustion temperatures. The combustion process and thus also the formation of pollutants is affected by many processes: Most important is the ratio of air to fuel as well as the residence time in the burning chamber. Interactions with the chamber wall, temperature and pressure in the combustion chamber, structural dimensions of the combustion chamber and contaminations in the fuel influence the combustion and pollutants. Moreover, revolution speed and load crucially determine the production of pollutants.

Due to a higher efficiency during partial load, the fuel consumption for diesel engines is lower than for gasoline engines. Thus, vehicles containing a diesel engine emit about 20 % less CO_2 than gasoline engines. Moreover, diesel engines work under air excess. Hence, CO and VOC emissions are also lower for diesel than gasoline engines. However, NO_x emissions are significantly larger. In gasoline engines, the fuel is evaporated before combustion. In comparison in diesel engines, the fuel is sputtered first and then needs to evaporate during combustion. This works well for low loads. But otherwise, soot is formed at the remaining droplets leading to higher PM emissions of diesel than gasoline engines. For gasoline cars, high soot emissions are mainly found during cold start and warm-up period of the engine. (e.g. Breuer et al., 2015; Winkler et al., 2015; Pucher et al., 2015)

The reduction of exhaust emissions caused by vehicles is crucial. However, it is challenging to reduce emissions of VOC, PM and NO_x at the same time. For example, combustion of fuel during air excess decreases VOC and PM but increases NO_x emissions. A common technique is the exhaust gas recirculation (EGR) which recycles a portion of the exhaust gas into the combustion chamber. This drops the burning temperature and thus reduces the emissions of NO_x. Furthermore, catalytic converters reduce the emission of pollutants. Three way catalytic converters (TWC) are used for gasoline engines. The catalytic converter consists of a ceramic honeycomb structure which is coated with the noble metals platinum, palladium and rhodium (so called wash coat). When the exhaust gas streams through the catalytic converter, VOC and CO react with O_2 in the exhaust gas and are thus oxidised to CO_2 and H_2O. NO_x reacts with VOC, CO or H_2 and is reduced to N_2 and H_2O. At operation temperature, the three way catalytic converter can reduce the emissions of the harmful species VOC, CO and NO_x by up to 98 %.

For diesel engines, diesel oxidation catalytic converters (DOC) reduce VOC and CO emissions. As diesel engines run under air excess, there are still high O_2 concentrations in the exhaust gas. The remaining VOC and CO in the exhaust gas prefer to react with O_2 instead of NO_x. Thus a NO_x reduction as it is performed by three way catalytic converters is not possible. Instead, NO_x emissions are either

reduced by NO_x storage catalyst or selective catalytic reduction. NO_x storage catalyst (NSC) stores NO_x by converting it to, for example, barium nitrate. After the maximum storage capacity is reached, the NSC needs to be discharged by shortly lowering the oxygen content of the exhaust gas which rises the VOC and CO concentrations. At first, they react with the barium nitrate releasing again NO_x. Then VOC and CO further reduce the released NO_x to N_2 and H_2O. After the NSC has been discharged, a new cycle of storing NO_x starts. Selective catalytic reduction (SCR) decreases NO_x emissions continuously. Urea ($(NH_2)_2CO$) is injected into the exhaust gas. It decomposes to ammonia (NH_3) which reduces NO_x. Furthermore, diesel particle filters (DPF) minimize soot emissions. As the exhaust gas streams through the filter, particles adsorb at porous ceramics. After approximately 500 km, particle filters need to regenerated by burning the accumulated soot particles. Such filters can reduce the soot emissions up to 95 %. (e.g. Breuer et al., 2015; Winkler et al., 2015; Pucher et al., 2015)

In total, road traffic contributes significantly to anthropogenic emissions. Fig. 2.1 shows the historical development of road traffic emissions from 1900 to 2000. During the first half of the 20th century, road traffic emissions are moderate. Since 1950 emissions strongly rise. At the end of the 20th century, the introduction of catalytic converters significantly reduced the road traffic emissions of certain species, however CO_2 continues to rise. Although the fuel efficiency of the combustion engines is progressing, the overall fuel consumption is steadily increasing and is expected to continue to rise in future. The covered distances, the comfort (e.g. air conditioners), the number of registered vehicles as well as larger and more powerful vehicles are responsible for the ongoing emission increase. (e.g. Joumard, 2005; Uherek et al., 2010)

In the year 2000, global road traffic emits about 4000 Tg CO_2 which corresponds to 14 % of total anthropogenic CO_2 emissions (Sausen et al., 2012). NO_x and CO emissions from road traffic contribute about 25 % to total anthropogenic NO_x and CO emissions, VOC emissions about 18 % respectively. The contribution of road traffic emissions to anthropogenic SO_2, CH_4 and N_2O emissions is rather low (below 3 %). Consequently, they are not further considered in this work. Black carbon (BC) originating from soot emissions of road traffic contributes about 10 % to global anthropogenic emissions. Most BC originates from diesel engines (98.7 %). (Nam et al. (2004); Uherek et al. (2010), EDGAR database Janssens-Maenhout et al. (2017), data from EU project QUANTIFY `http://www.pa.op.dlr.de/quantify/`)

Estimates of road traffic emissions are still very uncertain. In particular developing countries such as China, India and South East Asia have rapidly increased their vehicle stock which makes it difficult to estimate their emissions. Global road traffic CO_2 emissions presents an uncertainty of up to 10 %. Uncertainties of emissions from SO_2, NO_x, CO and VOC vary between 30 – 50 %. Highest uncertainty are given for the emissions of particulate matter (about 66 %). (Borken-Kleefeld et al., 2007; Uherek et al., 2010)

A further source of emissions due to road traffic are the mobile air conditioners in vehicles. In 2000, about 50 % of the global car fleet owns mobile air conditioners with a fast growing tendency (IPCC/TEAP, 2005). As a coolant agent CFC-12

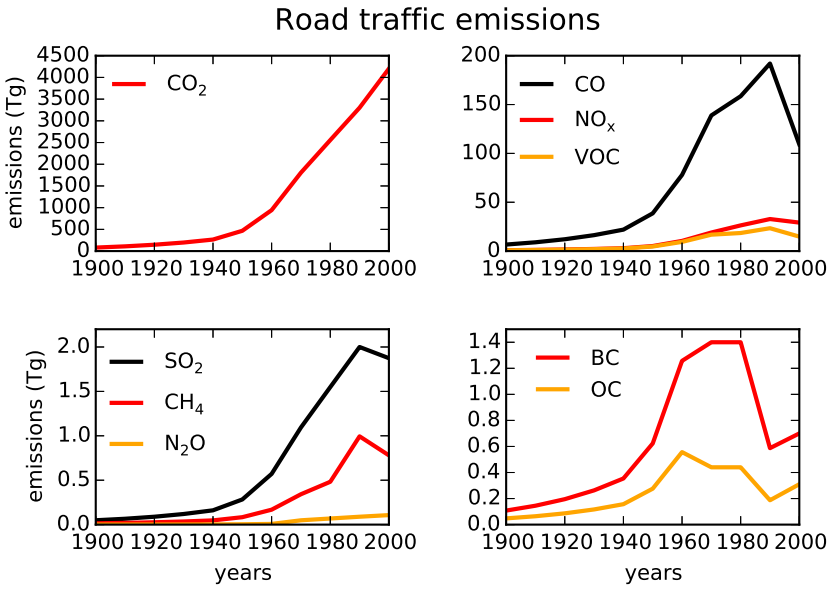

Figure 2.1: Historical development of global road traffic emissions of carbon dioxide (CO_2), carbon monoxide (CO), nitrogen oxides (NO_x), volatile organic compounds (VOC), sulphur dioxide (SO_2), methane (CH_4), nitrous oxide (N_2O), black carbon (BC) and organic carbon (OC) from 1900 to 2000. The emissions are taken from the EU project QUANTIFY (`http://www.pa.op.dlr.de/quantify`).

(CCl_2F_2) is used. If released, CFC-12 causes O_3 depletion in the stratosphere. Since 1990s, CFC-12 is steadily replaced by HFC-134a (CH_2FCF_3). HFC-134a has a shorter lifetime (14 yr) than CFC-12 and thus has a smaller effect on stratospheric O_3. The emission of cooling agents CFC-12 and HFC-134a occurs during accidents, during waste disposal (42.5 % – 69 %) as well as during leakage and service (10.9 %). (DeAngelo et al., 2006; Uherek et al., 2010)

Road traffic implies also indirect emissions. Brake wear, road wear, tyre wear and road dust resuspension contribute at least as much to PM as exhaust emissions (Amato et al., 2014). The emissions produced by building and maintaining the infrastructure, such as roads, bridges and tunnels, correspond to about 20 % of global exhaust emissions. Furthermore, production of fuels as well as construction and maintenance of vehicles cause emissions. The latter emits also approximately 20 % of global exhaust emissions (Samaras and Meisterling, 2008; Chester and Horvath, 2009). Usually, the construction and maintenance is accounted to different emission sectors such as industry or construction sector. Indirect emissions due to road traffic are not further considered in this study.

This thesis focuses on exhaust emissions. In particular the effect of NO_x, CO, VOC and particulate matter on the atmosphere are discussed in the following sections.

2.2. Effect of road traffic emissions on atmospheric chemistry

As discussed in section 2.1, road traffic emits NO_x, VOC and CO. These gases modify the composition of the atmosphere. The abundance of radiative active gases is influenced and thus impacts the radiation budget and climate. In the troposphere, NO_x, VOC and CO produce the greenhouse gas O_3. Moreover, the atmospheric concentration of OH radicals is influenced which in turn affects the lifetime of the greenhouse gas CH_4. The chemical processes are described in the following sections. The explanations are extracted from Seinfeld and Pandis (2006), Monks (2005), Fowler et al. (2008) and Monks et al. (2015).

2.2.1. Effect of road traffic emissions on tropospheric ozone

Road traffic emits NO and NO_2. Since both chemical species closely intertwine (their interconversion timescale is about 5 min), they are generally referred together as nitrogen oxides (NO_x). NO_x acts as a catalyst for O_3 production in the troposphere. During daytime, O_3 is formed by the photolysis of NO_2 (at wavelengths shorter than 424 nm):

$$NO_2 + h\nu \longrightarrow NO + O \tag{R1}$$
$$O + O_2 + M \longrightarrow O_3 + M \tag{R2}$$

M indicates an inert collision partner, usually N_2 or O_2. As the oxygen radical (O) is very reactive, it almost immediately reacts with O_2 forming O_3 (reaction R2). O_3 in turn is depleted by NO producing NO_2:

$$O_3 + NO \longrightarrow NO_2 + O_2 \tag{R3}$$

These three reactions form a cycling process which continuously produces and destroys O_3. However, NO_x is not destroyed by this photochemical cycle. During daytime, the photolysis of NO_2 initializes the production of O_3. During nighttime, NO_2 is not photolysed and thus produces no O_3. All NO reacts quickly with O_3 (reaction R3). As a results, NO almost completely vanishes during night. O_3 also reacts with NO_2 forming a nitrate radical (NO_3):

$$O_3 + NO_2 \longrightarrow NO_3 + O_2 \tag{R4}$$

Consequently during night, O_3 concentration decreases significantly while NO_2 and NO_3 concentrations increase.

Carbon monoxide (CO) is also emitted by road traffic. Reacting with the hydroxyl radical (OH), it initializes a chain of reactions:

$$\begin{aligned} \mathrm{CO} + \mathrm{OH} &\longrightarrow \mathrm{CO_2} + \mathrm{H} \\ \mathrm{H} + \mathrm{O_2} + \mathrm{M} &\longrightarrow \mathrm{HO_2} + \mathrm{M} \\ \mathrm{HO_2} + \mathrm{NO} &\longrightarrow \mathrm{OH} + \mathrm{NO_2} \\ \mathrm{NO_2} + h\nu &\longrightarrow \mathrm{NO} + \mathrm{O} \\ \mathrm{O} + \mathrm{O_2} + \mathrm{M} &\longrightarrow \mathrm{O_3} + \mathrm{M} \end{aligned} \tag{R5}$$

$$\text{net:} \quad \mathrm{CO} + 2\mathrm{O_2} + h\nu \longrightarrow \mathrm{CO_2} + \mathrm{O_3}$$

The produced hydroperoxyl radical (HO_2) reacts with NO to NO_2. (OH and HO_2 frequently react back and forth and are thus referred together as HO_x.) NO_2 in turn activates the photochemical cycle and forms O_3 (reaction R1 and R2). In theory, one CO molecule produces one O_3 molecule. However, the reactions

$$\mathrm{HO_2} + \mathrm{HO_2} \longrightarrow \mathrm{H_2O_2} + \mathrm{O_2} \tag{R6}$$

$$\mathrm{NO_2} + \mathrm{OH} + \mathrm{M} \longrightarrow \mathrm{HNO_3} + \mathrm{M} \tag{R7}$$

can terminate the reaction chain earlier before O_3 is produced. These reactions constitute a loss of HO_x and NO_x.

Due to incomplete combustion in the vehicle engines, road traffic also emits volatile organic compounds (VOC). In the troposphere, they are mainly oxidised by reacting with OH. To simplify the reaction chain, the chemical family VOC is denoted as RH with H being hydrogen and R indicating the residual molecule. The reaction chain is as follows:

$$\begin{aligned} \mathrm{RH} + \mathrm{OH} &\longrightarrow \mathrm{R} + \mathrm{H_2O} \\ \mathrm{R} + \mathrm{O_2} + \mathrm{M} &\longrightarrow \mathrm{RO_2} + \mathrm{M} \\ \mathrm{RO_2} + \mathrm{NO} &\longrightarrow \mathrm{RO} + \mathrm{NO_2} \\ \mathrm{RO} + \mathrm{O_2} &\longrightarrow \mathrm{R'CHO} + \mathrm{HO_2} \\ \mathrm{HO_2} + \mathrm{NO} &\longrightarrow \mathrm{OH} + \mathrm{NO_2} \\ 2(\mathrm{NO_2} + h\nu &\longrightarrow \mathrm{NO} + \mathrm{O}) \\ 2(\mathrm{O} + \mathrm{O_2} + \mathrm{M} &\longrightarrow \mathrm{O_3} + \mathrm{M}) \end{aligned} \tag{R8}$$

$$\text{net:} \quad \mathrm{RH} + 4\mathrm{O_2} + 2h\nu \longrightarrow \mathrm{R'CHO} + 2\,\mathrm{O_3} + \mathrm{H_2O}$$

The reaction forming alkyl peroxy (RO_2) is very fast. Higher carbonyl molecules (R'CHO) are further oxidised (not treated in this thesis). Finally, two NO_2 molecules are formed in the oxidation process of RH which produces in turn two O_3 molecules.

Summing up, NO_x closely intertwines with CO and VOC forming O_3. The hydroxyl radical (OH) is the key species. NO_x, CO and VOC are competing for an reaction with the OH radical. Hence, the ratio of CO to NO_x and the ratio of VOC to NO_x crucially determine the production of O_3. Fig. 2.2 shows an O_3 isopleth

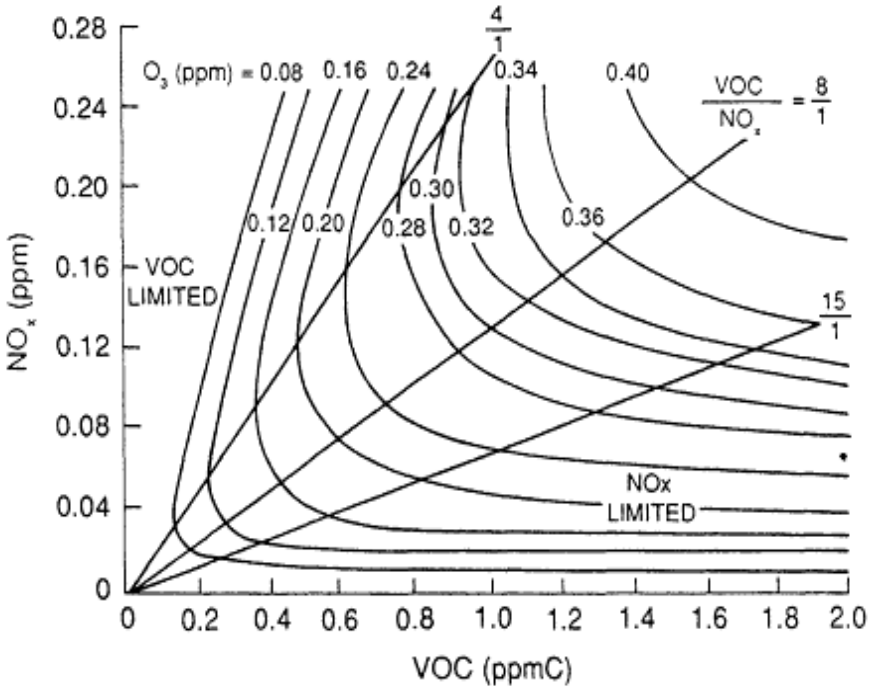

Figure 2.2: Ozone isopleth diagram showing the O_3 mixing ratio depending on NO_x and VOC mixing ratios. Values are derived from a combination of smog chamber data and photochemical modeling techniques. Reprinted with permission from "Rethinking the Ozone Problem in Urban and Regional Air Pollution", 1991 by the National Academy of Sciences, Courtesy of the National Academies Press, Washington, D.C. (Council, 1991). Figure is adapted from Dodge (1977).

diagram only for NO_x and VOC. As can be seen from fig. 2.2, the O_3 mixing ratio depends *non-linearly* on the NO_x and VOC mixing ratios. The concentration of NO_x crucially determines the O_3 formation.

- For high NO_x concentrations, which are typically found close to the emission source in polluted areas, O_3 decreases with increasing NO_x emissions. The reaction

$$OH + NO_2 + M \longrightarrow HNO_3 + M \tag{R9}$$

becomes more and more important removing HO_x and NO_x. Thus, less HO_x and NO_x are available to produce O_3. However, an increase of CO and VOC cause an increase of O_3 because higher concentrations of CO and VOC compete more efficiently with reaction (R9) for OH. Thus, this regime is called "VOC-limited". The ratio of VOC/NO_x is rather low (see fig. 2.2).

- In rural areas of industrialised countries with intermediated NO_x concentrations, an increase of NO_x concentration rises the O_3 formation. This region is therefore called "NO_x-limited" which is characterised by high VOC/NO_x ratios (see fig. 2.2). The reactions take place according to the reaction chains (R5) and (R8). The O_3 production is rather insensitive to variations of CO and VOC. Thus an increase of VOC emissions may not necessarily increase the O_3 production (see fig. 2.2).

- In very remote areas such as South Pacific, NO_x concentrations are very small. Here, the reactions of NO with hydroperoxyl radical (HO_2) and alkyl peroxy radical (RO_2), which usually lead to O_3 production (reaction chain R8), become very unlikely. Instead, the following reactions occur

$$\begin{aligned} HO_2 + HO_2 &\longrightarrow H_2O_2 + O_2 \\ RO_2 + HO_2 &\longrightarrow ROOH + O_2 \\ HO_2 + O_3 &\longrightarrow OH + 2\,O_2 \end{aligned}$$

  which destroy HO_x and O_3 leading to a net O_3 loss.

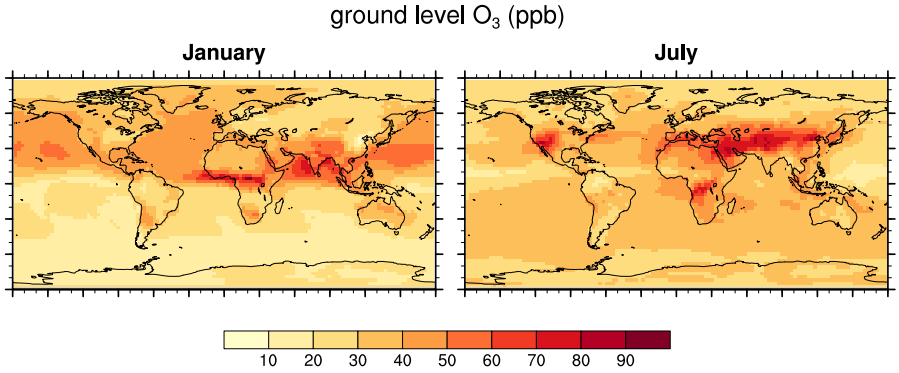

Figure 2.3: Ground level ozone mixing ratios in ppb in January and July for the year 2010. Values are taken from a simulation with the global chemistry climate model EMAC. The model setup and the emission inventory are explained in sect. 3.

Figure 2.3 shows the ground level O_3 mixing ratio in January and July for the year 2010. The O_3 patterns vary between the seasons. The maximum values of ground level O_3 are found in local summer when the solar radiation is strongest and thus can produce more O_3 by the photolysis of reaction (R1). The tropospheric O_3 burden is estimated to be around 337 ± 23 Tg (intermodel mean for the year 2000; Young et al., 2013).

Several studies exist which determine the contribution of road traffic emissions to tropospheric O_3. In the following, an overview over various studies is given. Values

vary among the studies as they use not only different chemistry climate models and emission inventories but also different methods to determine the contributions (Mertens et al., 2018). A detailed discussion about the different methods is found in sect. 4.1.

In general, road traffic emissions cause an increase of tropospheric O_3. Close to the source region, road traffic emissions contribute the most to the ground level O_3 in local summer (Hoor et al., 2009; Uherek et al., 2010). Over the industrialised countries such as North America, Europe, Southeast Asia and Japan, the contribution of road traffic emissions reaches up to 10 – 40 % of the ground level O_3 in summer (Granier and Brasseur, 2003; Niemeier et al., 2006; Mertens et al., 2018). The Mediterranean and the Arabian Peninsula show high contributions of road traffic emissions because their dry and sunny weather favours the photolysis of NO_2 (R1) and thus the production of O_3 (Uherek et al., 2010; Mertens et al., 2018). Lower contributions of road traffic emissions are found in Asia than in Europe or North America because the fraction of other anthropogenic emissions to road traffic emissions is larger (Mertens et al., 2018). In general, one NO_x molecule from road traffic emissions is not as efficient in producing O_3 in polluted areas than in pristine areas with lower NO_x concentrations (Granier and Brasseur, 2003). Globally, road traffic emissions produce 8 % of the tropospheric annual O_3 burden (Mertens et al., 2018).

As the photolysis rate of NO_2 (R1) depends on the solar radiation, O_3 produced by road traffic emissions shows a pronounced seasonal cycle. While in July road traffic emissions contribute up to 12 % to the zonal mean in the Northern hemispheric mid-latitudes, the contribution in January drops down to 8 % as less NO_2 is photolysed (Niemeier et al., 2006; Matthes et al., 2007). In winter, even an O_3 decrease due to road traffic emissions is observed over Europe, Russia and Northeastern US (Niemeier et al., 2006; Hoor et al., 2009). As the solar heating is reduced during winter, the air masses in the boundary layer are not as well mixed so that species from road traffic emissions can accumulate. The increased NO_x concentration leads to a destruction of O_3 (Niemeier et al., 2006).

Through convection, O_3 from road traffic emissions and its precursors are transported upwards and impact the O_3 concentration in higher altitudes. In particular in summer, it is very likely that road traffic emissions are transported into the free troposphere up to the tropopause region where O_3 is more radiative active (Hoor et al., 2009; Uherek et al., 2010). In general, O_3 contributions of road traffic emissions decrease with height (Granier and Brasseur, 2003; Hoor et al., 2009). In the Northern hemispheric summer at 500 hPa, road traffic emissions contribute 5 – 10 % to O_3. In contrast in the upper troposphere, the contribution drops down to 2 – 8 % (Granier and Brasseur, 2003; Niemeier et al., 2006).

Road traffic emissions can produce or destroy O_3 in pristine areas far away from the source region. NO_x from road traffic emissions can be transformed into peroxyacyl nitrates (PAN) which is lifted upwards into the upper troposphere, where it has a lifetime of several days (about 13 days). Thus PAN can be transported over long distances. When it sinks down, it thermally decomposes releasing again NO_x which in turn influences O_3. Thus, this O_3 change is attributed to road traffic

emissions. For example, PAN is increased by 75 ppt due to road traffic emissions in the arctic in spring. This rises the O_3 contribution by about 15 %. (Matthes et al., 2007; Roberts, 2007)

2.2.2. Effect of road traffic emissions on hydroxyl radical

The hydroxyl radical (OH) plays a crucial role in the tropospheric chemistry. The radical reacts with many chemical species in Earth's atmosphere and thus has only a lifetime of a few seconds (Seinfeld and Pandis, 2006). OH is formed by the photolysis of O_3. At wavelengths smaller than 319 nm O_3 is photolysed producing either a ground state O or an excited singlet $O(^1D)$. In most cases, $O(^1D)$ descends to ground state by colliding with N_2 or O_2. But it also reacts with H_2O forming OH:

$$O_3 + h\nu \longrightarrow O_2 + O(^1D) \tag{R10}$$

$$O(^1D) + H_2O \longrightarrow 2OH \tag{R11}$$

As OH is very reactive, it decomposes pollutants and is involved in the production of ozone and secondary organic aerosols in the boundary layer (e.g. Lawrence et al., 2001; Heard and Pilling, 2003). Hence, OH determines the self-cleaning effect of the atmosphere and thus crucially controls regional air quality (Lelieveld et al., 2002, 2004). In general, estimations of tropospheric OH concentrations generate a value of approximately $11 \cdot 10^5$ molec cm^{-3} (Naik et al., 2013; Prinn et al., 2005; Liang et al., 2017).

OH also destroys the greenhouse gases CH_4 and O_3 regulating their atmospheric lifetimes (e.g. Stevenson et al., 2006; Voulgarakis et al., 2013). Consequently, OH indirectly influences the radiation budget of the Earth (see sect. 2.4).

The atmospheric OH concentration strongly depends on the ratio of NO_x and VOC (Heard and Pilling, 2003). Consequently, road traffic emissions modify the OH concentration. Larger NO_x concentrations due to road traffic emissions shift the HO_2/OH balance to OH by reaction $HO_2 + NO \longrightarrow OH + NO_2$. Moreover, larger O_3 concentrations increase OH by reaction (R11). Thus in general, road traffic emissions enhance OH. In contrast, as CO has a long lifetime of about 1-2 months, it can be transported away from the source regions in remote areas where it destroys OH by the reaction $CO + OH \longrightarrow CO_2 + H$ (Niemeier et al., 2006; Uherek et al., 2010). Hence, the ratio of NO_x/CO determines the sign of OH change (Niemeier et al., 2006).

OH variations due to road traffic emissions are confined to the source regions: OH increases the most over industrialised countries (Eastern USA, central Europe, Eastern Asia) by up to $2.5 \cdot 10^4$ molec cm^{-3} (Hoor et al., 2009). During summer, in coastal areas with a high degree of urbanization, road traffic emissions increase the OH concentration by up to 5 – 10 % (Niemeier et al., 2006). In contrast, in certain regions such as UK or along ship tracks, road traffic emissions also decreases OH (Niemeier et al., 2006). With increasing altitude, the effect of road traffic emissions on OH decreases. At 300 hPa, OH increase due to road traffic is negligible (Granier and Brasseur, 2003).

However, the OH concentration change is dominated by the seasonal cycle, in particular in the Northern Hemisphere. In the Northern summer, the zonal mean of OH increases by up to 5 % of the total OH in the continental boundary layer (Niemeier et al., 2006). At the same time, the additional OH enhances the local O_3 production. In winter, the reduced solar radiation causes the emissions of CO and VOC to efficiently destroy OH (see reaction chains R5 and R8).

2.2.3. Effect of road traffic emissions on methane

As explained in the previous section, OH oxidises greenhouse gases such as CH_4. Consequently, OH largely controls their lifetimes. It reacts with CH_4 to the methyl radical (CH_3) which quickly recombines with O_2 to the methyl peroxy radical (CH_3O_2):

$$\mathrm{CH_4 + OH \xrightarrow{O_2} CH_3O_2 + H_2O} \tag{R12}$$

In general, the atmospheric lifetime of a species against OH is determined by the total mass of this species Q divided by the rate of removal of this species R by OH:

$$\tau = \frac{Q}{R} \tag{2.1}$$

The resulting tropospheric CH_4 lifetime varies among chemistry climate models. Stevenson et al. (2006) state a multi-model mean for 26 models of 8.67 ± 1.32 years for CH_4. Naik et al. (2013) compare 17 global model participating in the Atmospheric Chemistry and Climate Model Intercomparison Project (ACCMIP) finding a multi-model mean for CH_4 lifetime of 9.7 ± 1.5 yr.

CH_4 lifetime is also derived from observations. Therefore, OH is estimated by emissions of methyl chloroform (CH_3CCl_3). In general, CH_4 lifetime derived by observations are larger than derived by models. Prinn et al. (2005) estimate a CH_4 lifetime against tropospheric OH of $10.2^{+0.9}_{-0.7}$ years, Prather et al. (2012) derive 11.2 ± 1.3 years.

The oxidation of CH_4 initiates a chain of reactions producing in the end 4 O_3 molecules:

$$\begin{aligned}
\mathrm{CH_4 + OH} &\xrightarrow{\mathrm{O_2}} \mathrm{CH_3O_2 + H_2O} \\
\mathrm{CH_3O_2 + NO} &\xrightarrow{\mathrm{O_2}} \mathrm{HCHO + HO_2 + NO_2} \\
\mathrm{HCHO} + h\nu &\xrightarrow{\mathrm{2O_2}} \mathrm{CO + 2\,HO_2} \\
\mathrm{3(HO_2 + NO} &\longrightarrow \mathrm{NO_2 + OH)} \\
\mathrm{4(NO_2} + h\nu &\xrightarrow{\mathrm{O_2}} \mathrm{NO + O_3)}
\end{aligned} \tag{R13}$$

$$\text{net:} \quad \mathrm{CH_4 + 8O_2} + 5h\nu \longrightarrow \mathrm{CO + H_2O + 2\,OH + 4\,O_3}$$

In addition, one CO molecule is formed which in turn produces one O_3 molecule. Thus in total, one CH_4 molecule can yield to maximal five O_3 molecules. The ozone

change caused by CH_4 change is called *primary mode ozone (PMO)* (Prather, 1996; Wild and Prather, 2000; Wild et al., 2001). Usually, the change of O_3 lasts only a few months as the O_3 lifetime is only 23.4 ± 2.2 days (Young et al., 2013). However, the change of PMO lasts as long as the change of CH_4 lifetime does (Sausen et al., 2012). Additionally, the reduction of CH_4 further decreases the formation of stratospheric water vapour by reaction (R12).

In general, road traffic emissions increase OH which in turn reduces the atmospheric lifetime of CH_4. The reduction of CH_4 lifetime varies among the studies. Myhre et al. (2011) compare 5 models finding a model mean of -1.32 % (min -1.78 %, max 0.12 %) while Hoor et al. (2009) present a 6-model-mean of -1.61 ± 0.25 %. Matthes (2003) find a rather small reduction of -0.7 %. Granier and Brasseur (2003) state a CH_4 lifetime reduction at the upper end of -3 %.

To put it in a nutshell, road traffic emissions of NO_x, VOC and CO influence the atmospheric composition. They generally increase tropospheric O_3. In particular, ground level O_3 close to the source region is raised the most during summer when photolysis rates are largest. Even O_3 in pristine areas can be affected by road traffic emissions. In contrast, the effect on OH is rather restricted to the source region. Increased concentrations of NO_x and O_3 due to road traffic emissions rise in turn the OH concentrations. Additionally, increased OH concentrations oxidise more CH_4 which reduces the lifetime of CH_4. The oxidation of CH_4 impacts in turn the O_3 production (primary mode ozone). Consequently, lower CH_4 concentrations due to road traffic emissions decreases tropospheric O_3. However in total, tropospheric O_3 is increased by road traffic emissions of NO_x, VOC and CO.

2.3. Effect of road traffic emissions on aerosols

Road traffic emissions also influence atmospheric aerosols. Aerosols are small solid or liquid particles floating in the air. Their diameters vary between a few nanometers to several hundred micrometers. Aerosols originate from natural sources such as sea spray, desert dust, volcanoes as well as from anthropogenic sources such as combustion of fuels in cars or industrial plants. Aerosols are either directly emitted or they are formed by aerosol precursor gases. They mostly consist of mineral dust, sea salt, black carbon, organic carbon, sulphate, nitrate, ammonium and water. (Seinfeld and Pandis, 2006; Hendricks et al., 2012)

Aerosols influence the atmosphere and climate in multiple ways:

1. Aerosols directly impact the radiation budget by scattering and absorbing shortwave and longwave radiation. Aerosols (in particular sulphate particles) scatter shortwave radiation back into space, thus causing a negative forcing. Moreover, aerosols (in particular soot and dust particles) also absorb radiation, thus heating the surrounding air and causing a positive radiative forcing (Sausen et al., 2012). Both processes are called the *direct effect* (Ångström, 1962).

2. Aerosols indirectly impact the climate through their interactions with clouds. Aerosols serve as cloud condensation nuclei. Hence, the abundance of aerosols influences the cloud formation, modifies their microphysical properties and their lifetime (Lohmann and Feichter, 2005). Clouds crucially influence the climate as they are tied to the hydrological cycle and affect the radiation budget. This effect is called the *indirect effect* (Twomey, 1977; Albrecht, 1989).

3. Aerosols can also reduce the cloud coverage on a regional scale. Solar insulation heats up dark haze including soot so that cloud droplets evaporate and the clouds dissolve. This process is mostly found over the Northern Indian Ocean during the North East monsoon and affects the radiation budget on a regional scale. The effect is called the *semi-direct effect* (Ackerman et al., 2000).

4. Aerosols further influence the concentrations of greenhouse gases. Condensable species such HNO_3 are adsorbed by aerosols. Thus their gas phase concentrations are reduced. For example, this process influences NO_x and HO_x concentrations affecting O_3 production and destruction. At the surface of aerosols, heterogeneous reactions occur which transform several gases. For example, the chlorine radical can be activated at the surface of aerosols which can subsequently destroy O_3 in the stratosphere. (e.g. Dentener and Crutzen, 1993; Sausen et al., 2012; Hendricks et al., 2012)

Due to the combustion of fossil fuels in passenger cars and heavy goods vehicles, road traffic directly emits aerosol particles. They mainly consist of black and organic carbon but also contain small proportion of sulphate (SO_4). Moreover, road traffic emits the aerosol precursor gas sulphur dioxide (SO_2) which is transformed to sulfuric acid (H_2SO_4). H_2SO_4 in turn produces sulphate aerosols. Road traffic emissions of NO_x produce nitrate (NO_3) which is then transformed to nitrate aerosols. (e.g. Sausen et al., 2012; Hendricks et al., 2012; Righi et al., 2013)

The amount and the distribution of black carbon (BC) and nitrate aerosols produced by road traffic emissions have been investigated in several studies. The abundance of BC which originates from road traffic emissions is confined to source regions. In Europe and Eastern USA, 50 % of BC originates from road traffic emissions (Sausen et al., 2012). Köhler et al. (2001) state that road traffic emissions contribute up to 20 % of the BC mass concentration at the surface in Northern midlatitudes (in the mid-1990s). Righi et al. (2013) obtain larger values than Köhler et al. (2001) and Sausen et al. (2012). In the year 2000, up to 70 % (about 1 µg m^{-3}) of BC in central Europe, Eastern USA as well as Southern and Eastern Asia arises from road traffic emissions[1]. The relative contribution of road traffic emissions to BC in Europe and North America is higher than in Asia due to high background BC concentration in Asia originating from industry, energy production and households. Thus, Europe and North America have a high potential to reduce BC from road traffic emissions (Righi et al., 2015).

[1] In fact, Righi et al. (2013) considers all land transport modes. However, as explained in sect. 3.4, road traffic emissions are by far the largest contributors to land transport emissions. Consequently for simplification, land transport is denoted as road traffic.

Convection and long scale transport disperse aerosols upwards into the free troposphere. Thus road traffic emissions also contribute to aerosols in the upper troposphere. For example, BC from Asian road traffic emissions contributes 10 % to the total BC concentration in the upper troposphere in July (Köhler et al., 2001).

Road traffic emissions largely accounts for nitrate aerosols in many regions. In contrast to BC, which are rather restricted to their source region, nitrate aerosols from road traffic emissions are distributed more homogeneously in the atmosphere. This is explained as nitrate aerosols are formed by NO_3 while the polluted air masses are dispersed. Southern Europe and Northern India show the largest concentrations with over 1 µg m^{-3} (contributing about 10 – 60 % to total nitrate aerosols). In North and South America, 50 – 70 % of nitrate aerosols originate from road traffic emissions (Righi et al., 2013).

Due to road traffic emissions, more aerosols and thus more cloud condensation nuclei are available in the atmosphere. Hence, more but smaller cloud droplets are formed. As small droplets scatter radiation stronger than large droplets, clouds with smaller droplets are optically thicker, i.e. more solar radiation is reflected back to space. Moreover, clouds with smaller droplets live longer as the droplets do not grow as fast. Thus, it takes longer before the droplets have grown large enough to fall down as precipitation.

The specific radiative forcings of each aerosol effect are given in sect. 2.4.

2.4. Effect of road traffic emissions on climate

Road traffic emissions alter climate directly and indirectly. Earth's climate is determined by the global energy balance of incoming shortwave (solar) and outgoing longwave (terrestrial) radiation. Solar radiation warms the Earth increasing its surface temperature. Absorbed solar energy is re-emitted by the Earth as terrestrial radiation. In steady state, shortwave and longwave radiation balance each other at top of the atmosphere (TOA) and thus determine the surface temperature of the Earth.

The atmosphere plays a crucial role for the radiation budget. It contains several gases which absorb radiation. Such *greenhouse gases* are for example water vapour, carbon dioxide, ozone, methane and nitrous dioxide. Water vapour is the most important natural greenhouse gas, followed by CO_2 (e.g. Ponater et al., 2012). Natural causes (e.g. volcanic eruptions) as well as anthropogenic emissions alter the atmospheric composition and hence perturb the radiation budget: they cause a change in the net radiation flux (in Wm^{-2}) which is called *radiative forcing (RF)* (Myhre et al., 2013). The concept of radiative forcing is widely used to quantify and compare these natural and anthropogenic perturbations of climate.

Once the radiation budget is perturbed, climate variables such as surface temperature adapt to re-establish the radiative balance at TOA. A net downward flux change at the respective surface (e.g top of the atmosphere, tropopause) is defined as positive RF. It causes a larger energy uptake into the climate system inducing a warming and thus a rise of surface temperature. Accordingly, a negative RF corresponds to an upward flux change causing a cooling. (Wallace and Hobbs, 2006; Zdunkowski et al., 2007)

In a first approximation, the change in global mean equilibrium surface temperature (ΔT_S) depends linearly on the RF

$$\Delta T_S \approx \lambda \cdot RF \tag{2.2}$$

with λ being the *climate sensitivity*. Eq. 2.2 applies the transition from one equilibrium climate state to another. While the RF is computed when the climate is perturbed, ΔT_S describes the surface temperature once the climate could adapt to the perturbation. However, the climate sensitivity λ varies not only amongst climate models, but also for different strength and types of perturbations within the same climate model (Cess et al., 1990; Hansen et al., 1997; Berntsen et al., 2005; Stuber et al., 2005; Soden and Held, 2006).

Several definitions of radiative forcing exist, each has its advantages and its limitations. *Instantaneous RF* determines the flux change which results immediately after the climate is perturbed. *Stratosphere adjusted RF* describes the flux change after the stratospheric temperature has adjusted to the perturbation. The stratosphere typically adapts within a few weeks to months. In contrast, the troposphere adjusts within several decades to millennia as the ocean response is very slow. *Zero-surface-temperature-change RF* is the flux change if the temperature in troposphere and stratosphere is allowed to adapt but the surface temperature is set constant. *Effective RF* describes the flux change at TOA after temperature, water vapour and clouds could adjust. In general, sea surface temperature and sea ice cover is kept constant for the determination of effective RF. Land surface properties such as temperature and vegetation can adapt to the perturbation. (Hansen et al., 1997; Stuber et al., 2001; Vial et al., 2013; Myhre et al., 2013)

Road traffic emissions affect climate in several ways. Passenger cars and heavy good vehicles emit greenhouse gases, precursor of greenhouse gases as well as aerosols and thus perturb the radiative energy transfer of the Earth. The radiative forcing of the different effects are listed in table 2.1 which compares the RF of road traffic emissions[1] with the total anthropogenic RF. As the effect of primary mode ozone (see sect. 2.2.3) is rather uncertain and comparably small, it is not included in the table.

CO_2 has a rather long lifetime (varying between 5 – 200 year, Albritton et al., 2001) and thus is well mixed in tropo- and stratosphere. CO_2 from road traffic emissions causes by far the largest climate impact. It generates a RF of about 150 mW^{-2} which corresponds to 8 % of total anthropogenic CO_2 RF since pre-industrial times (Fuglestvedt et al., 2008; Uherek et al., 2010).

Formation of ozone in the troposphere due to road traffic emissions is the second largest RF. It results in a RF of about 54 mW m^{-2} which corresponds to 14 % of total anthropogenic O_3 RF since pre-industrial times (Niemeier et al., 2006; Fuglestvedt et al., 2008). Other studies obtain similiar values: A 5-model-mean delivers a O_3 RF for road traffic emissions of about 31 mW m^{-2} ranging between 15 and 42 mW m^{-2}

[1] Uherek et al. (2010) presents RF values for land transport. However, as road traffic emissions are by far the largest contributor to land transport emissions, it is justified to simplify the representation and call it "road traffic" here.

Effect	**Road traffic RF in mW m^{-2}**	**Total RF in mW m^{-2}**
Carbon dioxide (CO_2)	150 (143 to 166)	1820 (1630 to 2010)
Ozone (O_3)	54 (19 to 91)	400 (200 to 600)
Methane (CH_4)	-12 (-29 to -5)	-157
Sulphate aerosols (direct)	-12 (-7 to -5)	-350 (-850 to 150)
Soot aerosols (direct)	23 (14 to 32)	
Aerosol indirect effect	*	-45 (-1200 to 0)
TOTAL	223	1540

* no reliable estimates available

Table 2.1: Global mean of road traffic and total anthropogenic radiative forcing in mW m^{-2} (Uherek et al., 2010; Sausen et al., 2012; Myhre et al., 2013). Road traffic RF represents the year 2000. In contrast, total RF indicates the RF for the year 2011 taken from Myhre et al. (2013). Only the tropospheric O_3 is regarded for O_3 RF. Total RF of aerosol-radiation interaction (direct effect) considers both aerosols types (sulphate and soot aerosols) together. No range for the total RF are given when they are not explictily stated in Myhre et al. (2013).

(Myhre et al., 2011). A 6-model-mean by Hoor et al. (2009) gives a RF of 27.9 ± 5 mW m^{-2} for the year 2003. Using the tagging method to attribute road traffic emissions to O_3 (see chapt. 4), Mertens et al. (2018) find the largest RF of 92 mW m^{-2}. They further pointed out that methodical deficiencies lead to a large underestimations of the contribution of road traffic emissions to O_3 radiative forcing. Due to larger O_3 concentrations from road traffic emissions in Northern summer than in Northern winter, the O_3 RF is larger in July than in January (Niemeier et al., 2006). Furthermore, RF of tropospheric O_3 strongly depends on height and latitude (Lacis et al., 1990; Berntsen et al., 1997; Hansen et al., 1997; Worden et al., 2008; Bowman et al., 2013). In the upper troposphere, an O_3 increase causes a larger RF than in the lower troposphere.

The climate effect due to direct CH_4 emissions of road traffic is negligible (Uherek et al., 2010). The main part is caused indirectly by changes in CH_4 lifetime due to OH variation caused by road traffic emissions (see sect. 2.2.3). Uherek et al. (2010) and Fuglestvedt et al. (2008) find a CH_4 RF of about -12 mW m^{-2}. Hoor et al. (2009) find a stronger RF of -14.5 ± 2.3 mW m^{-2} for 2003. The effect of the CH_4 lifetime change on O_3 (primary mode O_3, PMO, see sect. 2.2.3) is yet not well quantified (Sausen et al., 2012). Dahlmann et al. (2016) estimates the PMO being 0.29 × RF(CH_4), while Hoor et al. (2009) state a PMO of 0.42 × RF(CH_4) and thus estimate a RF of -6.1 ± 1.0 mW m^{-2} for 2003. Myhre et al. (2011) include also the effect of CH_4 on stratospheric water vapour and obtains a RF of 16 ± 13 mW m^{-2}

(5-model-mean).

The direct effect of aerosols is twofold. On the one hand, mainly due to radiation absorption, soot aerosols warm the climate with about 23 mW m^{-2}. Fuglestvedt et al. (2008) estimate a RF of BC ranging from 14 – 32 mW m^{-2}. In contrast, Köhler et al. (2001) state a larger RF of about 80 mW m^{-2}. On the other hand, sulphate aerosols cool the climate with about -12 mWm^{-2}. In total, the RF of the direct aerosol effect is positive. Balkanski et al. (2010) report a direct aerosol RF between 29.1 – 41.4 mW m^{-2}, Fuglestvedt et al. (2008) find a RF of 3.3 ± 11 mW m^{-2} of road traffic emissions.

Considerding the direct, semi-direct and indirect effects of aerosols together, Righi et al. (2013) reveal a RF of -80.7 to -11.8 mW m^{-2} which is dominated by radiation impact of clouds. In general, aerosol-cloud interaction are very uncertain and cause a large spread of RF (Sausen et al., 2012).

As described above, the radiative forcings of road traffic emissions differ largely among the various studies. The reasons for these differences are that the cited studies use different emission inventories, different chemistry climate models and different techniques to derive the climate effect of road traffic emissions (Mertens et al., 2018).

Further influences on the atmospheric compositions and radiation budget caused by road traffic emissions are only briefly mentioned here and not further discussed: The changes in O_3 and OH affect the atmospheric sulphate burden and stratospheric water vapour (e.g. Unger et al., 2006; Shindell et al., 2009). Moreover, O_3 influences the vegetation and thus the carbon cycle (e.g. Sitch et al., 2007). In addition, as NO_2 absorbs shortwave radiation, the emissions of NO_x has a small direct RF (Kvalevåg and Myhre, 2007).

2.5. Effect of road traffic emissions on environment

Road traffic emissions impact not only climate but also contribute to air pollution affecting human health and environment. In general, emissions from road traffic are related to diseases of the respiratory system (e.g. asthma), of the cardiovascular system (e.g. strokes and heart diseases) and are also related to carcinogenic diseases (e.g. lung cancer). Consequently, road traffic emissions increase the morbidity and mortality (e.g. WHO, 2006a, 2016, 2017). In particular, people living close to major roads face an increased risk of coronary heart diseases, diabetes and mortality. (Nyberg et al., 2001; Finkelstein et al., 2004; Chen et al., 2007; Gan et al., 2010)

Particulate matter (PM) emitted by road traffic imposes the greatest risk to human health (WHO, 2006a; Uherek et al., 2010). Particles can enter deep into the lung where they penetrate into the bloodstream. Small particles with diameters less than 2.5 µm (PM2.5) are especially harmful to human as they can penetrate deeper into the lung than larger particles (Fang et al., 2013). The specific size distribution of the particles strongly depends on the meteorological situation and on the traffic volume. Vehicles mainly produce fine and ultrafine PM (Despiau and Croci, 2007; Rodriguez et al., 2007). Break and road wear cause rather coarse mode particles (Manoli et al., 2002). PM concentrations rapidly diminish with the distance from the road (Wrobel et al., 2000). Moreover, PM causes inflammations and cerebrovascular

accidents. It also impacts cardiovascular and respiratory systems. Additionally, emissions of PM containing arsenic, chrome, nickel and lead are carcinogenic and thus are associated with lung cancer. According to the World Health Organization, the annual average concentration of 10 µg/m^3 for PM2.5 and 20 µg/m^3 for PM10 (PM with diameters less than 10 µm) should not be exceeded (WHO, 2006b). In 2000, the average loss of life expectancy due to PM2.5 is estimated to be 8.6 months in Europe varying for different regions (Amann et al., 2004).

Due to its low solubility, O_3 also penetrates deep into the lungs where it harms the respiratory system. It reduces lung function, causes breathing problems, triggers asthma and causes respiratory diseases. For elderly people and those with respiratory diseases, O_3 can cause an inflammation of airways. Moreover, O_3 triggers allergies and induces eye irritations (Krzyzanowski et al., 2005). Independent from PM, O_3 itself increase the mortality (e.g. Mudway and Kelly, 2000; Gryparis et al., 2004; Bell et al., 2006). An exposure of the 8-hour mean 100 µg/m^3 should not be exceeded (WHO, 2006a).

Additionally, road traffic emits NO_2 which is also considered to be harmful for humans. It affects the respiratory system, causes infections, reduces the lung function and growth. It further induces bronchitis and asthma. At very high concentrations, NO_2 is toxic and inflames the airways (WHO, 2006a). Consequently, WHO (2006a) suggests a threshold of 1-hour mean 200 µg/m^3.

Exhaust emissions from road traffic also contains CO and small amounts of SO_2. CO is only harmful in high concentrations when CO replaces oxygen in the bloodstream. The exhaust emission of SO_2 has been largely reduced. Thus the health impact of SO_2 from road traffic emissions is less relevant any more.

Not only the exhaust emissions but also the noise emitted by road traffic impacts human health. For example, road traffic noise is associated with an increased risk of strokes (Sørensen et al., 2011), with hypertension (Leon Bluhm et al., 2007), with ischemic heart diseases (van Kempen et al., 2002) and with increased myocardial infarction (Selander et al., 2009).

Besides the health impact of road traffic emissions, the environment is also affected. PM from road traffic contains heavy metal which contaminates the soil after being deposited. SO_2 and NO_x from road traffic emissions also contribute the formation of acid rain. The deposition of NO_x cause acidification and eutrophication of soils (Uherek et al., 2010). Furthermore, O_3 harms sensitive plant species (Ainsworth et al., 2012). It enters the plant through their stomata where it destroys the plant's cells and leads to a reduction of photosynthesis (Reich and Amundson, 1985). Additionally for plants with broad leaves, O_3 causes visible leaf defects (Günthardt-Goerg and Vollenweider, 2007). This can lead to a significant reduction of quantity and quality of crop yield (Mills et al., 2007). Consequently, road traffic emissions damage soil, vegetation, water sources and whole ecosystems (Uherek et al., 2010).

3

Global chemistry climate model EMAC

To quantify the effect of road traffic emissions on global climate, the global chemistry climate model ECHAM/MESSy Atmospheric Chemistry (EMAC) model is used. It is a numerical chemistry climate simulation system which contains submodels describing tropospheric, stratospheric and mesospheric processes. Interaction with oceans, land and human influences (e.g. anthropogenic emissions) are also implemented (Jöckel et al., 2010). In this work, EMAC utilises the second version of the Modular Earth Submodel System (MESSy 2.53) to link multi-institutional computer codes. The core atmospheric model bases on the 5th generation European Centre Hamburg general circulation model (ECHAM5; Roeckner et al., 2006). This section presents the atmospheric model ECHAM5 and the Modular Earth System Model MESSy. Subsequently, the specific model setup as well as the emission inventory of road traffic used in this work are described in detail.

3.1. Atmospheric model ECHAM5

The dynamical core of ECHAM is developed from a global numerical weather prediction model of the European Centre for Medium-Range Weather Forecasts, **EC**MWF (Simmons et al., 1989). To adapt the model for climate simulations further developments were performed at the Max-Planck Institute for Meteorology in **HAM**burg (Roeckner et al., 2003).

ECHAM5 has a spectral dynamical core which solves the primitive equations for the hydrostatic approximation: continuity equation, conservation of momentum and thermal energy equation. The prognostic variables vorticity, divergence, temperature and the logarithm of surface pressure are given in spectral space (truncated series of spherical harmonics). The prognostic water species such as vapour, liquid and solid are represented in grid space (Gaussian grid). To define the vertical model structure, ECHAM applies an hybrid sigma-pressure system. Close to the

surface, the hybrid coefficients follow the orography, where as at higher altitudes (above 35 hPa), they describe pressure levels. Roeckner et al. (2003) gives a detailed description of ECHAM5.

3.2. Modular Earth Submodel System MESSy

The software package MESSy links various submodels to a base model which enables the construction of an Earth system model (Jöckel et al., 2005). These submodels contain infrastructure components for the data management, physical process or diagnostics. Examples for submodels are the calculations of the radiative fluxes or the calculations of the chemical reaction rates.

The basic concept of MESSy is to divide the code into four layers (see fig. 3.1; Jöckel et al., 2005): (1) The base model layer BML contains, in this thesis, the base model ECHAM5. (2) The base model interface layer BMIL contains base-model specific implementation to provide data exchange between the base model and the submodels. (3) The submodel interface layer SMIL passes the information from BMIL to the submodels. It further provides the communication between the different submodels. (4) The submodel core layer SMCL finally contains the various submodels such as calculation of the radiative and convective fluxes.

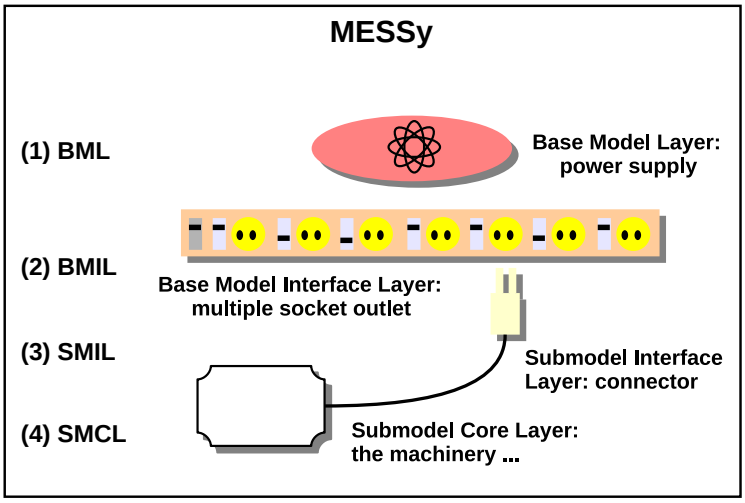

Figure 3.1: Sketch of MESSy with its four layer structure, adapted from Kerkweg and Jöckel (2012a).

3.3. Model setup

The combination of ECHAM and MESSy is called EMAC and enables to set up a flexible Earth system model. Various submodels can be added to an EMAC simulation. In the following, only these submodels which are relevant for the simulations performed in this work are described in more detail. A complete list of all submodels is given in the appendix A.2. The general setup resembles the model setup of *RC1SD-base-10a* which is described in Jöckel et al. (2016) in more detail.

For the present thesis, EMAC is applied in the resolution T42L90MA. T42 corresponds to a quadratic Gaussian grid of approx. 2.8° by 2.8° in latitude and longitude. L90MA describes 90 vertical hybrid pressure levels up to 0.01 hPa. The time step length is 12 minutes. The simulation is free running, i.e. only the initial values are prescribed and the simulated values are not adapted to measurements (nudging).

The submodel MECCA (Module Efficiently Calculating the Chemistry of the Atmosphere) is used for solving the chemical mechanism (Jöckel et al., 2010; Sander et al., 2011). The chemical mechanism is based on 218 gas phase, 12 heterogeneous and 68 photolysis reactions. Overall, 188 species are regarded. The principle chemistry of tropo- and stratosphere is considered which includes the species OH, HO_2, O_3, CH_4, nitrogen oxides, alkanes, alkenes, chlorine and bromine.

The radiative calculations are performed with the submodel RAD (Dietmüller et al., 2016). The terrestrial (i.e. longwave) radiative spectrum is divided into 16 spectral bands (3.33 to 1000 μm) and is determined after Mlawer et al. (1997). The solar (i.e. shortwave) radiation spectrum is split up into 4 spectral bands (ultraviolet, visible and near-infrared 0.25 - 4.00 μm) and is calculated after Fouquart and Bonnel (1980). To achieve higher resolution in the shortwave spectrum, the submodel FUBRAD increases the spectral bands up to 55 in the stratosphere and mesosphere (Nissen et al., 2007).

In general, it is difficult to detect small perturbations (such as changes in road traffic emissions) with a chemistry climate model, since the dynamics and the chemistry are coupled within the model. For example, small variations of road traffic emissions change the chemical state. Through radiation transfer and water vapour cycle, the dynamics of the simulation are changed as well which in turn feed back to the chemical state. This can lead to very different meteorological situations and thus can produce very different results even for small perturbations. This effect is known as the "butterfly effect" which makes it impossible to detect the climate effect of small changes from the inheret noise of a chemistry climate model. To eliminate the detection problem, Deckert et al. (2011) developed the Quasi Chemistry Transport Model (QCTM) mode for EMAC. This mode decouples the dynamics from the chemistry. It prescribes climatologies for the radiation calculation using monthly means of CO_2, CH_4, O_3, N_2O, CF_2Cl_2 and $CFCl_3$. Climatologies of OH, $O(^1D)$ and Cl as well as a climatology of HNO_3 are used to decouple the formation of polar stratospheric clouds and the oxidation of CH_4 from the chemistry (submodels MSBM and CH4). For the climatologies, the monthly means are taken from the *RC1SD-base-10a* simulation (detailed description of the simulation *RC1SD-base-10a* are found in Jöckel et al. (2016)). By using climatologies, this QCTM mode breaks

the feedback processes between chemistry and dynamics. It suppresses the inherent noise of a chemistry climate model and thus enables to quantify the climate effect of small perturbations.

As EMAC is run in the QCTM mode, the calculation of the radiative fluxes, which feed back to the model simulation, is based on climatologies of CO_2, CH_4, O_3, N_2O, CF_2Cl_2 and $CFCl_3$ (radiation call rad01). To determine the radiative forcing of the O_3 change caused by road traffic emissions, additional calculations of the radiative fluxes are necessary. First, the radiative fluxes of the O_3 field which is modified by the model chemistry (provided by the submodel MECCA) are calculated (radiation call rad02). Second, to determine the contribution of road traffic emissions to ozone ${O_3}^{tra}$, the radiative fluxes of (O_3 – ${O_3}^{tra}$) are computed (radiation call rad03). In a post processing step, the radiation calls rad02 and rad03 are subtracted to finally obtain the radiative fluxes due to ${O_3}^{tra}$. For rad02 and rad03, the stratospheric adjusted radiative fluxes are computed. This enables to determine the stratospheric adjusted radiative forcing (see sect. 2.4).

The MACCity emission inventory (Granier et al., 2011) provides anthropogenic emissions such as emissions from road traffic, ships, aviation, industry, agricultural waste burning and biomass burning. A detailed description of the emissions are given in the following sect. 3.4. The submodel ONEMIS (Kerkweg et al., 2006b) calculates emissions during the simulation (so called online emissions) for EMAC. It provides NO_x emissions from soil according to Yienger and Levy (1995) and biogenic isporene (C_5H_8) emissions according to Guenther et al. (1995). In the model setup used here, CH_4 is not directly emitted. Instead, the submodel TNUDGE (Kerkweg et al., 2006b) provides pseudo-emissions: the CH_4 mixing ratios in the lowest model layer are adapted to measurement by Newton relaxation (further details are given in Jöckel et al. (2016)). The lightning NO_x emissions are parameterised according to Grewe et al. (2001) and scaled to approximately 5 Tg(N) per year (submodel LNOX).

As the focus of the thesis is the effect of road traffic emissions of NO_x, VOC and CO on O_3 and CH_4, other effects are represented with lower accuracy. For example, atmospheric aerosols are prescribed to consider their interactions with the heterogeneous chemistry and radiation. Volcanic aerosols are included as well. The aerosol properties are calculated by the submodel AEROPT (Dietmüller et al., 2016).

To specify the contribution of road traffic emissions to O_3 production, the submodel TAGGING is used. A detailed description can be found in Grewe et al. (2010, 2017). It considers ten source categories: emissions from anthropogenic non-traffic (e.g. industry and households), road traffic, ship traffic, air traffic, biogenic sources, biomass burning, lightning, methane and nitrous oxide decompositions and stratospheric ozone production. The submodel calculates the contribution of these source categories to the species O_3, CO, OH, HO_2, peroxyacyl nitrates (PAN), reactive nitrogen compounds (NO_y = NO, NO_2, HNO_4,...) and non-methane hydrocarbons (NMHC). Further details are explained in chapt. 4. Within the scope of this thesis, I further developed the tagging method of OH and HO_2 and improved certain shortcomings. A detailed description is presented in sect. 4.4. The further developed

tagging method V1.1 (submodel TAGGING 1.1) is used in this thesis to perform the simulations.

If not indicated otherwise, the time period of July 2009 to December 2010 is simulated. The first half year is taken as spin-up period, the remaining year is used for the analysis. Due to limited computational resources, it is only possible to use one year for the analysis. An EMAC simulation for a three years time period shows that the year-to-year variability is quite low which justifies to use only 1 year for evaluation (see appendix A.1 and Hoor et al. (2009)).

3.4. Emissions in EMAC

The anthropogenic emissions for the EMAC simulations are taken from the emission inventory MACCity (Monitoring atmospheric composition & climate (MACC)/City Zero (carbon) Energy (CityZEN); Granier et al., 2011). MACCity provides data for the period 1990 - 2010. It bases on two data set: ACCMIP and RCP8.5. ACCMIP (Atmospheric Chemistry and Climate - Model Intercomparison Project; Lamarque et al., 2010) is a historical emission dataset for the period 1850-2000. It combines several existing global and regions emission inventories. The emissions of trace gases and aerosols are given on a decadal basis. RCP8.5 (Representation Concentration Pathways) was developed within the scope of fifth Assessment Report (AR5) of the IPCC (IPCC, 2013; van Vuuren et al., 2011; Riahi et al., 2007). The emission projections RCP8.5 describe a steady emission increase throughout the 21st century. It leads to a radiative forcing of 8.5 W m^{-2} in the year 2100 which approximately corresponds to 1370 ppm CO_2. For MACCity, the anthropogenic emissions are obtained by a linear interpolation on a yearly basis between the year 1990, 2000, 2005 and 2010. The years 1990 and 2000 are taken from ACCMIP, the year 2005 and 2010 from RCP8.5. In order to obtain the emissions from biomass burning, the ACCMIP dataset is also expanded.

The emission data is provided on a monthly basis to reconstruct the seasonal cycle of the emissions. The resolution of the data is $0.5° \times 0.5°$. Anthropogenic emissions of the species CH_4, CO, NO_x, SO_2, BC, OC, NH_3 and a large set of VOCs is given. For the EMAC simulations performed in this thesis, anthropogenic emissions are summarised to sectors agricultural waste burning, biomass burning, industry[1], road traffic, shipping and aviation.

Fig. 3.2 shows the road traffic emissions for NMVOC[2], CO and NO_x. In total, road traffic emits in 2010 20.3 Tg(NO) NO_x, 145.8 Tg(CO) CO and 17.2 Tg(C) VOC. In fact, MACCity merges emissions from road traffic, railways and inland shipping into the same emission sector "land transport". However, the emissions of railways and inland shipping are very small compared to the emissions of road traffic. Railways contribute to the land transport by about 3 % for CO_2, 7 % for NO_x, 0.4 % for CO and 1 % for VOC. Inland shipping is even less: 0.9 % for CO_2, 2 % for NO_x, 0.1 % for CO and 0.3 % for VOC (e.g. QUANTIFY

[1]Emissions from the industry sector are determined by subtracting road traffic and agricultural waste burning emissions from the anthropogenic land emissions.

[2]NMVOC stands for non-methane volatile organic compounds. In this thesis, it is called only VOC to simplify the representation.

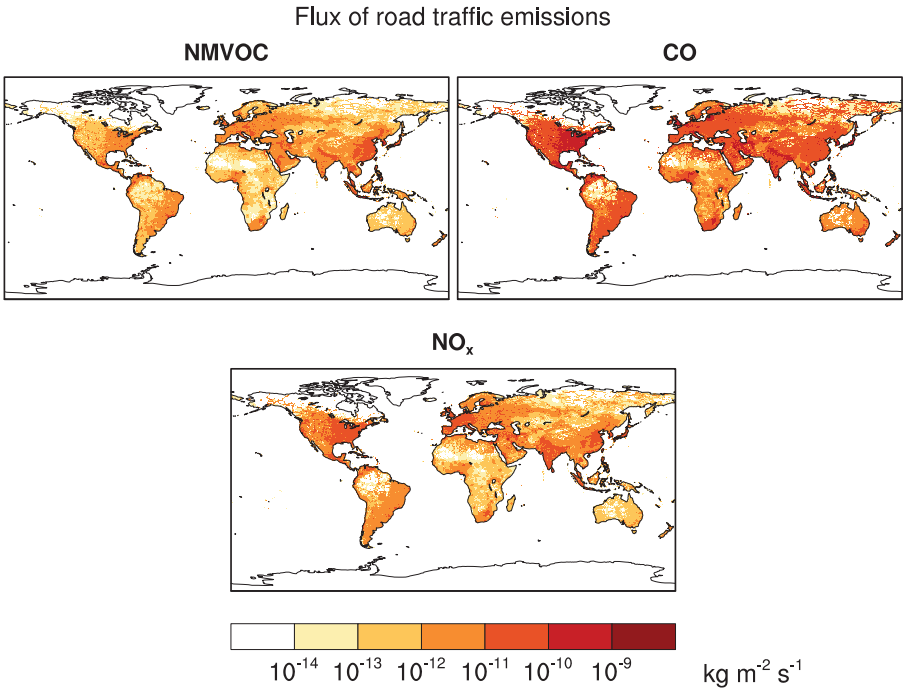

Figure 3.2: Emission flux of road traffic in kg m^{-2} s^{-1} for NMVOC, CO and NO_x are shown. Annual mean for the year 2010 is presented.

`http://www.pa.op.dlr.de/quantify/`; Uherek et al., 2010). As mentioned in sect. 2.1, the uncertainties concerning road traffic emissions vary around 30 - 50 % for NO_x, VOC and CO. Thus, the uncertainties for road traffic emissions are substantially larger than the contributions of railways and inland shipping to the land transport emissions. Consequently, the sector "land transport" is considered as "road traffic" in the following.

4

Tagging method

The tagging method attributes trace gases to emission sectors. It is used in this work to attribute changes of tropospheric O_3, OH and CH_4 to road traffic emissions of NO_x, VOC and CO. At first, the general idea of the tagging method is described in sect. 4.1 and also compared to the perturbation method. Sect. 4.2 presents the ten source categories implemented in EMAC. One of these source categories indicates road traffic emissions which is later used in TransClim to determine the contribution of road traffic emissions to O_3, OH and CH_4. Subsequently, the implementation of the tagging method for long-lived species such as O_3 is presented in sect. 4.3. I further developed the tagging method for short-lived species such as OH and HO_2. Sect. 4.4 describes the advanced tagging method V1.1 and compares it to the former version V1.0. Part of this section is also submitted to *Geoscientific Model Development* as the paper "Further development of the TAGGING 1.1 submodel based on the Modular Earth Submodel System (MESSy 2.53): An enhanced method of contributing emissions to short-lived chemical species (OH and HO_2)" by V.S. Rieger, M. Mertens and V. Grewe. Finally, I introduce a new method to determine the contributions of source categories to CH_4 concentration in sect. 4.5.

4.1. General tagging method

Pollutants such as species from road traffic emissions can be transported over long distances and thus be distributed far away from their emission source. Consequently, they influence air quality and human health not only on local scale but also on global scale. Under these circumstances, it is crucial to attribute pollutants to different regions and emission sources. Therefore, the concept of "tagging" is very helpful. Imaginary "tags" are added to certain species and their transport and chemical reaction pathways are tracked.

The quantification of source attributions has been the goal of many studies. The principle of tagging is applied to attribute CO to different emission types and regions (e.g. Granier et al., 1999; Pfister et al., 2004, 2011), to attribute the transport of air

masses to various regions (Lawrence et al., 2003), to attribute NO_x concentrations to different emission sources (Horowitz and Jacob, 1999), to trace stable isotopic compositions (Gromov et al., 2010) or to trace aerosol particles (Wang et al., 2009). For the attribution of tropospheric O_3 to emission sources, several tagging methods are applied. Tropospheric O_3 can be traced back only to NO_x sources (Lelieveld and Dentener, 2000; Grewe, 2004; Grewe et al., 2012; Emmons et al., 2012) or only to VOC sources (Butler et al., 2011; Coates and Butler, 2015). Dunker et al. (2002) determine whether O_3 is produced in the NO_x- or VOC- sensitive regime. Furthermore, Grewe et al. (2017) purpose a tagging scheme which considers NO_x, CO and VOC emissions simultaneously.

Another common approach to determine the impact of an emission change to O_3 is the perturbation method. It compares two simulations with different emission strengths. Typically, one simulation contains all emissions and the second simulation contains a reduction of an emission sector (e.g. road traffic). If the underlying processes are linear, the perturbation and tagging methods produce the same result (Grewe et al., 2010; Clappier et al., 2017). However, the O_3 chemistry is very non-linear (see sect. 2.2.1) and so the perturbation and tagging method differ strongly. In general, the perturbation method underestimates the emission effect on O_3 by a factor 2 to 5 (Grewe et al., 2012; Emmons et al., 2012; Mertens et al., 2018). The perturbation method gives the *impact* of an emission change on a certain trace gas (Wu et al., 2009; Grewe et al., 2012). In contrast, the tagging method gives the *contribution* of an emission to a certain trace gas (Grewe et al., 2017).

In this thesis, the tagging method introduced by Grewe et al. (2010); Grewe (2013); Tsati (2014) and Grewe et al. (2017) is used and will be briefly explained in the following. As an example, a bimolecular reaction of the chemical species A and B forming the species C is considered:

$$A + B \longrightarrow C \tag{4.1}$$

Consequently, each species A, B and C is split up into N subspecies A^i, B^i and C^i (with N being the number of source categories). Thus, A^i describes the contribution of the source category i to the concentration of A (the same holds for B^i and C^i). This implies that the budget of the sum over all contributions and the total concentration is closed:

$$A = \sum_{i=1}^{N} A^i, \qquad B = \sum_{i=1}^{N} B^i, \qquad C = \sum_{i=1}^{N} C^i \tag{4.2}$$

These tagged species (A^i, B^i, C^i) go through the same reactions as their main species (A, B, C). In general, if A from the category i reacts with B from category j, the formed C is counted half to the category i and half to the category j:

$$A^i + B^j \longrightarrow \frac{1}{2}C^i + \frac{1}{2}C^j \tag{4.3}$$

Considering the C^i production, following reactions can occur: (1) A^i and B^i originates from the same category i, then the formed C is fully attributed to the category

i. (2) A^i reacts with B^j from one of the $N-1$ remaining categories ($\forall j,\ j \neq i$). Then, half of C is attributed to the category i. (3) B^i reacts with A^j from one of the $N-1$ remaining categories ($\forall j,\ j \neq i$) forming half of C^i. Regarding all possible combinations, the production of C^i is determined as follows:

$$\begin{aligned} ProdC^i &= k\left(A^iB^i + \sum_{j=1,j\neq i}^{N}\frac{1}{2}A^iB^j + \sum_{j=1,j\neq i}^{N}\frac{1}{2}A^jB^i\right) \\ &= k\left(A^iB^i + \frac{1}{2}A^i\left(B-B^i\right) + \frac{1}{2}\left(A-A^i\right)B^i\right) \\ &= \frac{1}{2}kAB\left(\frac{A^i}{A} + \frac{B^i}{B}\right) \end{aligned} \tag{4.4}$$

with k being the reaction rate coefficient of reaction 4.1. Consequently, this combinatorial approach enables a full partitioning of the reaction rate.

4.2. Implementation in EMAC

In the realisation of the tagging method used in this work, seven chemical species are tagged: ozone (O_3), carbon monooxide (CO), reactive nitrogen compounds (NO_y = NO, NO_2, HNO_4,...), non-methane hydrocarbons (NMHC), peroxyacyl nitrates (PAN), hydroxyl (OH) and hydroperoxyl (HO_2) (presented in Grewe et al. (2017)). For these chemical species, the contributions of ten source categories are determined. The ten categories are indicated in table 4.1. Consequently, O_3 is divided into O_3 from road traffic O_3^{tra}, from ships O_3^{shp}, from air traffic O_3^{air}, from anthropogenic

Category	Description	Origin
tra	road traffic emissions	anthropogenic
shp	ship emissions	anthropogenic
air	air traffic emissions	anthropogenic
ind	anthropogenic non-traffic (industry): all anthropogenic emissions without traffic and agricultural waste burning	anthropogenic
lig	NO_x emissions from lightnings	natural
bio	biogenic emissions: isoprene and soil-NO_x emissions (online), biogenic emissions and agricultural waste burnging (online)	natural
bb	emissions from biomass burning	anthropogenic, natural
CH_4	decomposition of CH_4	natural
N_2O	decomposition of N_2O	natural
str	stratospheric O_3 production	natural

Table 4.1: Overview of the ten categories for the tagging method implemented in EMAC.

non-traffic emissions O_3^{ind}, from lightnings O_3^{lig}, from biogenic emissions O_3^{bio}, from biomass burning O_3^{bb}, from CH_4 decomposition $O_3^{CH_4}$, from N_2O decomposition $O_3^{N_2O}$ and from stratospheric ozone production O_3^{str}.

Two different implementations are chosen for long-lived tracers (such as O_3, NO_y, NMHC and PAN) and short-lived tracers (such as OH and HO_2). These two methods are presented in the following sections.

4.3. Tagging method for long-lived species

Road traffic emissions impact the distributions of NO_y, CO and NMHC. Through chemical processes as described in sect. 2.2.1, the global distributions of O_3 and PAN are also influenced. In general, road traffic emissions increase the concentration of all these species. However, to determine the contribution of road traffic emissions to O_3, NO_y, CO, NMHC and PAN, the tagging method for long-lived[1] species is applied.

The tagging method is briefly explained in this section. Further details are found in Tsati (2014) and Grewe et al. (2017). Each of the five chemical species or families are divided into ten tagged species for ten source categories (see table 4.1). Accordingly to the main species, each tagged species is transported, receives the respective online and offline emissions, is removed by wet and dry deposition and reacts with the same chemical species as the main species.

		reaction	**rate**
1	O_3 production	$NO_y + HO_2$	R_1
2	O_3 production	$NO_y + NMHC$	R_2
3	O_3 loss	$O_3 + OH$	R_3
4	O_3 loss	$O_3 + HO_2$	R_4
5	O_3 loss	$O_3 + NO_y$	R_5
6	O_3 loss	$O_3 + NMHC$	R_6
7	O_3 loss	$O_3 + X$	R_7

Table 4.2: Overview of reaction channels of the tagging method for O_3 as implemented in EMAC. All reactions of the O_3 chemistry are summarised in two production and five loss reactions. X indicates all chemical species which are not tagged.

Exemplary, the tagging of long-lived species is explained for O_3. In fact, all chemical species which are frequently produced by O_3 and in turn frequently react back to O_3 are regarded as an "O_3 storage" (Crutzen and Schmailzl, 1983). Hence, they are treated as one chemical family "ozone" in the tagging scheme. Table 4.2 shows the seven main reaction channels of O_3. Based on table 4.2, the O_3 production $ProdO_3^i$ and loss $LossO_3^i$ are determined according to the tagging theory described

[1] To simplify the notation, the chemical species O_3, NO_y, CO, NMHC and PAN are called long-lived species because their lifetime is considerably longer than the lifetime of OH and HO_2.

in the sect. 4.1 (compare to eqs. (13) and (14) in Grewe et al. (2017)):

$$ProdO_3^i = \frac{1}{2} R_1 \left(\frac{NO_y^i}{NO_y} + \frac{HO_2^i}{HO_2} \right) + \frac{1}{2} R_2 \left(\frac{NOy^i}{NO_y} + \frac{NMHC^i}{NMHC} \right) \tag{4.5}$$

$$\begin{aligned} LossO_3^i = & \frac{1}{2} R_3 \left(\frac{OH^i}{OH} + \frac{O_3^i}{O_3} \right) + \frac{1}{2} R_4 \left(\frac{HO_2^i}{HO_2} + \frac{O_3^i}{O_3} \right) + \frac{1}{2} R_5 \left(\frac{NO_y^i}{NO_y} + \frac{O_3^i}{O_3} \right) \\ & + \frac{1}{2} R_6 \left(\frac{NMHC^i}{NMHC} + \frac{O_3^i}{O_3} \right) + R_7 \frac{O_3^i}{O_3} \end{aligned} \tag{4.6}$$

The tagged O_3 is determined by an ordinary differential equation:

$$\frac{d}{dt} O_3^i = ProdO_3^i - LossO_3^i \tag{4.7}$$

This approach enables a closed budget, i.e. the sum over all emission contributions equals the total concentration (Grewe et al., 2010). Consequently, the O_3 concentration is fully split up into the ten source categories (table 4.1):

$$O_3 = \sum_{i=1}^{N} O_3^i \tag{4.8}$$

The species CO, NO_y, NMHC and PAN are tagged in a similar way. CH_4 is not explicitly tagged. However, the oxidation products of CH_4 are accounted to NMHC. N_2O is not tagged either, but the decomposition products of N_2O contribute to NO_y^{str}. This tagging method enables to tag long-lived species which are in particular important for the production and destruction of tropospheric O_3. It is applied to EMAC simulations performed in this work (sect. 3.3).

4.4. Tagging method for short-lived species

As described in section 2.2.2, the hydroxyl radical (OH) is crucial for the atmospheric chemistry. It decomposes the greenhouse gases CH_4 and O_3 which affects Earth's climate. Road traffic emissions generally increase OH concentrations, in particular in the lower troposphere. Thus, to fully determine the road traffic emissions effect on the climate, it is essential to quantify the contribution of road traffic emissions to OH. The attribution of OH to road traffic emissions is carried out by the tagging method for short-lived species.

The tagging of short-lived and long-lived species bases on the same principles (sect. 4.1). However, due to their different lifetimes, the implementation of tagging for short-lived species such as OH and HO_2 deviates from the tagging for long-lived species. HO_x[1] is neither transported nor emitted nor deposited. Thus, the

[1] In many reactions OH is transformed to HO_2 and vice verca. Thus, OH and HO_2 are referred together as HO_x.

implementation of the tagging approach for long-lived species as describes in section 4.3 does not apply. Tsati (2014) and Grewe et al. (2017) introduce an alternative: the production and destruction of HO_x is assumed to be in steady-state.

However, the HO_x tagging mechanism V1.0, described by Tsati (2014) and Grewe et al. (2017), had certain shortcomings: First, the main HO_2 source by the reaction $H + O_2 \longrightarrow HO_2$ was only partly taken into account. Second, certain reactions of the HO_x chemistry which are in particular important in the stratosphere were not considered. Third, the sum of all contributions did not equal the total concentration.

I further developed the HO_x tagging method and corrected these shortcomings. In the recent HO_x tagging method V1.1, I increased the number of reactions from 12 to 30. Many new reactions are now considered which are important in the troposphere and stratosphere. To fully account for the main HO_2 source by the reaction of H and O_2, I introduced the tagging of the hydrogen radical H. The closure of the sum of all contributions and the total concentrations is achieved by adding rest terms to the tagging mechanisms. Part of this chapter is published in the Journal *Geoscientific Model Development* as the paper "Further development of the TAGGING 1.1 submodel based on the Modular Earth Submodel System (MESSy 2.53): An enhanced method of contributing emissions to short-lived chemical species (OH and HO_2)" by V.S. Rieger, M. Mertens and V. Grewe.

The results obtained in this section are also received by an EMAC simulation described in sect. 3.3. However, the NO_x emissions from lighting are scaled to 4 Tg(N) per year. This enables a better comparison the results of the former HO_x tagging scheme V1.0 presented in Grewe et al. (2017).

The tagging method for short-lived species presented in the following is also implemented in the EMAC setup (sect. 4.5) which is used to execute the simulations for TransClim.

4.4.1. The former HO_x tagging method V1.0

The tagging method V1.0 described by Grewe et al. (2017) determines the contribution of source categories to O_3, NO_y, CO, NMHC, PAN, OH and HO_2 concentrations. Ten source categories are considered and every species included in the tagging method is decomposed into these categories (see table 4.1). These tagged species go through the same chemical reactions and the same deposition loss processes as O_3. The tagging method uses a combinatoric approach to determine the contributions: It redistributes the production and loss rates of each species to the ten source categories according to the concentrations of the tagged species. Details on the tagging theory and implementation in EMAC are found in Grewe (2013) and Grewe et al. (2017), respectively.

For the first time, V1.0 determined the contribution of source categories to OH and HO_2 concentrations. The tagging method V1.0 was based on 12 reactions for the HO_x chemistry (reactions marked with "o" in last column of table 4.3). It included the main production and loss reactions of HO_x with O_3, NO_y, NMHC, CO and CH_4. V1.0 only regarded reactions which are important in the troposphere. Reactions which mainly occur in the stratosphere were not taken into account. However, the main HO_2 production by the reaction (1) $H + O_2 \longrightarrow HO_2$ (see table 4.3) was not

regarded. It was combined with reaction (11) CO + OH $\longrightarrow$ H + CO_2 (see table 4.3) to

$$\begin{aligned} CO + OH &\longrightarrow CO_2 + H \\ &\xrightarrow{O_2} CO_2 + HO_2 \\ \Longrightarrow CO + OH &\xrightarrow{O_2} CO_2 + HO_2 \end{aligned}$$

But not all H radicals in the troposphere are produced by the reaction of CO + OH. Also the reactions (7) OH + O(^{3}P), (10) H_2 + OH and (28) HCHO + $h\nu$ produce H (table 4.4). These reactions were neglected in V1.0. Thus, only 80 % of the H production and therefore only 80 % of the HO_2 production by reaction (1) was considered in the troposphere. In the stratosphere, the reaction of CO + OH becomes less important and most of H is produced by reactions (7) and (28). Consequently, only 6 % of H and also of HO_2 production by reaction (1) was regarded by this approach. (Numbers are derived from the EMAC simulation described in sect. 3.3.)

In the troposphere, the most important reactions not covered in V1.0 are reaction (1) H + O_2 as well as reaction (15) NO_2 + HO_2 and (18) decomposition of HNO_4. In the stratosphere, reactions (1) H + O_2, (5) HO_2 + O(^{3}P) and (7) OH + O(^{3}P) play a leading role and were not included in V1.0.

Most reaction rates used in the tagging method corresponds to the production and loss rates directly provided by the chemical scheme MECCA of EMAC. However for reactions with NMHC, the reaction rates were obtained indirectly. The reaction rate of OH with NMHC (reaction 21, table 4.3) was determined via the production rates of CO by assuming that each reaction of OH with NMHC produces one CO molecule. This method neglects all intermediate oxidation reactions of NMHC and considers only these reactions when NMHC is finally oxidised to CO. For the reaction rates of NO_y and HO_2 with NMHC (reaction 22 and 23), only the reaction of HO_2 with methylperoxy radical (CH_3O_2) was considered.

To derive the contributions to OH and HO_2, steady-state between HO_x production and loss was assumed. However, the steady-state assumption was not completely fulfilled for V1.0 (see Sect. 4.4.4). Moreover, the sum over the contributions of the ten source categories to the OH and HO_2 concentrations did not equal the total OH and HO_2 concentrations. It deviated by about 70 %.

4.4.2. Reduced HO_x reaction system in V1.1

OH and HO_2 react with many chemical species. To minimize the calculation time of a simulation, the HO_x chemistry used in chemical scheme MECCA is reduced to the most important reactions which occur in the troposphere and stratosphere. Only reactions with a tropospheric or stratospheric annual mean reaction rate larger than 10^{-15} mol mol^{-1} s^{-1} are considered (see table 4.3). Hence, the number of reactions is increased from 12 (V1.0) to 27 (V1.1), which still constitutes a reduced set of reactions compared to the full chemical scheme used in EMAC. In the following, this set is called *reduced HO_x reaction system V1.1.*

	reaction			rates	tro	str	V1.1
1	$H + O_2$	$\longrightarrow$	HO_2	R_1	x	x	(x)
2	$H_2O + O(^1D)$	$\longrightarrow$	$2\ OH$	R_2	x	x	o
3	$HO_2 + HO_2$	$\longrightarrow$	$H_2O_2 + O_2$	R_3	x		o
4	$HO_2 + O_3$	$\longrightarrow$	$OH + 2\ O_2$	R_4	x	x	o
5	$HO_2 + O(^3P)$	$\longrightarrow$	$OH + O_2$	R_5		x	x
6	$OH + O_3$	$\longrightarrow$	$HO_2 + O_2$	R_6	x	x	o
7	$OH + O(^3P)$	$\longrightarrow$	$H + O_2$	R_7		x	x
8	$HO_2 + OH$	$\longrightarrow$	$H_2O + O_2$	R_8	x	x	o
9	$H_2O_2 + OH$	$\longrightarrow$	$H_2O + HO_2$	R_9	x		x
10	$H_2 + OH$	$\longrightarrow$	$H_2O + H$	R_{10}	x		x
11	$CO + OH$	$\longrightarrow$	$H + CO_2$	R_{11}	x	x	o
12	$CH_4 + OH$	$\longrightarrow$	$CH_3 + H_2O$	R_{12}	x	x	o
13	$ClO + OH$	$\longrightarrow$	$0.94\ Cl + 0.94\ HO_2$	R_{13}		x	x
		$\longrightarrow$	$+ 0.06\ HCl + 0.06\ O_2$				
14	$NO + HO_2$	$\longrightarrow$	$NO_2 + OH$	R_{14}	x	x	o
15	$NO_2 + HO_2$	$\longrightarrow$	HNO_4	R_{15}	x	x	x
16	$NO + OH$	$\longrightarrow$	$HONO$	R_{16}		x	x
17	$NO_2 + OH$	$\longrightarrow$	HNO_3	R_{17}		x	o
18	HNO_4	$\longrightarrow$	$NO_2 + HO_2$	R_{18}	x		x
19	$HONO + h\nu$	$\longrightarrow$	$NO + OH$	R_{19}		x	x
20	$HNO_3 + h\nu$	$\longrightarrow$	$NO_2 + OH$	R_{20}		x	x
21	$NMHC + OH$	$\longrightarrow$	$NMHC$	R_{21}	x		o
22	$NMHC + HO_2$	$\longrightarrow$	$NMHC$	R_{22}	x		o
23	$NMHC + NO_y$	$\longrightarrow$	$HO_2 + NMHC + NO_y$	R_{23}	x	x	o
24	$NMHC + OH$	$\longrightarrow$	$NMHC + HO_2$	R_{24}	x		x
25	$NMHC + h\nu$	$\longrightarrow$	$NMHC + HO_2$	R_{25}	x		x
26	$ClO + HO_2$	$\longrightarrow$	$HOCl + O_2$	R_{26}		x	x
27	$BrO + HO_2$	$\longrightarrow$	$HOBr + O_2$	R_{27}		x	x

Table 4.3: Reduced HO_x reaction system V1.1 describes the main reactions of HO_x chemistry in troposphere and stratosphere. These 27 reactions are used for the tagging method V1.1. In the column "tro" ("str"), reactions which are important in the troposphere (stratosphere) are marked. In the column "V1.1", reactions marked with "o" were already included in V1.0. Reactions marked with "x" are added in V1.1. Reactions marked with "(x)" were only partly taken into account in V1.0. The numbers of reactions are referenced in the text.

The reactions which are important in the troposphere are indicated in table 4.3. As stated above, reaction (1) of H and O_2 dominates the HO_2 production in the troposphere. It produces 49 % of tropospheric HO_2. In V1.0, only part of this HO_2 source was regarded (see sect. 4.4.1). The most important HO_2 loss is the reaction with NO (reaction 14) followed by the reaction with itself producing H_2O_2 (reaction 3) which accounts for 32 % and 12 % of tropospheric HO_2 loss. The production via H_2O and $O(^1D)$ produces about 21 % of tropospheric OH (reaction 2). The excited oxygen radical ($O(^1D)$) originates from the photolysis of O_3. Also reaction (14) of NO and HO_2 produces 32 % of tropospheric OH. OH is mostly destroyed by CO (reaction 11, 38 %) followed by the destruction by NMHC (reaction 21, 25 %).

In the stratosphere different chemical reactions become important. Here, OH is mainly destroyed by O_3, producing 40 % of stratospheric HO_2. The reaction is partly counteracted by the reaction (14) which produces 21 % of OH and destroys 24 % of HO_2. Since large quantities of O_3 are found in the stratosphere, O_3 or the excited oxygen radical ($O(^3P)$) destroys about 62 % of HO_2. Reactions with NMHC, CO and CH_4 play only a minor role in the stratosphere.

Reactions of OH and HO_2 with chlorine and bromide were not considered in V1.0. These reactions, which take place only in the stratosphere, are added to the tagging method V1.1. Reactions (21) to (25) involve the chemical family NMHC which contains several species such as formaldehyde (HCHO), ethylene (C_2H_4) and propane (C_3H_8). For example, the rate for reaction (21) is determined by adding up the rates of all reactions of OH with each single species of the family NMHC. Reaction rate (23) contains all rates of the reactions between the species of the chemical families NO_y and NMHC. All reaction rates are directly derived by MECCA mechanism of EMAC.

Table 4.3 does not consider all reactions with annual reaction rates larger than 10^{-15} mol mol^{-1} s^{-1}. The photolysis of hydrogen peroxide (H_2O_2), hypochlorous acid (HOCl) and hypobromous acid (HOBr) are excluded from the reduced HO_x reaction system V1.1 as the tagging method can not be applied. The specific reasons are explained in appendix A.3.2.

4.4.3. Deductions of tagged species

To derive how much OH and HO_2 is produced and destroyed by a source category i, the tagging approach described in Grewe et al. (2010, 2017) is used. In general, bimolecular reactions with two chemical species A + B $\longrightarrow$ C are tagged as follows: the production P and loss L of a species from the category i (here $LossA^i$, $LossB^i$ and $ProdC^i$) is determined after equation 4.4

$$LossA^i = LossB^i = ProdC^i = \frac{1}{2} R \left(\frac{A^i}{A} + \frac{B^i}{B} \right) \tag{4.9}$$

with k being the reaction rate coefficient and $R = kAB$ being the respective reaction rate. For unimolecular reactions A $\longrightarrow$ B + C, the distribution of categories from the educts is completely passed to the products:

$$LossA^i = LossB^i = ProdC^i = R\frac{A^i}{A} \tag{4.10}$$

	reaction			rates	tro	str
1	$H + O_2$	$\longrightarrow$	HO_2	R_1	x	x
7	$OH + O(^3P)$	$\longrightarrow$	$H + O_2$	R_7		x
10	$H_2 + OH$	$\longrightarrow$	$H_2O + H$	R_{10}	x	
11	$CO + OH$	$\longrightarrow$	$H + CO_2$	R_{11}	x	x
28	$HCHO + O_2 + hv$	$\longrightarrow$	$H + CO + HO_2$	R_{28}	x	

Table 4.4: Reduced H reaction system describes the main reactions of H. In the column "tro" ("str"), reactions which are important in the troposphere (stratosphere) are marked. The numbers of the reactions correspond to the numbers in table 4.3.

As described above, the long-lived species O_3, CO, NO_y and NMHC are tagged according to tagging method described in Grewe et al. (2017). Due to limited computational resources, other species such as H, H_2, H_2O_2, CH_4, ClO and BrO are not tagged (as in V1.0). Here, different approaches are derived to retain the ratio of contribution to total concentration $\frac{A^i}{A}$:

1. If a tagged species reacts with a non-tagged species, the non-tagged species does not contribute and the tagging method for a unimolecular reaction is applied (see reaction 4.10). Examples are reactions (9), (10) and (14).

2. Using the family concept as described in Grewe et al. (2017) allows the assumption that all tags are distributed equally among the species in the same chemical family. It follows:

$$\frac{NO^i}{NO} = \frac{NO_2^i}{NO_2} = \frac{HNO_4^i}{HNO_4} = \frac{NO_y^i}{NO_y} \tag{4.11}$$

   As mentioned in Grewe et al. (2017), all species which are frequently converted back and forth to ozone are considered as an "ozone storage" (Crutzen and Schmailzl, 1983). These species together with O_3 are lumped into one chemical family "ozone". Both $O(^1D)$ and $O(^3P)$ belong to this chemical family. Hence, as in Grewe et al. (2017), the family concept is applied which sets:

$$\frac{O(^1D)^i}{O(^1D)} = \frac{O(^3P)^i}{O(^3P)} = \frac{O_3^i}{O_3} \tag{4.12}$$

3. In reaction (1), neither H nor O_2 are tagged. To obtain the ratio $\frac{HO_2^i}{HO_2}$, an extra tagging of H itself is set up. The H radical is very reactive, so H production balances H loss. Table 4.4 presents the main reactions for H which still constitute a subset of full H chemistry implemented in MECCA. Based on table 4.4, H production $ProdH^i$ and H loss $LossH^i$ for the contribution of

a source category i is:

$$\begin{aligned} ProdH^i =& \frac{1}{2} R_7 \left(\frac{OH^i}{OH} + \frac{O_3^i}{O_3} \right) + R_{10} \frac{OH^i}{OH} \\ &+ \frac{1}{2} R_{11} \left(\frac{CO^i}{CO} + \frac{OH^i}{OH} \right) + R_{28} \frac{NMHC^i}{NMHC} \end{aligned} \tag{4.13}$$

$$LossH^i = R_1 \frac{H^i}{H} \tag{4.14}$$

As mentioned above, the family concept also sets $\frac{HCHO^i}{HCHO} = \frac{NMHC^i}{NMHC}$. Since the steady-state assumption applies for H (see sect. 4.4.4), the H production per source category i $ProdH^i$ equals the loss $LossH^i$. After setting eq. (4.13) and (4.14) equal to each other, the following equation is deduced:

$$\begin{aligned} \frac{H^i}{H} =& \frac{1}{2} \frac{R_7}{R_1} \left(\frac{OH^i}{OH} + \frac{O_3^i}{O_3} \right) + \frac{R_{10}}{R_1} \frac{OH^i}{OH} \\ &+ \frac{1}{2} \frac{R_{11}}{R_1} \left(\frac{CO^i}{CO} + \frac{OH^i}{OH} \right) + \frac{R_{28}}{R_1} \frac{NMHC^i}{NMHC} \end{aligned} \tag{4.15}$$

These different approaches are applied to the reduced HO_x reaction system V1.1 (table 4.3) to derive the contributions of source categories to OH and HO_2 in sect. 4.4.5.

4.4.4. Steady-state assumption

The steady-state assumption of the HO_x chemistry is the basic principle of the tagging method for short-lived species introduced by Tsati (2014) and Grewe et al. (2017). In steady-state, the production and loss of OH and HO_2 balance each other. Table 4.5 shows annual means of HO_x and H production and loss rates of the reduced reaction system for the tagging methods V1.0 and V1.1 as well as the total production and loss rates derived from the complete chemical scheme MECCA in EMAC. The production and loss rates are obtained from an EMAC simulation following the setup described in sect. 3.3. Note that for V1.0 no values for the H production and loss are available since the tagging of H was not considered in V1.0.

In general, total OH production (derived by MECCA) equals total OH loss in the troposphere and stratosphere. The same holds for HO_2 and H. In the troposphere, the annual mean of the total OH production and loss rates are $0.49 \cdot 10^{-13}$ mol mol^{-1} s^{-1} (table 4.5). The OH loss of V1.1 and V1.0 represents well the total OH loss in the troposphere. However, the OH production for V1.1 and V1.0 differs by 12 % from the total OH production. Considering HO_2 in the troposphere, the total production and loss rates are well reflected by the reduced HO_x reaction system V1.1. In contrast, the HO_2 production and loss of V1.0 differs by 14 % and 41 % from the total rates.

In the stratosphere, the total OH and HO_2 production equals the total loss. V1.1 represents the total rates in the stratosphere very well. However, the OH production

		OH		HO_2		H	
		prod.	loss	prod.	loss	prod.	loss
total - MECCA	tro	0.49	0.49	0.49	0.49	0.24	0.24
	str	*2.78*	*2.78*	*2.48*	*2.48*	*7.09*	*7.09*
reduced - V1.1	tro	0.43	0.48	0.47	0.49	0.24	0.24
	str	*2.49*	*2.76*	*2.47*	*2.48*	*7.06*	*5.99*
reduced - V1.0	tro	0.43	0.47	0.29	0.42	-	-
	str	*0.86*	*1.30*	*1.19*	*0.84*	-	-

Table 4.5: Annual mean of OH, HO_2 and H production and loss rates (air mass weighted) in 10^{-13} mol mol^{-1} s^{-1} for the total rates (derived from the complete chemical scheme MECCA in EMAC) and for the rates of the reduced reaction system of the tagging method V1.0 and V1.1. The first row gives the rates for the troposphere, the second row for the stratosphere (written in italic).

of V1.1 misses 10 % of the total OH production. Since V1.0 was only developed for the troposphere, not all reactions which are important in the stratosphere were considered. Thus, the OH and HO_2 production and loss rates of V1.0 considerably underestimated the total production and loss rates.

The reduced H reaction system in V1.1 (table 4.4) represents the total H production and loss in the troposphere very well. However in the stratosphere, H loss in V1.1 deviates by 17 % from the total H loss.

Summing up, the reduced HO_x reaction system V1.1 represents well the total HO_x production and loss in the troposphere and stratosphere. V1.1 reproduces the HO_x chemistry better than V1.0. However, OH production in troposphere and stratosphere as well as H loss in the stratosphere of V1.1 deviates from the total rates derived by MECCA. Thus, the steady-state for the reduced HO_x and H reaction system (tables 4.3 and 4.4) is not completely fulfilled.

But steady-state between production and loss is crucial for the tagging method for short-lived species. To re-establish the steady-state assumption, it would be necessary to include the complete HO_x and H chemistry in the tagging method. However, this is not possible as the tagging method does not apply to all reactions of the HO_x and H chemistry (for examples see appendix A.3.2). Consequently, rest terms *resOH*, *resHO*$_2$ and *resH* for OH, HO_2 and H are introduced to compensate for the deviations from steady-state. Each rest term is calculated by subtracting the production rates of the reduced reaction system (tables 4.3 and 4.4) from the loss rates:

$$\begin{aligned} resOH &= R_6 + R_7 + R_8 + R_9 + R_{10} + R_{11} + R_{12} + R_{13} + R_{16} + R_{17} + R_{21} + R_{25} \\ &\quad - (2 \cdot R_2 + R_4 + R_5 + R_{14} + R_{19} + R_{20}) \\ resHO_2 &= 2 \cdot R_3 + R_4 + R_5 + R_8 + R_{14} + R_{15} + R_{22} + R_{26} + R_{27} \\ &\quad - (R_1 + R_6 + R_9 + 0.94 \cdot R_{13} + R_{18} + R_{23} + R_{24} + R_{25}) \\ resH &= R_1 - (R_7 + R_{10} + R_{11} + R_{28}) \end{aligned}$$

Finally, the rest terms are equally distributed over the categories as is it unknown by which source the missing HO_x is produced or destroyed. Therefore, they are divided by the number of source categories n. The resulting rest terms are shown in the appendix A.3.3.

Considering the rest terms *resOH*, *resHO*$_2$ and *resH* leads to the closure of the budget. In V1.0, the sum over the contributions from all source categories did not balance the total concentration. The averaged deviations for OH and HO_2 in troposphere were about 70 % of the total concentrations. Since the stratosphere was not considered in V1.0, the deviations were even larger (104 % for OH and 89 % for HO_2). In V1.1, the sum of OH and HO_2 now perfectly balances the total OH and HO_2 concentrations. The deviations are negligible (below 10^{-4} % for OH and below 10^{-3} % for HO_2). Consequently, including the rest terms to the tagging method is mandatory for the steady-state assumption and also closes the budget.

4.4.5. Determination of HO_x contributions

Taking the above considerations into account, the OH and HO_2 production and loss terms per source category i are finally derived. In the reduced HO_x reaction system V1.1 (table 4.3), OH is produced by the reactions (2) $H_2O + O(^1D)$, (4) $HO_2 + O_3$, (5) $HO_2 + O(^3P)$, (14) $NO + HO_2$, (19) HONO + $h\nu$ and (20) $HNO_3 + h\nu$. Applying the partitioning described in sect. 4.4.3, the OH production for a source category i $ProdOH^i$ is determined as follows:

$$\begin{aligned} ProdOH^i =& 2 \cdot R_2 \frac{O_3^i}{O_3} + \frac{1}{2} R_4 \left(\frac{HO_2^i}{HO_2} + \frac{O_3^i}{O_3} \right) + \frac{1}{2} R_5 \left(\frac{HO_2^i}{HO_2} + \frac{O_3^i}{O_3} \right) \\ &+ \frac{1}{2} R_{14} \left(\frac{NO_y^i}{NO_y} + \frac{HO_2^i}{HO_2} \right) + R_{19} \frac{NO_y^i}{NO_y} + R_{20} \frac{NO_y^i}{NO_y} \end{aligned} \tag{4.16}$$

OH is destroyed by the reactions (6) OH + O_3, (7) OH + $O(^3P)$, (8) HO_2 + OH, (9) H_2O_2 + OH, (10) H_2 + OH, (11) CO + OH, (12) CH_4 + OH, (13) ClO + OH, (16) NO + OH, (17) NO_2 + OH, (21) NMHC + OH and (24) NMHC + OH. The OH loss per source category i $LossOH^i$ is:

$$\begin{aligned} LossOH^i =& \frac{1}{2} R_6 \left(\frac{OH^i}{OH} + \frac{O_3^i}{O_3} \right) + \frac{1}{2} R_7 \left(\frac{OH^i}{OH} + \frac{O_3^i}{O_3} \right) \\ &+ \frac{1}{2} R_8 \left(\frac{HO_2^i}{HO_2} + \frac{OH^i}{OH} \right) + \frac{1}{2} R_9 \left(\frac{HO_2^i}{HO_2} + \frac{OH^i}{OH} \right) + R_{10} \frac{OH^i}{OH} \\ &+ \frac{1}{2} R_{11} \left(\frac{CO^i}{CO} + \frac{OH^i}{OH} \right) + R_{12} \frac{OH^i}{OH} \\ &+ R_{13} \frac{OH^i}{OH} + \frac{1}{2} R_{16} \left(\frac{NO_y^i}{NO_y} + \frac{OH^i}{OH} \right) + \frac{1}{2} R_{17} \left(\frac{NO_y^i}{NO_y} + \frac{OH^i}{OH} \right) \\ &+ \frac{1}{2} R_{21} \left(\frac{NMHC^i}{NMHC} + \frac{OH^i}{OH} \right) + \frac{1}{2} R_{24} \left(\frac{NMHC^i}{NMHC} + \frac{OH^i}{OH} \right) \end{aligned} \tag{4.17}$$

HO_2 is produced by reactions (1) H + O_2, (6) OH + O_3, (9) H_2O_2 + OH, (13) ClO + OH, (18) HNO_4, (23) NMHC + NO_y, (24) NMHC + OH and (25) NMHC

+ $h\nu$. However, H in reaction (1) is not tagged. To be able to determine the HO_2 production by reaction (1) $R_1 \frac{H^i}{H}$, the introduced H tagging (see sect.4.4.3) is applied and $\frac{H^i}{H}$ is replaced with equation (4.15). Reaction (13) constitutes a simplified reaction producing $0.94 \cdot HO_2$. Consequently, the HO_2 production per source category i $ProdHO2^i$ is determined:

$$\begin{aligned} ProdHO_2^i = &\frac{1}{2}R_6\left(\frac{OH^i}{OH}+\frac{O_3^i}{O_3}\right)+\frac{1}{2}R_7\left(\frac{OH^i}{OH}+\frac{O_3^i}{O_3}\right) \\ &+\frac{1}{2}R_9\left(\frac{HO_2^i}{HO_2}+\frac{OH^i}{OH}\right)+R_{10}\frac{OH^i}{OH}+\frac{1}{2}R_{11}\left(\frac{CO^i}{CO}+\frac{OH^i}{OH}\right) \\ &+0.94\cdot R_{13}\frac{OH^i}{OH}+R_{18}\frac{NO_y^i}{NO_y}+\frac{1}{2}R_{23}\left(\frac{NMHC^i}{NMHC}+\frac{NO_y^i}{NO_y}\right) \\ &+\frac{1}{2}R_{24}\left(\frac{NMHC^i}{NMHC}+\frac{OH^i}{OH}\right)+R_{25}\frac{NMHC^i}{NMHC}+R_{28}\frac{NMHC^i}{NMHC} \end{aligned} \tag{4.18}$$

The HO_2 loss is determined by reactions (3) $HO_2 + HO_2$, (4) $HO_2 + O_3$, (5) $HO_2 + O(^3P)$, (8) $HO_2 + OH$, (14) $NO + HO_2$, (15) $NO_2 + HO_2$, (22) $NMHC + HO_2$, (26) $ClO + HO_2$ and (27) $BrO + HO_2$. Hence, the HO_2 loss per source category i $LossHO2^i$ is:

$$\begin{aligned} LossHO_2^i = &R_3\frac{HO_2^i}{HO_2}+\frac{1}{2}R_4\left(\frac{HO_2^i}{HO_2}+\frac{O_3^i}{O_3}\right)+\frac{1}{2}R_5\left(\frac{HO_2^i}{HO_2}+\frac{O_3^i}{O_3}\right) \\ &+\frac{1}{2}R_8\left(\frac{HO_2^i}{HO_2}+\frac{OH^i}{OH}\right)+\frac{1}{2}R_{14}\left(\frac{NO_y^i}{NO_y}+\frac{HO_2^i}{HO_2}\right) \\ &+\frac{1}{2}R_{15}\left(\frac{NO_y^i}{NO_y}+\frac{HO_2^i}{HO_2}\right)+\frac{1}{2}R_{22}\left(\frac{NMHC^i}{NMHC}+\frac{HO_2^i}{HO_2}\right) \\ &+R_{26}\frac{HO_2^i}{HO_2}+R_{27}\frac{HO_2^i}{HO_2} \end{aligned} \tag{4.19}$$

Sect. 4.4.4 shows that the steady-state assumption for OH and HO_2 is justified when the rest terms $resOH$, $resHO_2$ and $resH$ are regarded. Therefore, the rest terms are divided by the number of source categories n to add them to the contributions of a category i. In a steady-state, production of OH^i and HO_2^i equals the loss:

$$ProdOH^i - LossOH^i + resOH/n = 0 \tag{4.20}$$

$$ProdHO_2^i - LossHO_2^i + resHO_2/n + resH/n = 0 \tag{4.21}$$

The equations (4.20) and (4.21) are rewritten as follows:

$$0 = A^i - L^{OH}\frac{OH^i}{OH} + P^{OH}\frac{HO_2^i}{HO_2} + \frac{resOH}{n} \tag{4.22}$$

$$0 = B^i + P^{HO_2}\frac{OH^i}{OH} - L^{HO_2}\frac{HO_2^i}{HO_2} + \frac{resHO_2}{n} + \frac{resH}{n} \tag{4.23}$$

with the variables P^{OH}, L^{OH}, P^{HO_2}, L^{HO_2}, A^i and B^i (compare to Grewe et al. (2017) equations (25) to (28)):

$$P^{OH} = \frac{1}{2}R_4 + \frac{1}{2}R_5 + \frac{1}{2}R_{14} - \frac{1}{2}R_8 \tag{4.24}$$

$$L^{OH} = \frac{1}{2}R_6 + \frac{1}{2}R_7 + \frac{1}{2}R_8 + R_9 + R_{10} + \frac{1}{2}R_{11} \tag{4.25}$$

$$+ R_{12} + R_{13} + \frac{1}{2}R_{16} + \frac{1}{2}R_{17} + \frac{1}{2}R_{21} + \frac{1}{2}R_{24} \tag{4.26}$$

$$P^{HO_2} = \frac{1}{2}R_6 + \frac{1}{2}R_7 + R_9 + R_{10} + \frac{1}{2}R_{11} + 0.94 \cdot R_{13} + \frac{1}{2}R_{24} - \frac{1}{2}R_8 \tag{4.27}$$

$$L^{HO_2} = 2 \cdot R_3 + \frac{1}{2}R_4 + \frac{1}{2}R_5 + \frac{1}{2}R_8 + \frac{1}{2}R_{14} + \frac{1}{2}R_{15} + \frac{1}{2}R_{22} + R_{26} + R_{27} \tag{4.28}$$

$$\begin{aligned} A^i = {} & 2 \cdot R_2 \frac{O_3^i}{O_3} + \frac{1}{2}R_4 \frac{O_3^i}{O_3} + \frac{1}{2}R_5 \frac{O_3^i}{O_3} + \frac{1}{2}R_{14} \frac{NO_y^i}{NO_y} + R_{19} \frac{NO_y^i}{NO_y} + R_{20} \frac{NO_y^i}{NO_y} \\ & - \frac{1}{2}R_6 \frac{O_3^i}{O_3} - \frac{1}{2}R_7 \frac{O_3^i}{O_3} - \frac{1}{2}R_{11} \frac{CO^i}{CO} - \frac{1}{2}R_{16} \frac{NO_y^i}{NO_y} - \frac{1}{2}R_{17} \frac{NO_y^i}{NO_y} \\ & - \frac{1}{2}R_{21} \frac{NMHC^i}{NMHC} - \frac{1}{2}R_{24} \frac{NMHC^i}{NMHC} \end{aligned} \tag{4.29}$$

$$\begin{aligned} B^i = {} & \frac{1}{2}R_6 \frac{O_3^i}{O_3} + \frac{1}{2}R_7 \frac{O_3^i}{O_3} + \frac{1}{2}R_{11} \frac{CO^i}{CO} + R_{18} \frac{NO_y^i}{NO_y} \\ & + \frac{1}{2}R_{23} \left(\frac{NMHC^i}{NMHC} + \frac{NO_y^i}{NO_y} \right) + \frac{1}{2}R_{24} \frac{NMHC^i}{NMHC} + R_{25} \frac{NMHC^i}{NMHC} \\ & + R_{28} \frac{NMHC^i}{NMHC} - \frac{1}{2}R_4 \frac{O_3^i}{O_3} - \frac{1}{2}R_5 \frac{O_3^i}{O_3} - \frac{1}{2}R_{14} \frac{NO_y^i}{NO_y} \\ & - \frac{1}{2}R_{15} \frac{NO_y^i}{NO_y} - \frac{1}{2}R_{22} \frac{NMHC^i}{NMHC} \end{aligned} \tag{4.30}$$

Solving equations (4.22) and (4.23), the contributions of a source category i to the OH and HO_2 concentration are finally obtained (same equations as equations (29) and (30) in Grewe et al. (2017), but with differently defined coefficients):

$$\frac{OH^i}{OH} = \frac{A^i L^{HO_2} + B^i P^{OH}}{L^{OH} L^{HO_2} - P^{OH} P^{HO_2}} \tag{4.31}$$

$$\frac{HO_2^i}{HO_2} = \frac{A^i P^{HO_2} + B^i L^{OH}}{L^{OH} L^{HO_2} - P^{OH} P^{HO_2}} \tag{4.32}$$

These equations are implemented in the TAGGING submodel and EMAC simulations according to sect. 3.3 are performed. Note that for this EMAC simulation the time period from July 2007 to December 2008 is considered as this period overlaps with time period chosen by Grewe et al. (2017). Furthermore, to be consistent with Grewe et al. (2017), the NO_x emissions from lightning are scaled to 4 Tg(N) per year. The results of the OH and HO_2 contributions for the year 2008 are analysed and compared with V1.0 in the following section.

4.4.6. Results

4.4.6.1. Contribution of short-lived species (HO_x) in the troposphere

Figures 4.1 and 4.2 show the zonal mean of OH and HO_2 contributions up to 200 hPa for the ten source categories derived by V1.1 (first and third columns) and V1.0 (second and forth columns). First, the OH and HO_2 contributions of V1.1 are described in the following. For the categories which are determined by anthropogenic emissions, such as "shipping", "road traffic" and "anthropogenic non-traffic", the maximum values of OH and HO_2 contributions occur in the lower troposphere in the Northern Hemisphere. This clearly shows that for anthropogenic dominated categories the OH and HO_2 contributions are caused by anthropogenic emissions. The contributions vary among these categories of surface emissions as not only the amount but also the composition of the emissions differs. For the category "aviation", maximum OH contribution are found in the Northern Hemisphere between 200 and 250 hPa. However, HO_2 contribution has a minimum in this region and a maximum in the lower troposphere. The OH values for the categories "CH_4 decomposition", "N_2O decomposition", "lightning" and "biogenic emissions" are largest in the upper troposphere. Most OH contributions of "biomass burning" are found in lower tropical troposphere. In contrast, negative values occur in the upper tropical troposphere. Concerning the HO_2 contribution, the residual categories show a maximum in the tropical lower troposphere. In addition, the category "lightning" shows a strong HO_2 loss in the upper tropical troposphere which is caused by reaction (14).

The results obtained by V1.1 are compared to the OH and HO_2 zonal profiles of V1.0 only in the troposphere (figs. 4.1 and 4.2). The HO_x tagging method V1.0 was only developed for the troposphere. Hence, a comparison in the stratosphere is not reasonable. In general, contributions to OH and HO_2 mixing ratios of V1.1 are larger in the troposphere compared to V1.0. This overall shift towards larger values is explained by the re-establishment of the steady-state and thus the closure of the budget in V1.1. In V1.0 the budget was not closed and thus the contributions were underestimated.

For OH, the categories "lightning" and "aviation" show no large changes in the general pattern of the zonal means between V1.0 and V1.1. Considering the HO_2 contributions, no large changes are found for the categories "biomass burning", "anthropogenic non-traffic", "road traffic" and "shipping".

The contribution of the category "aviation" to HO_2 in V1.1 shows roughly the same pattern compared to V1.0. However, the HO_2 destruction along the flight path is not as pronounced any more which is caused by the inclusion of reaction (15) and (18) to V1.1. Reaction (15) adds the term $\frac{1}{2} R_{15} \frac{NO_y^i}{NO_y}$ to the HO_2 loss (eq. 4.4.5) and reaction (18) adds the term $R_{18} \frac{NO_y^i}{NO_y}$ to the HO_2 production (eq. 4.4.5). As reaction rate R_{15} equals the rate R_{18}, this leads to a larger HO_2 production than HO_2 loss $\left(R_{18} \frac{NO_y^i}{NO_y} > \frac{1}{2} R_{15} \frac{NO_y^i}{NO_y} \right)$. Consequently, the addition of reaction (15) and (18) to the reduced HO_x reaction system V1.1 constitutes an extra HO_2 source.

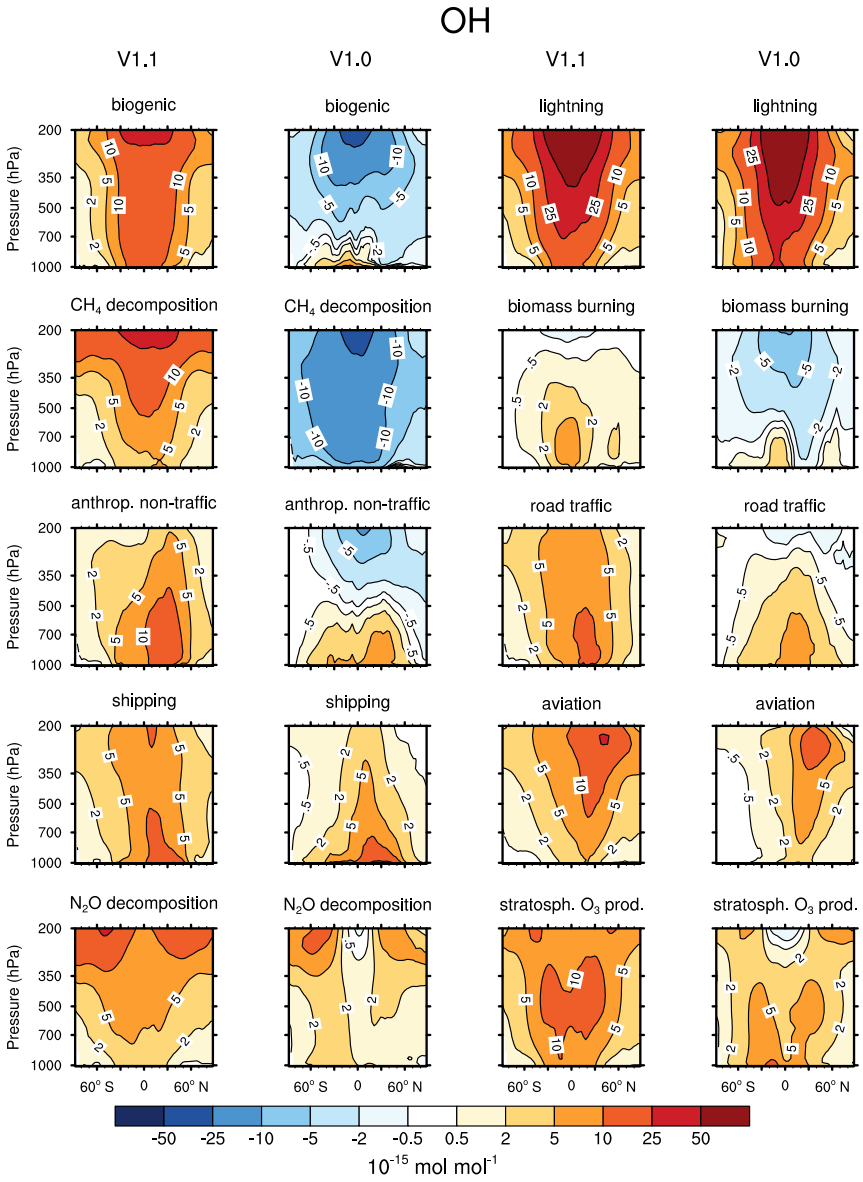

Figure 4.1: Contribution of ten source categories to OH in 10^{-15} mol mol^{-1}. Zonal means of the year 2008 are shown. First and third columns show the tagging method V1.1. Second and forth columns show the tagging method V1.0. Simulation is performed with EMAC.

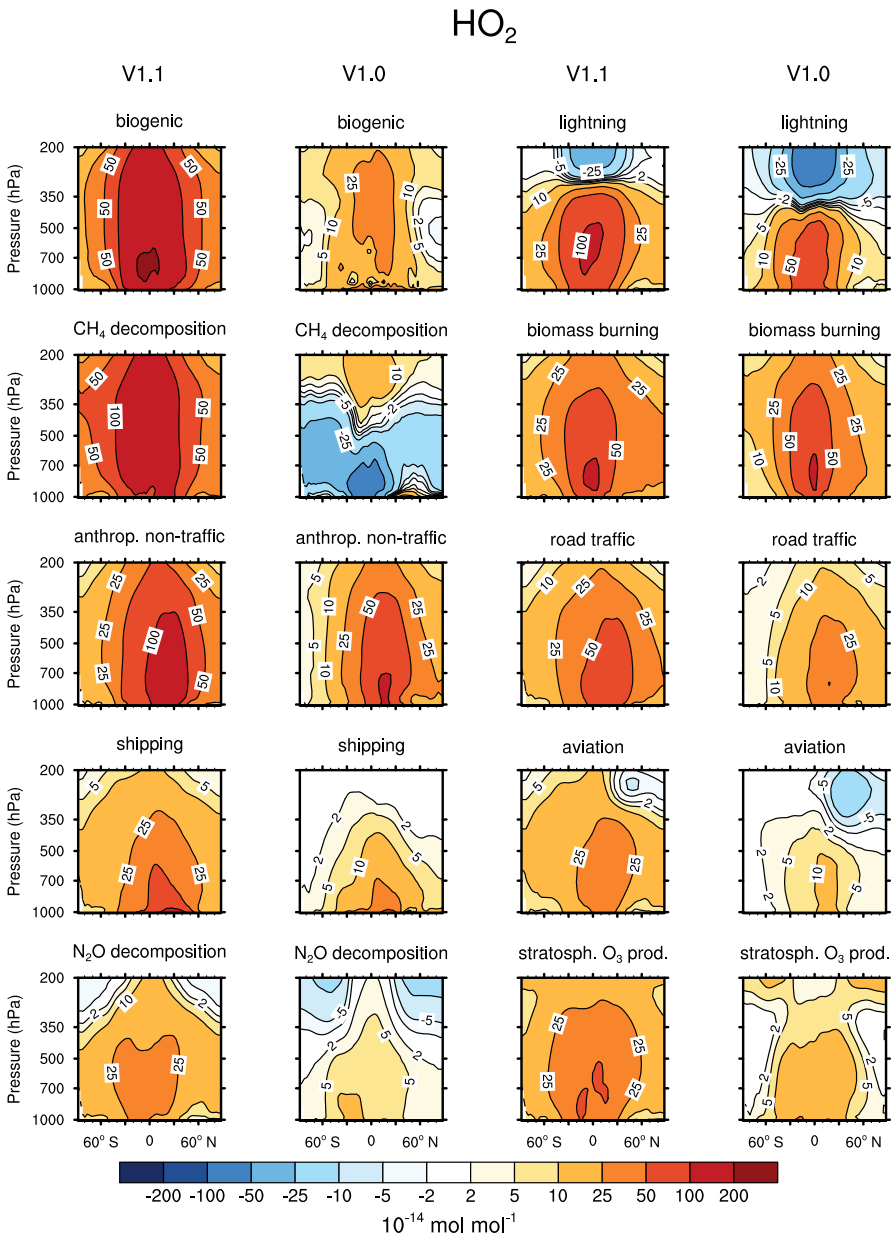

Figure 4.2: Contribution of ten source categories to HO_2 in 10^{-15} mol mol^{-1}. Zonal means of the year 2008 are shown. First and third columns show the tagging method V1.1. Second and forth columns show the tagging method V1.0. Simulation is performed with EMAC.

Larger values of the categories "N_2O decomposition" and "lightning" to HO_2 in the upper troposphere are explained by a larger HO_2 production in V1.1 compared to V1.0. The H tagging in V1.1 considers all relevant HO_2 sources (reaction (7), (10), (11) and (28)) leading to a larger HO_2 production. Also the addition of reactions (15) and (18) (explanation see above) as well as the addition of reaction (23) which considers more reactions than in V1.0 increase the HO_2 contribution of the categories "N_2O decomposition" and "lightning".

Large changes in pattern are observed for the contributions of "biogenic emissions" and "CH_4 decomposition" to OH and HO_2 as well as for the contributions of "biomass burning" and "anthropogenic non-traffic" to OH. In V1.1, these categories mainly constitute a source of OH and HO_2 in the troposphere. The addition of reaction (24) and (25) to the reduced HO_x reaction system V1.1 presents a HO_2 source increasing OH and HO_2 contributions. Furthermore, reactions of NMHC with OH, HO_2 and NO_y (reaction 21, 22 and 23) are important throughout the whole troposphere. In contrast to V1.0, V1.1 considers all reactions of NMHC with OH, HO_2 and NO_y (see sect. 4.4.2) significantly changing the pattern of "biogenic emissions", "CH_4 decomposition", "biomass burning" and "anthropogenic non-traffic".

To summarize, the contributions to OH and HO_2 mixing ratios show generally larger values in V1.1 compared to V1.0. This is explained by the re-establishment of the steady-state which leads to more consistent results than V1.0. For OH, no large changes are found in the categories "lightning" and "aviation". However, large changes are found for "biomass burning", "CH_4 decomposition" and "biogenic emissions". For HO_2, no large differences occur in the categories "biomass burning", "anthropogenic non-traffic", "road traffic" and "shipping". In comparison, the categories "biogenic emissions" and "CH_4 decomposition" differ strongly. The differences between the contributions of V1.1 and V1.0 are traced back to the addition of certain reactions to the reduced reaction system considered in the HO_x tagging method.

4.4.6.2. Contribution of short-lived species (HO_x) in the stratosphere

Figs. 4.3 and 4.4 show the zonal mean of OH and HO_2 from 1 to 200 hPa. Note the logarithmic scale of the contour levels. As OH mixing ratio strongly rises with increasing height, so do the contributions to OH. The category "biomass burning" shows negative OH values in the tropopause region. In this region, also large CO values from "biomass burning" occur. CO effectively destroys OH by reaction (11) which causes the observed OH loss. The large OH loss in the lower stratosphere of the category "stratospheric O_3 production" is mainly caused by the destruction of OH by O_3 (reaction 6).

The contributions to HO_2 in the stratosphere increases with height as well. The categories "biogenic emissions", "lightning", "biomass burning", "anthropogenic non-traffic", "road traffic", "shipping" and "aviation" show a local maximum at around 5 hPa which is caused by omitting the photolysis of HOCl (see appendix A.3.2).

HO_2 loss occurs in tropopause region for the category "lightning" which is induced reaction (14) destroying HO_2. The category "N_2O decomposition" shows negative values in the lower stratosphere and a strong negative minimum at around 10 hPa which is also caused by reaction (14). The local maximum with positive

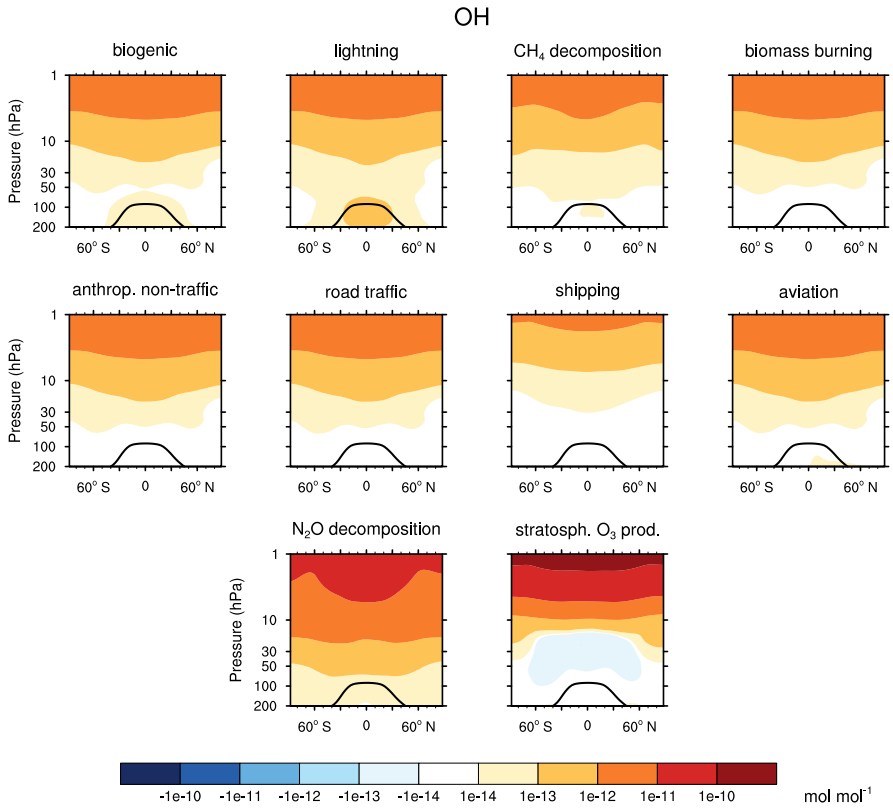

Figure 4.3: Contribution of ten source categories to OH in the stratosphere. Zonal mean of the year 2010 are shown. Black line indicates the tropopause. Simluation is performed with EMAC including tagging method V1.1. Note the logarithmic scale of the contour levels.

HO_2 contributions indicates that in this region the HO_2 production via reaction (1) and (6) dominates the HO_2 loss via reaction (14).

4.4.6.3. Effects on long-lived species

The tagging of short-lived and long-lived species closely intertwine. Changes in the contributions to OH and HO_2 influence the contributions to the long-lived tracers O_3, NO_y, CO, NMHC and PAN. For example, figure 4.5 shows the zonal mean of the contributions of the ten source categories to O_3. Grewe et al. (2017) presents the same figure for the HO_x tagging method V1.0 (their fig. 4). For consistency, the results obtained in this study are compared with the results of Grewe et al. (2017) only for the year 2008.

In general, no large differences between V1.1 and V1.0 for long-lived species are found. The category "biogenic emissions" and "CH_4 decomposition" show an

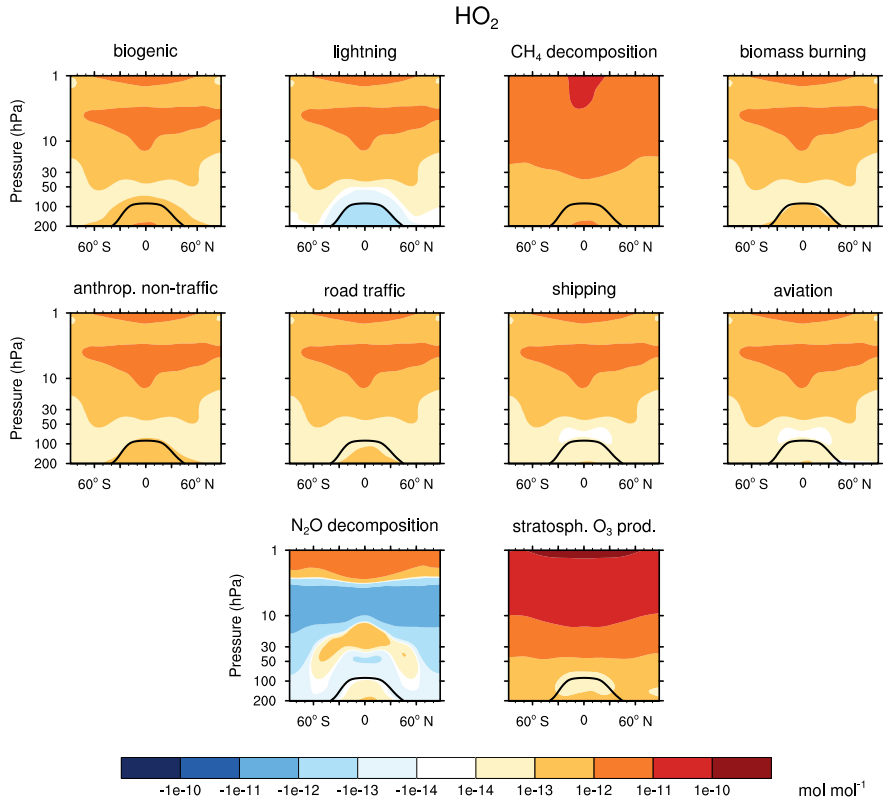

Figure 4.4: Contribution of ten source categories to HO_2 in the stratosphere. Zonal mean of the year 2010 are shown. Black line indicates the tropopause. Simluation is performed with EMAC including tagging method V1.1. Note the logarithmic scale of the contour levels.

O_3 increase in the tropical troposphere. "Stratospheric O_3 production" slightly increases in the Southern Hemisphere. Small O_3 changes are found for the categories "lightning" and "N_2O decomposition". Regarding the remaining long-lived species, the contribution of "biomass burning" to CO decreases while the contributions of "biogenic emissions" to CO increases in the Southern Hemisphere. The remaining sectors stay rather unchanged. NO_y, NMHC and PAN show only minor changes. Although major differences in OH and HO_2 occur between V1.0 and V1.1, these do not have a large effect on the long-lived species. This shows that the contributions of long-lived species are rather determined by long-lived species than by short-lived species.

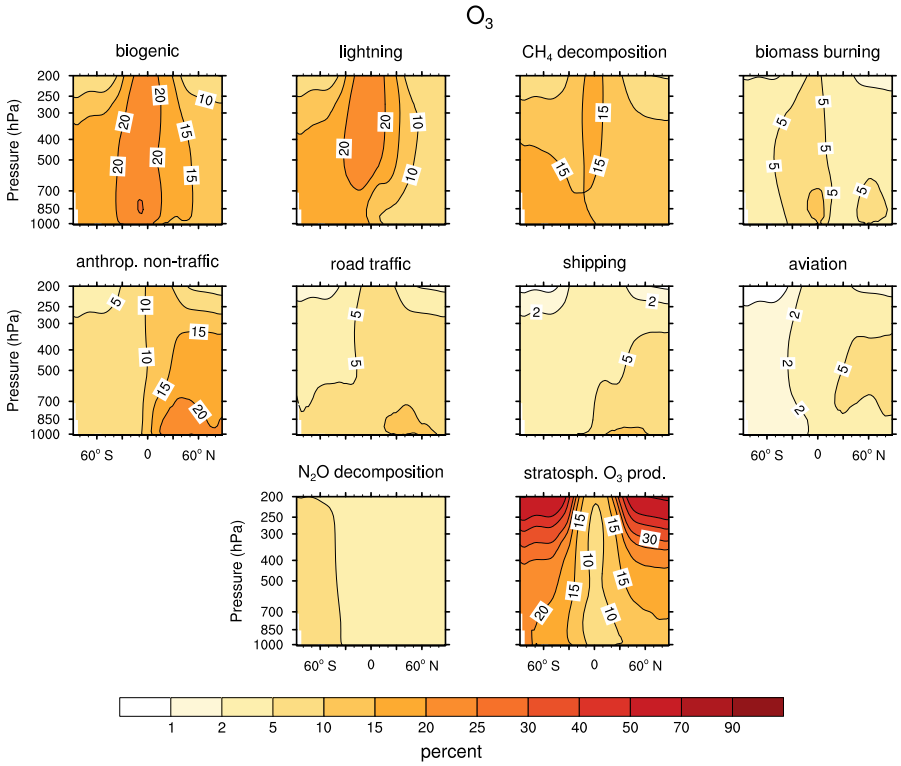

Figure 4.5: Annual mean contributions of ten source categories to O_3 mixing ratio in %.

4.4.7. Summary

This section presented a further developed HO_x tagging mechanism. 15 new reactions producing and destroying HO_x are added to tagging meachnism. In Grewe et al. (2017), the HO_x tagging mechanism V1.0 was restricted to the troposphere only. In this thesis, I further included the reactions which are essential for HO_x production and loss in the stratosphere. In particular the production of HO_2 by H and O_2 and the reaction of OH and HO_2 with $O(^3P)$ are important in the stratosphere and are now taken into account. Thus, the HO_x tagging method is now applicable not only in the troposphere but also in the stratosphere. Moreover, I introduced an equivalent tagging mechanism to obtain the contributions to the H radical. This step is mandatory to fully account for the main HO_2 source: the reaction of H with O_2.

In V1.0, the budget of the sum of the HO_x contributions and the total HO_x concentration deviated by about 70 %. The addition of 15 new reactions to the reaction system leads to a better closure (deviation of 25 %). However, since certain reactions are omitted from the tagging mechanism, the production and loss rates are

less balanced. Since this is a crucial assumption for the HO_x tagging mechanism, rest terms to balance the deviation of HO_x production and loss are explicitly introduced. The rest terms are equally distributed over the source categories. This leads to the closure of the budget. Consequently, the contributions computed by V1.1 represent more realistic results than V1.0.

The further developed HO_x tagging method V1.1 can now be used to quantify the effect of anthropogenic emissions on the concentrations of OH and HO_2 in the troposphere and stratosphere. It enables to explicitly determine the contribution of road traffic emissions to OH. Road traffic emissions contribute with $5.93 \cdot 10^{-15}$ mol mol^{-1} to tropospheric OH mixing ratio, representing 6.6 % of the total tropospheric OH. Hoor et al. (2009) state that road traffic emissions show the largest effect on OH in Northern Hemisphere in summer. They find a maximum value in the continental boundary layer of 0.18 % for a 5 % perturbation method which corresponds to 3.6 % for a 100 % perturbation method (scaled with the factor 20). Using the HO_x tagging method V1.1 reveals a maximum contribution of 21 % for the same region. This value is significantly larger than the value found by Hoor et al. (2009) which is caused by the fact that contributions determined by a tagging method are generally larger than determined by a perturbation method (Grewe et al., 2010; Mertens et al., 2018).

In the present thesis, the advanced HO_x method V1.1 is applied in the following to further assess the effect of mitigation options of the road traffic emissions on OH mixing ratios. Therefore, I implemented the HO_x tagging V1.1 into the TAGGING submodel (see sect. 3.3). Thus, the EMAC simulations performed in the following sections of this thesis include the HO_x tagging V1.1.

4.5. Tagging method for methane

In this thesis, I introduce a new concept to determine the contribution of emissions to CH_4. In particular, this concept enables to quantify the contribution of road traffic emissions to CH_4 and the corresponding radiative forcing.

A change in road traffic emissions causes also changes in the OH distribution (see sect. 2.2). OH in turn is the main component which destroys CH_4 (see sect. 2.2.3):

$$CH_4 + OH \xrightarrow{O_2} CH_3O_2 + H_2O \tag{R14}$$

Reaction (R14) performs 90 % of the global CH_4 loss (Stenke et al., 2012). Thus, OH controls the CH_4 lifetime τ by reaction (R14) which in turn affects the CH_4 concentration. Consequently, a variation in road traffic emission changes the CH_4 concentration. In a first order approximation, the CH_4 concentration is determined by production processes $P(t)$ and by the destruction process through OH expressed by the atmospheric lifetime τ (Grewe and Stenke, 2008):

$$\frac{\partial}{\partial t} CH_4 = P(t) - \frac{1}{\tau} \cdot CH_4 \tag{4.33}$$

To determine the contribution CH_4^i of a specific source category i to CH_4, the linear differential equation (4.33) needs to be split up into the source categories. Therefore,

the generalised tagging method presented by Grewe (2013) is applied. In general, the temporal evolution of the state variables $\vec{x}$ is described by various processes $x_j (j = 1, ..., n)$. The state variables $\vec{x}$ is determined by external forcings $\vec{P}(t)$ and the state variables $\vec{F}(\vec{x})$:

$$\frac{\partial}{\partial t}\vec{x} = \vec{P}(t) + \vec{F}(\vec{x}) \tag{4.34}$$

For m source categories, the variables are split up into their contributions to each category i:

$$P_j(t) = \sum_{i=1}^{m} P_j^i(t) \tag{4.35}$$

$$F_j(\vec{x}) = \sum_{i=1}^{m} F_j^i(\vec{x}) \tag{4.36}$$

$$x_j(t) = \sum_{i=1}^{m} x_j^i \tag{4.37}$$

As derived in Grewe (2013), the impact Q_j^i of the category i on $F_j(\vec{x})$ is defined as the state variable $\vec{x}^i$ multiplied with the sensitivity of $F_j(\vec{x})$ due to the category i:

$$Q_j^i = \vec{x}^{i^T} \frac{\partial F_j(\vec{x})}{\partial \vec{x}^i} \tag{4.38}$$

Thus, the contribution $F_j^i(\vec{x})$ is the relative contribution of the impact Q_j^i from category i versus the total impact of all categories. For the contribution of a source category i to the state variable x_j it follows (compare to Grewe (2013) eq. (10)):

$$\frac{\partial}{\partial t}x_j^i = P_j^i(t) + F_j^i(\vec{x}) = P_j^i(t) + F_j(\vec{x}) \cdot \frac{Q_j^i}{\sum_{i=1}^{m} Q_j^i} \tag{4.39}$$

$$= P_j^i(t) + F_j(\vec{x}) \cdot \frac{\vec{x}^{i^T} \nabla F_j(\vec{x})}{\vec{x}^T \nabla F_j(\vec{x})} \tag{4.40}$$

Since CH_4 and $\frac{1}{\tau}$ determine the CH_4 concentration (eq. 4.33), they are set to processes describing state variables:

$$\vec{x} = \begin{pmatrix} \frac{1}{\tau} \\ CH_4 \end{pmatrix} \tag{4.41}$$

$$\text{with} \quad CH_4 = \sum_{i=1}^{m} CH_4^i, \quad \frac{1}{\tau} = \sum_{i=1}^{m} \frac{1}{\tau^i} \tag{4.42}$$

CH_4 and the reciprocal lifetime[1] are split up into their contributions. It follows:

$$F_{CH_4}(\vec{x}) = -\frac{1}{\tau} CH_4 \tag{4.43}$$

$$\nabla F_{CH_4}(\vec{x}) = \begin{pmatrix} -CH_4 \\ -\frac{1}{\tau} \end{pmatrix} \tag{4.44}$$

Inserting eqs. (4.43) and (4.44) in eq. (4.40) delivers for the contribution of a source category i to the state variable CH_4:

$$\frac{\partial}{\partial t} CH_4^i = P^i(t) - \frac{1}{\tau} CH_4^i \frac{\left(\frac{1}{\tau^i}\ ,\ CH_4^i\right) \begin{pmatrix} -CH_4 \\ \frac{1}{\tau} \end{pmatrix}}{\left(\frac{1}{\tau}\ ,\ CH_4\right) \begin{pmatrix} -CH_4 \\ \frac{1}{\tau} \end{pmatrix}} \tag{4.45}$$

$$= P^i(t) - \frac{1}{2} \left(\frac{1}{\tau^i} CH_4 + \frac{1}{\tau} CH_4^i \right) \tag{4.46}$$

$$= P^i(t) - \frac{1}{2\tau} CH_4^i \left(\frac{\tau}{\tau^i} + \frac{CH_4^i}{CH_4} \right) \tag{4.47}$$

Eq. (4.47) determines the temporal development of the contribution of a source category to the CH_4 concentration. It requires not only the CH_4 concentration and CH_4 lifetime τ, but also the contribution of the lifetime τ^i. The latter describes the CH_4 loss which is determined by OH from the contribution i:

$$\tau^i = \frac{CH_4}{CH_4 loss^i} = \frac{CH_4}{k\ CH_4\ OH^i} \tag{4.48}$$

with k being the reaction rate coefficient of reaction (R14).

In the following, the general contribution CH_4^i (eq. 4.47) is transferred to the source category "road traffic". Road traffic only emits a very small amount of CH_4 (see sect. 2.1). Hence, the CH_4 production processes from road traffic are negligible i.e. $P^{tra}(t) \approx 0$. Consequently it follows from eq. (4.47):

$$\frac{\partial}{\partial t} CH_4^{tra} = -\frac{1}{2} \left(\frac{1}{\tau^{tra}} CH_4 + \frac{1}{\tau} CH_4^{tra} \right) \tag{4.49}$$

Road traffic emissions contribute to OH which in turn influences the CH_4 concentration. Relation (4.49) enables to determine the contribution of road traffic emissions to CH_4 by its lifetime change.

The following example demonstrates how the tagging of CH_4 is applied. The contribution of road traffic emissions to CH_4 is compared to the impact of road traffic emissions on CH_4. The contribution of road traffic emissions to CH_4 is

[1] The reciprocal lifetimes are additive as the rate of removal R from independent processes are additive: $\frac{1}{\tau} = \frac{R}{Q} = \frac{\sum_{i=1}^{m} R^i}{Q} = \sum_{i=1}^{m} \frac{1}{\tau^i}$ (see sect. 2.2.3).

derived from the CH_4 tagging developed in this thesis (eq. 4.49). The $CH_4{}^{tra}$ lifetime of 94.5 years is derived from an EMAC simulation (see sect. 3.3) according to eq. (4.48). The impact of road traffic emissions on CH_4 is calculated by the perturbation method which compares two simulations with and without road traffic emissions (see sect. 4.1). The CH_4 change (ΔCH_4) due to road traffic emissions is determined according to the following relation which was introduced by Grewe and Stenke (2008):

$$\frac{\partial}{\partial t}\Delta CH_4 = \frac{\delta}{1+\delta}\tau^{-1}CH_4 - \frac{1}{1+\delta}\tau^{-1}\Delta CH_4 \tag{4.50}$$

Road traffic emissions decreases the lifetime of CH_4. Many different values exists (see sect. 2.2.3). For this example, a CH_4 lifetime change δ of -1.61 % derived with the perturbation method by Hoor et al. (2009) is chosen.

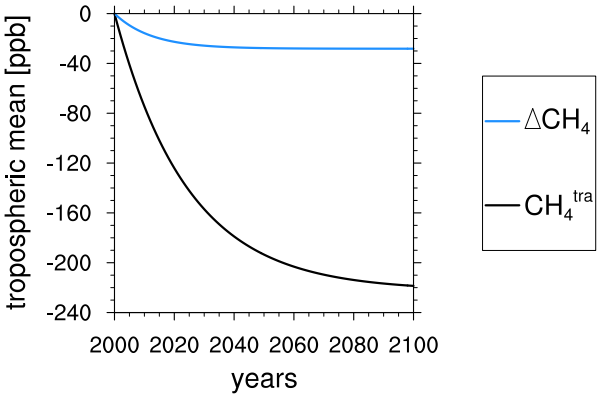

Figure 4.6: Impact (ΔCH_4) derived by the perturbation method and contribution ($CH_4{}^{tra}$) derived by the tagging method of global road traffic emissions.

Both relations (eq. 4.49 and eq. 4.50) are solved using the Euler backward method. The CH_4 background mixing ratio is set to a constant value of 1.8 ppm. The methane perturbation lifetime (τ) is set to 12 years. The resulting impact (ΔCH_4) and contribution ($CH_4{}^{tra}$) are shown in fig. 4.6. In 2100, road traffic emissions decreases CH_4 by -28 ppb. However, the contribution of road traffic emissions of CH_4 has a values of -222 ppb and is by far larger than the impact determined by the perturbation method. This shows that the perturbation method underestimates the contribution derived by the tagging method.

Summing up, this novel method of tagging CH_4 contributions, which is introduced in this thesis, enables to determine the contribution of source categories to CH_4 concentration. It is used in the model TransClim to determine the contribution

as well as the uncertainty range of road traffic emissions to CH_4 and its respective radiative forcing (see sect. 5.5).

This chapter presented an advanced tagging method for OH and HO_2 as well as a novel tagging method for CH_4 which is based on lifetime changes caused by OH. Both methods enable to determine the contributions of anthropogenic emissions such as road traffic emissions to OH, HO_2 and CH_4. The tagging method for HO_x and CH_4 operate reliably. The uncertainties of the HO_x tagging method result from the rest terms which are added to the contributions. As the added rest terms are about one order of magnitude lower than the contributions itself, the uncertainties caused by the rest terms are limited. The tagging method for CH_4 itself possess no uncertainty as the splitting up of the CH_4 contributions is consistent and complete. Uncertainties may originate from the calculation of CH_4 lifetime as different methods exist (Lawrence et al., 2001). Furthermore, the determination of the OH concentration is very sensitive to the input parameter of the simulation setup. Overall, the tagging methods for HO_x and CH_4 offer a great opportunity to assess the climate effect of mitigation strategies for road traffic and are used in the following in the response model TransClim.

5

Development of TransClim

This chapter presents the development of the chemistry-climate response model TransClim. Fig. 5.1 shows an overview of how TransClim is developed and thus guides the reader through this chapter:
At first, sect. 5.1 motivates TransClim and describes its basic model idea. Based on TransClim's objective to asses the climate effect of road traffic emissions of NO_x, VOC and CO, specific requirements for its algorithm are derived in sect. 5.2. To fulfil these requirements an adequate algorithm needs to be selected. Therefore, several algorithms are tested in sect. 5.3. As the O_3 chemistry is non-linear, the algorithm selection focuses only the determination of O_3 concentration originating from the emissions. The effect on CH_4 is expected to be rather linear because CH_4 has a long lifetime of about 8.67 ($\pm$ 1.32) years (Stevenson et al., 2006). Thus, the determination of CH_4 concentration is easier and is regarded later in sect. 5.5. To simplify the testing, a test environment (called "4-box-model") is built up in sect. 5.3.1. It consists of four boxes representing four emission regions. Each box contains a simplified three component O_3 chemistry. Sect. 5.3.2 gives two examples to demonstrate the applicability of the "4-box-model" in simulating non-linearities similar to tropospheric O_3 chemistry. It also supports that the "4-box-model" is well suited for testing possible algorithms for TransClim.

Various algorithms are tested in sect. 5.3.3. Each algorithm is tested against the requirements formulated in sect. 5.2. If an algorithm does not pass the test, it is discarded. The algorithms are chosen in such a way that the whole spectra of possible options are covered: The relation between emissions and O_3, the relation between O_3 precursors and O_3 as well as the separation of O_3 chemistry and transport is regarded. At first, a direct relation of O_3 precursors and O_3 is tested in the "4-box-model" (sect. 5.3.3.1 "Linear combination of precursors"), but discarded as the non-linearities of O_3 chemistry hampers this approach. Subsequently, two approaches separating non-linear O_3 chemistry and transport processes are tested (sect. 5.3.3.2 "Coupled linear equation system", sect. 5.3.3.3 "Iteration method"). Also these two algorithms fail showing that chemistry and transport are not separa-

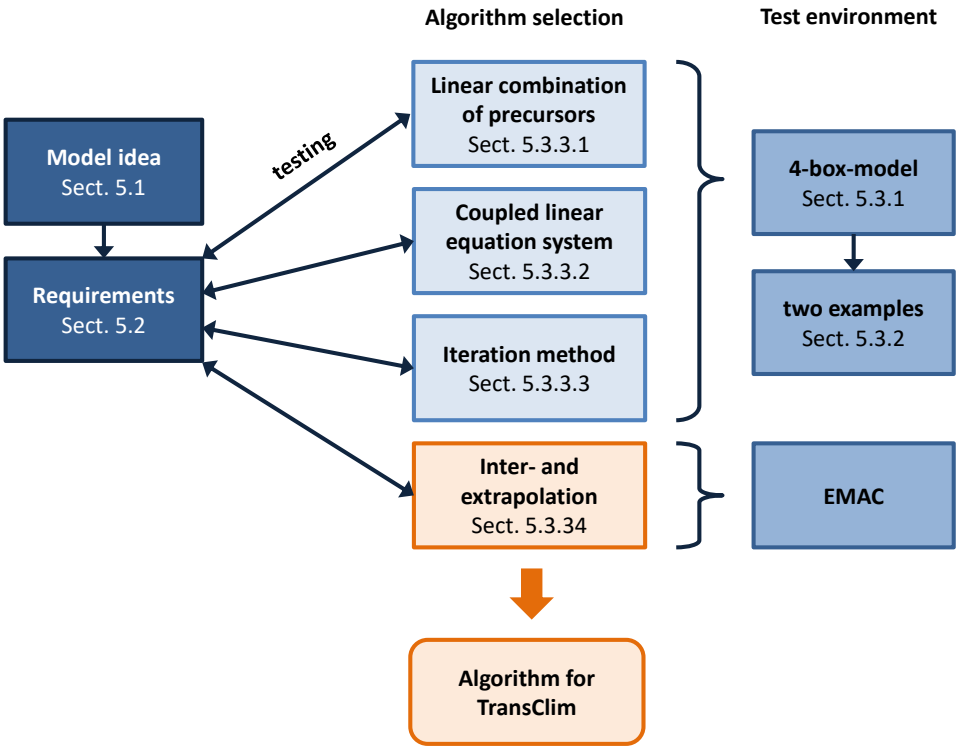

Figure 5.1: Structure of chapter 5. It demonstrates the development path of TransClim.

ble. Last but not least, it is tested whether a combination of emissions is promising (sect. 5.3.3.4 "Inter- and extrapolation within look-up table"). As for this approach, the magnitude of O_3 change is particularly important, this algorithm is not tested in the "4-box-model" but in the global chemistry climate model EMAC (sect. 3). This algorithm fulfils almost all requirements set in sect. 5.2. Thus, it is chosen as final algorithm for TransClim.

Sect. 5.4 describes the setup of the LUT needed for this algorthim. The implementation of TransClim is shown in sect. 5.5. In the version, presented in this thesis, TransClim calculates the climate effect of road traffic emissions of NO_x, VOC and CO on O_3 and CH_4. The effect of CO_2 and aerosols are computed by the climate-response model *AirClim* (Grewe and Stenke, 2008) and by climate-response functions (Hendricks et al., 2017).

After TransClim is implemented, it needs to be evaluated with EMAC simulations (sect 5.6). Two examples are chosen: one direct comparison to an EMAC simulation and one comparison to the simulations performed within the scope of the VEU1 project (Hendricks et al., 2017). Finally, an assessment over the general performance of TransClim is given in sect. 5.7.

5.1. Motivation and model idea of TransClim

To reduce the effect of road traffic emissions on climate, mitigation strategies need to be developed. On the one hand, new technological trends such as new fuels for passenger cars, heavy goods vehicles and buses (e.g. Karavalakis et al., 2012; Suarez-Bertoa et al., 2015; Jedynska et al., 2015) change the vehicle's emissions of NO_x, VOC and CO and thus impact Earth's climate. On the other hand, political decisions such as financial support for electrical cars and car pooling also influence the climate.

To assess the effect of road traffic emissions of NO_x, VOC and CO on climate, complex global chemistry climate models are usually considered. However, their application is very computational expensive which hampers the evaluation of many possible mitigation scenarios. Therefore, a tool is needed which efficiently determines the climate effect of mitigation strategies.

Hence, I developed a new chemistry-climate response model called *TransClim* ("Modelling the effect of surface **Trans**portation on **Clim**ate"). To quickly determine the climate effect of an road traffic emission scenario, TransClim does not explicitly calculate the chemical and physical processes. Instead, it combines precalculated relations between emissions and their climate effect. Figure 5.2 shows the basic principle of TransClim. Road traffic emissions of NO_x, VOC and CO are varied and the corresponding O_3 change is simulated with the global chemistry climate model EMAC. Note that the relation between the emission variation and the O_3 change is non-linear (see sect. 2.2.1). These relations between emission variation and O_3 change are used to create a lookup table (LUT) for TransClim. TransClim interpolates within this LUT and determines the climate effect (e.g. O_3 change) of a specific road traffic emission scenario. In this manner, TransClim determines the climate effect of any road traffic emission scenario. Hence, it enables to assess the climate effect of a broad range of emission scenarios.

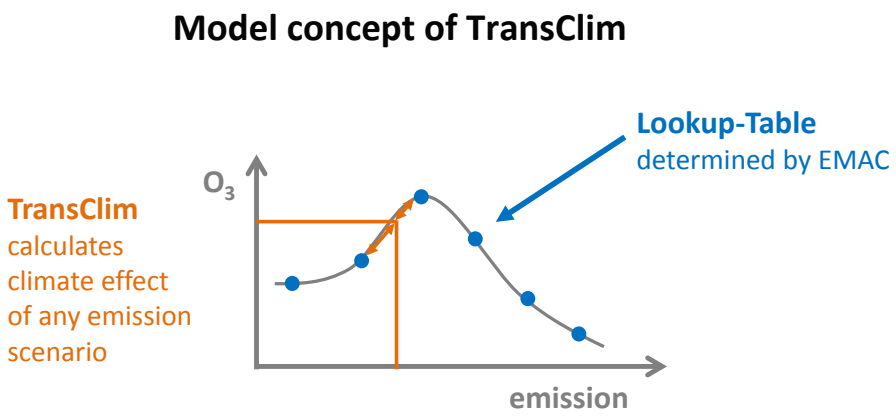

Figure 5.2: TransClim is based on a lookup-table (LUT) determined with the global chemistry climate model EMAC. By interpolating within the LUT TransClim determines the climate effect of any road traffic emission scenario.

5.2. Requirements

The objective of TransClim is to assess the effect of road traffic emissions of NO_x, VOC and CO on tropospheric O_3 and CH_4 and their respective effect on climate. Therefore it is important that the algorithm of TransClim, which combines pre-calculated relations between emission and climate effect, fulfils certain requirements:

1. It shall consider the road traffic emissions of NO_x, VOC and CO. These species produces O_3 in the troposphere (see sect. 2.2.1). Thus, the algorithm shall be able to calculate the resulting total O_3 concentration as well as the contribution of road traffic O_3^{tra} to the total O_3 concentration (derived by the tagging method, see sect. 4.3).

2. It shall consider the non-linearity of the tropospheric O_3 chemistry.

3. It shall regard different emission regions (such as Europe, Germany, North America, ...) of road traffic emissions. Within these emission regions, the road traffic emissions are varied.

4. It shall further determine the pattern of O_3 and O_3^{tra} caused by a road traffic emission scenario. This enables to determine not only the global but also the regional effect. It shall be able to detect the emission plume of the emission regions since the downwind effect can differ from the source region effect.

5. It shall calculate the radiative forcing of O_3 and O_3^{tra}.

6. It shall determine the change of CH_4 and CH_4^{tra}. Furthermore, the respective radiative forcing of CH_4 and CH_4^{tra} shall be calculated as well.

7. It shall take the background concentration of O_3 and CH_4 into account. This will enable to consider different future emission scenarios such as the Representative Concentration Pathways RCP (van Vuuren et al., 2011). The O_3 and CH_4 background concentration can vary in a future emission scenario and thus also the climate effect of the road traffic emissions changes.

5.3. Algorithm selection for TransClim

In this section, an efficient algorithm for TransClim, which is fast enough to assess many emission scenarios and which simultaneously generates errors of less than 10 %, is developed. Several approaches are evolved and tested whether they fulfil the requirements formulated in the previous section 5.2. This section focuses on finding an algorithm to determine the change of tropospheric O_3. The method for assessing CH_4 change caused by road traffic emissions is discussed later in sect. 5.5. Due to the non-linearity of the tropospheric O_3 chemistry, finding a suitable algorithm for O_3 is expected to be more complicated than for CH_4.

To simplify the development, I built up a test environment. It consists of four boxes (Eurasia, Pacific, North America and Atlantic). Each of the boxes contains a simplified three component O_3 chemistry imitating the non-linear tropospheric O_3 chemistry. The boxes are connected by transport. This *4-box-model* represents the

basic behaviour concerning tropospheric O_3 chemistry and transport processes of a complex chemistry climate model such as EMAC. It enables to better understand the fundamental processes of transport and chemistry. Additionally, it is computational expensive to frequently run a global chemistry climate model. Hence, a simplified environment offers a suitable test bed to develop an algorithm for TransClim. If the tested approach does not fulfil the requirements (sect. 5.2) in the 4-box-model, it will also not fulfil the requirements in EMAC and thus it is discarded.

5.3.1. Description of 4-box-model

This sections describes the *4-box-model* which acts as a test environment for finding a suitable algorithm for TransClim.

The Northern Hemisphere is split up into four boxes, representing Eurasia, Pacific, North America and Atlantic (see fig. 5.3). Each box has a zonal dimension of approximately $7.7 \cdot 10^3$ km, a meridional dimension of $2.2 \cdot 10^3$ km and a height of 8 km (representing the average height of the tropopause at these latitudes).

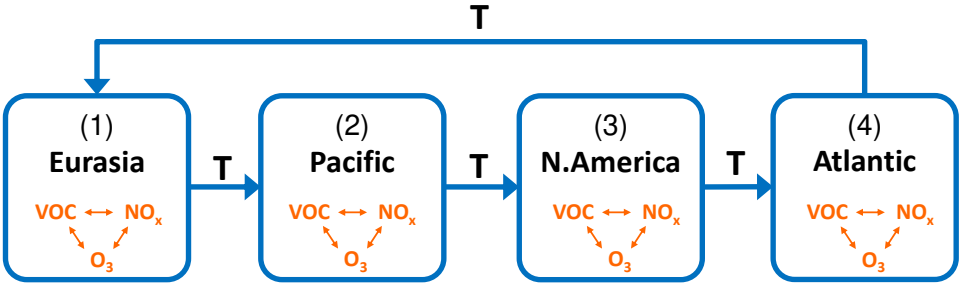

Figure 5.3: 4-box-model containing the regions Eurasia, Pacific, North America and Atlantic. In each box, NO_x and VOC are emitted and produce and destroy O_3 by a simplified three component chemistry. Chemical species are transported from box to box (indicated with T).

Each box contains a simplified three component O_3 chemistry. Usually, many chemical components are involved in the ozone production and destruction (see sect. 2.2). As Grewe et al. (2010) proposed as a test bed, the principal components are summarised in two chemical families: nitrogen oxides ($NO_x = NO + NO_2$) and volatile organic compounds (VOC[1]). (Note that CO is not regarded explicitly as its behaviour regarding the tropospheric O_3 chemistry is similar to VOC.) Hence, the complex ozone chemistry in the troposphere is boiled down to the following three chemical reactions:

- Ozone is produced by the precursors VOC and NO_x with the chemical rate coefficient p:

$$\mathrm{VOC} + \mathrm{NO_x} \xrightarrow{air} \mathrm{O_3} + \mathrm{VOC} + \mathrm{NO_x} \qquad \text{(R15)}$$

[1]In fact, the non-methane volatile organic compounds (NMVOC) are considered. However, in this thesis, only the expression VOC is used to simplify the syntax.

- Ozone is destroyed by VOC or NO_x with the chemical rate coefficients d_x or d_y:

$$\mathrm{VOC} + \mathrm{O_3} \xrightarrow{air} \mathrm{VOC} \tag{R16}$$

$$\mathrm{NO_x} + \mathrm{NO_x} + \mathrm{O_3} \xrightarrow{air} \mathrm{NO_x} + \mathrm{NO_x} \tag{R17}$$

Note that these three reactions are artificial. Reaction (R17) is constructed in such a way that a non-linear chemical reaction system in NO_x is formed. The combination of the reaction (R15), (R16) and (R17) leads to the following O_3 production P and destruction D rates:

$$P = p \cdot x \cdot y \tag{5.1}$$

$$D = d_x \cdot x \cdot z + d_y \cdot y \cdot y \cdot z \tag{5.2}$$

Here, the concentrations of VOC, NO_x and O_3 are abbreviated with x, y and z. The change in net O_3 concentration is formed by subtracting the O_3 loss (eq. 5.2) from the O_3 production (eq. 5.1). The steady-state solution leads to following O_3 concentration (compare to Grewe et al. (2010) their eq. (4) and (36)):

$$\frac{dz}{dt} = P - D = pxy - d_x xz - d_y y^2 z = 0 \tag{5.3}$$

$$\Rightarrow z = \frac{pxy}{d_x x + d_y y^2} \tag{5.4}$$

The resulting O_3 mixing ratios are shown in an isopleth diagram in fig. 5.4a. According to Grewe et al. (2010), the reaction rate coefficients of reactions (R15) to (R17) in the 4-box-model are set to: $p = 8.9 \cdot 10^{-8}$ ppb^{-1} s^{-1}, $d_x = 2.5 \cdot 10^{-8}$ ppb^{-1} s^{-1} and $d_y = 2.5 \cdot 10^{-9}$ ppb^{-2} s^{-1}. The isopleth pattern of the three component chemistry corresponds well with mixing ratios of a complex chemistry model (see fig. 5.4b). Hence, the three component chemistry sufficiently describes the principal non-linearities in the tropospheric ozone chemistry and thus, the three component chemistry are used to conduct test simulations.

Additionally, the 4 boxes are interacting by transport representing advection of chemical species (in fig. 5.3 indicated with T). As a first approximation, it is assumed that the boxes are located in the west wind zone. Thus, the transport of trace gases occurs only in one direction. With an average wind speed of 4 m s^{-1}, the trace gases are transported from one box to the neighbouring. This is implemented by setting $T = 0.5 \cdot 10^{-6} s^{-1}$ in the 4-box-model[1]. For example, the trace gases are transported from the box Eurasia to the box Pacific and so on.

[1]The transport coefficient T describes the ratio of transported particles (N_t) to total particles of one box (N_{total}) per time unit t. It is computed by the ratio of distance x (covered with an average wind speed of 4 m s^{-1}) to the average length of a box (about 7700 km):

$$T = \frac{N_t}{N_{total}} \cdot \frac{1}{t} = \frac{x}{7700\ km} \cdot \frac{1}{t} = \frac{4\ m\ s^{-1}}{7700\ km} \approx 0.5 \cdot 10^{-6} s^{-1}.$$

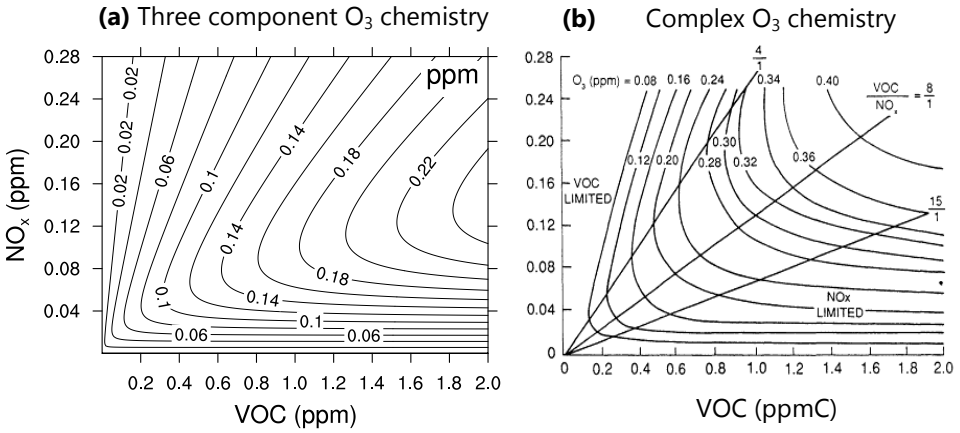

Figure 5.4: O_3 isopleth diagram for (a) simplified three component chemistry (according to Grewe et al. (2010)) and (b) simulation with complex chemistry model (The values are derived from a combination of smog chamber data and photochemical modeling techniques. Reprinted with permission from "Rethinking the Ozone Problem in Urban and Regional Air Pollution", 1991 by the National Academy of Sciences, Courtesy of the National Academies Press, Washington, D.C. (Council, 1991). Figure is adapted from Dodge (1977).)

In each box, emissions of NO_x and VOC occur. The strength of the emissions depends on the box: In the box Eurasia, the emissions are rather high since this region is highly industrialised. In contrast, the emissions in the box Pacific are small. As a sink process, VOC and NO_x are destroyed with the atmospheric lifetime τ_x and τ_y. The lifetime of NO_x in the troposphere varies strongly: between 1.8 days at the surface and 18.6 days in the upper troposphere (Seinfeld and Pandis, 2006). Also the lifetime of VOC ranges largely between minutes to months (Williams and Koppmann, 2007). Consequently, an average value of one week is assumed for τ_x and τ_y. This assumption reduces the accuracy of the 4-box-model. But as a first approximation, it can be applied for simplified test environment.

For VOC and NO_x (represented as x and y), the change in concentration of the trace gases due to emission E, loss processes (expressed by lifetime τ) and the transport T is described by (indices indicate the box number):

$$\begin{aligned}
\frac{dx_1}{dt} &= E_1^x - \frac{1}{\tau_x}x_1 - Tx_1 + Tx_4 = 0 \\
\frac{dx_2}{dt} &= E_2^x - \frac{1}{\tau_x}x_2 - Tx_2 + Tx_1 = 0 \\
\frac{dx_3}{dt} &= E_3^x - \frac{1}{\tau_x}x_3 - Tx_3 + Tx_2 = 0 \\
\frac{dx_4}{dt} &= E_4^x - \frac{1}{\tau_x}x_4 - Tx_4 + Tx_3 = 0
\end{aligned} \tag{5.5}$$

$$\begin{aligned}
\frac{dy_1}{dt} &= E_1^y - \frac{1}{\tau_y} y_1 - T y_1 + T y_4 = 0 \\
\frac{dy_2}{dt} &= E_2^y - \frac{1}{\tau_y} y_2 - T y_3 + T y_1 = 0 \\
\frac{dy_3}{dt} &= E_3^y - \frac{1}{\tau_y} y_3 - T y_3 + T y_2 = 0 \\
\frac{dy_4}{dt} &= E_4^y - \frac{1}{\tau_y} y_4 - T y_4 + T y_3 = 0
\end{aligned} \tag{5.6}$$

Also O_3 (represented as z) is transported from one box to the next. But no direct emission occurs. O_3 is formed by chemical processes from the precursors NO_x and VOC. Combining the chemical O_3 production (reaction R15) and destruction (reactions R16, R17) with the transport between the boxes, the change in O_3 is described as follows:

$$\begin{aligned}
\frac{dz_1}{dt} &= p x_1 y_1 - d_x x_1 z_1 - d_y y_1 y_1 z_1 - T z_1 + T z_4 = 0 \\
\frac{dz_2}{dt} &= p x_2 y_2 - d_x x_2 z_2 - d_y y_2 y_2 z_2 - T z_2 + T z_1 = 0 \\
\frac{dz_3}{dt} &= p x_3 y_3 - d_x x_3 z_3 - d_y y_3 y_3 z_3 - T z_3 + T z_2 = 0 \\
\frac{dz_4}{dt} &= p x_4 y_4 - d_x x_4 z_4 - d_y y_4 y_4 z_4 - T z_4 + T z_3 = 0
\end{aligned} \tag{5.7}$$

This set of equations (5.7) forms a coupled differential equation system which is non-linear in y. Only the steady-state solution is considered, so all temporal derivations are set to zero. Analytically solving the equation systems (5.5) and (5.6) provides the following solutions for $\vec{x}^{\,T} = (x_1, x_2, x_3, x_4)$ and $\vec{y}^{\,T} = (y_1, y_2, y_3, y_4)$:

$$\vec{x} = \frac{1}{\alpha^4 - T^4} \cdot \begin{pmatrix} \alpha^3 & T^3 & \alpha T^2 & \alpha^2 T \\ \alpha^2 T & \alpha^3 & T^3 & \alpha T^2 \\ \alpha T^2 & \alpha^2 T & \alpha^3 & T^3 \\ T^3 & \alpha T^2 & \alpha^2 T & \alpha^3 \end{pmatrix} \cdot \overrightarrow{E^x} \tag{5.8}$$

$$\vec{y} = \frac{1}{\beta^4 - T^4} \cdot \begin{pmatrix} \beta^3 & T^3 & \beta T^2 & \beta^2 T \\ \beta^2 T & \beta^3 & T^3 & \beta T^2 \\ \beta T^2 & \beta^2 T & \beta^3 & T^3 \\ T^3 & \beta T^2 & \beta^2 T & \beta^3 \end{pmatrix} \cdot \overrightarrow{E^y} \tag{5.9}$$

with $\alpha = \frac{1}{\tau_x} + T$, $\beta = \frac{1}{\tau_y} + T$, $\overrightarrow{E^x}^{\,T} = (E_1^x, E_2^x, E_3^x, E_4^x)$ and $\overrightarrow{E^y}^{\,T} = (E_1^y, E_2^y, E_3^y, E_4^y)$. The solution of $\vec{z}^{\,T} = (z_1, z_2, z_3, z_4)$ has a similar structure:

$$\vec{z} = \frac{1}{\gamma^4 - T^4} \cdot \begin{pmatrix} \gamma_2\gamma_3\gamma_4 & T^3 & \gamma_2 T^2 & \gamma_2\gamma_3 T \\ \gamma_3\gamma_4 T & \gamma_1\gamma_3\gamma_4 & T^3 & \gamma_3 T^2 \\ \gamma_4 T^2 & \gamma_1\gamma_4 T & \gamma_1\gamma_2\gamma_4 & T^3 \\ T^3 & \gamma_1 T^2 & \gamma_1\gamma_2 T & \gamma_1\gamma_2\gamma_3 \end{pmatrix} \cdot \vec{\epsilon} \tag{5.10}$$

with $\epsilon_b = p x_b y_b$ and $\gamma_b = d_x x_b + d_y y_b y_b + T$ (b is the box number). The eqs. (5.8) to (5.10) provide a setting to determine the total VOC, NO_x and O_3 concentrations in the 4-box-model.

Furthermore, the **contributions** of an emission to VOC, NO_x and O_3 concentrations is determined. To calculate the contributions, the general tagging method after Grewe et al. (2010) (see sect. 4.1) is introduced in the 4-box-model. Therefore, the emissions in each box b ($b = 1 \dots 4$) are split up into background emissions E_b^{BG} and additional emissions E_b^{add}:

$$\overrightarrow{E^x} = \overrightarrow{E^{x,BG}} + \overrightarrow{E^{x,add}} \tag{5.11}$$

$$\overrightarrow{E^y} = \overrightarrow{E^{y,BG}} + \overrightarrow{E^{y,add}} \tag{5.12}$$

Consequently, each summand in eqs. (5.8) and (5.9) describes the contribution of the corresponding emission to x_b and y_b. For example, the contributions of additional emissions and background emissions of the four boxes to x_1 are:

$$\begin{aligned}
x_1^{E_1^{x,add}} &= \frac{1}{\alpha^4 - T^4} \cdot \alpha^3 \cdot E_1^{x,add} \\
x_1^{E_2^{x,add}} &= \frac{1}{\alpha^4 - T^4} \cdot T^3 \cdot E_2^{x,add} \\
x_1^{E_3^{x,add}} &= \frac{1}{\alpha^4 - T^4} \cdot \alpha T^2 \cdot E_3^{x,add} \\
x_1^{E_4^{x,add}} &= \frac{1}{\alpha^4 - T^4} \cdot \alpha^2 T \cdot E_4^{x,add}
\end{aligned} \tag{5.13}$$

$$\begin{aligned}
x_1^{E_1^{x,BG}} &= \frac{1}{\alpha^4 - T^4} \cdot \alpha^3 \cdot E_1^{x,BG} \\
x_1^{E_2^{x,BG}} &= \frac{1}{\alpha^4 - T^4} \cdot T^3 \cdot E_2^{x,BG} \\
x_1^{E_3^{x,BG}} &= \frac{1}{\alpha^4 - T^4} \cdot \alpha T^2 \cdot E_3^{x,BG} \\
x_1^{E_4^{x,BG}} &= \frac{1}{\alpha^4 - T^4} \cdot \alpha^2 T \cdot E_4^{x,BG}
\end{aligned} \tag{5.14}$$

Analogously, the same holds for the box (2) to (4) and $\vec{y}$. To tag the contribution of emissions in box i to O_3 in box b, the general tagging method described in sect. 4.1 is applied. According to eq. (4.4), the contributions of box i (x^i, y^i and z^i) to O_3 production (reaction R15) and destruction (reactions R16 and R17) in box b are (compare to Grewe et al. (2010) eq. (17) and (20)):

$$\hat{P}_b^i = \frac{1}{2} p \left(x_b^i y_b + x_b y_b^i \right) \tag{5.15}$$

$$\hat{D}_b^{x,i} = \frac{1}{2} d_x \left(x_b^i z_b + x_b z_b^i \right) \tag{5.16}$$

$$\hat{D}_b^{y,i} = d_y \left(\frac{2}{3} y_b^i y_b z_b + \frac{1}{3} y_b^2 z_b^i \right) \tag{5.17}$$

Note that the factors $\frac{1}{3}$ and $\frac{2}{3}$ result from the trimolecular reaction (R17). Thus, the change in contribution of an emission from box i to z in box b is written as:

$$\frac{dz_b^i}{dt} = \hat{P}_b^i - \hat{D}_b^{x,i} - \hat{D}_b^{y,i} - Tz_b^i + Tz_{b-1}^i \tag{5.18}$$

The box $b-1$ indicates the previous box, i.e. for the box 1 the previous box is the box 4. As equation system (5.7), the equation system (5.18) is solved analytically for steady-state.

Summing up, the 4-box-model consists of four boxes containing a simplified three component O_3 chemistry. VOC and NO_x are emitted in each box and are transported. They produce and destroy O_3 which is also transported from box to box. The differential equations for NO_x, VOC, O_3 and their respective contributions are solved for steady-state. The 4-box-model enables to calculate the O_3 concentrations and contributions of various emission scenarios.

5.3.2. Applicability of 4-box-model

To demonstrate the applicability of the 4-box-model, two examples are given in the following section. The first example illustrates the behaviour of O_3 contributions when NO_x emissions are increased. The second examples shows the effect on O_3 contributions when road traffic emissions are omitted.

5.3.2.1. Example 1: Increase of NO_x emissions

Fig. 5.5 shows an example of an emission increase and the effect on the O_3 contributions in the 4-box-model. An additional NO_x emission is introduced to the background emissions in the box Pacific and then stepwise increased up to $3.5 \cdot 10^{-4}$ ppb s^{-1} to demonstrate the different chemical regimes of O_3. The respective contributions of the additional emission and of the background NO_x and VOC emissions of each box to O_3 in the box Pacific are determined with the 4-box-model and shown in fig. 5.5.

At first, the additional NO_x emission produces additional O_3 in the box Pacific (green line). This indicates that the chemical regime of box Pacific is "NO_x-limited". The O_3 production peaks at a NO_x emission of around $1.0 \cdot 10^{-4}$ ppb s^{-1}. Then, the production decreases showing that the chemical regime switched to "VOC-limited" as the NO_x concentration is high enough to finally decrease O_3 production (see sect. 2.2.1). For high NO_x emissions (above approx. $2.3 \cdot 10^{-4}$ ppb s^{-1}), O_3 is even destroyed.

The contributions of the background NO_x (red lines) and VOC (blue lines) emissions to O_3 show very different behaviour. The contributions of the VOC background emissions increases with increasing NO_x emission, while the contribution of NO_x background emissions decreases. The contributions of NO_x and VOC background emissions from the box Eurasia are larger than for the box Pacific. This results from larger background emissions in Eurasia than in Pacific. These large background emissions cause large NO_x and VOC mixing ratios which are transported to the Pacific where they contribute to O_3 production or destruction. Moreover, fig. 5.5

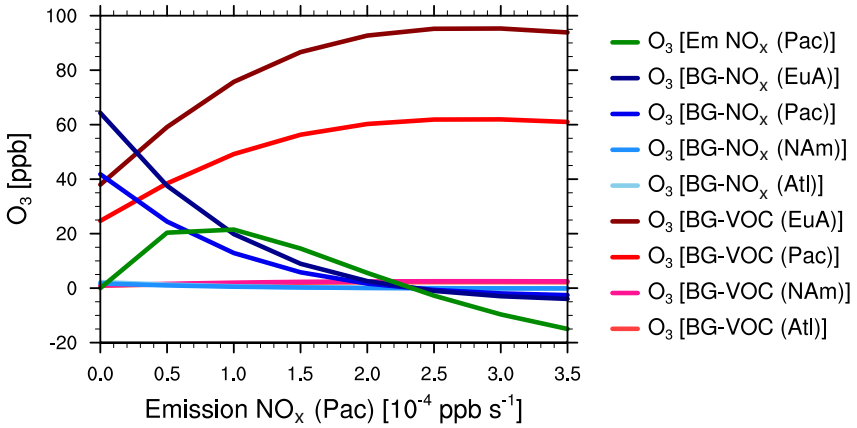

Figure 5.5: O_3 contributions in the box Pacific of a NO_x emission increase in the same box. The O_3 contributions of the additional emission (Em) and the background emissions (BG) for NO_x and VOC of each box Eurasia (EuA), Pacific (Pac), North America (NAm) and Atlantic (Atl) is shown.

shows that at first the NO_x background from Eurasia dominates the O_3 mixing ratio in the Pacific. With increasing NO_x emissions in the Pacific, the NO_x background loses its importance and is replaced by the VOC background from Eurasia. Emissions from the box Atlantic and North America only play a minor role. Here, the transport over two boxes is too far to cause a large effect.

This example emphasizes that the 4-box-model reproduces the non-linearity of the O_3 chemistry and the transport processes between the 4 boxes very well.

5.3.2.2. Example 2: Effect of road traffic emissions

In the following example, the emissions are split up into different sectors: emissions from road traffic, shipping, aviation, industry and a residual sector which contains emissions from agricultural waste, biomass burning, biogenic and lightnings. The amount of NO_x and VOC emissions in each box are deduced from the emission inventory MACCity described in sect. 3.4 (specific amounts see appendix A.4). Fig. 5.6 shows the NO_x and VOC emissions in each box being split up into the emission sectors (first and second row). In all boxes, the residual sector contributes most to the emissions. In the Pacific and Atlantic, NO_x and VOC emissions are small. Only ships largely emit NO_x here. In Eurasia, the total emissions are about $4.2 \cdot 10^{-5}$ ppb s^{-1} for NO_x and $1.4 \cdot 10^{-4}$ ppb s^{-1} for VOC. In North America, the NO_x road traffic emissions dominate over the industry sector while in Eurasia both sectors have about the same size.

Based on these emissions, the 4-box-model enables to calculate the respective total O_3 mixing ratios and contributions (third row in fig. 5.6). Corresponding to the high emissions in Eurasia and North America the resulting O_3 mixing ratios are also large (44.6 ppb in Eurasia and 34.1 ppb in North America). In contrast, in Pacific

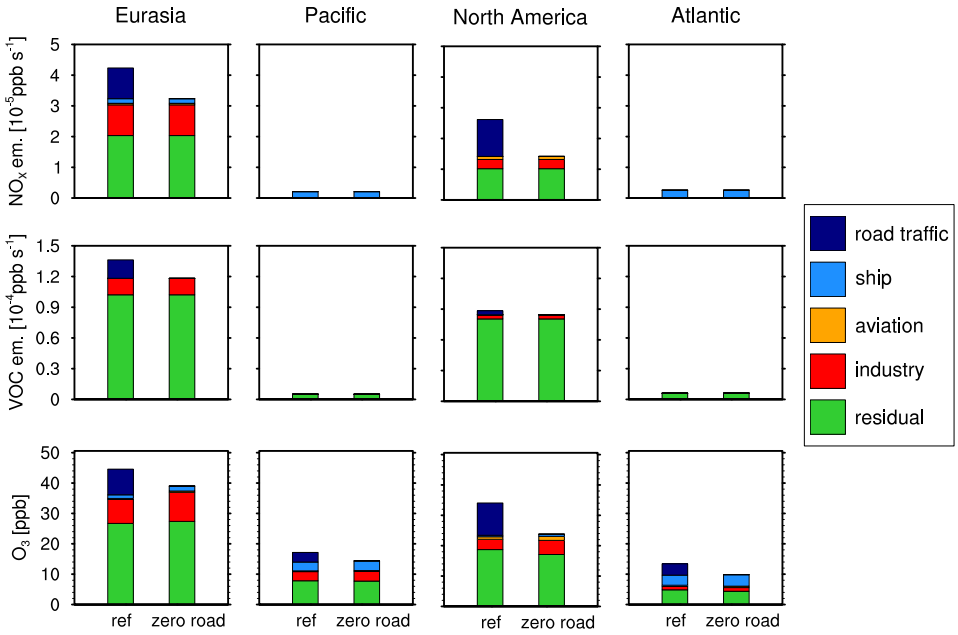

Figure 5.6: The first and second row show the NO_x and VOC emissions for the 4 boxes, split up into the emission sectors road, ship, aviation, industry and residual. The third row shows the respective contributions to O_3 determined by the 4-box-model. *ref* indicates the reference simulation. *zero road* indicates the simulation in which all road traffic emissions are set to zero.

and Atlantic, the total emissions are very low which results in low total O_3 mixing ratios (17.2 ppb in Pacific and 13.4 ppb in Atlantic). The boxes with high emissions (Eurasia and North America) show a different behaviour for the contributions than the boxes with low emissions (Pacific and Atlantic). For Eurasia and North America, the ratios of the sectors to the total emissions are approximately represented in the O_3 contributions. For the Pacific and Atlantic, although only shipping, aviation and the residual sector contributes to the emissions, all sectors contributes to O_3. This effect is caused by the transport of the emissions from box to box and by the non-linearity of the O_3 chemistry.

The second bar in fig. 5.6 shows the case when all NO_x and VOC emissions from road traffic are set to zero (*zero road*). The total emissions in Eurasia and North America are thus reduced by 24 % and 46 % for NO_x and 13 % and 5 % for VOC. No emissions are changed in Pacific and Atlantic. Omitting emissions from road traffic causes a decrease in O_3 in all four boxes. In Pacific and Atlantic, total O_3 decreases by 16 % and 27 %. In Eurasia and North America, the reduction of the total O_3 by lack of road traffic emissions (12 % and 30 %) is compensated by the remaining emission sectors. In particular, the sector ship, aviation and industry become more

efficient in producing O_3. The behaviour of the residual term varies: in Eurasia it becomes slightly more efficient, in North America less efficient in producing O_3.

The effect that an O_3 decrease, which is caused by a reduction of road traffic emissions, is compensated by the other emission sectors was also found by Grewe et al. (2012, 2017) in the global chemistry climate model E39C (a predecessor of EMAC; Hein et al., 2001). This shows that the 4-box-model represents well the basic principle of the non-linearity of the O_3 chemistry and tracer transport. It is able to reproduce the contribution of road traffic emissions to O_3. Hence, the 4-box-model is used as a test bed to find a solution algorithm for TransClim. In the following section, various solution algorithms based on the results of the 4-box-model are tested.

5.3.3. Testing of solution algorithms

In the following section, an efficient algorithm for TransClim which reproduces the total O_3 concentration (requirement (1), see sect. 5.2) is developed. Sect. 5.3.4 assesses whether the algorithm also fulfils the remaining requirements (2) – (7). Four different algorithms are tested and described in this section. The first algorithm tests linear combinations of O_3 precursors (sect. 5.3.3.1). The second and third algorithms investigates the separation of the non-linear O_3 chemistry and the transport processes (sect. 5.3.3.2, sect. 5.3.3.3). The forth approach tests interpolations and extrapolations within a look-up table (LUT) (sect. 5.3.3.4). The first three algorithms (sect. 5.3.3.1 to 5.3.3.3) are set up in the test environment 4-box-model which has been derived in sect. 5.3.1. For the last algorithm (sect. 5.3.3.4), the magnitude of O_3 changes is particularly important, thus this algorithm is tested with the global chemistry climate model EMAC (see fig. 5.1). For each algorithm, the road traffic emissions of NO_x and VOC are varied either in the 4-box-model or in EMAC. These simulations provide input for the LUT as indicated in fig. 5.2. The specific setup for the LUT varies for each algorithm and is explicitly explained in the corresponding section. Subsequently, the data points in the LUT shall be combined in an efficient way to determine the total O_3 concentrations in each box for a specific emission scenario.

For the first three algorithms (sect. 5.3.3.1 to 5.3.3.3), which are tested in the 4-box-model, the determination of the O_3 concentration is performed in two steps: First, the NO_x and VOC concentration are derived from the NO_x and VOC emissions. Second, the O_3 concentration is deduced from the NO_x and VOC concentration.

As a first step, the relation between NO_x and VOC emissions and NO_x and VOC mixing ratios is regarded in the 4-box-model. It is straightforward to determine NO_x and VOC mixing ratios from their emissions: The NO_x and VOC mixing ratios depend linearly on emissions, transport processes and destruction through lifetime (see eqs. (5.5) and (5.6)). Based on eqs. (5.8) and (5.9), the NO_x and VOC mixing ratios are written as a linear combination of the additional VOC and NO_x emissions

($E_b^{x,add}$ and $E_b^{y,add}$) :

$$x_b = \sum_{b=1}^{n} \mu_b \cdot E_b^{x,add} + x_b^{BG}$$
$$y_b = \sum_{b=1}^{n} \lambda_b \cdot E_b^{y,add} + y_b^{BG} \tag{5.19}$$

The coefficients μ_b and λ_b are determined for each box b by linear regression. x_b^{BG} and y_b^{BG} indicate the background mixing ratios in each box. As an example, the additional NO_x emissions ($\overrightarrow{E^{y,add}}$) are increased 7 times in each of the 4 boxes while the remaining emissions are kept constant. This forms a LUT which contains 113 data points describing the NO_x mixing ratios in each box due to $\overrightarrow{E^{y,add}}$ increase. Fig. 5.7a shows the NO_x mixing ratios in the box Eurasia depending on $\overrightarrow{E^{y,add}}$ increase in the boxes Eurasia (EuA), Pacific (Pac), North America (NAm) and Atlantic (Atl). The relations between the emissions and the corresponding mixing ratios is clearly affine linear. Fig. 5.7b presents the relative frequency distribution of the relative errors between the NO_x mixing ratios determined according to eqs. (5.19) and the original values derived for 32 simulations with the 4-box-model for the box Eurasia. The relative errors of about 10^{-8} are very small, hence the determination of NO_x and VOC according to eqs. (5.19) works very well.

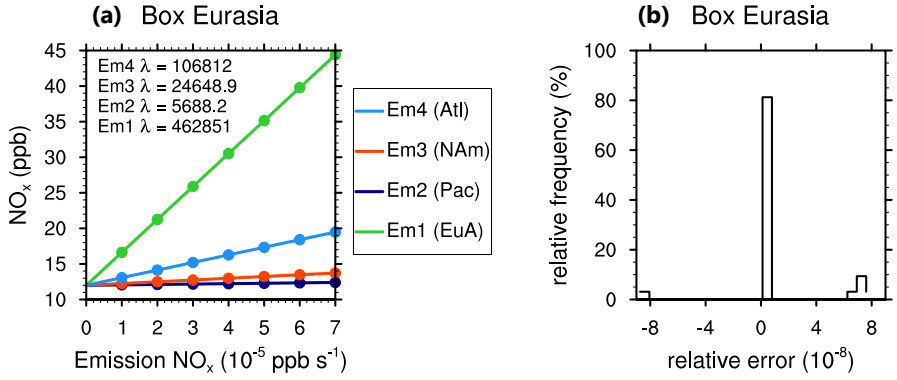

Figure 5.7: (a) NO_x mixing ratios in box Eurasia depending on an increase of additional NO_x emissions (Em) in box Eurasia (EuA), Pacific (Pac), North America (NAm) and Atlantic (Atl). The dots indicate the data points of the LUT. The regressions coefficients λ are also given. (b) Relative frequency distribution of the relative error between the NO_x mixing ratios determined after eqs. (5.19) and the original values derived from 32 simulations performed with the 4-box-model for all four boxes.

However, the determination of the O_3 concentration from the precursors NO_x and VOC is challenging as the non-linearity of the O_3 chemistry and the transport closely intertwine. To find an algorithm which determines the O_3 concentration, different approaches are tested in the following. Algorithms described in sect. 5.3.3.1 to 5.3.3.3 fail, but sect. 5.3.3.4 presents an efficient algorithm which computes the climate effect fast enough to enable the assessment of many road traffic emission scenario and which generates errors of less than 10 %. This algorithm is finally used for the implementation in TransClim.

5.3.3.1. Linear combination of precursors

This approach checks whether a linear combination of the precursors $\vec{x}$ and $\vec{y}$ can be used to fulfil the requirements in sect. 5.2. As a first step, this approach is tested against requirement (1): Can a linear combination of the precursors be used to calculate the correct O_3 concentration caused by an emission scenario? Therefore, this approach is tested in the 4-box-model.

At first, the concentrations of the precursors $\vec{x}$ and $\vec{y}$ is determined from the emissions by eqs. (5.19). Then, $\vec{x}$ and $\vec{y}$ are combined linearly to retrieve the O_3 concentration in the 4 boxes ($\vec{z}$). Therefore, $\vec{x}$ and $\vec{y}$ are described by a function $f(x_b, y_b)$ which is weighted with transport coefficients t_b. The general form for z in box i is:

$$z_i = \sum_{b=1}^{4} t_b \cdot f(x_b, y_b) \tag{5.20}$$

To calculate z_i the transport coefficients t_b need to be determined under the condition that $f(x_b, y_b)$ is known. Three sets of linear combinations are formed in such a way that they take into account the non-linear O_3 chemistry (by s_b) and the linear transport effects (by transport coefficients (a, b, c) for (1), (n_1, n_2, n_3, n_4) for (2) and (t_1, t_2, t_3, t_4) for (3)):

$$\begin{aligned}
&(1) \quad z_b = s_b + a \cdot (s_{b-1} - s_b) + b \cdot (s_{b-2} - s_b) + c \cdot (s_{b-3} - s_b) \\
&(2) \quad z_b = n_1 s_b + n_2 s_{b-1} + n_3 s_{b-2} + n_4 s_{b-3} \\
&(3) \quad z_b = s_b + t_{b-1} s_{b-1} + t_{b-1} t_{b-2} s_{b-2} + t_{b-1} t_{b-2} t_{b-3} s_{b-3} - t_b s_b \\
&\text{with} \quad s_b = \frac{p x_b y_b}{d_x x_b + d_y y_b^2}
\end{aligned} \tag{5.21}$$

As previously, index b indicates the box number. The expression s_b describes the O_3 concentration when no transport occurs and is computed by the simplified three component chemistry (compare to eq. (5.4)). Linear combination (1) describes the case that z_b is mainly determined by the simplified three component chemistry s_b in the same box b. The influences of the remaining boxes are regarded by adding the O_3 changes (caused by different chemical states of the three component chemistry in each box) multiplied with transport coefficients. Linear combination (2) adds the O_3 concentration determined by the three component chemistry in each box linearly to z_b. Linear combinations (1) and (2) of eqs. 5.21 assume that each box contributes to z_b with constant transport coefficients. In contrast, linear combination (3) assumes that the transport coefficients between the boxes are constant. For example, the

O_3 concentration determined by the three component chemistry in box $b-2$ (s_{b-2}) contributes to z_b by multiplying the transport coefficients of these boxes which s_{b-2} has to cross ($t_{b-1}t_{b-2}$). The transport coefficients (a,b,c) of linear combination (1), (n_1, n_2, n_3, n_4) of linear combination (2) and (t_1, t_2, t_3, t_4) of linear combination (3) are determined by analytically solving the eqs. (5.21).

Subsequently, a LUT is set up with the 4-box-model. The additional NO_x emission is increased seven times in each of the four boxes and the corresponding O_3 concentrations in each box is computed with the 4-box-model. These 28 simulations deliver the input for the LUT. For each data point in the LUT, the transport coefficients are computed.

For linear combination (3), the numbers of transport coefficients become complex. Thus, this linear combination is not reasonable. The results of linear combinations (1) and (2) are presented in fig. 5.8. As fig. 5.8 shows, the transport coefficients of the linear combinations (1) and (2) scatter broadly. In particular, the transport coefficients of linear combination (1) vary strongly. They even change their signs. Although the transport coefficients of linear combination (2) differ not as strongly (values deviate from the mean by less than 45 %), the variation is still too large to ensure a reliable determination of z.

Consequently, all three linear combinations in eqs. (5.21) fail to produce confident transport coefficients. Hence, they are not able to fulfil requirement (1) and compute the correct O_3 concentration of an emission scenario. This is explained as the analytical solution of z (eq. 5.10) can not be split up into a linear combination of the form eq. (5.20). The pre-factor $(\gamma_1\gamma_2\gamma_3\gamma_4 - T^4)^{-1}$ in eq. (5.10) depends on x_b and y_b of all four boxes. Hence, a splitting up into four individual terms $f(x_b, y_b)$ which depend only x_b and y_b of one box b, as proposed in eq. (5.20), is not possible.

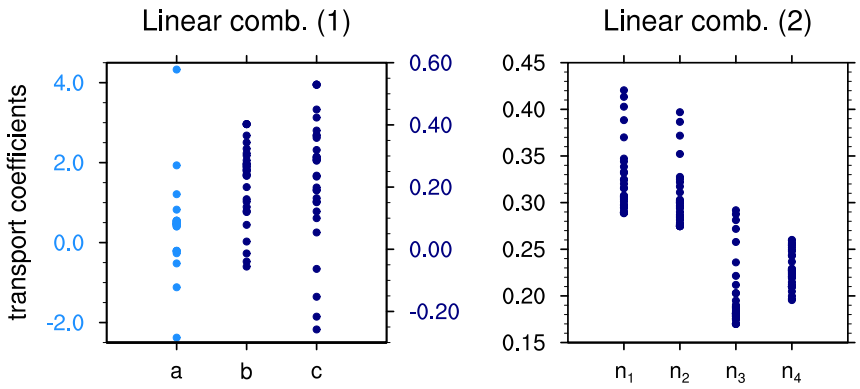

Figure 5.8: Transport coefficients (a,b,c) and (n_1, n_2, n_3, n_4) for linear combination (1) and (2). Note the different axis for the transport coefficient a compared to b and c.

5.3.3.2. Coupled linear equation system

The second approach separates the non-linear O_3 chemistry and the transport processes. By means of a coupled linear equation system, this algorithm determines the O_3 concentrations which are compared to the original values obtained by the 4-box-model (requirement (1), sect. 5.2).

At first, the concentrations of the precursors $\vec{x}$ and $\vec{y}$ are computed by eqs. (5.19). Subsequently, the approach assumes that in equation system (5.7) the transport T is known. It is supposed that the transport T can be deduced directly from source-receptor relations in the 4-box-model. Then, only the behaviour of the ozone chemistry in equation system (5.7) is unknown and needs to be determined. In the following, the ozone chemistry is indicated with the function $C_b(x_b, y_b, z_b)$. For example, derived from the simplified O_3 chemistry (eq. 5.1 and 5.2), it is assumed that the chemistry function can be written as a polynomial function:

$$C_b(x_b, y_b, z_b) = a_0 x_b y_b + a_1 y_b^2 z_b + a_2 x_b z_b \tag{5.22}$$

with parameters a_i which need to be determined. $C_b(x_b, y_b, z_b)$ describes the simplified three component chemistry (eq. 5.3). Thus, the temporal evolution of $\vec{z}$ (equation system 5.7) is set to steady-state and is rewritten in a matrix notation:

$$\begin{pmatrix} x_b y_b & y_b^2 z_b & x_b z_b & \cdots \\ \vdots & \vdots & \vdots & \vdots \end{pmatrix} \cdot \begin{pmatrix} a_0 \\ a_1 \\ a_2 \\ \vdots \end{pmatrix} = \begin{pmatrix} -T z_b + T z_{b-1} \\ \vdots \end{pmatrix} \tag{5.23}$$

The index $b-1$ indicates the previous box $b-1$ of box b. For example, the previous box of box 1 is the box 4. Thus, the equation system is shortly written as:

$$\boldsymbol{K} \cdot \vec{a} = \vec{d} \tag{5.24}$$

The vector $\boldsymbol{K} \cdot \vec{a}$ describes the chemistry. The vector $\vec{a}$ contains the unknown parameters. The vector $\vec{d}$ denotes the O_3 transport from one box to the next. However, this linear equation system (5.24) is under-determined (as for 4 boxes 4 equations with 12 unknown parameters need to be solved). To obtain all parameters a_i in $\vec{a}$, it is necessary to combine several 4-box-model simulations with different initial conditions (for example, simulations with different additional NO_x emissions):

$$\begin{aligned} \boldsymbol{K_1} \cdot \vec{p_1} &= \vec{d_1} \\ \boldsymbol{K_2} \cdot \vec{p_2} &= \vec{d_2} \\ &\vdots \\ \boldsymbol{K_n} \cdot \vec{p_n} &= \vec{d_n} \end{aligned} \tag{5.25}$$

The index indicates the different 4-box-model simulations. The number of simulations n equals the size of $\vec{a}$, i.e. the number of unknown parameters (in this example 12). Thus, the equation system (5.25) is rewritten as

$$\boldsymbol{M} \cdot \vec{A} = \vec{D} \tag{5.26}$$

Finally, the linear matrix equation (5.26) is solved analytically to obtain the solution of $\vec{A}$. Subsequently, $\vec{z}$ is determined for any emission scenario.

In the following, the results of $\vec{z}$ computed by eq. (5.26) are tested with the 4-box-model whether they correspond to the original $\vec{z}$. Usually, the chemistry function $C_b(x_b, y_b, z_b)$ in eq. (5.22) is not as well known as in the 4-box-model. Therefore, three different polynomial functions are chosen which are assumed to described the main aspects of the O_3 chemistry:

$$\begin{aligned}
\text{poly1: } C_b(x_b, y_b, z_b) &= a_0 x_b y_b + a_1 x_b z_b + a_2 y_b^2 z_b \\
\text{poly2: } C_b(x_b, y_b, z_b) &= a_0 x_b y_b + a_1 x_b z_b + a_2 y_b z_b + a_3 x_b^2 z_b + a_4 y_b^2 z_b \\
\text{poly3: } C_b(x_b, y_b, z_b) &= a_0 + a_1 x_b + a_2 y_b + a_3 x_b y_b + a_4 x_b^2 + a_5 y_b^2 \\
&\quad + a_6 z_b + a_7 x_b z_b + a_8 y_b z_b + a_9 x_b y_b z_b + a_{10} x_b^2 z_b + a_{11} y_b^2 z_b
\end{aligned}$$

The polynomial poly1 describes the simplified O_3 chemistry used in the 4-box-model (see eq. 5.3). The polynomial poly2 represents also a similar non-linear system as poly1, but x_b and y_b contribute equally to the chemistry function $C_b(x_b, y_b, z_b)$. Furthermore, poly3 denotes a polynomial function which is symmetric in x_b and y_b. Thus, it describes a chemistry function $C_b(x_b, y_b, z_b)$ when only little information about O_3 chemistry is available.

To solve eq. (5.26) for the three chemistry functions $C_b(x_b, y_b, z_b)$, a LUT needs to be set up. Therefore, simulations with the 4-box-model are performed by varying the additional emissions of $\vec{x}$ and $\vec{y}$. For poly1, 3 simulations with the 4-box-model are needed to solve the coupled linear equation system; hence 3 simulations are taken as input for the LUT. For poly2 and ploy3, 5 and 12 simulations are needed. Subsequently, eq. (5.26) is solved for the three chemistry functions $C_b(x_b, y_b, z_b)$ and three sets of parameters $\vec{A}$ are computed.

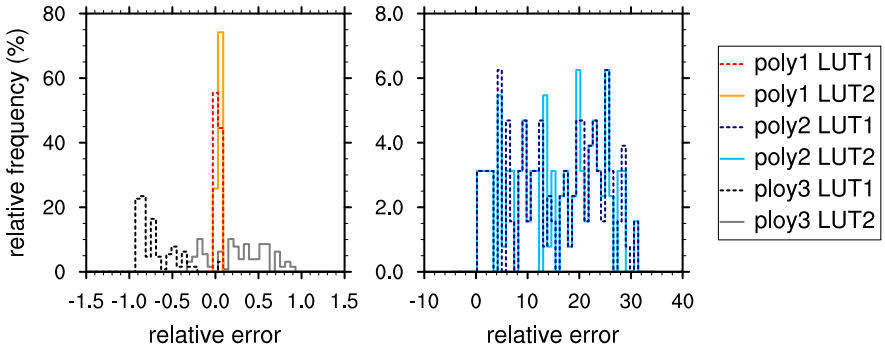

Figure 5.9: Relative frequency distribution of the relative errors of $\vec{z}$ determined by eq. 5.26 for three polynomial functions (poly1, poly2, poly3) and the original $\vec{z}$ values determined by 4-box-model. Given are the distributions for two different LUT (LUT1 and LUT2). Note that the relative errors of poly2 are divided by 10.

Subsequently, the computed parameters $\vec{A}$ are used to determine the O_3 concentrations $\vec{z}$ for the three chemistry functions (poly1, poly2, poly3) by eq. (5.26) for 32 emission scenarios. The obtained values of $\vec{z}$ are compared with the orignial values for the same 32 emission scenarios computed by the 4-box-model. Fig. 5.9 shows the resulting relative errors. As can be seen in fig. 5.9, the relative errors vary strongly with the chosen polynomial. The polynomial poly1 obtains very good results since it corresponds very well with the underlying three component O_3 chemistry (compare to eq. (5.7)). However, poly2 and poly3 deviates largely. This shows that $\vec{z}$ strongly depends on the chosen chemistry function $C_b(x_b, y_b, z_b)$. For polynomials with more than 5 terms, the determinant of $\boldsymbol{M}$ becomes close to 0. Then, $\boldsymbol{M}$ is a singular matrix and not invertible any more. Thus, eq. (5.26) can not be solved. Furthermore, fig. 5.9 shows the relative errors for different LUT. Here, different emission variation simulations performed with the 4-box-model are used as input for the LUT to determine $\vec{A}$ with eq. (5.26) for poly1, poly2 and poly3. Each LUT for each polynomial produces different results for $\vec{z}$ and thus also different relative frequency distributions. This shows that the results strongly vary with the chosen polynomial function $C_b(x_b, y_b, z_b)$ and with the simulations taken as input for the LUT to train eq. (5.26). Hence, this method does not deliver reliable results for O_3 and thus does not fulfil requirement (1) (sect. 5.2). The approach of a coupled linear equation system is therefore discarded.

5.3.3.3. Iteration method

The third approach also tests whether the O_3 chemistry and transport processes can be split up. It determines the O_3 concentration by an iteration method. The approach is tested within the 4-box-model and examines whether it satisfies requirement (1) stated in sect. 5.2.

The temporal evolution of $\vec{z}$ (equation system 5.7) is split up in a chemistry term C_b describing the net O_3 production in box b and a transport term $\hat{T}$:

$$f_b(\vec{z}) = \frac{dz_b}{dt} = C_b(x_b, y_b, z_b) + \hat{T}(z_b, z_{b-1}) \tag{5.27}$$

The transported z depends on the considered box z_b itself and its previous box z_{b-1}. Hence, for 4 boxes, the equation system (5.7) is set to steady-state and is rewritten as:

$$\vec{f}(\vec{z}) = \begin{pmatrix} f_1(\vec{z}) \\ f_2(\vec{z}) \\ f_3(\vec{z}) \\ f_4(\vec{z}) \end{pmatrix} = 0 \tag{5.28}$$

As before, it is assumed that the transport $\hat{T}$ is known and can be deduced from source-receptor relations in the 4-box-model (and later in EMAC). Thus, it is only necessary to determine the function $C_b(x_b, y_b, z_b)$. To do so, a LUT with the 4-box-model is set up for $C_b(x_b, y_b, z_b)$ for each box b. Therefore, the additional emissions of VOC $\overrightarrow{E^{x,add}}$ and NO_x $\overrightarrow{E^{y,add}}$ are varied in each box b. The resulting net O_3 production is used as input for the LUT.

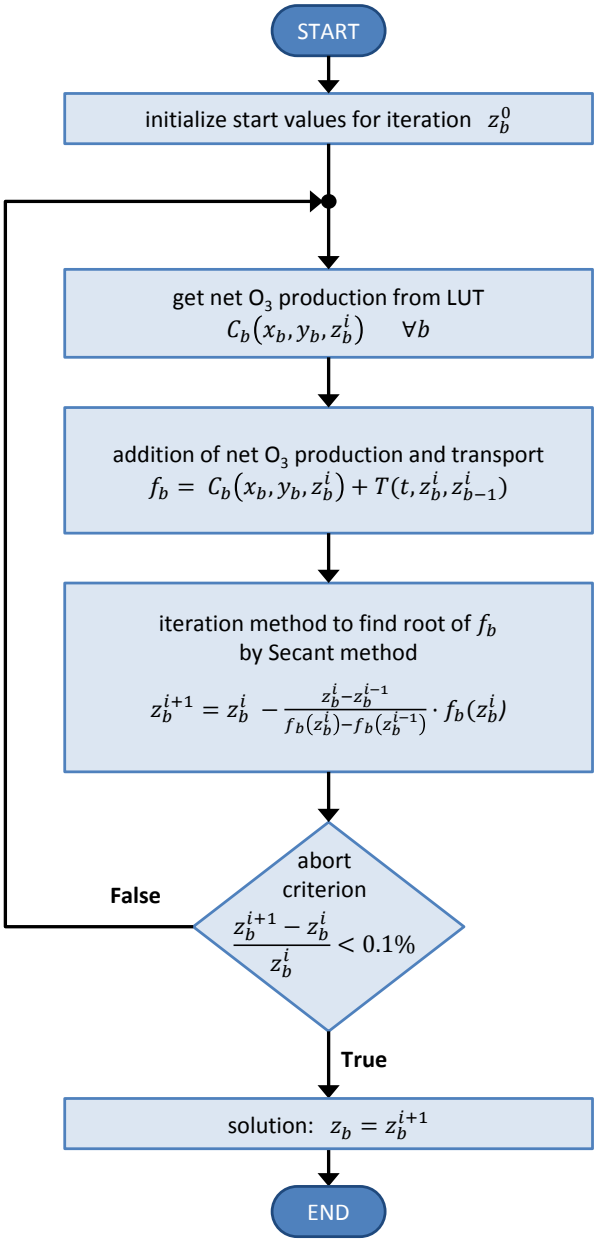

Figure 5.10: Flow chart of the iteration method. The precursors x_b and y_b are determined for a specific emission scenario after eq. (5.19). The index b indicates the box number.

Thus, to obtain $\vec{z}$, one needs to find the root of the equation system $\vec{f}(\vec{z}) = 0$. There are several options for finding the root of an equation system. In this study, the iterative Secant method (e.g. Hanke-Bourgeois, 2009) is chosen because it does not need the derivative of the function f_b (compared to the Newton method). It solves eq. 5.28 by:

$$z_b^{k+1} = z_b^k - \frac{z_b^k - z_b^{k-1}}{f_b(\vec{z}^{\,k}) - f_b(\vec{z}^{\,k-1})} \cdot f_b(\vec{z}^{\,k}) \tag{5.29}$$

To derive $\vec{z}$ for a specific emission scenario, the precursors $\vec{x}$ and $\vec{y}$ are computed according to eq. (5.19) first. Subsequently, $\vec{z}$ is determined as presented in the flow chart (fig. 5.10) and explained in the following: After setting an initial value for $\vec{z}^{\,0}$, the respective net O_3 productions C_b for each box b is searched in the corresponding LUT by linear interpolation. Then, eq. (5.28) is solved for $\vec{z}^{\,i+1}$ by the Secant method. The following iteration step searches again the corresponding $C_b(x_b, y_b, z_b)$ in the LUT for the new $\vec{z}^{\,i}$ and solves again eq. (5.28). The iteration continues until the change per iteration step is less than a certain threshold. In this case, the iteration loop is aborted once the relative change in $\vec{z}$ is less than 0.1 %.

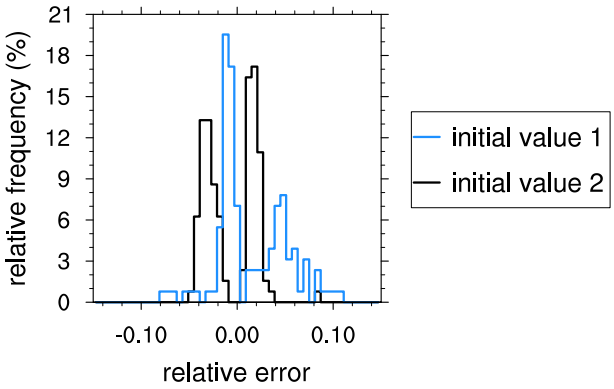

Figure 5.11: Relative frequency distribution of the relative errors of $\vec{z}$ determined after the iteration method. Shown are the distributions for two different initial values.

Fig. 5.11 shows the relative frequency distribution of the relative errors between $\vec{z}$ determined after the iteration algorithm and the original values directly calculated with the 4-box-model for 32 emission scenarios. The distribution for two initial values are shown. The initial value 2 is decreased by 30 % compared to value 1. In this example, the LUT for $C_b(x_b, y_b, z_b)$ has a high resolution containing 1000 entries. Overall, this algorithm produces good results. The deviations are less than 15 %. However, the results obtained by the Secant method depends on the initial value. Moreover, further iteration steps will not improve the precision of the results. As the Secant method approaches the root, z_b^k and z_b^{k-1} as well as $f_b(\vec{z}^{\,k})$ and $f_b(\vec{z}^{\,k-1})$ become almost equal. Subtracting two nearly equal numbers leads to a loss of significance.

This algorithm produces good results in the 4-box-model and is worth further considerations. However when transferring this iteration method to a global chemistry climate model such as EMAC, the determination of the transport coefficients T becomes problematic. For four boxes which are ordered meridional around the Earth (like the 4-box-model) there are four different transport coefficients T which are to be determined. However, if the system is extended to 8 boxes (4 meridional and 2 zonal), 12 transport coefficients need to be determined. Thus, an under-determined equation system is formed. Hence, it is not possible to deduce the transport coefficients from only one simulation. To obtain the transport coefficients it is necessary to combine several simulations. The more boxes are used, the more the equation system becomes under-determined. Thus, more simulations need to be combined. As was shown in sect. 5.3.3.2, the combination of several simulations may be misleading. Hence, this approach is also discarded.

5.3.3.4. Inter- and extrapolation within look-up table

The algorithm approach "Coupled linear equation system" (sect. 5.3.3.2) and "Iteration method" (sect. 5.3.3.3) showed that a separation of chemistry and transport is not promising. Therefore, the forth approach checks the applicability of inter- and extrapolations within a look-up table. The possibility to extrapolate outside of the range of emission scenarios, which were used to train the LUT, enables to extend the applicability of TransClim.

As the magnitude of O_3 changes is particularly important for this approach, it is not tested in 4-box-model but in the global chemistry climate model EMAC (see sect. 3). This enables to base the inter- and extrapolation on realistic magnitudes of O_3 chemistry and transport effects. The specific EMAC simulation setup used here is explained in sect. 3.3. However for this analysis, a coarse resolution of T21L19 (approximately $5.6° \times 5.6°$ Gaussian grid in horizontal dimensions and 19 vertical levels up to 10 hPa) is used to save computational resources. To obtain the regional effects of the O_3 chemistry and the transport, two small and close boxes or emission regions are chosen: Western and Eastern Europe (see appendix A.5). In each emission region, road traffic emissions of NO_x and VOC are varied and simulations are performed with EMAC: road traffic emissions of NO_x and VOC are scaled with scaling factors between 0 and 3. A sketch of the resolution of these emission variation simulations is also given in the appendix A.5. These emission variation simulations deliver input for the LUT.

Table 5.1 presents four different methods of interpolating within the LUT. For each method, the emission variation simulations performed with EMAC are combined in a different way to serve as input for the LUT. The methods and the corresponding LUT are explained in the following:

1. For the first method "Linear interpolation", the LUT contains four dimensions: emissions of x and y for the two boxes Western Europe (1) and Eastern Europe (2). The method interpolates linearly within this LUT to obtain z. No extrapolation for emissions outside the LUT is possible. As the LUT general contains an irregular grid, this method becomes very slow when the dimension of the LUT increases.

2. The second method "Addition of LUT" consists of several LUT: each box owns its LUT. The LUT contains then only two dimensions. After interpolating linearly within one LUT of a box, the corresponding changes of z are added to the reference z. However, an extrapolation to emission variations outside the LUT is not possible.

3. The third method "Fit spline" bases on one LUT containing all emission variations of both boxes (as method (1)). It fits a multidimensional spline to the data in the LUT by applying generalised additive models. An extrapolation of the data outside the regime of the LUT is possible.

4. The forth method "Fit function" adds the change of z (Δz_b) in each box to the reference value. Δz_b for each box b is obtained by fitting the data per box to the function

$$\Delta z_b = \frac{a_1 \cdot \Delta E_b^x \cdot \Delta E_b^y}{a_2 \cdot \Delta E_b^x \cdot \Delta E_b^x + a_3 \cdot \Delta E_b^y} \tag{5.30}$$

which resembles the three component O_3 chemistry of sect. 5.3.1. However, the NO_x and VOC concentration is replaced with the corresponding emissions. This method enables also an extrapolation.

	Method	LUT design	Extra-polation	Mean deviations in 10^{-3}	
				(a)	(b)
1.	Linear interpolation	$z = LUT(E_1^x, E_1^y, E_2^x, E_2^x)$	no	-0.059	-2.3
2.	Addition of LUT	$z = z^{ref} + \Delta z_1 + \Delta z_2$	no	-0.052	0.0028
		$\Delta z_b = LUT(E_b^x, E_b^y)$			
3.	Fit spline	$z = LUT(E_1^x, E_1^y, E_2^x, E_2^x)$	yes	-0.094	-0.022
4.	Fit function	$z = z^{ref} + \Delta z_1 + \Delta z_2$	yes	0.88	-1.7
		$\Delta z_b = \frac{a_1 \Delta E_b^x \Delta E_b^y}{a_2 (\Delta E_b^x)^2 + a_3 \Delta E_b^y}$			

Table 5.1: Concepts of interpolating within LUT. As an example, only two boxes Western Europe (1) and Eastern Europe (2) are considered. The last two columns show the mean relative deviations of emission scenarios (a) and (b) indicated in fig. 5.12.

Fig. 5.12 shows the relative frequency distribution of the relative errors between O_3 derived from the four interpolation methods and O_3 directly derived from EMAC simulations for two different emission scenarios: In example (a) road traffic emissions of NO_x and VOC are scaled with 1.2 and 0.8 in Western and Eastern Europe to demonstrate the performance of the four interpolation methods under simultaneous increase and decrease of emissions. In example (b) NO_x and VOC road traffic emissions are increased by 2.2 and 2.5 in both emission regions to investigate a strong increase of emissions. Only values for the Northern Hemisphere up to 850 hPa are taken into consideration as most errors are expected to occur in this region. The mean of the relative deviations for emission scenarios (a) and (b) are indicated in table 5.1.

Method (4) "Fit Function" shows the largest errors in both emission scenarios. Moreover, this method strongly depends on the chosen function in eq. (5.30). Method (1) "Linear interpolation" gives good results in the emission scenario (a), but fails for emission scenario (b). Very good results (average relative errors below $9 \cdot 10^{-5}$) are delivered by method (3) "Fit spline". However, method (2) "Addition of LUT" produces the best results (average relative errors below $5 \cdot 10^{-5}$) and thus fulfils requirement (1): it reproduces the total O_3 concentration very well. Hence, this method will be used as a solution algorithm for TransClim.

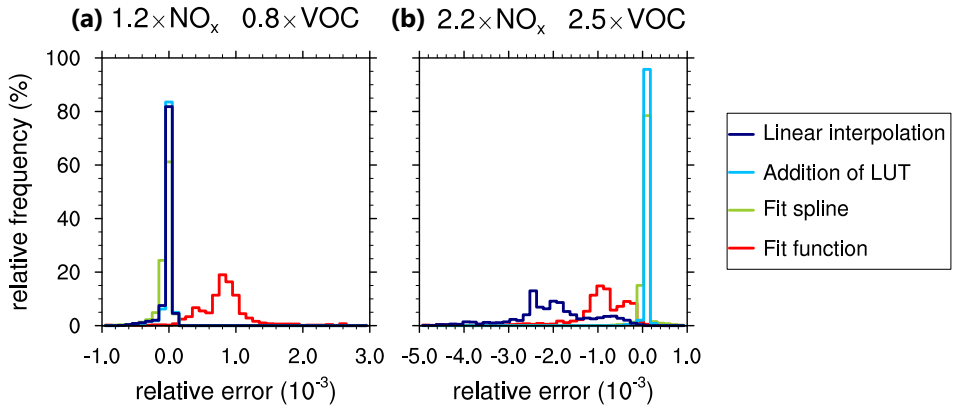

Figure 5.12: Relative frequency distribution of the relative errors of O_3 determined after the four interpolation methods indicated in table 5.1 and original values from EMAC simulations. As an example, two emission scenarios are presented: (a) 1.2×NO_x, 0.8×VOC (b) 2.2×NO_x, 2.5×VOC emission scaling in Western and Eastern Europe simultaneously.

5.3.4. TransClim's algorithm

The previous sect. 5.3.3 tested different solution algorithms whether they fulfil requirements (1) (see sect. 5.2). Finally, the method "Addition of LUT" was identified to produce very good results, i.e. very small errors of 1 ‰. This section assesses how well the remaining requirements formulated in sect. 5.2 are fulfilled.

Fig. 5.13 shows a sketch of the method for only two emission regions (e.g. Western and Eastern Europe) and for only two road traffic emission species NO_x and VOC. For each emission region, a LUT with the emission scaling factor for NO_x, VOC and CO road traffic emissions ($sNOx$, $sVOC$, sCO) is created to determine the variable change ($x - x^{ref}$):

$$\Delta x(i) = x(i) - x^{\mathrm{ref}}(i) = \mathrm{LUT}\,(\ sNOx(i),\quad sVOC(i),\quad sCO(i)\ )$$

The emission scaling factor indicates the factor by which the reference emission is scaled. Thus, each LUT has three dimensions (in fig. 5.13, two dimensions). To obtain the new variable x^{new} for an emission scenario, the change $\Delta x(i)$ for each emission region i is obtained by linearly interpolating within the respective LUT. Finally, the computed $\Delta x(i)$ is added to the reference x^{ref} (see fig. 5.13). This method is performed for all grid boxes of an EMAC simulation. Thus, it

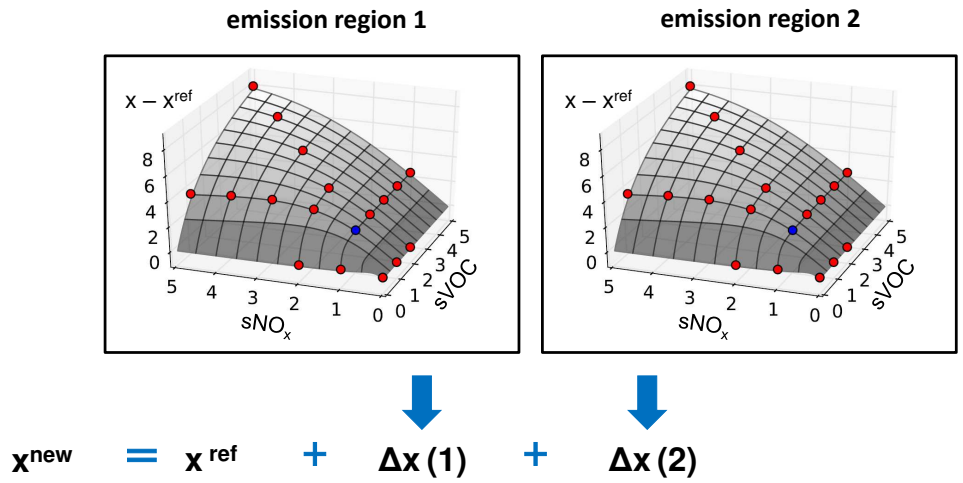

Figure 5.13: Sketch of interpolation algorithm in TransClim. For each emission region a LUT contains the change in variable x ($x - x^{\mathrm{ref}}$) and the emission scaling factors for NO_x and VOC emissions ($sNOx, sVOC$). The blue dot indicates the reference simulation ($sNOx = 1, sVOC = 1$). The red dots indicate the emission variation simulations performed with EMAC. After linearly interpolating within the LUT of each emission region i, the resulting changes $\Delta x(i)$ are added to reference x^{ref}. This procedure is performed for every grid box. The variable x can be one- or multidimensional.

applies for 1 dimensional variables, such as global radiative forcing, as well as for multidimensional variables, such as the O_3 concentration.

This approach offers a fast algorithm. It takes about 15 minutes to calculate the climate effect of an emission scenario in one emission region (with 3 dimensional variables). For the determination of O_3 the algorithm obtains very good results: the computed O_3 concentration deviates only little from the original values (less than 1 ‰ see fig. 5.12). Moreover, this method fulfils most requirements formulated in sect. 5.2. Although, the method is only tested for NO_x and VOC road traffic emissions, it is easily expendable to CO road traffic emissions (requirement 1). Furthermore, the method is not only applicable for the determination of O_3, but also for other variables such as road traffic O_3^{tra}, methane CH_4 as well as the radiative forcings of O_3 and road traffic ${O_3}^{tra}$ (requirement 1, 5 and 6). By interpolating within the LUT, the non-linearity of tropospheric O_3 chemistry is regarded (requirement 2). The transport effects, which are linear, are taken into account by adding $\Delta x(i)$ of each emission region to x^{ref}. Each emission region has its own LUT, so the effect of different emission regions is considered (requirement 3). Since the method is applied to each grid box of an EMAC simulation, it is also possible to determine the pattern of O_3 and O_3^{tra} (requirement 4). Moreover, road traffic emissions modify CH_4 lifetime which affects CH_4 concentration on a longer time scale compared to O_3. Hence, the determination of the radiative forcing of CH_4 and road traffic CH_4^{tra} as well as its dependence on the CH_4 background requires different tools which are explained in sect. 5.5 (requirement 6 and 7).

However, the consideration of O_3 background is not given with the current approach (requirement 7). The emission variation are bound to a specific base year with a certain O_3 background. Varying the road traffic emissions for this base year results in specific O_3 changes. Since the tropospheric O_3 chemistry is strongly non-linear, varying the road traffic emissions for different O_3 background may result in a complete different O_3 change. The influence of the O_3 background concentration will be regarded in future studies.

5.4. Setup of lookup table

After a suitable algorithm for TransClim was found in sect. 5.3, the following section describes the procedure of how the lookup-table (LUT) for TransClim is set up. At first, seven emission regions are defined in sect. 5.4.1. Subsequently, the specific emission variations performed with EMAC are described in sect. 5.4.2.

5.4.1. Emission regions

To determine the effect of road traffic emissions from different emission regions, seven emission regions are defined (fig. 5.14): Germany, Western Europe, Northern Europe, Eastern Europe, Southern Europe, North America and Asia. One single emission region is dedicated to Germany as road traffic emission scenarios in Germany are used for evaluating TransClim (sect. 5.6.2) as well as to demonstrate the applicability of TransClim (sect. 6.1). The borders of the emission region Germany are chosen carefully so that the neighbouring countries extend only little into

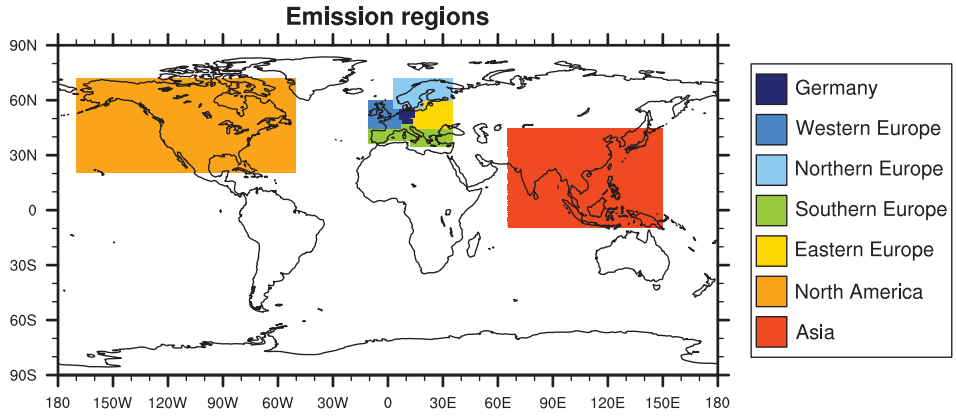

Figure 5.14: Seven emission regions which are defined for the LUT of TransClim.

this region. The emission region Western Europa contains most of France, Great Britain and Ireland. Scandinavia is merged to Northern Europe. Eastern Europe consists of not only the Eastern European countries but also some parts of the Baltic countries: Slovenia, Croatia, Romania and the Northern part of Bosnia and Herzegovina and Serbia. The emission region Southern Europe contains the whole European Mediterranean such as Iberian Peninsula, Italy, the Southern Baltic countries, Greece, Cyprus and the Western Turkey. The region North America merges USA, Canada, the Northern Mexico and Cuba. The emission region Asia contains India, Pakistan, China, Japan, the South-East Asian countries as well as Indonesia, Malaysia and Papa New Guinea.

Table 5.2 gives the road traffic emission inventories of NO_x, CO and VOC for the seven emission regions, the remaining part of the world and the global values derived from the emission inventory MACCity (see sect. 3.4; Granier et al., 2011). The emission region Germany has low VOC road traffic emissions of only 0.09 Tg(C) yr^{-1} compared to the other European emission regions. Eastern and Southern Europe presents high CO road traffic emission of about 4 Tg(CO) yr^{-1}. In general, the emission regions North America and Asia show high road traffic emissions which correlates to their large domains they cover. The global road traffic emissions for NO_x are 20.31 Tg(NO) yr^{-1}, for CO 145.80 Tg(CO) yr^{-1} and for VOC 17.22 Tg(C) yr^{-1}.

Russia, Australia, Africa and South America are not considered yet as they are not the main focus of this study. Nevertheless, it is easy to expand the LUT to include further emission regions.

	NO_x in Tg(NO) yr^{-1}	CO in Tg(CO) yr^{-1}	VOC in Tg(C) yr^{-1}
Germany	0.486	1.148	0.089
Western Europe	0.730	2.331	0.205
Northern Europe	0.342	0.831	0.167
Eastern Europe	0.561	4.245	0.408
Southern Europe	0.839	4.050	0.430
North America	4.473	35.829	1.276
Asia	5.853	37.371	8.289
Rest of the world	7.027	59.991	6.348
GLOBAL	20.311	145.796	17.222

Table 5.2: Road traffic emissions per emission regions for the year 2010 derived from the emission inventory MACCity (see sect. 3.4; Granier et al., 2011). Global emissions are given in the last row.

5.4.2. Emission variation simulations with EMAC

To obtain the data points for the LUT, simulations with the global chemistry climate model EMAC (sect. 3) are performed. The specific setup of the EMAC simulations is described in sect. 3.3. The emission inventory for EMAC is split up into the seven emission regions indicated in fig. 5.14. The implementation in EMAC is described in appendix A.6. The emission scaling factors are set in the MESSy run script `xmessy_mmd_TransClim_LUT`.

At first, a reference simulation is set up. Therefore, an EMAC simulation with

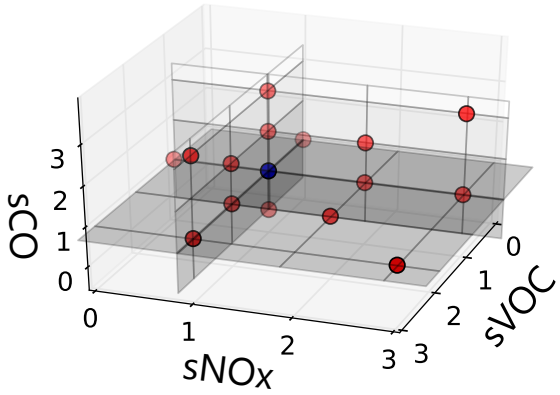

Figure 5.15: Scheme of variation of NO_x, VOC and CO road traffic emission for each emission region. Presented are the emission scaling factors sNOx, sVOC and sCO. The reference simulation is indicated by a blue circle and has emission scaling factors for NO_x, VOC and CO of 1.

all emission scaling factors ($sNOx, sVOC, sCO$) in all emission regions are set to 1. Subsequently, $sNOx, sVOC$ and sCO are varied in each of the seven emission regions while the factors in the residual regions are set to 1. The schematic in fig. 5.15 shows the principle of emission variations for the three species for one emission regions. It is too computational expensive to span the whole space for the emission scaling of NO_x, VOC and CO. Thus, only two emission scaling factors are varied at the same time while the third factor is kept constant at 1. Emission scaling factors between 0 (corresponding to a total reduction of the emission) and 3 (corresponding to a triplication of the emission) are chosen. Additionally, an emission variation simulation with $sNOx, sVOC$ and sCO set to 0 in each emission region is performed. In appendix A.7, table A.3 presents a list of the emission variation simulations per emission region used in this thesis.

5.5. Model description of TransClim

This section describes the implementation of the chemistry-climate response model TransClim. Fig. 5.16 shows a flow chart of the calculation steps performed in TransClim. To prepare a simulation with TransClim, the output of the emission variation simulations performed with EMAC (as described in sect. 5.4.2) is read in first. Table 5.3 indicates the necessary input data for TransClim. For the reference and emission variation simulations, ozone (O_3), road traffic ozone ($O_3{}^{tra}$), methane (CH_4), methane loss by OH (CH4loss) and methane loss by OH^{tra} (CH4losstra) are read in. Furthermore, stratospheric adjusted solar and thermal fluxes of the 2nd radiation call in EMAC (flxs(rad02) and flxt(rad02)) are read in as well. These fluxes correspond to ozone field which is modified by the emission variation (see EMAC model setup sect. 3.3). TransClim also reads in the stratospheric adjusted solar and thermal radiation fluxes of the 3rd radiation call (flxs(rad03) and flxt(rad03)). They represent the radiation fluxes due to the field (O_3 – $O_3{}^{tra}$). The general setup of the EMAC simulations is described in sect. 3.

Subsequently, lifetime of CH_4 and $CH_4{}^{tra}$ is computed by the following relation:

$$\tau_{CH4} = \frac{m(CH4)}{m(CH4loss)} \tag{5.31}$$

$$\tau_{CH4tra} = \frac{m(CH4)}{m(CH4losstra)} \tag{5.32}$$

with $m(CH4), m(CH4loss)$ and $m(CH4losstra)$ being the tropospheric mass of CH_4, CH4loss and CH4losstra. The lifetimes are only calculated for the tropospheric domain as over 90 % of CH_4 is destroyed in the troposphere (Ciais et al., 2013). Additionally, the net radiative fluxes due to O_3 and $O_3{}^{tra}$ (flxn(O_3) and flxn($O_3{}^{tra}$) are determined:

$$flxn(O_3) = flxs(rad02) + flxt(rad02) \tag{5.33}$$

$$flxn(O_3 - O_3^{tra}) = flxs(rad03) + flxt(rad03) \tag{5.34}$$

$$flxn(O_3^{tra}) = flxn(O_3) - flxn(O_3 - O_3^{tra}) \tag{5.35}$$

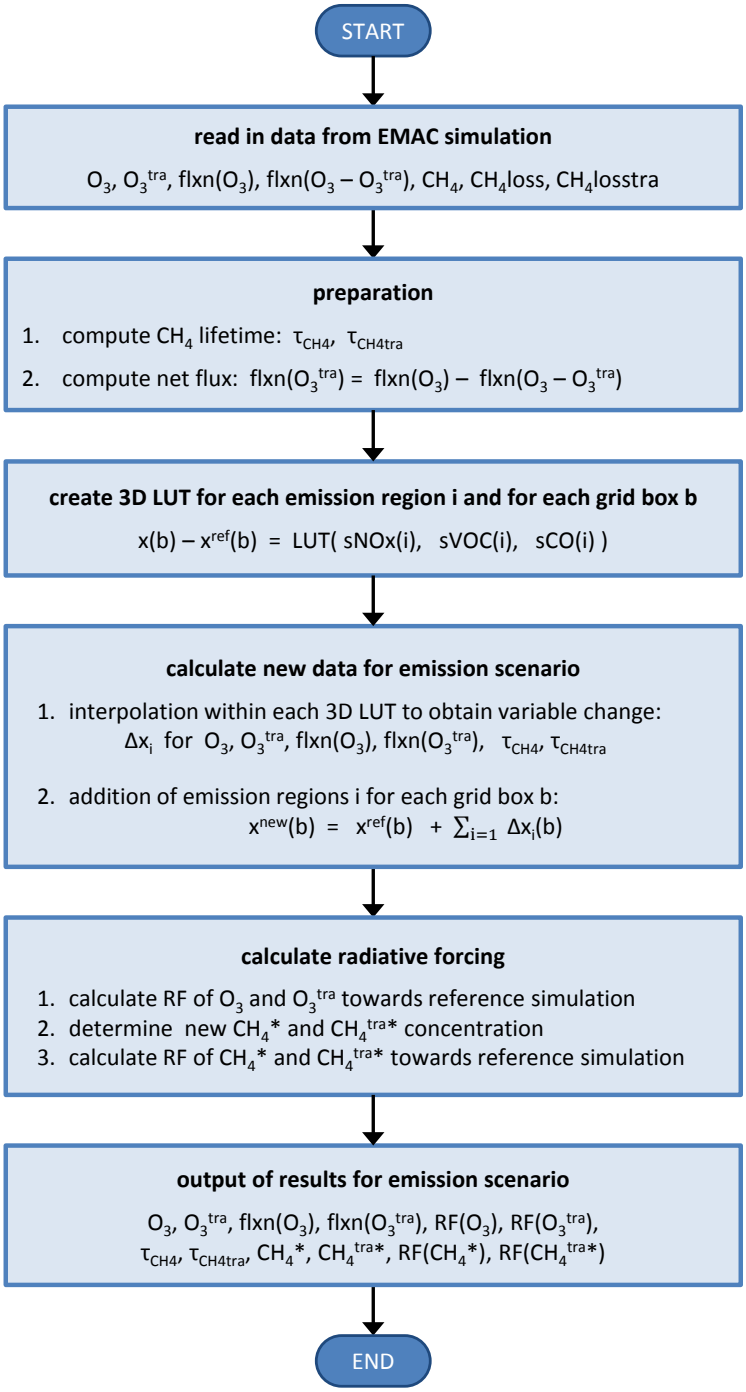

Figure 5.16: Flow chart of TransClim showing the main steps.

In the following step, TransClim creates three dimensional LUT with the dimensions $sNOx$, $sVOC$ and sCO representing the variable change $x - x^{ref}$ for each emission region and each grid box. Two LUT in three dimensional resolution (levels, latitude, longitude) for the variables O_3 and $O_3{}^{\mathrm{tra}}$, two LUT in two dimensional resolution (latitude, longitude) for the net flux flxn(O_3) and flxn($O_3{}^{\mathrm{tra}}$) and two LUT with the tropospheric means of τ_{CH4} and τ_{CH4tra} are produced. In the file `namelist.py` it is possible to set the emission variation simulations (see sect. 5.4.2) per emission region which are used as input for the LUT. The emission variation simulations used in this thesis are specified in appendix A.7. This procedure of creating the LUT for each simulation makes TransClim very flexible: the LUT is easily extendable to more emission variation simulations.

Subsequently, TransClim determines the variables for O_3, $O_3{}^{\mathrm{tra}}$, flxn(O_3) and flxn($O_3{}^{\mathrm{tra}}$), τ_{CH4} and τ_{CH4tra} for an emission scenario by the solution algorithm described in sect. 5.3.4. The emission scenario is set in the file `main.py`. To determine the new variables, the algorithm first linearly interpolates in the corresponding LUT for each variable x of each emission region i to obtain the difference: $\Delta x_i(b) = x(b) - x^{ref}(b)$. Second, the results of each emission region is added to the value of the reference simulation: $x^{new}(b) = x^{ref}(b) + \sum_{i=1}^{n} \Delta x_i(b)$, with n being the number of emission regions (here $n = 7$). For multidimensional variables, this procedure is repeated for all grid boxes b (levels, latitudes and longitudes).

Afterwards, the radiative forcings are determined. For O_3 and $O_3{}^{\mathrm{tra}}$, the radiative forcings are computed by subtracting the reference fluxes from the interpolated ones:

$$RF(O_3) = flxn(O_3^{interpolated}) - flxn(O_3^{ref}) \tag{5.36}$$

$$RF(O_3^{tra}) = flxn(O_3^{tra,interpolated}) - flxn(O_3^{tra,ref}) \tag{5.37}$$

For the radiative forcings of CH_4 and $CH_4{}^{\mathrm{tra}}$, a different procedure has to be applied. The change in lifetimes τ_{CH4} and τ_{CH4tra} caused by the emission scenario modifies the concentration of CH_4 and $CH_4{}^{\mathrm{tra}}$. At first, the new concentrations $CH_4{}^*$ and $CH_4{}^{\mathrm{tra}*}$ (denoted with *) need to be determined. Based on $CH_4{}^*$ and $CH_4{}^{\mathrm{tra}*}$, the respective radiative forcings are then computed. To obtain $CH_4{}^*$ and $CH_4{}^{\mathrm{tra}*}$, the following concepts are chosen:

1. To determine the $CH_4{}^*$ concentration caused the lifetime change of τ_{CH4}, the concept introduced by Grewe and Stenke (2008) is applied. It calculates the change of CH_4 (ΔCH_4) by:

$$\frac{d}{dt}\Delta CH_4 = \frac{\delta}{1+\delta}\tau_{CH4}^{-1} - \frac{1}{1+\delta}\tau_{CH4}^{-1}\Delta CH_4 \tag{5.38}$$

   with δ being the relative change of CH_4 lifetime and CH_4^{BG} being the CH_4 background concentration. The Euler backward method is used to solve the differential equation:

$$\Delta CH_4(t_{n+1}) = \frac{\Delta CH_4(t_n) + h \cdot \frac{\delta}{1+\delta} \cdot \tau_{CH4}^{-1} \cdot CH_4^{BG}(t_{n+1})}{1 + h \cdot \frac{1}{1+\delta} \cdot \tau_{CH4}^{-1}} \tag{5.39}$$

with h being the step size (here h is set to 1 year). The change of CH_4 is calculated for a certain time span, e.g. from pre-industrial time to the year 2100. Then, $CH_4{}^{\mathrm{BG}}$ varies with time. Subsequently, the CH_4 change is added to the CH_4^{BG} concentration to obtain the new concentration $CH_4{}^*$.

2. To determine the contribution $CH_4{}^{\mathrm{tra}*}$ adapted to the lifetime change of τ_{CH4tra}, the method introduced in sect. 4.5 is used. Eq. 4.49 determines the temporal evolution of $CH_4{}^{\mathrm{tra}}$:

$$\frac{\partial}{\partial t} CH_4^{tra} = -\frac{1}{2}\left(\frac{1}{\tau_{CH4tra}} CH_4 + \frac{1}{\tau_{CH4}} CH_4^{tra}\right) \tag{5.40}$$

According to the Euler backward method, $CH_4{}^{\mathrm{tra}*}$ is calculated by:

$$CH_4^{tra*}(t_{n+1}) = \frac{CH_4^{tra}(t_n) - \frac{h}{2} \cdot \tau_{CH4tra}^{-1} \cdot CH_4^{BG}(t_{n+1})}{1 + \frac{h}{2} \cdot \tau_{CH4}^{-1}} \tag{5.41}$$

with h being the step size (set to 1 year). To execute the iteration (eq. 5.41), the start value $CH_4{}^{\mathrm{tra}}(\mathrm{t_0})$ for pre-industrial time (year 1850) is set to zero as there was no emissions from road traffic at that time.

Finally, after the adapted values for $CH_4{}^*$ and $CH_4{}^{\mathrm{tra}*}$ are determined, the corresponding radiative forcings are calculated by the formula based on Ramaswamy et al. (2001):

$$RF(CH_4) = \alpha \cdot \left(\sqrt{M} - \sqrt{M_0}\right) - (f(M, N_0) - f(M_0, N_0)) \tag{5.42}$$
$$f(M, N) = 0.47 \cdot \ln\left(1 + 2.01 \cdot 10^{-5}(MN)^{0.75} + 5.31 \cdot 10^{-15} M (MN)^{1.52}\right)$$

with $\alpha = 0.12$ and M (N) being the CH_4 (N_2O) mixing ratios in ppb. For $CH_4{}^*$, the radiative forcing $\mathrm{RF}(CH_4{}^*)$ is computed with respect to the reference state ($M = CH_4{}^*$, $M_0 = CH_4{}^{\mathrm{ref}}$ in eq. (5.42)). For $CH_4{}^{\mathrm{tra}*}$, the radiative forcing $\mathrm{RF}(CH_4{}^{\mathrm{tra}*})$ is determined by:

$$RF(CH_4^{tra*}) = RF(CH_4^*) - \widetilde{RF} \tag{5.43}$$

$\widetilde{RF}$ is calculated according to eq. (5.42) with $M = CH_4^* - CH_4^{tra*}$ and $M_0 = CH_4^{BG} - CH_4^{tra,ref}$.

In the end, the interpolated values for the emission scenario O_3, $O_3{}^{\mathrm{tra}}$, $\mathrm{flxn}(O_3)$, $\mathrm{flxn}(O_3{}^{\mathrm{tra}})$, $\mathrm{RF}(O_3)$, $\mathrm{RF}(O_3{}^{\mathrm{tra}})$, τ_{CH4}, τ_{CH4tra}, $CH_4{}^*$, $CH_4{}^{\mathrm{tra}*}$ as well as $\mathrm{RF}(CH_4{}^*)$ and $\mathrm{RF}(CH_4{}^{\mathrm{tra}*})$ are written to netCDF output files. Table 5.3 shows an overview of the output variables of TransClim.

Variable		Dimension	Unit
	INPUT OF TRANSCLIM		
ozone O_3	`O3`	lev, lat, lon	mol mol^{-1}
road traffic ozone $O_3{}^{tra}$	`O3tra`	lev, lat, lon	mol mol^{-1}
str. adj. solar flux of O_3 at TOA	`flxs(rad02)`	lat, lon	W m^{-2}
str. adj. thermal flux of O_3 at TOA	`flxt(rad02)`	lat, lon	W m^{-2}
str. adj. solar flux of (O_3-O_3^{tra}) at TOA	`flxs(rad03)`	lat, lon	W m^{-2}
str. adj. thermal flux of (O_3-O_3^{tra}) at TOA	`flxt(rad03)`	lat, lon	W m^{-2}
methane CH_4	`CH4`	lev, lat, lon	mol mol^{-1}
methane loss by OH	`CH4loss`	lev, lat, lon	mol mol^{-1} s^{-1}
methane loss by road traffic OH^{tra}	`CH4losstra`	lev, lat, lon	mol mol^{-1} s^{-1}
	OUTPUT OF TRANSCLIM		
interpolated ozone	`O3`	lev, lat, lon	mol mol^{-1}
interpolated road traffic ozone	`O3tra`	lev, lat, lon	mol mol^{-1}
interpolated str. adj. net flux of O_3 at TOA	`flxn_O3`	lat, lon	W m^{-2}
interpolated str. adj. net flux of $O_3{}^{tra}$ at TOA	`flxn_O3tra`	lat, lon	W m^{-2}
interpolated net radiative forcing O3	`RF_O3`	global mean	W m^{-2}
interpolated net radiative forcing O3tra	`RF_O3tra`	global mean	W m^{-2}
interpolated CH_4 lifetime	`tau_CH4`	tropospheric mean	s
interpolated $CH_4{}^{tra}$ lifetime	`tau_CH4tra`	tropospheric mean	s
adapted $CH_4{}^*$ to lifetime change	`CH4_adp`	global mean	mol mol^{-1}

Continued on next page

Table 5.3 – *Continued from previous page*

Variable		**Dimension**	**Unit**
adapted $CH_4{}^{tra*}$ to lifetime change	`CH4tra_adp`	global mean	mol mol^{-1}
net radiative forcing of $CH_4{}^{*}$	`RF_CH4`	global mean	W m^{-2}
net radiative forcing of $CH_4{}^{tra*}$	`RF_CH4tra`	global mean	W m^{-2}

Table 5.3: Input and output variables of TransClim. All variables are annual means on model levels. The abbreviations lev, lat and lon denote levels, latitudes and longitudes. The abbreviation str. adj. stands for stratospheric adjusted.

5.6. Evaluation of TransClim

After setting up TransClim, the model is evaluated in the following section. Two different evaluations are presented: First, TransClim is directly evaluated with an EMAC simulation. Second, TransClim is compared to the simulations performed in the DLR project VEU1 (Verkehrsentwicklung und Umwelt 1, i.e. Transport and the Environment 1, `www.dlr.de/VEU`; Hendricks et al., 2017).

5.6.1. Direct comparison to EMAC simulation

In this section, a TransClim simulation is directly compared with an EMAC simulation. A specific set of the emission scaling factors for each emission region is chosen in such a way that, based on the LUT used in this thesis (indicated in appendix A.7), a broad range of emission variation is performed. In Germany, only NO_x emissions are reduced. In Western and Northern Europe, the emissions of NO_x, VOC and CO are increased or decreased simultaneously. In contrast, all emissions are enhanced or lowered by the same factor in the regions Eastern and Southern Europe. The values for the emission scaling factors are presented in table 5.4. The road traffic emissions of NO_x, VOC and CO are only changed in Europe to test if the solution algorithm of TransClim also works on a regional scale. Here, the non-linearities of the O_3 chemistry are expected to be larger than on global scale. Hence, this emission scenario with a broad range of emission variation in Europe is expected to be difficult to reproduce with TransClim.

Emission region	**Emission scaling**		
	sNOx	**sVOC**	**sCO**
Germany	0.3	1.0	1.0
Western Europe	0.1	1.0	0.9
Northern Europe	1.6	0.7	1.0
Eastern Europe	1.3	1.3	1.3
Southern Europe	0.5	0.5	0.5
North America	1.0	1.0	1.0
Asia	1.0	1.0	1.0

Table 5.4: Emission scaling factors (factors by which the reference emissions are scaled) for evaluating TransClim simulation with EMAC simulation.

The comparison is performed by using the emission scaling factors of table 5.4 for a simulation with EMAC (described in sect. 3.3) and for a simulation with TransClim (based on the LUT as described in sect. 5.4.2). Fig. 5.17 shows the results of ozone (O_3) and the contribution to ozone (O_3^{tra}) over Europe for the TransClim simulation and the relative difference to the EMAC simulation. The tropospheric O_3 and O_3^{tra} columns (in Dobson units) are shown. At lower latitudes, photolysis rates are generally larger producing more O_3. The differences between

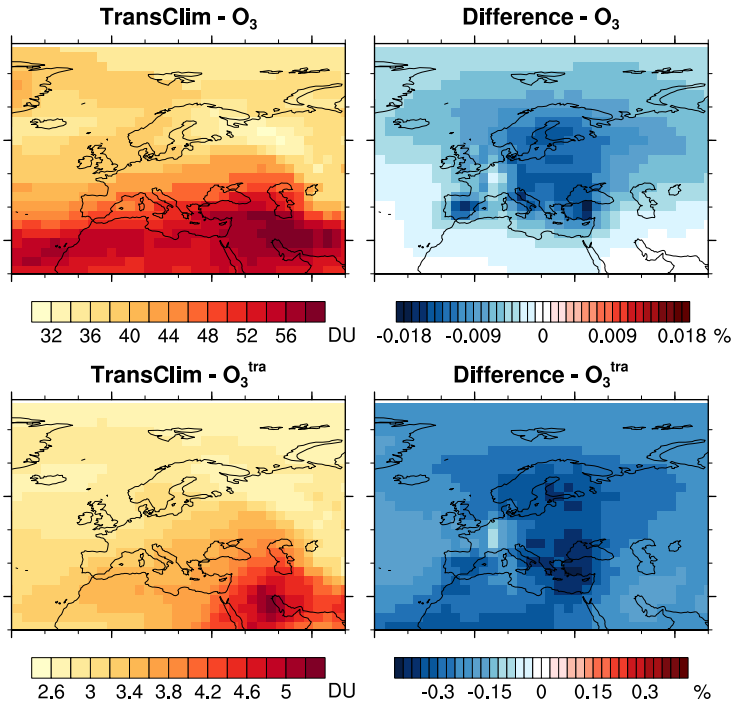

Figure 5.17: Comparison between simulations performed with TransClim and EMAC. Ozone (O_3) and the contribution to ozone ($O_3{}^{tra}$) are shown. Tropospheric ozone (O_3) and road traffic ozone ($O_3{}^{tra}$) columns are given in Dobson unit (DU). The relative differences of the TransClim with respect to the EMAC simulation are shown for the tropospheric columns.

the TransClim and EMAC simulations are very low, i.e. for O_3 the deviations are below 0.018 % and for $O_3{}^{tra}$ below 0.4 %. In general, TransClim underestimates O_3 and $O_3{}^{tra}$ compared to EMAC (the reason for this is explained below). The largest deviations occurs in the Mediterranean and Baltic countries.

The relative differences of ozone (O_3), methane loss (CH4loss) and net flux at top of the atmosphere (flxn(O_3)) as well as the corresponding contributions ($O_3{}^{tra}$, CH4losstra, flxn($O_3{}^{tra}$)) obtained by TransClim in comparison to EMAC are shown in fig. 5.18. (For this simulation, CH4loss and CH4losstra are additionally interpolated by TransClim.) For the tropospheric O_3 column, the largest deviations of -0.018 % are found in Europe and span over the Northern Hemisphere. Generally, TransClim underestimates the CH4loss over whole Europe. Only between the emission regions Western Europe and Germany, small overestimations are observed. For flxn(O_3), almost no change is found. The variables which describe the contribution of road traffic emissions ($O_3{}^{tra}$, CH4losstra, flxn$O_3{}^{tra}$) show larger differences of up

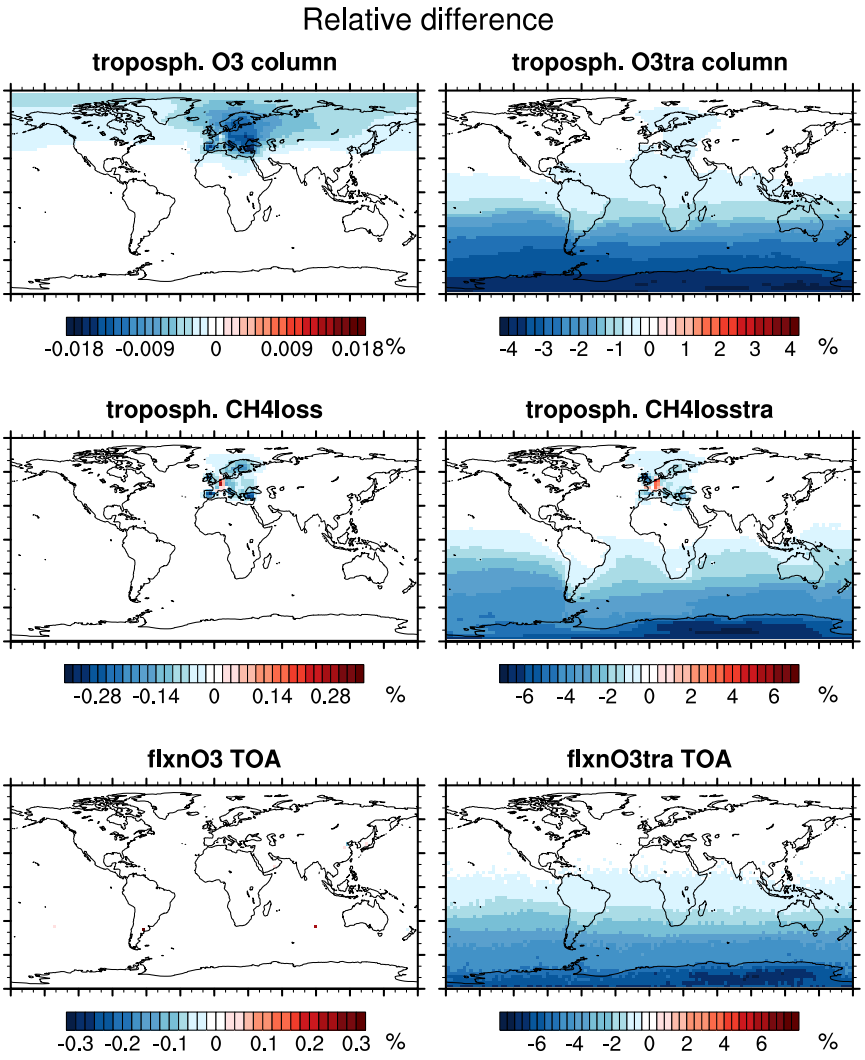

Figure 5.18: Relative difference between TransClim and EMAC simulation. Ozone (O_3), methane loss (CH4loss) and ozone fluxes (flxn(O_3)) as well as the contribution to ozone ($O_3{}^{tra}$), to methane loss (CH4losstra) and to ozone fluxes (flxn($O_3{}^{tra}$)) are shown. For the O_3 and $O_3{}^{tra}$, the relative difference of the tropospheric columns are shown. For CH4loss and CH4losstra, the deviations of the tropospheric means are displayed. The values at top of the atmosphere (TOA) are shown for flxn(O_3) and flxn($O_3{}^{tra}$).

to 6 % in the Southern Hemisphere. However, the contributions of road traffic emissions in the Southern Hemisphere are generally very small. Dividing the absolute differences by these small values in the Southern Hemisphere to compute the relative differences causes the large differences in the Southern Hemisphere. Additionally, the relative frequency distributions of the relative differences and the global means of O_3, O_3^{tra}, τ_{CH4}, τ_{CH4}^{tra}, flxn(O_3) and flxn(O_3^{tra}) derived by TransClim and by EMAC are displayed in appendix A.8. These comparisons also show that the deviations between the EMAC and TransClim simulation are generally very small.

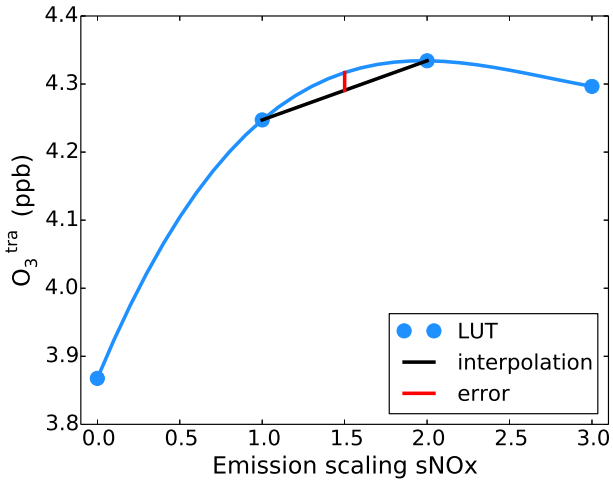

Figure 5.19: Sketch of interpolation error

Fig. 5.19 shows a sketch of the interpolation error caused by TransClim. Blue dots indicates the LUT for O_3^{tra} depending on NO_x emission scaling in Germany. The blue line presents the non-linear relationship between the NO_x emission and O_3^{tra}. The LUT is 3 dimensional and the data is arranged on an irregular grid. For such data structure, the used interpolation algorithm (implemented in python) only supports a linear interpolation. The curvature of the non-linear relationship between NO_x emission and O_3^{tra} is negative. Thus, a linear interpolation within the LUT (indicated with the black line) causes an underestimation of the interpolated value. The error which is caused by the linear interpolation is indicated with the red line. However, the resulting errors are so small that the application of a linear interpolation is justified.

Despite the general slight underestimation of TransClim, the deviations between the results obtained by TransClim and EMAC are very low (below 6 %). This shows that TransClim reproduces this EMAC simulation very well.

5.6.2. Comparison to VEU1 simulations

In this section, simulations performed within the project VEU1 are imitated with TransClim to assess the performance of TransClim. The DLR project VEU1 (Verkehrsentwicklung und Umwelt 1, i.e. Transport and the Environment 1, Henning et al. (2015), `www.dlr.de/VEU`) examined the German transport and its effect on the environment (Hendricks et al., 2017). EMAC simulations were performed to quantify the climate impact of a future road traffic emission scenario. Road traffic emissions for the year 2030 were determined and their influence of NO_x, O_3 and OH was computed with EMAC. This offers a good opportunity to test the performance of TransClim.

Within the scope of the project VEU1, German road traffic emissions were derived for present day conditions as well as for possible future scenarios. Based on socio-economic data such as population, households, income levels, economic development and demographic trends, the transport demand was determined. To compute the emissions for road traffic, railways and inland shipping, both the passenger as well as the freight transport were regarded. For the passenger transport, different transport modes such as motorised private transport, public transport, bicycles and pedestrians were taken into account. Additionally, different vessel and fuel types as well as the emission classes were considered. The development of new technologies in the transport sectors were modelled as well. Considering all these different factors, a *baseline emission scenario* for German road traffic emissions for the years 2008, 2020 and 2030 was created.

In VEU1, the climate impact of this baseline emission scenario was simulated with EMAC only for the year 2030. To obtain the impact of German road traffic emissions, the perturbation method (see sect. 4.1) was used. This method compares two EMAC simulations: one simulation contains all emissions and another simulation neglects the road traffic emissions. In order to obtain a robust signal of the German road traffic emissions, the perturbation signal was enhanced. Thus not only the road traffic emissions in Germany but the road traffic emissions in all European countries were set to zero. This method determines the climate impact of the European road traffic emissions. Subsequently, the resulting European radiative forcing was in turn downscaled to receive the radiative forcing of the German road traffic emissions. In this manner, the radiative forcing of the O_3 change caused by German road traffic emissions was computed. The specific setup of the EMAC simulations is described in Gottschaldt et al. (2013) and Hendricks et al. (2017).

Additionally, the CH_4 lifetime change for German road traffic emissions was deduced from the EMAC simulation described above. With the climate-response model AirClim (Grewe and Stenke, 2008; Grewe et al., 2012; Dahlmann et al., 2016) the corresponding radiative forcing was calculated using the same method as TransClim (see sect. 5.5). The effect of primary mode ozone is calculated by $0.29 \times \mathrm{RF}(CH_4)$ (see sect. 2.4; Dahlmann et al., 2016). The CH_4 background concentration were taken from Meinshausen et al. (2011).

The results obtained by the project VEU1 offer the opportunity to evaluate TransClim with respect to climate impact of O_3 and CH_4 lifetime change caused by regional transport emissions. TransClim uses the road traffic emissions of VEU1 and

imitates the EMAC simulation performed in VEU1. The emission scaling factors (factors by which the reference emissions are scaled) for TransClim are presented in table 5.5. For this simulation, the resulting NO_x and OH mixing ratios are also computed by TransClim (see sect. 5.5).

Emission region	**Emission scaling**			**year**
	sNOx	**sVOC**	**sCO**	
Germany	1.136	1.509	1.032	2008
Germany	0.514	0.802	0.422	2020
Germany	0.298	0.724	0.382	2030
Western Europe	0.729	0.462	0.490	
Northern Europe	0.379	0.305	0.723	
Eastern Europe	0.677	0.415	0.366	
Southern Europe	0.725	1.388	0.521	
North America	1.000	1.000	1.000	
Asia	1.000	1.000	1.000	

Table 5.5: Emission scaling factors in TransClim for imitating VEU1 simulations. The emission scaling factors in Germany for the years 2008, 2020 and 2030 are also indicated. For the remaining regions (Western Europe to Asia), the emission scaling factors remain constant for the years 2008, 2020 and 2030.

The zonal means of NO_x, O_3 and OH change caused by the European road traffic emissions (i.e. difference between the "reference simulation" and "no European road traffic simulation") for the year 2030 is shown in fig. 5.20. The first and second column show the relative and absolute change derived from TransClim. The third column presents the absolute changes obtained with EMAC in VEU1 (Hendricks et al., 2017). European road traffic emissions increase NO_x over the Northern Hemisphere. The increase (up to 4 %) is very confined to the latitudes where the European road traffic emits. Furthermore, European road traffic emissions increase O_3 in the Northern Hemisphere. The O_3 rise is not only bound to the lower troposphere but reaches high up to the tropopause region. It even stretches into the lower stratosphere where O_3 from European road traffic emissions is found over the tropics. The zonal mean is increased by up to 0.5 % in the Northern lower troposphere. Moreover, European road traffic emissions cause an OH increase in the lower troposphere which is rather confined to the emission region and OH decrease in the upper troposphere. TransClim reproduces the pattern of NO_x and O_3 increases very well. However, TransClim underestimates the OH increase caused by European road traffic emissions. In VEU1, the OH increase reaches the tropopause region in the Northern Hemisphere. In contrast, TransClim confines the OH increase below 500 hPa. In VEU1, a different emission inventory is used than for TransClim. As the OH chemistry is very sensitive to emissions, this can lead to different OH mixing

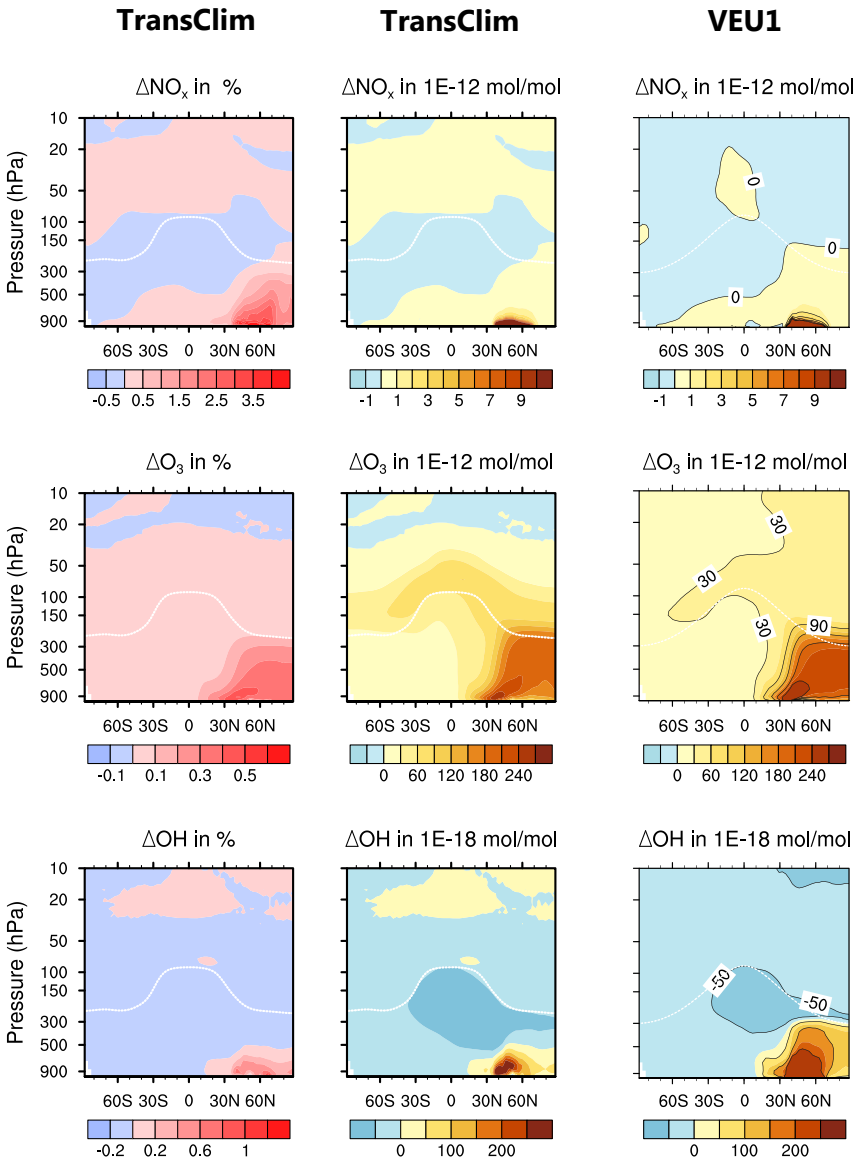

Figure 5.20: Zonal mean of relative and absolute NO_x, O_3 and OH change caused by European road traffic emissions for the year 2030. Simulations performed with TransClim and VEU1 are compared. The first and second columns show the relative and absolute changes simulated with TransClim. The third column shows the absolute changes simulated with EMAC (Hendricks et al., 2017). The white line indicates the tropopause.

ratios in VEU1 than for TransClim.

The results of VEU1 simulations in fig. 5.20 are averaged over three years. In contrast, TransClim shows a 1-year-average. The good agreement between TransClim and VEU1 shows that a LUT consisting of 1 year simulations is sufficiently good to described the NO_x, O_3 and OH change derived from a three years EMAC simulation.

TransClim also enables to determine the climate impact of only German road traffic emissions. An additional simulation with TransClim is performed in which all road traffic emissions in Germany are neglected. To obtain the climate impact of German road traffic emissions, the TransClim simulation without German road traffic emissions is subtracted from the reference simulation ("reference simulation" - "no German road traffic emissions simulation"). The resulting O_3 and OH change

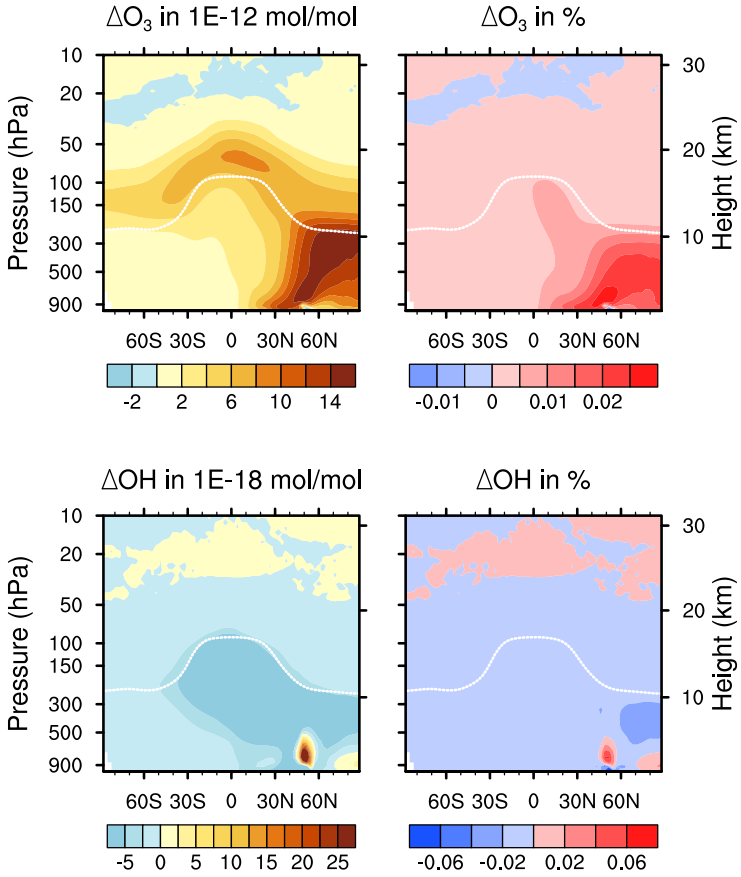

Figure 5.21: Zonal mean of relative and absolute NO_x, O_3 and OH change caused by German road traffic emissions for the year 2030. The simulation is performed with TransClim. The white line indicates the tropopause.

are shown in fig. 5.21. The pattern of the O_3 increase is very similar to O_3 change caused by the European road traffic emissions (fig. 5.20). But the magnitude of O_3 change is not as pronounced for German as for European road traffic emissions as the amount of road traffic emissions released by Germany is smaller. The zonal mean of O_3 rises by up to 0.03 % in the lower Northern troposphere. Noteworthy, a small O_3 decrease is observed just above 50°N. In this region, NO_x is strongly increased by German road traffic emissions. The O_3 decrease due to a NO_x increase indicates that this region is "VOC-limited" (see sect. 2.2.1). Considering OH, a decrease due to German road traffic is found in the free troposphere. However, a small increase of up to 0.06 % is observed just above 50°N.

The O_3 radiative forcings and the change in CH_4 lifetime are derived from the TransClim simulations and compared with the VEU1 results in table 5.6. The O_3 radiative forcing caused by European road traffic emissions is 1.34 mW m^{-2} and deviates by only 4 % from the VEU1 value. The O_3 forcing for the German road traffic emissions is 0.089 mW m^{-2} (derived with TransClim). It differs from the value obtained in VEU1 by 24 %. This is not surprising, as in VEU1 the German values are obtained by downscaling the forcing from the European road traffic emissions (see above). For the change in CH_4 lifetime caused by European road traffic emissions, TransClim obtains a significantly lower value than VEU1. On the one hand, the OH increase obtained by TransClim is smaller than in VEU1 (compare to fig. 5.20). On the other hand, the CH_4 lifetimes of the simulation for TransClim's LUT (about 7.7 years) are generally lower than in the EMAC simulations used for VEU1 (about 8.5 years). This is caused by the different emission inventories used for TransClim and VEU1 simulations. Moreover, different methods for calculating the CH_4 lifetime are responsible for the different CH_4 lifetimes (Lawrence et al., 2001). Interestingly, the CH_4 lifetime change due to European road traffic emissions is negative. But for German road traffic emissions, TransClim computes a positive lifetime change. Due to the downscaling in VEU1, this change in sign can not be represented in the VEU1 results. The shift in sign of the CH_4 lifetime is caused as for the European road traffic emissions tropospheric OH increases by 0.03 %. However, for the German road traffic emissions tropospheric OH decreases by -0.003 %.

Variable	**Model**	**Europe**	**Germany**
RF(O_3) in mW m^{-2}	VEU1	1.29	0.072
	TransClim	1.34	0.089
τ_{CH4} change in %	VEU1	-0.084	-0.0047
	TransClim	-0.018	0.00089

Table 5.6: Ozone radiative forcing (RF(O_3)) and CH_4 lifetime (τ_{CH4}) change for the simulation derived in VEU1 (Hendricks et al., 2017) and computed by TransClim. The column Europe indicates the values induced by the European road traffic emissions, the column Germany for the German road traffic emissions.

Variable	Model	2008	2020	2030
RF(O_3)	VEU1	0.28	0.13	0.07
	TransClim	0.25	0.11	0.09
RF(O_3^{tra})	TransClim	0.44	0.22	0.15

Table 5.7: Radiative forcing of impact on ozone (O_3) and contribution change to ozone (O_3^{tra}) in mW m^{-2} due to German road traffic emissions for the years 2008, 2020, 2030. The results for VEU1 (Hendricks et al., 2017) and TransClim are given.

To compute the O_3 radiative forcing for different years in VEU1, Hendricks et al. (2017) scaled the O_3 radiative forcing with the NO_x emissions from road traffic. Using the VEU1 emission inventories given for the years 2008, 2020 and 2030 (see Hendricks et al., 2017), TransClim also computes the O_3 radiative forcings for these years. The emission scaling factors for 2008, 2020 and 2030 in Germany are indicated in table 5.5. Table 5.7 presents the O_3 radiative forcing for VEU1 and TransClim. The O_3 radiative forcing obtained by VEU1 decreases in future. This decreasing trend is well reproduced by TransClim. However, the values differ by 0.02 mW m^{-2}. TransClim obtains lower forcings for 2008 and 2020 and a larger forcing for 2030. The radiative forcing of O_3^{tra} from German road traffic emissions is also indicated in table 5.7. It is about twice as large as the radiative forcing due to total O_3. This indicates that the effect of German road traffic emission on the radiative forcing is underestimated by a factor of two when only the total O_3 mixing ratios and not the O_3 contributions are regarded.

Fig. 5.22 shows the radiative forcing caused by the change of CH_4 lifetime for VEU1 and TransClim. In VEU1, the radiative forcing of CH_4 is computed by AirClim[1]. AirClim and TransClim use the same method for deriving the CH_4 radiative forcing from the change of CH_4 lifetime (see sect. 5.5). The RF is computed for the timespan from 1850 to 2100. Before 2000, historic CH_4 background concentrations are considered. After 2000, the CH_4 background concentrations are taken from RCP8.5 (Meinshausen et al., 2011; van Vuuren et al., 2011). Note that the primary mode ozone is included in both simulations ($0.29 \times RF(CH_4)$; Dahlmann et al., 2016). As the obtained CH_4 lifetime change strongly differs for TransClim and VEU1 (see table 5.6), the corresponding RF differs as well. VEU1 results in negative forcing corresponding to the negative lifetime change. TransClim obtains a slight positive forcing due to the positive CH_4 lifetime. Furthermore, the CH_4 radiative forcing due to German road traffic emissions is determined after the tagging method as described in sect. 4.5 and 5.5. It is indicated in fig. 5.22 with "tag". In contrast to OH which decreases due to German road traffic emissions, the contribution of road traffic to OH (OH^{tra}) increases due to German road traffic emissions by 0.064 % in the troposphere. This leads to a decrease of the contribution CH_4^{tra} and thus to a large negative radiative forcing.

[1] Due to an error in the RF calculation in AirClim, the values slightly differs from the ones indicated in Hendricks et al. (2017)

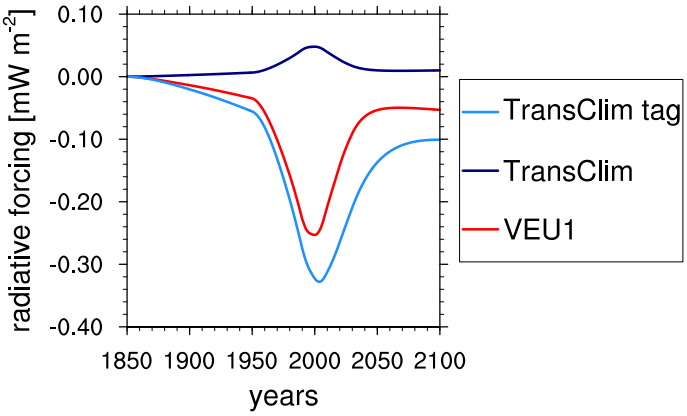

Figure 5.22: Radiative forcing due to CH_4 lifetime change for the year 1850 to 2100. The forcings for VEU1 and TransClim are given. TransClim computes the RF as described in sect. 5.5. The abbreviation "tag" indicates the contribution of road traffic emissions to radiative forcing of methane ($RF(CH_4{}^{tra})$).

Summing up, TransClim reproduces the results obtained by EMAC very well. Although TransClim underestimates the results of EMAC slightly, it performs very well when being directly compared to EMAC (deviations are below 6 %). It also imitates the simulation performed in VEU1 satisfactorily. Moreover, the overall pattern of European road traffic emissions is described very well by TransClim. Only OH is largely underestimated leading to a smaller CH_4 lifetime change and smaller radiative forcings of CH_4.

5.7. Assessment of TransClim

This section gives an overall assessment about the applicability and performance of the model TransClim.

TransClim is a chemistry-climate response model which efficiently determines the climate effect of road traffic emission scenarios. It considers the road traffic emissions of NO_x, VOC and CO and computes the change of O_3 and CH_4 as well as the respective radiative forcings. Seven emission regions are defined (Germany, Western Europe, Northern Europe, Eastern Europe, Southern Europe, North America and Asia) which allows for varying the road traffic emissions of NO_x, VOC and CO from 0 to 200 % in each emission region.

The algorithm of TransClim enables to determine the climate effect of a road traffic emission scenario very quickly. Using a standard computer, it is approximately 6000 times faster than a complex chemistry climate model such as EMAC running on a high performance computer. For example, to compute the global mean climate effect of an emission scenario in Germany, TransClim needs 0.2 s. In other words, TransClim requires about $4.5 \cdot 10^5$ times less computing time than a climate simulation with EMAC. Consequently, TransClim provides a suitable tool to assess

Category	Performance	Restrictions	Future solutions
Global effect	very good (deviations below 0.9 %)	linear interpolation within LUT	non-linear interpolation with generalised additive models
Local effect	not possible	–	extension of LUT with high resolution climate models
Pattern	good (deviations 0.02 – 6 %)	linear interpolation within LUT	non-linear interpolation with generalised additive models
Future scenarios	not possible	–	extension of LUT with different background emissions
Speed	fast, 6000 times faster than a complex chemistry climate model (e.g. 0.02 node-h per TransClim simulation)	number of emission regions and grid points	–
Flexibility	very good, easily extendable to more emission regions, other climate models and other emission sectors	–	–
Applicability	good, broad range of road traffic emission scenarios	only within the range of LUT, only road traffic	extrapolation outside the LUT with generalised additive models, extension of LUT to other emission sectors (railways, shipping)

Table 5.8: Performance, restrictions and future solutions of the response model TransClim.

the climate effect of a broad range of road traffic emission scenarios. Using the tagging method, it considers the contribution of O_3 and CH_4. This enables to calculate not only the impact but also the contribution of road traffic emissions to O_3 and CH_4 as well as to their respective radiative forcings.

TransClim reproduces the O_3 and CH_4 changes as well their radiative forcings derived by the complex chemistry climate model EMAC very well. A direct comparison of TransClim and EMAC for one emission scenario simulation shows that the differences are below 6 %. Additionally, TransClim is able to reproduce the pattern of the changes. The general small underestimation caused by TransClim arises from the interpolation algorithm. The errors are still small enough (0.02 – 6 %) to be uncritical for the application of TransClim.

However, the current implementation restricts the application of TransClim. The LUT bases on simulations of the global model EMAC which allows for calculating the global and regional effect of road traffic emissions. To determine the climate effect on a local scale, it would be necessary to train the LUT with other models such as the climate model MECO(n) (coupled model system MESSyfied ECHAM and COSMO models nested n-times; Kerkweg and Jöckel, 2012a,b) which can simulate a fine resolution of 0.44°. Moreover, the LUT used in this work considers only road traffic emissions of the year 2010. For different years, the O_3 background concentration changes and thus the current LUT is not valid any more. To compute the O_3 effect of road traffic emissions for very different O_3 background concentration, a new LUT needs to be set up. Furthermore, the current LUT enables TransClim to compute the climate effect of only road traffic emissions. The determination of the climate effect of other land based traffic modes such as railways and shipping requires additional EMAC simulations. Also the calculation of the climate effect of road traffic emissions from other regions than the seven emission regions of this work needs an extension of the LUT.

Overall, the interpolation algorithm of TransClim is very flexible. It allows for easily extending the LUT for additional years, traffic modes and emission regions. However, the computational resources which are needed to set up the LUT restrict the applicability of TransClim. But once the LUT is set up for specific emission regions and traffic modes (e.g. road traffic), TransClim enables to simulate quickly a broad range of emission scenarios. Table 5.8 presents an overview of the performance of TransClim. A comparison to other response model is given in the conclusion (chapt. 7).

In the following chapter, two examples of emission scenarios are presented and their climate effect on O_3 and CH_4 is determined with TransClim.

6

Assessment of road traffic mitigation options

Mitigation strategies for road traffic aim for reducing traffic congestion, fossil fuel use as well as emissions of greenhouse gases and pollutants. Politics have many possibilities to achieve these aims by managing the rising demand of road traffic. The introduction of efficient policies in road traffic market is challenging as economical growth, social benefits and emissions need to be regarded at the same time. Some policies can be applied national, but most operate on a local scale.

A broad range of mitigation options exist regulating the choice of fuel, the energy efficiency of vehicles, the use of vehicles or pricing instruments. Politics have the possibility to foster the use of biofuels or low carbon fuels such as natural gas. They can also support other propulsion techniques such as hydrogen or electrical vehicle minimizing the direct emissions of greenhouse gases. Furthermore, policies can reduce emissions of road traffic by setting emission and fuel consumption limits. Moreover, regulations for vehicle size, shape and weight as well as new techniques for reducing air drag and rolling resistance also influence the fuel consumptions and thus the emissions. Also the use of vehicles itself can be reduced by mitigation options. A change in land use pattern, greater support of public transportation as well as an improved traffic management can reduce traffic volume. Real time information for searching parking space further reduces mileage. Financial support of ride, car and bicycle sharing as well as temporal driving bans can also diminish traffic volume. Moreover, limitations for vehicle registration reduce the vehicle stock. Motor fuel taxes, vehicle registration fee, road tolls and higher parking fee make the use of private vehicles less attractive and thus reduce the traffic volume as well. (Sims et al., 2014)

However, to efficiently change road traffic and reduce emissions, one mitigation strategy is not sufficient. For instance, the introduction of motor fuel taxes alone have only little effect on the driving behaviour of vehicle owners (Sims et al., 2014). Therefore, a combination of several policies is necessary to significantly modify road

traffic.

Two sets of mitigation options described above are investigated with TransClim in the following chapter. The first example presents a combination of policies such strong regulation of emissions and large financial support for public transport, car sharing and public bike rentals (sect. 6.1). The second example describes a single mitigation option: the introduction of biofuels in Europe (sect. 6.2). In sect. 6.1, the climate effect of possible future road traffic emission scenarios in Germany, deduced from the combination of different policies, is quantified with TransClim. These emission scenarios are developed in the DLR project VEU2 (Verkehrsentwirklung und Umwelt 2, i.e. Transport and the Environment 2, `www.dlr.de/VEU`). VEU2 is the follow-up of the project VEU1 which has been used to evaluate TransClim (sect. 5.6.2). In sect. 6.2, the climate effect of biofuels in Europe is investigated with TransClim. Two scenarios describe the emissions caused when passenger cars and heavy goods vehicles in Europe run with fuel containing low and high biofuel content.

6.1. Climate effect of mitigation options in Germany

The climate effect of a set of several mitigation strategies for German road traffic is quantified with TransClim in the following section. The DLR project VEU2 (Verkehrsentwirklung und Umwelt 2, i.e. Transport and the Environment 2, `www.dlr.de/VEU`) investigates the future development of German transport and its effect on society and environment. Political demands, technical innovations and social developments are taken into account to trigger changes in the German traffic system. Within the scope of this project, three possible future scenarios are developed for the year 2030 and 2040 (Seum et al., 2017a,b):

1. The scenario **regulated shift (rShift)** represents a scenario in which political and technological impulses push the society towards a strong conservation of resources and environment. The international community of states strongly cooperates and establishes a global emission trading which includes aviation and shipping. In view of shortage of fossil fuels, the principle policies follow the goal of saving resources, reducing emissions and gaining independence from fossil fuels. Energy production from alternative sources such as wind and solar energy are further extended. In 2040, the ratio of renewable energies to conventional production is significantly increased to 80 %. Strong regulation of greenhouse gas and pollutant emissions exists in traffic sectors. Public transport is funded intensively. Railway network is further extended, the intervals of trains and buses are increased and public transport has priority which significantly decrease the travel time. This makes public transport more attractive. Car sharing and public bike rentals are supported by the government. Consequently, less people own a car and if they do, they tend to possess smaller ones.

2. The scenario **free play (fPlay)** represents a scenario with loose regulations for conserving environment and resources. The international community of

states cooperates less and acts more on a national base. The European emission trading is stopped. Existing climate policies are not tightened. Fossil fuels are sufficiently available and can cover the increasing demand. In Germany, the economical interests are prioritised compared to environmental interests. The government offers no funding for alternative technologies and rather supports existing structures. The ratio of renewable energy for energy production is raised to only 40 % in 2040. Combustion engines remain the dominating propulsion technique for road traffic. Investments into public transportation are missing. The public transport is only concentrated on highly frequented routes. In peripheral regions, public transport strongly decreases which increases travel time and costs. Private cars still dominate. The fleet of private cars is steadily growing and people tend to buy larger vehicles.

3. **Reference scenario (ref)** describes a scenario which continues the present day trends of climate policy. The emission trading continues to persist only on European scale and is not extended to global scale. Principle goals of protecting environment and climate exist, but are not gaining a dominant role in German politics. Thus, the goals of climate protection are not completely enforced. The main structures of energy production remain unchanged and the ratio of renewable energy towards conventional production reaches a moderate level of 60 % in 2040. The traffic sector receives a moderate support for new inventions regarding emission reduction and efficiency increase. Moreover, the emission thresholds on vehicles are only slightly tightened. The financial support of public transport remains rather constant which increases travel expenses. Public transport is extended in large cities and diminished in peripheral regions. Car sharing and public bike rentals are supported moderately. Consequently, the fleet of private vehicles remains unchanged. However, a trend towards larger vehicles is noticeable.

For these three emission scenarios, road traffic emissions are provided by the VEU2 project for the years 2010, 2030 and 2040. Based on these road traffic emissions of NO_x, VOC and CO, the climate effect is determined with TransClim in the following. However, the VOC emission provided by VEU2 includes also CH_4 emissions. As TransClim only takes road traffic emissions of VOC without CH_4, the fraction of CH_4 has to be subtracted from the provided VOC emissions. Based on the EDGAR emission inventory (Crippa et al., 2016), the fraction of CH_4 to VOC emissions for the road traffic sectors in Germany is about 4 %. Thus, only 96 % of the provided VOC emissions are considered in the following. The emission scaling factors (factors by which the reference emissions are scaled) for the three emission scenarios are given in table 6.1. For the year 2010, all three emission scenarios are identical.

Fig. 6.1 shows the impact on ozone (O_3) and change in contribution to ozone ($O_3{}^{tra}$) as well as the corresponding radiative forcings caused by the three German road traffic emission scenarios ref, fPlay and rShift. The values are computed by subtracting the TransClim simulations with the German road traffic emissions and the TransClim simulation with no German road traffic emissions. Furthermore, I

Emission scenario	years	Emission scaling		
		sNOx	sVOC	sCO
ref	2010	0.778	1.116	0.713
	2030	0.200	0.663	0.416
	2040	0.177	0.592	0.395
fPlay	2010	0.778	1.116	0.713
	2030	0.204	0.664	0.491
	2040	0.165	0.590	0.574
rShift	2010	0.778	1.116	0.713
	2030	0.152	0.501	0.362
	2040	0.111	0.370	0.306

Table 6.1: Emission scaling factors for the emission scenarios ref, fPlay and rShift.

assumed that the German road traffic emissions of NO_x, VOC and CO possess each an uncertainty of 10 %. Based on this assumption, the error bars displayed in fig. 6.1 are computed by TransClim.

For the year 2010, German road traffic emissions of NO_x, VOC and CO cause globally a tropospheric O_3 change of 7.5 ppt and ${O_3}^{tra}$ change of 19 ppt. As the emissions of NO_x, VOC and CO from German road traffic decrease for the years 2030 and 2040, so do the O_3 and ${O_3}^{tra}$ changes. Corresponding to the largest emissions of the scenario fPlay, the O_3 and ${O_3}^{tra}$ changes are the largest as well. In contrast, the emission scenario rShift causes the lowest O_3 and ${O_3}^{tra}$ changes. The ${O_3}^{tra}$ changes for the year 2010 is about 2.5 times larger than the O_3 changes, for the year 2030 and 2040 1.7 times respectively. The contribution ${O_3}^{tra}$ is stronger influenced by German road traffic emissions than the total O_3. In accordance to the O_3 and ${O_3}^{tra}$ changes, the RF caused by German road traffic emissions decreases for the years 2030 and 2040 compared to 2010. Largest RF is generally caused by the scenario fPlay, lowest RF by the scenario rShift. The RF of ${O_3}^{tra}$ as well as its change between the years is larger than the RF of O_3. This shows that the RF of ${O_3}^{tra}$ is stronger affected by mitigation options than the RF of O_3 which is explained by the fact that ${O_3}^{tra}$ is also stronger reduced than O_3. ${O_3}^{tra}$ describes only the contribution of road traffic emissions, in contrast O_3 contains also the contributions of other emission sectors such as aviation or shipping. Hence, a change of only road traffic emissions is partly compensated by the other emission sectors (Grewe et al., 2012, 2017). Consequently, ${O_3}^{tra}$ is stronger influenced by mitigation options than O_3. Assuming a 10 % uncertainty of German road traffic emissions reveals that the mitigation options of VEU2 decrease the climate effect of O_3 after 2010 efficiently. However, the difference between the scenarios might not be significant.

German road traffic emissions influence not only ozone but also methane. The CH_4 lifetime changes caused by German road traffic emissions for the three emis-

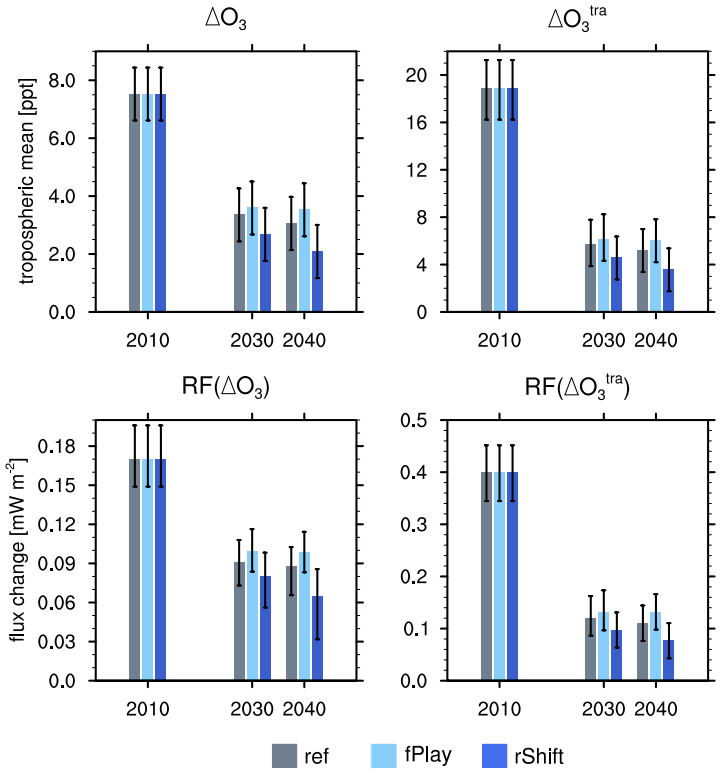

Figure 6.1: Impact on ozone (O_3) and change in contribution to ozone (O_3^{tra}) as well as stratospheric adjusted radiative forcing of O_3 and O_3^{tra} caused by German road traffic emissions of NO_x, VOC and CO for the three VEU2 scenarios ref, fPlay and rShift. The error bars are displayed as well.

sion scenarios are calculated by TransClim (see table 6.2). The resulting RF of CH_4 and CH_4^{tra} are presented in fig. 6.2. The radiative forcing of the impact on methane ($RF(\Delta CH_4)$) and the radiative forcing of the contribution to methane ($RF(\Delta CH_4^{tra})$) are computed according to VEU1 (Hendricks et al., 2017, , see also eqs. 5.39, 5.41, 5.42 and 5.43). The primary mode ozone (PMO) is regarded as well ($PMO = 0.29 \times RF(CH_4)$; Dahlmann et al., 2016). CH_4 background concentrations are taken from the RCP8.5 scenario (Meinshausen et al., 2011). The shaded areas correspond to the uncertainty range determined by TransClim under the assumption that the German road traffic emissions possess an uncertainty of 10 %.

As the change of CH_4 lifetime is scaled with normalised NO_x emissions from road traffic to create a temporal evolution (same procedure as in VEU1; Grewe and Stenke, 2008; Hendricks et al., 2017), the $RF(\Delta CH_4)$ closely follows the behaviour of NO_x emissions (compare to fig. 2.1). German road traffic emissions induce a negative

Emission scenario	years	τ_{CH4} in 10^{-5}	τ_{CH4tra} in 10^{-3}
ref	2010	$-3.09^{+0.40}_{-0.41}$	$-3.51^{+0.49}_{-0.44}$
	2030	$2.94^{+0.43}_{-0.40}$	$-0.12^{+0.22}_{-0.40}$
	2040	$2.95^{+0.44}_{-0.42}$	$-0.10^{+0.22}_{-0.22}$
fPlay	2010	$-3.09^{+0.40}_{-0.41}$	$-3.5^{+0.49}_{-0.44}$
	2030	$3.82^{+0.44}_{-0.40}$	$-0.13^{+0.22}_{-0.40}$
	2040	$5.47^{+0.42}_{-0.44}$	$-0.06^{+0.22}_{-0.22}$
rShift	2010	$-3.09^{+0.40}_{-0.41}$	$-3.51^{+0.49}_{-0.44}$
	2030	$2.82^{+0.42}_{-0.44}$	$-0.09^{+0.22}_{-0.22}$
	2040	$2.59^{+0.44}_{-0.43}$	$-0.06^{+0.22}_{-0.22}$

Table 6.2: Relative change in τ_{CH4} and τ_{CH4tra} for the emission scenarios ref, fPlay and rShift caused by German road traffic emissions. The values are computed towards the case that all road traffic emissions in Germany are set to zero. The given uncertainty range is determined under the assumption that German road traffic emissions own an uncertainty of 10 %.

RF(ΔCH_4) up to the year 2020. After that the RF switches its sign and the RF becomes positive. The change in sign is traced back to the CH_4 lifetime change (see table 6.2). For the year 2010, TransClim determines a negative CH_4 lifetime change, i.e. German road traffic emissions decrease CH_4 lifetime. In contrast, for the years 2030 and 2040, the CH_4 lifetime change is positive, i.e. German road traffic emissions increase CH_4 lifetime. Consequently, CH_4 lifetime change in Germany is very sensitive to the assumptions in road traffic emissions.

After the year 2020, the emission scenario fPlay causes the largest RF(ΔCH_4) due to German road traffic emissions, in contrast the emission scenario rShift induces the lowest RF(ΔCH_4). This is caused by a larger increase of CH_4 lifetime for fPlay than for rShift (see table 6.2).

RF($\Delta {CH_4}^{tra}$) indicates the RF caused by the change of contribution of German road traffic emissions to CH_4. It is approximately 10 times larger than RF(ΔCH_4). RF($\Delta {CH_4}^{tra}$) stays negative over the whole time period. The time period of 2070 to 2100 of RF($\Delta {CH_4}^{tra}$) is enlarged and displayed in the second row of fig. 6.2. The differences between the scenarios in RF($\Delta {CH_4}^{tra}$) are within the same magnitude as for RF(ΔCH_4). The emission scenario ref presents the strongest RF. In contrast, the difference between the scenarios fPlay and rShift is small (below 6 %) as the change of τ_{CH4tra} is also little (see table 6.2). However, the uncertainties of the

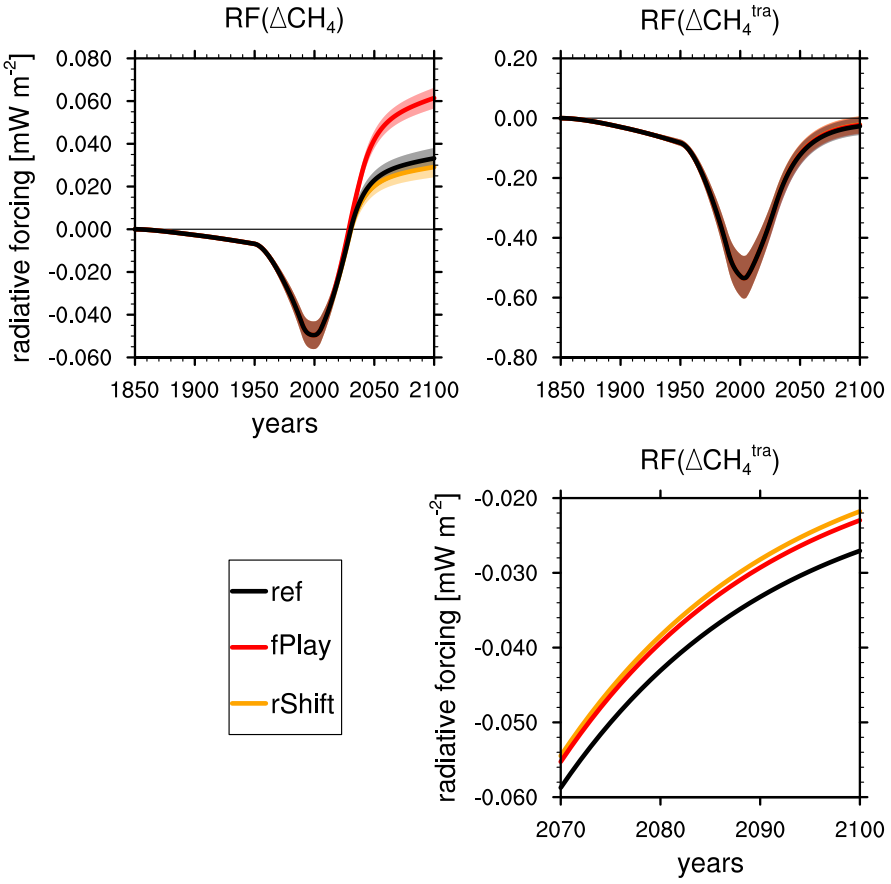

Figure 6.2: Temporal evolution of radiative forcing of impact on methane (CH_4) and contribution change to methane ($CH_4{}^{tra}$) caused by German road traffic emissions of NO_x, VOC and CO for the three VEU2 scenarios ref, fPlay and rShift. The shaded areas correspond to the 10 % uncertainty range assumed for the VEU2 emissions.

three scenarios are larger than the differences between the scenarios. Thus, it is challenging to deduce reliable statements from the presented results of RF(ΔCH_4).

Summing up, the scenario rShift imposes the lowest RF of O_3 and the $O_3{}^{tra}$. Also the RF of CH_4 and $CH_4{}^{tra}$ is the weakest. Largest changes in O_3 and $O_3{}^{tra}$ as well as in RF(ΔO_3) and RF($\Delta O_3{}^{tra}$) are observed for the scenario fPlay. The RF(ΔCH_4) is largest for fPlay. However, for RF($\Delta CH_4{}^{tra}$), the contribution of the scenario ref is the largest. In general, the RF caused by O_3 is significantly larger than by CH_4. In a nutshell, corresponding to its large emissions, the scenario fPlay imposes the greatest impact on climate. In contrast, the scenario rShift results in the lowest impact. The scenario ref indicates a medium climate effect situated

between the scenarios fPlay and rShift. This study of prospective mitigation options of German road traffic shows that the political and technological impulses executed in the scenario rShift (see above) presents a good option to reduce the global climate effect of German road traffic emissions of NO_x, VOC and CO.

Most existing literature investigates the climate effect of global road traffic emissions (e.g. Granier and Brasseur, 2003; Niemeier et al., 2006; Matthes et al., 2007; Hoor et al., 2009; Uherek et al., 2010; Mertens et al., 2018). Only Hendricks et al. (2017) also examine the effect of road traffic emissions in Germany. Using the perturbation method, they find an O_3 RF of German road traffic emissions of 0.28 mW m^{-2} for the year 2008 which lies between the RF of the impact on ozone of 0.17 mW m^{-2} and the contribution to ozone of 0.40 mW m^{-2} for the year 2010 found in this thesis. For the year 2030, Hendricks et al. (2017) estimate a decrease of O_3 RF to 0.07 mW m^{-2} being lower than the radiative forcings found here. The radiative forcing of the impact of German road traffic emissions on methane is lower while the contribution of German road traffic emissions to methane is larger than the values found by Hendricks et al. (2017).

Comparing the impact on ozone reveals that German road traffic emissions account for 0.1 – 0.6 % to the O_3 RF of global road traffic emissions (Fuglestvedt et al., 2008; Hoor et al., 2009; Myhre et al., 2011). Considering the radiative forcing of the contribution to ozone, German road traffic emissions contribute with 0.4 % to global road traffic emissions (Mertens et al., 2018). Niemeier et al. (2006) and Matthes et al. (2007) state that global road traffic emissions account for 8 to 12 % to the zonal mean of O_3. In comparison, German road traffic emissions contribute about 0.18 % to the zonal mean which is approximately 56 times less than the global road traffic emissions. In total, German road traffic emissions of NO_x, VOC and CO contribute 0.03 % to the tropospheric O_3 burden while the global road traffic contributes 8 % (Mertens et al., 2018). Moreover, German road traffic emissions cause a CH_4 lifetime change of 0.003 % in 2010 (see table 6.2), thus contributing by 0.3 – 0.4 % to CH_4 RF of global road traffic emissions (Hoor et al., 2009; Uherek et al., 2010).

6.2. Climate effect of biofuels in Europe

In this section, the climate effect of a single mitigation strategy is quantified with TransClim: Replacing standard gasoline and diesel fuels with biofuels offers an opportunity to reduce the effect of road traffic emissions of NO_x, VOC and CO on climate. In the following, the climate effect of the introduction of biofuels in Europe is investigated.

Blends of ethanol and biodiesel are the most common renewable fuel for gasoline and diesel vehicles. Bioethanol is produced by the fermentation of sugar, by the hydrolysis and fermentation of starch and by the breakdown of cellulosic biomass. Therefore, typically sugar cane, corn, cereals as well as stalks of wheat and woods are used. Biodiesel is formed from frying oils, vegetable oils or animal fats. Transesterification of these oils and fats produce fatty acid methyl esters, so called biodiesel. The oils are usually extracted from rapeseed, sunflower, soya and palm. (Bringezu et al., 2009)

Fuel blends containing biofuels change the exhaust emissions. Ethanol containing fuel blends usually reduce exhaust emissions of CO, VOC and CO_2. However, no significant trend for NO_x emissions is observed. Certain VOC such as formaldehydes, acetaldehydes and ethanol increase which leads to an enhanced O_3 forming potential (e.g. Karavalakis et al., 2012; Suarez-Bertoa et al., 2015). The use of biodiesel blends also reduces the exhaust emissions of CO, VOC, CO_2 and particulate matter. Most studies find an increase of NO_x emissions. However, some studies state lower NO_x emissions (Karavalakis et al., 2009; Jedynska et al., 2015).

Several studies exist investigating the effect of biofuels on exhaust emissions of vehicles. However, only few studies address the emission change of fuel blends with a low and high biofuel content at the same time. Two of these studies have been chosen for the example presented in this section:

- Suarez-Bertoa et al. (2015) investigate the emissions of different ethanol containing gasoline blends. They use blends with low contents of ethanol (5 %, 10 % and 15 %) as well as blends with high contents of ethanol (75 % and 85 %). They measure the emissions of the blends with a Euro 5a flex-fuel vehicle over the World harmonized Light-duty vehicle Test Cycle. For this example, the blends containing 10 % and 85 % are considered. The emission changes with respect to standard gasoline are given in table 6.3. Interestingly, the change in NO_x emissions varies strongly. The gasoline blend containing 10 % ethanol increases NO_x emissions by 30 % while the blend containing 85 % decreases NO_x emissions by 40 %.

- Jedynska et al. (2015) test different biodiesel blends using a Euro 3 truck engine. The blends contain 5 %, 10 %, 20 % and 100 % biodiesel produced by rapeseed oil. The measurements were performed for the European Transient Cycle. The blends containing 10 % and 100 % biodiesel are taken into account for this example. The emission changes towards standard diesel are displayed in table 6.3. NO_x emissions increase while CO emissions decease with increasing fraction of biodiesel.

Fuel blend	Biofuel proportion	Emission change NO_x	VOC	CO
Ethanol	10 %	+30 %	-73 %	+7 %
	85 %	-40 %	-43 %	+3 %
Biodiesel	10 %	+1 %	+36 %	-2 %
	100 %	+26 %	+1 %	-42 %

Table 6.3: Emission change in percent caused by the different fuel blends with respect to standard gasoline and diesel. The values are derived from Suarez-Bertoa et al. (2015) and Jedynska et al. (2015). For ethanol, the values refer to the percent change of NO_x, VOC and CO emissions in mg/km. For biodiesel, the values refer to the percent change of NO_x and CO emissions in g/kWh and of VOC emissions in ppb.

The emission changes found by Suarez-Bertoa et al. (2015) and Jedynska et al. (2015) (see table 6.3) are generalised onto all vehicle types and transferred to the European vehicle fleet. I constructed two emission scenarios:

1. The scenario **biofuel low** assumes that all European passenger cars, heavy goods vehicles and buses drive with fuels containing a low biofuel content. Thus all gasoline and diesel driven vehicles experience the same emission changes as indicated by the fuel blend containing 10 % ethanol and 10 % biodiesel presented in table 6.3.

2. The scenario **biofuel high** describes the case in which all vehicles in Europe use fuel blends with a high content of biofuels. The vehicles containing a gasoline engine use the fuel with 85 % ethanol and thus experience the emission changes as indicated in table 6.3. The emission of diesel vehicle are changed according to the emission changes of 100 % biodiesel as displayed in table 6.3.

The composition of the vehicle fleet in Europe are taken from the data set of Eurostat[1]. For each emission region, the number of gasoline and diesel vehicles is multiplied by the emission changes as indicated in table 6.3. The resulting emission scaling factors (factors by which the reference emissions are scaled) for the emission region Germany, Western, Northern, Eastern and Southern Europe are given in table 6.4. The factors of the emission regions North America and Asia are set to 1.

Taking the emission scaling factors displayed in table 6.4, TransClim computes the mixing ratio of ozone (O_3) and the contribution to ozone ($O_3{}^{tra}$) as well as the RF of O_3, $O_3{}^{tra}$, CH_4 and $CH_4{}^{tra}$. Fig. 6.3 displays the impact on ozone (O_3) and the change in contribution to ozone ($O_3{}^{tra}$) caused by the two emission scenarios towards the reference simulation. The reference simulation constitutes the simulation when

[1]Download from `http://ec.europa.eu/eurostat/en/data/database` at 08 January 2018

Emission scenario	Emission region	Emission scaling sNOx	sVOC	sCO
biofuel low	Germany	1.195	0.598	1.030
	Western Europe	1.155	0.723	1.015
	Northern Europe	1.186	0.675	1.033
	Eastern Europe	1.163	0.670	1.014
	Southern Europe	1.172	0.683	1.023
	North America	1.000	1.000	1.000
	Asia	1.000	1.000	1.000
biofuel high	Germany	0.794	0.697	0.879
	Western Europe	0.869	0.745	0.824
	Northern Europe	0.845	0.731	0.858
	Eastern Europe	0.835	0.721	0.839
	Southern Europe	0.846	0.731	0.845
	North America	1.000	1.000	1.000
	Asia	1.000	1.000	1.000

Table 6.4: Emission scaling factors of the emission scenarios "biofuel low" and "biofuel high" for the seven emission regions in TransClim.

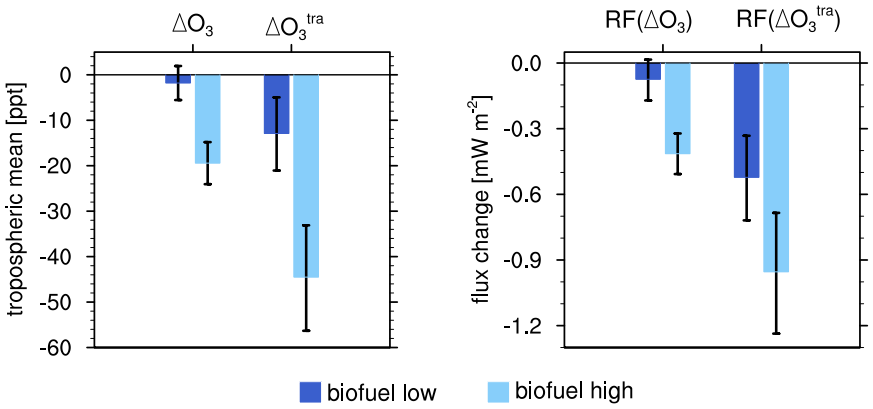

Figure 6.3: Tropospheric mean of the impact on ozone (ΔO_3) and the change in contribution to ozone ($\Delta O_3{}^{tra}$) as well as stratospheric adjusted O_3 and $O_3{}^{tra}$ radiative forcing caused by road traffic emissions of NO_x, VOC and CO for the scenarios "biofuel low" and "biofuel high". Values display the differences against the reference simulation. Error bars are given as well.

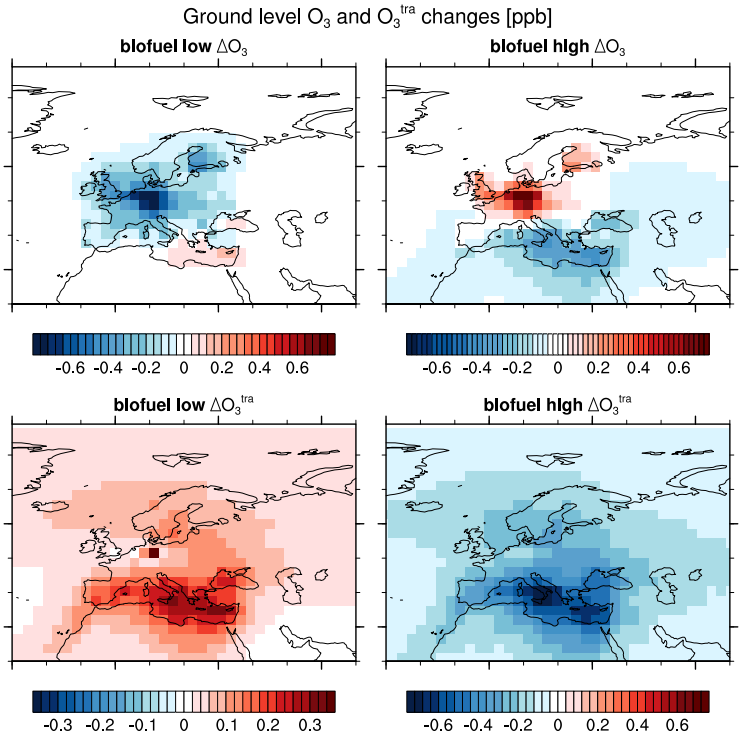

Figure 6.4: Impact on ground level ozone (O_3) and change in contribution to ground level ozone (O_3^{tra}) for the scenarios "biofuel low" and "biofuel high". Values indicate the difference towards the reference simulation.

all emission scaling factors are set to 1. Jedynska et al. (2015) give 95 % confidence interval for their emission measurements. Values for NO_x and CO emissions for the different type of biofuels vary only below 2.6 % while VOC emissions show uncertainties of up to 14 %. These uncertainties are taken into account to derive the error bars presented in fig. 6.3. Both emission scenarios cause a decrease of the tropospheric O_3 and O_3^{tra}. However, the change of O_3 for "biofuel low" is so small that even the sign of the change is not ensured. The scenario "biofuel high" reduces O_3 and O_3^{tra} approximately 11 times and 3 times stronger than "biofuel low". Thus, the effect of biofuels is larger on O_3 than on the contribution O_3^{tra}. Corresponding to the O_3 and O_3^{tra} decreases, biofuels in Europe decrease the RF of O_3 and O_3^{tra} caused by road traffic emissions. The scenario "biofuel low" reduces the O_3 RF by about 0.07 ± 0.10 mW m^{-2}, while "biofuel high" leads to a stronger decline of about 0.41 ± 0.10 mW m^{-2}. Thus the scenario "biofuel high" lowers the RF of O_3 and O_3^{tra} about 6 times and 2 times stronger than "biofuel low".

Fig. 6.4 shows the impact on ground level ozone (O_3) and the change in contribution to ground level ozone (O_3^{tra}) caused by the scenarios "biofuel low" and "biofuel

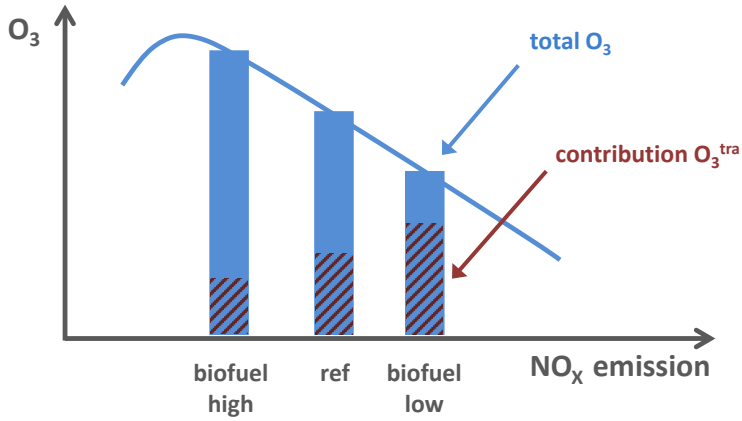

Figure 6.5: Sketch of relation between ground level O_3 depending on NO_x emission in a VOC-limited region (e.g. Europe). The total O_3 mixing ratios are displayed as columns for the scenarios "biofuel low" and "biofuel high" as well as for the reference simulation (ref). The hatched part of the columns present the contribution of road traffic emissions to ozone (O_3^{tra}).

high". The difference against the reference simulation are displayed. Interestingly, the two scenarios show different behaviour for the ground level O_3 and O_3^{tra}. O_3 decreases while O_3^{tra} increases over central Europe for "biofuel low". In contrast, O_3 increases while O_3^{tra} decreases over central Europe for "biofuel high". The sketch in fig. 6.5 explains this behaviour. The near surface O_3 chemistry over central Europe is VOC-limited (see sect. 2.2.1). On the one hand, the scenario "biofuel low" causes an approximately 17 % increase of NO_x emissions in Europe which leads in a VOC-limited regime to an O_3 decrease. On the other hand, NO_x emissions for "biofuel high" decrease by approximately 16 % leading to an increase of ground level O_3. The non-linearity of O_3^{tra} is not as strongly pronounced as for O_3: a NO_x increase leads to an O_3^{tra} increase while a NO_x decrease also reduces O_3^{tra}. For "biofuel low", more NO_x is available to contribute to the O_3 production than for "biofuel high" which leads to larger contributions to ozone (O_3^{tra}). Moreover, large changes of O_3^{tra} are observed over Southern Europe. In this region, O_3 mixing ratios are generally higher than over Northern Europe leading also to larger absolute O_3^{tra} changes.

The change in radiative forcings of the impact on methane (CH_4) and of the contribution change to methane (CH_4^{tra}) caused by the scenarios "biofuel low" and "biofuel high" is displayed in fig. 6.6. The radiative forcing is computed with respect to the reference simulation of the year 2010. Both scenarios decrease CH_4 and cause a negative CH_4 RF. Taking the uncertainties of the emission changes into account, a negative CH_4 RF for "biofuel high" is very likely, but not total ensured. The scenario "biofuel low" cause a stronger RF than "biofuel high" as CH_4 lifetime is stronger enhanced for this scenario. In contrast, "biofuel low" causes almost no

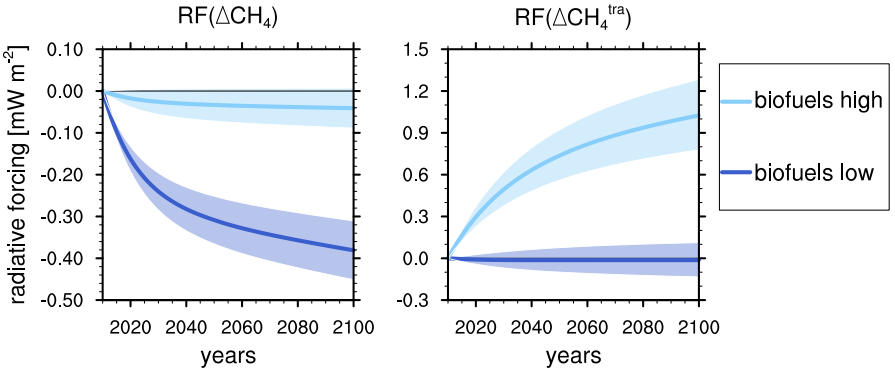

Figure 6.6: Radiative forcing of the impact on methane (CH_4) and of contribution to methane (CH_4^{tra}) caused by the scenarios "biofuel low" and "biofuel high". Values indicate the change towards the reference simulation. The time period from 2010 to 2100 is presented. The range of radiative forcings related to the emission uncertainty is displayed as well.

change of $RF(\Delta CH_4^{tra})$ as the CH_4^{tra} lifetime is almost not affected. The scenario "biofuel high" results in a positive $RF(\Delta CH_4^{tra})$ as the CH_4^{tra} lifetime is decreased.

Overall, the introduction of biofuels in Europe offers a potential to reduce the effect of road traffic emissions on climate. Fuels with a low content of biofuels ("biofuel low") induces a small negative O_3 forcing, but a large negative CH_4 RF. Thus in this scenario the cooling caused by the CH_4 RF is largely dominating the O_3 RF. In contrast, the O_3 RF caused by fuels containing a high content of biofuels ("biofuel high") induces a strong negative O_3 RF. However, the effect of the CH_4 is negligible small. Summing up, both scenarios have a high potential to reduce climate effect of European road traffic emissions. Fuel blends with low biofuel contents reduce the climate effect by reducing the greenhouse gas CH_4. Fuels with high biofuel contents reduce the climate effect by reducing tropospheric O_3.

Concerning air quality, fuels with low content of biofuels increases NO_x emissions but decreases O_3. In contrast, fuels with high content of biofuels decreases NO_x emissions, but increase O_3 in central Europe. As both NO_x and O_3 impact human health (see sect. 2.5), a further assessment of the impact on air quality is required. However, this is beyond the scope of this thesis and would require different tools: For example, regional climate models such MECO(n) (Kerkweg and Jöckel, 2012a,b) can be used the refine the resolution and determine the effect of biofuels on smaller scale.

Several studies exist stating that the substitution of conventional fuels with biodiesel and ethanol fuel blends result in higher ozone forming potential (e.g. Gaffney and Marley, 2009; Suarez-Bertoa et al., 2015). For example, Milt et al. (2009) finds an increase of ground level ozone of about 16 ppb in Bangkok, Thailand, if conventional fuel would be replaced with 10 % biofuels. However, all these studies investigate the effect of biofuel substitution on ozone on a local scale. So

far, no study exists which investigates the effect on regional or global scale. This hampers a comparison of the mitigation option presented here with existing literature. For fuel blends with a high content of biofuel, this study reveals an increase of ground level ozone which agrees with Suarez-Bertoa et al. (2015) who found that in particular blends with high ethanol contents have larger potential to increase ozone formation than blends with low contents.

In the mitigation scenario presented in this section, the emission changes caused by different biofuel blends are deduced from only two studies: Suarez-Bertoa et al. (2015) and Jedynska et al. (2015). However, these emissions are only valid under idealised conditions for certain engines and driving cycles. Due to lack of measurements under more realistic conditions, the emission changes as indicated in table 6.3 are assumed to be valid for all vehicle types as a first approximation. This hampers the transfer of emission changes to the European vehicle fleet. Nevertheless, this examples shows the opportunity offered by TransClim to quickly assess the climate effect of different kind of emission scenarios. TransClim also enables to determine the corresponding uncertainty range. The reliability of the computed climate effects depends on the uncertainty range of the input emissions. TransClim considers the uncertainty of the input emissions and computes their effect on the climate. This enables to determine the long-term climate effect of mitigation strategies and helps to assess these results.

7

Conclusion and Outlook

This thesis presents the development of the model TransClim. TransClim is a chemistry-climate response model which determines the climate effect of road traffic emission scenarios on O_3 and CH_4. It further computes the corresponding radiative forcings. TransClim is based on a look-up table (LUT) containing pre-calculated relations of emissions and their climate effect. These relations are computed by the complex chemistry climate model EMAC.

Within the scope of this thesis, I tested various approaches to find a suitable algorithm for combining the pre-calculated relations. The following algorithm revealed promising results: Road traffic emissions are split into seven emission regions: Germany, Western, Northern, Eastern and Southern Europe as well as North America and Asia. The road traffic emissions of NO_x, VOC and CO are varied individually in each emission region and their climate effect is simulated with EMAC. These simulations deliver the input for the LUT of each emission region. Then, for a particular emission scenario, TransClim interpolates within the LUT of each emission region to compute the O_3 change towards a reference simulation. These O_3 changes of each emission regions are added to the reference simulation to obtain the new O_3 concentration. The same procedure is performed to compute the contribution of road traffic emissions to ozone (${O_3}^{tra}$) as well as the radiative forcings $RF(O_3)$ and $RF({O_3}^{tra})$. This method enables to consider the non-linearity of the tropospheric O_3 chemistry by interpolating within each LUT. It also considers the linear transport processes by adding the obtained O_3 changes to the reference simulation. The advantage of the presented algorithm is that it determines the climate effect very fast. Depending on the research question, a TransClim simulation takes between several seconds to hours. For example, to compute 3 dimensional variables for an emission scenario in Germany, TransClim takes up to 15 min on a standard computer while a full simulation with a complex climate chemistry model takes up to 2 months on a high performance computer. Thus, TransClim is about 6000 times faster.

TransClim determines not only the impact but also the contribution of road

traffic emissions to climate change. To compute the contribution, a so-called tagging method is applied in this thesis (Grewe et al., 2010). The determination of the contribution of road traffic emissions on O_3 already exists (Grewe et al., 2010, 2017). However, the computation of the contribution of short-lived species (OH and HO_2) introduced by Tsati (2014) and Grewe et al. (2017) showed certain short-comings such as that the budget between total concentration and contribution was not closed. Moreover, there was no method to assess the contribution of emissions to CH_4. Within the scope of this thesis, I further improved the tagging method of short-lived species which enables to attribute OH and HO_2 concentrations to emission sources such as road traffic. It is now not only applicable in the troposphere but also in the stratosphere. Moreover, the sum of all contributions now equals the total concentration. I also introduced a new tagging method which enables the source attribution of CH_4. It computes the contribution of an emission sector to CH_4. These tagging methods are used in EMAC and in TransClim to determine the contribution of road traffic emissions on O_3, OH and CH_4.

The response model TransClim was evaluated with simulations of the complex chemistry climate model EMAC. It revealed that the results obtained by TransClim show only very small deviations from EMAC. Over the source region Europe, the deviations are below 0.4 %. In the Southern Hemisphere, the deviations reach up to 6 % as in this region the contributions of road traffic emissions are generally small. This comparison showed that TransClim reproduces the EMAC results very well.

Within the scope of this thesis, the impact and contribution of two road traffic emission scenarios were quantified with TransClim. First, I evaluated the climate effect of three prospective mitigation strategies in Germany. These three scenarios describe how German road traffic emissions evolve under strict, medium and loose environmental regulation and emission controls. Simulations with TransClim revealed that the scenario with strict regulations shows the smallest impact of German road traffic emissions on O_3 and CH_4 (0.065 and 0.014 mW m^{-2}) as well as the smallest contributions to O_3 and CH_4 (0.077 and -0.18 mW m^{-2}). Second, the climate effect of biofuels in Europe were quantified for the first time. Two scenarios were constructed describing the cases that all vehicles in Europe use fuel blends with low and high biofuel contents. Simulations with TransClim showed that blends with a high content of biofuels have a large potential to reduce tropospheric O_3 and its radiative forcing. But ground level O_3 increases over central Europe which imposes a risk for human health. Blends with a low content of biofuels strongly reduce CH_4 and its impact on climate.

These two examples investigated the climate effect of road traffic emissions on a regional scale, namely in Europe and Germany. It showed that road traffic emissions in Germany and Europe cause an ${O_3}^{tra}$ radiative forcing of about 0.4 and 4.4 mW m^{-2} for the year 2010. Within the scope of the study "Revisiting the contribution of land transport and shipping emissions to tropospheric ozone" by Mertens, M., Grewe, V., Rieger, V. S. and Jöckel, P. (Atmos. Chem. Phys., 2018), I found that the contribution of global road traffic emissions to O_3 cause a radiative forcing of approximately 92 mW m^{-2}. Thus, German and European road traffic emissions contribute with about 0.4 % and 5 % to global radiative forcing of ${O_3}^{tra}$. These

contributions are smaller than the fractions of German and European road traffic emissions of NO_x, VOC and CO to global road traffic emissions. This effect is caused by the non-linearity of the tropospheric O_3 chemistry pointing out again the importance of including this non-linearity in the assessments of mitigation strategies.

A direct comparison of the presented assessments with existing literature is difficult as only few studies examine the global climate effect of regional road traffic emission scenarios. Hendricks et al. (2017) investigate the climate effect of German road traffic emissions finding radiative forcings of O_3 which compare well with the values obtained here. However, the radiative forcing of CH_4 derived within the scope of this thesis deviates significantly from Hendricks et al. (2017) as TransClim computes a smaller and positive OH change due to German road traffic emissions. So far, there is no study investigating the global climate effect of emissions caused by substitution of conventional fuels with biofuels in road traffic. Suarez-Bertoa et al. (2015) state that fuel blends with a large content of biofuels possess a larger O_3 forming potential than blends with low biofuel content. This trend is reflected by the results of this thesis as emissions of fuels with a high content of biofuels significantly increase ground level O_3 in Central Europe. However, a direct comparison is difficult because Suarez-Bertoa et al. (2015) examine the local effect of exhaust emissions while this thesis focusses on the regional effect over Europe.

Within the scope of this thesis, two examples of mitigation options for road traffic were investigated with TransClim. But TransClim offers also the opportunity to examine the climate effect of erroneous emission data. For example, automobile companies such as Volkswagen, Porsche and Audi installed defeat devices in diesel-power vehicles to manipulate exhaust emissions. Under certification test conditions, these vehicles meet emission standards while under actual road conditions, they release significantly higher amounts of emissions such as NO_x (Schiermeier, 2015). Tanaka et al. (2018) examined the climate effect caused by the installation of defeat devices in diesel vehicles. They find that these vehicles cause a larger short-term warming generated by additional tropospheric O_3. These kind of assessments can also be performed with the response model TransClim.

This thesis only focussed on the direct effect of road traffic emissions on the atmospheric chemistry. However, a change of atmospheric chemistry modifies the radiation budget and dynamical processes. This triggers feedback processes which can amplify or dampen the global warming caused by road traffic emissions. In the study entitled "Can feedback analysis be used to uncover the physical origin of climate sensitivity and efficacy differences?" by Rieger V., Dietmüller S. and Ponater M. (Clim Dyn 2017), I investigated these feedback processes which are caused by a rise of NO_x and CO surface emissions. The surface emissions of NO_x and CO were increased 9 times and the resulting Planck, lapse-rate, stratospheric temperature, albedo, water vapour and cloud feedback were investigated. In general, enhanced NO_x and CO emissions lead to an amplification of global warming by the albedo, water vapour and stratospheric temperature feedback. Planck and lapse-rate feedback cause a dampening of global warming. The effect of the cloud feedback is uncertain. However, these simulations need to be long-term simulations in which chemistry and dynamic are coupled and can interact with each other. As long-

term simulations are computational expensive, they are only possible for particular emission scenarios and not for setting up a LUT of TransClim.

Other response models also investigate the effect of traffic emissions on climate and air quality. For example, the response models LinClim and AirClim determine the effect of aviation emissions on climate while the response model TM5-FASST determines the effect of pollutants on air quality (Lim et al., 2007; Grewe and Stenke, 2008; Grewe et al., 2012; Dahlmann et al., 2016; Leitão et al., 2013). In the following, a short assessment of the different methods used by these model for determining the O_3 concentration and radiative forcing is presented and compared to the interpolation algorithm used by TransClim.

LinClim computes the radiative forcings of CO, O_3, CH_4, water vapour, contrails and aerosols for an aviation emission scenario by using a linear approach (Lim et al., 2007). To compute the RF of O_3, LinClim scales the O_3 RF of a reference year with the aircraft fuel use per year and NO_x emissions per mass of fuel. This linearisation allows for determining the temporal evolution of the RF. The approach reproduces the basic results obtained by the complex chemistry climate model ECHAM4/OPYC3 (Roeckner et al., 1999). However, noticeable deviations are observed for O_3 RF. The response model AirClim computes the concentration of CO_2, O_3, CH_4, water vapour and contrails as well as their corresponding RF and temperature changes for aviation emissions (Grewe and Stenke, 2008; Dahlmann et al., 2016). It therefore uses a linear approach for the calculation of CO_2, O_3 and CH_4 and a non-linear approach for the calculation of contrails, RF and temperature changes. For this response model, 24 emission regions located between 52 and 967 hPa are defined. Using the chemistry climate model E39/C (Hein et al., 2001), one emission perturbation simulation is performed in each emission region. AirClim combines the precalculated E39/C simulations for an aviation emission scenario to determine concentration change of O_3. Subsequently, the temporal evolution is calculated by solving the linear equation $\frac{d\Delta C}{dt} = sP(t) - \frac{1}{\tau}\Delta C$ with τ being the lifetime and P the production term. The factor s normalizes the concentration change to the concentration change determined by the combination of the precalculated E39/C simulations. The corresponding radiative forcing is deduced in a similar way. The results obtained by AirClim are in good agreement with the values derived by the full chemistry climate model E39/C. O_3 presents a similar pattern and the RF agrees within 15 %. Summing up, LinClim and AirClim uses both a linear approach to determine the O_3 concentration. Both response models present good results which shows that the linearisation is working for O_3 changes in the stratosphere well. In this region, the O_3 chemistry is not characterised by strong non-linearities as it is in the troposphere. Consequently, a linear approach for determining tropospheric O_3 would lead to higher errors. Thus, a non-linear interpolation algorithm as used by TransClim is better suitable for computing O_3 concentrations in the troposphere.

The response model TM5-FASST, developed at Joint Research Centre (Italy), computes the impact of pollutants in the troposphere. It calculates the impact of precursors such as NO_x, SO_2, CO and BC on air quality. It further derives the radiative forcings and temperature changes as well as the mortality, statistical lifetime expectance and the effect of O_3 on vegetation and crop yield (Leitão et al.,

2013). However, TM5-FASST assumes a linear relation between precursors and pollutants such as O_3. For this response model, 56 emission regions are defined. In each region, the emissions of each precursors are reduced by 20 % and the resulting impact is simulated with the chemical transport model TM5-CTM (Krol et al., 2005). Subsequently, to compute for example the O_3 concentration for an emission scenario, the O_3 change of all emission region is scaled with the emission change of the emission scenario. Then, the resulting O_3 change of each O_3 precursor and of each emission region is added to the reference O_3 concentration. This approach performs well. In general, O_3 is overestimated (underestimated) for increased (decreased) emissions. In particular regions with high O_3 precursor emissions, such as Asia, Europe and North America, show deviations of up to 20 percent points. These large deviations are caused by the non-linearity of the tropospheric O_3 chemistry which is not regarded by this linear approach. The impact on O_3 of the three considered O_3 precursors NO_x, VOC and CO are only considered separately by adding up each O_3 change to the reference O_3. In comparison, TransClim interpolates within a three dimensional LUT of NO_x, VOC and CO emissions and thus considers the interaction of the three precursors in producing O_3. Both models add the resulting O_3 changes to the reference O_3 as the transport effects are linear. As the non-linear O_3 chemistry is considered in TransClim, it reveals deviations which are by far lower than the ones obtained by TM5-FASST. Although, TM5-FASST computes a broader range of impact metrics than TransClim, it does not account for the contribution of the precursors. Hence, no response model so far investigates the impact of road traffic emissions on climate as well as the contributions of these emissions. Therefore, TransClim is a unique response model.

The response model TransClim presented in this thesis is operational. It is able to compute the most import features of the climate effects of road traffic emissions on O_3 and CH_4. TransClim considers seven emission region (Germany, Western Europe, Northern Europe, Eastern Europe, Southern Europe, North America and Asia) and allows for varying the road traffic emissions of NO_x, VOC and CO from 0 to 200 % in each emission region. By assuming an uncertainty range of the input road traffic emissions, TransClim also enables to determine the uncertainty of the climate effects. However, the development of TransClim is not completed. There are still further development steps planned. An extension of the LUT onto more emission regions is desirable. The regions South East Asia and India show a strong increase of road traffic and thus present interesting regions for mitigation strategies. Moreover, the inclusion of other surface transportation modes such as shipping broadens the applicability of TransClim. Climate change can be determined with different metrics. So far, TransClim only uses the metric radiative forcing. The usage of other metrics such as surface temperature change shall also be implemented. The determination of the change of aerosols caused by an emission scenario would further deepen the understanding of the climate effect of a particular mitigation strategy. Furthermore, it would be desirable to extend the current approach of TransClim to include the effect of a change in O_3 background concentration. This would enable to determine the climate effect of future mitigation strategies. To further assess the effect on air quality with TransClim, simulations with a region model such as

MECO(n) (Kerkweg and Jöckel, 2012a,b) would be necessary.

Although further extensions of the response model TransClim are planned, the model is ready to assess the climate effect of many road traffic emission scenarios.

A

Appendix

A.1. EMAC simulation with three years time period

This section describes an EMAC simulation over a three years time period (2008 to 2010). To save computational resources, the same EMAC setup as described in sect. 3.3 is used but with a low resolution of T21L19. This corresponds to a Gaussian grid with approximately $5.6° \times 5.6°$ and 19 vertical layers reaching up to 10 hPa. The time step length is set to 30 minutes. The tropospheric O_3 and road traffic O_3^{tra} averaged up to 300 hPa for the years 2008 to 2010 are presented in fig. A.1. Additionally, the net radiative flux change caused by road traffic O_3^{tra} is shown. It is calculated by subtracting the 2nd radiation call (rad02 of O_3) and the 3rd radiation call (rad03 of O_3-O_3^{tra}).

Due to its photochemical production, O_3 has a pronounced seasonal cycle. Consequently, O_3 and O_3^{tra} vary strongly during the seasons. Maximum values are found in May and June. In January, the mixing ratios drop by 8 ppb and 0.6 ppb, respectively. The net flux of O_3^{tra} also varies strongly during the year which corresponds to the variation of the O_3^{tra} mixing ratio. Despite the large seasonal cycle, the year-to-year variability is very low. This justifies the simplification to use only one year of EMAC simulation for the analysis.

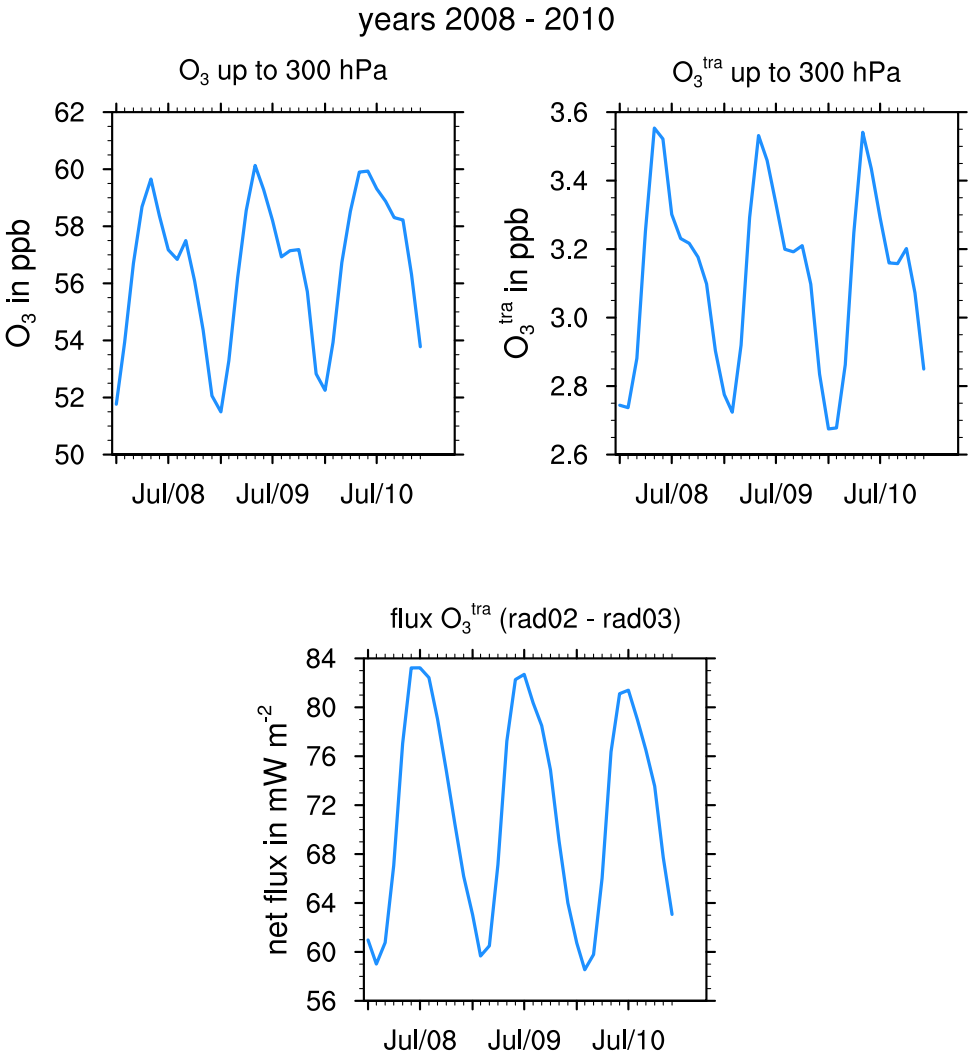

Figure A.1: Tropospheric O_3 and road traffic O_3^{tra} averaged up to 300 hPa as well as net radiative flux O_3^{tra}. The latter is computed by subtracting the 2nd radiation call (rad02) corresponding to the changed O_3 fields and the 3rd radiation call (rad03) corresponding to the net radiative flux change of O_3 – O_3^{tra} (rad02 - rad03). Monthly mean for the years 2008 to 2010 are shown.

A.2. List of submodels

Table A.1 gives a detailed overview of the submodels which are used for the simulation setup described in sect. 3.3.

Submodel	Description	References
AEROPT	aerosol optical properties	Dietmüller et al. (2016)
AIRSEA	air-sea exchange of tracers	Pozzer et al. (2006)
CH4	methane oxidation and linkage to hydrological cycle	
CHANNEL	memory and meta-data management, data export	Jöckel et al. (2010)
CLOUD	cloud parametrisation	Roeckner et al. (2006), and references therein
CLOUDOPT	cloud optical properties	Dietmüller et al. (2016)
CONVECT	convection parametrisation	Tost et al. (2006b)
CVTRANS	convective tracer transport	Tost et al. (2010)
DDEP	dry deposition of tracers and aerosols	Kerkweg et al. (2006a)
E5VDIFF	land-atmosphere exchange and vertical diffusion	Roeckner et al. (2003)
GWAVE	non-orographic gravity waves	Baumgaertner et al. (2013)
IMPORT	import data from external files	Kerkweg and Jöckel (2015)
JVAL	determination of photolysis rates	Sander et al. (2014)
LNOX	lightning NO_x production	Tost et al. (2007); Jöckel et al. (2010)
MECCA	chemistry in troposphere and stratosphere	Jöckel et al. (2010); Sander et al. (2011)
MSBM	multiphase chemistry in stratosphere	Jöckel et al. (2010)
OFFEMIS	offline emissions of tracers and aerosols	Kerkweg et al. (2006b)

Continued on next page

Table A.1 – *Continued from previous page*

Submodel	Description	References
ONEMIS	determination of online emissions	Kerkweg et al. (2006b)
ORBIT	Earth orbit calculations	
OROGW	orographic gravity wave drag	
PTRAC	testing with passive tracers	Jöckel et al. (2008)
QBO	Newtonian relaxation of the QBO (quasi-biennial oscillation)	Giorgetta and Bengtsson (1999); Jöckel et al. (2006)
RAD	radiative transfer calculation	Dietmüller et al. (2016)
RAD_FUBRAD	sub-submodel of RAD, high-resolution short-wave heating rate parametrisation	Nissen et al. (2007); Dietmüller et al. (2016)
SCALC	simple calculations	Jöckel et al. (2016)
SCAV	wet deposition and scavenging of tracers and aerosols	Tost et al. (2006a)
SEDI	aerosol sedimentation	Kerkweg et al. (2006a)
SURFACE	surface parameters	Jöckel et al. (2016)
TAGGING	attribution of source emissions to trace gases	Grewe et al. (2017)
TNUDGE	Newtonian relaxation of tracers	Kerkweg et al. (2006b)
TRACER	data and meta-data management of chemical tracers	Jöckel et al. (2008)
TROPOP	diagnostic calculation of tropopause height	Jöckel et al. (2006)

Table A.1: List of submodel used for the simulation setup described in sect. 3.3.

A.3. HO_x tagging method V1.1

A.3.1. Reaction rates

Fig. A.2 shows the reaction rates of all reactions including HO_x with a tropospheric or stratospheric annual mean reaction rate larger than 10^{-15} mol mol^{-1} s^{-1}. The reactions rates are received by an EMAC simulation (setup according to sect. 3.3). For this simulation, NO_x emissions from lightning are scaled to 4 Tg(N) per year.

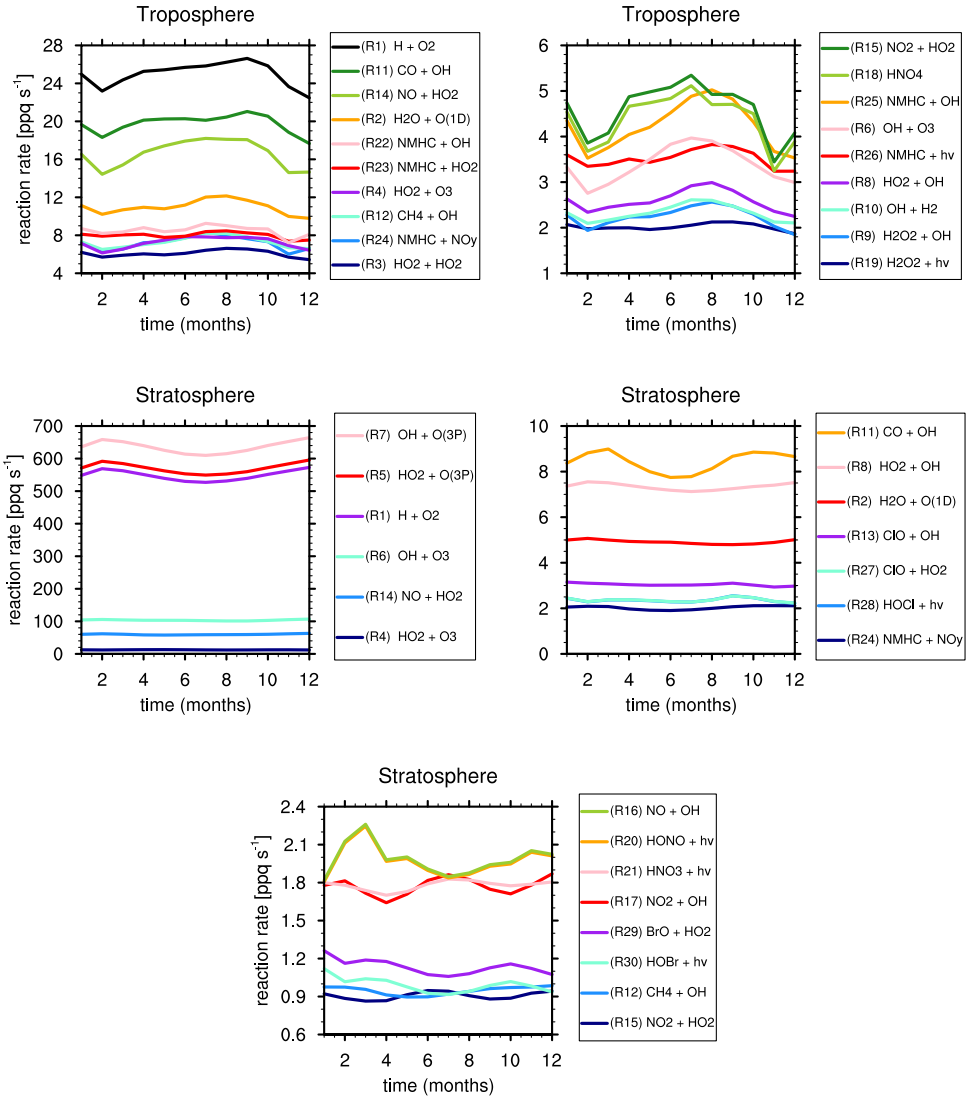

Figure A.2: Reaction rates of HO_x reactions with a tropospheric or stratospheric annual mean reaction rate larger than 10^{-15} mol mol^{-1} s^{-1}.

A.3.2. Exclusion of reactions from reduced HO_x reaction system V1.1

The annual mean reaction rates of the following three reactions are also greater than 10^{-15} mol mol^{-1} s^{-1} and thus would usually be accounted to the reduced HO_x reaction system V1.1.

$$H_2O_2 + h\nu \longrightarrow 2OH \tag{A.1}$$

$$HOCl + h\nu \longrightarrow OH + Cl \tag{A.2}$$

$$HOBr + h\nu \longrightarrow OH + Br \tag{A.3}$$

However, the tagging method can not be applied for these three reactions.

To include the OH production by the photolysis of H_2O_2 (reaction A.1), it would be necessary to tag H_2O_2. Since the production and the loss of H_2O_2 are not balanced, steady-state can not be assumed. Thus, a similar tagging approach as for HO_x and H is not valid for H_2O_2. Consequently, reaction (A.1) is excluded from the HO_x tagging method. This reaction contributes about 8 % to the total OH production in the troposphere.

Hypochlorous acid (HOCl) and hypobromous acid (HOBr) are photolysed in the stratosphere and produce OH (reaction A.2 and A.3), but HOCl and HOBr are not tagged. Although the steady-state assumption is globally valid, locally the production and loss of HOCl and HOBr are not balanced everywhere. In the stratosphere, for about 65 % of the model grid boxes the production deviates by more than 10 % from the loss of HOCl and HOBr. In particular, in the transition area between day and night in the polar region, the production deviates strongly from the loss. Also at night where the reactions mostly occur, the steady-state is not fulfilled everywhere. Moreover, since both species are not radicals, their lifetimes can not be assumed to be short. Hence, the tagging method can not be applied, so the reactions (A.2) and (A.3) are omitted from the OH production.

Considering reactions (A.1), (A.2) and (A.3) to the reduced HO_x reaction system V1.1 would lead to a significantly larger OH production in the troposphere representing about 98 % of the total OH production rate derived by MECCA. In the stratosphere, 91 % of the total OH production would be regarded. Hence, excluding these reactions from the reduced HO_x reaction system V1.1 worsens the steady-state between OH production and loss. The rest term *resOH* introduced in sect. 4.4.4 compensates this deviation from production and loss rate.

A.3.3. Rest term

Fig. A.3 shows the zonal mean of the rest terms *resOH*, *resHO2* and *resH*.

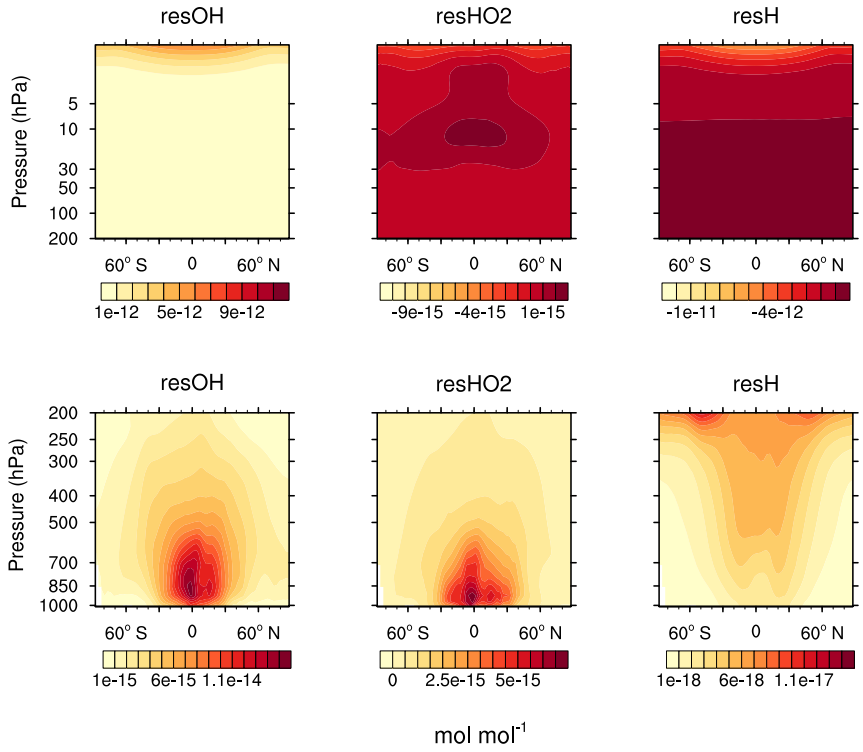

Figure A.3: Zonal mean of rest terms *resOH*, *resHO2* and *resH*. The first row ranges from 1 to 200 hPa, the second row from 1000 to 200 hPa.

A.4. Input emissions for 4-box-model

Table A.2 presents the NO_x and VOC emissions of the different emission sectors for the 4-box-model. The values are deduced from the emission inventory MACCity (Granier et al., 2011). Further explanations are found in sect. 3.4. These input variables are used for Example 2 "Effect of road traffic emissions" (sect. 5.3.2.2). Moreover, to obtain realistic results, the reaction rates are adapted to $p = 8.9 \cdot 10^{-4}$ ppb^{-1} s^{-1}, $d_x = 2.5 \cdot 10^{-4}$ ppb^{-1} s^{-1} and $d_y = 2.5 \cdot 10^{-6}$ ppb^{-2} s^{-1}.

		(1) Eurasia	(2) Pacific	(3) North America	(4) Atlantic
road traffic	NO_x	$1.0 \cdot 10^{-5}$	0	$1.2 \cdot 10^{-5}$	0
	VOC	$1.8 \cdot 10^{-5}$	0	$4.0 \cdot 10^{-6}$	0
shipping	NO_x	$1.5 \cdot 10^{-6}$	$2.0 \cdot 10^{-6}$	0	$2.5 \cdot 10^{-6}$
	VOC	$1.0 \cdot 10^{-7}$	$2.0 \cdot 10^{-7}$	0	$2.0 \cdot 10^{-7}$
aviation	NO_x	$5.0 \cdot 10^{-7}$	$8.0 \cdot 10^{-8}$	$1.0 \cdot 10^{-6}$	$8.0 \cdot 10^{-8}$
	VOC	0	0	0	0
industry	NO_x	$1.0 \cdot 10^{-5}$	0	$3.0 \cdot 10^{-6}$	0
	VOC	$1.6 \cdot 10^{-5}$	0	$4.0 \cdot 10^{-6}$	0
agricultural	NO_x	$2.5 \cdot 10^{-7}$	0	$1.0 \cdot 10^{-7}$	0
waste burning	VOC	$1.8 \cdot 10^{-6}$	0	$2.0 \cdot 10^{-7}$	0
biomass	NO_x	$9.1 \cdot 10^{-8}$	0	$6.8 \cdot 10^{-8}$	0
burning	VOC	$3.6 \cdot 10^{-7}$	0	$2.3 \cdot 10^{-7}$	0
background	NO_x	$2.0 \cdot 10^{-5}$	0	$1.0 \cdot 10^{-5}$	0
emissions	VOC	$1.0 \cdot 10^{-4}$	$5.0 \cdot 10^{-6}$	$8.0 \cdot 10^{-5}$	$6.0 \cdot 10^{-6}$

Table A.2: Input emissions in ppb s^{-1} for sect. 5.3.2.2 for the 4-box-model.

A.5. EMAC model setup for section 5.3.3.4

The EMAC simulations which are used for the analysis of the sect. 5.3.3.4 "Inter- and extrapolation of look-up table" has a coarse resolution of T21L19 (approx. 5.6° × 5.6°) with 19 vertical layers up to 10 hPa. The time step length is set to 30 minutes. The time period of July 2007 to December 2008 is simulated: after half a year of spin-up time, the year 2008 is analysed. The spin-up time of half a year is sufficient as the simulation branches off from the simulation *RC1SD-base-10a* which is already in steady-state (Jöckel et al., 2016). Moreover, an EMAC simulation over a three years time period further shows that the climate system is in steady-state after half a year of spin-up time (see fig. A.1). Otherwise, the model setup equals the setup descriped in sect. 3.3. The road traffic emissions are split up as described in appendix A.6. Two emission regions are chosen for the analysis: Western and Eastern Europe (see fig. A.4). These emission regions are used as both regions are situated in a strongly polluted area. Moreover, they are very close to each other. This enables to intensively study the effect of the non-linear O_3 chemistry and the transport. Within these two emission regions, the road traffic emissions of NO_x and VOC are varied between 0 and 3 (as shown in fig. A.5).

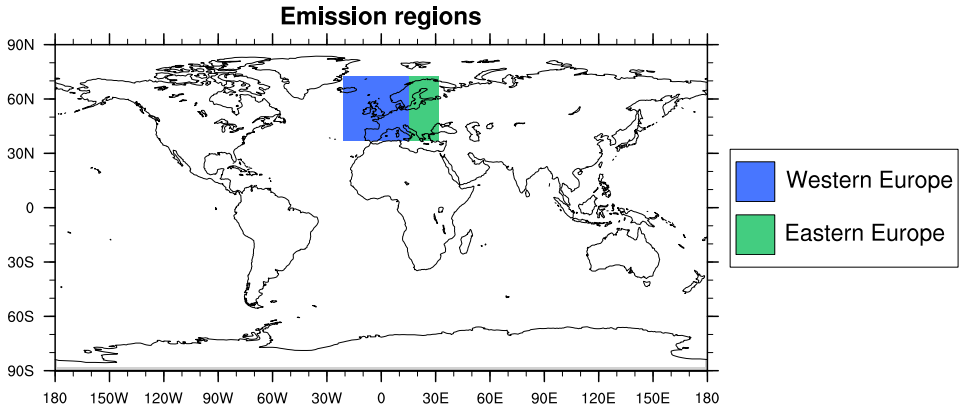

Figure A.4: Emission regions: Western and Eastern Europe.

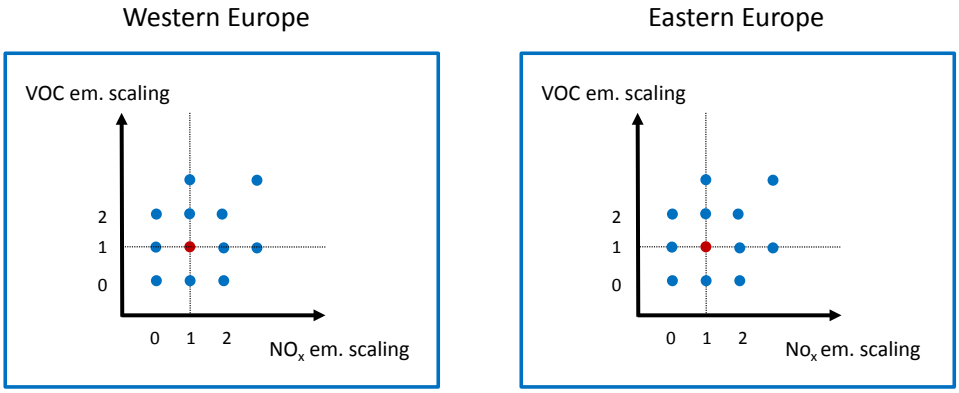

Figure A.5: Resolution of emission variation simulations performed with EMAC for emission regions Western and Eastern Europe. The emission scaling factors for the NO_x and VOC road traffic emissions are presented. The reference simulation is indicated with a red dot.

A.6. Split-up of emissions in EMAC

At first, the emission files, which are read in by EMAC, need to be split up into the emission regions. Thus, each emission region contains the emission data for its corresponding region. The rest is set to 0. However, to maintain the total emission amount, a residual files is created which contains the residual emissions.

Two examples are given for the emission region "GER" and the residual file "RES":

```
CCMI_DLR1.0_AR5-RCP8.5_road_MISC_195001-201012_GER.nc
CCMI_DLR1.0_AR5-RCP8.5_road_MISC_195001-201012_RES.nc
```

In MESSy, the emission files for the different emission regions are read in via the namelist structure `import.nml`:

```
! ROAD (LAND)
! (NO,CO,SO2,NH3,C2H4,C2H6,C3H6,C3H8,NC4H10,CH3CHO,CH3COCH3,CH3CO2H,
!  CH3OH,HCHO,HCOOH,MEK)

! emission region: Germany
!RG_TRIG(70) = 1,'months', 'first',0, 'ROAD_GER', 721,1,732,702,
'NML=./emregions/CCMI_DLR1.0_AR5-RCP8.5_road_MISC_195001-201012_regGER.nml',

! emission region: rest of the world
RG_TRIG(74) = 1,'months', 'first',0, 'ROAD_RES', 721,1,732,702,
'NML=./emregions/CCMI_DLR1.0_AR5-RCP8.5_road_MISC_195001-201012_regRES.nml',
```

For scaling the road traffic emissions, I explicitly introduced emission scaling factors for NO_x, VOC and CO emissions in the MESSy run script

```
### Scaling factors of emission regions
sNOx_GER=1.0
sVOC_GER=1.0
sCO_GER=1.0
...
```

These scaling factors are passed to `offemis.nml`. Here, the emissions of each emission region are scaled and then added to the corresponding tracer. An example for the emission region Germany (GER) is given:

```
! emission region: Germany
EMIS_IN(110) = 'NO,$sNOx_GER;NOytra,$sNOx_GER',       'import_grid','ROAD_GER_NO',      'GP=1'
EMIS_IN(111) = 'CO,$sCO_GER;COtra,$sCO_GER' ,         'import_grid','ROAD_GER_CO',      'GP=1'
EMIS_IN(112) = 'SO2' ,                                'import_grid','ROAD_GER_SO2',     'GP=1'
EMIS_IN(113) = 'C2H4,$sVOC_GER;NMHCtra,$sVOC_GER' ,   'import_grid','ROAD_GER_C2H4',    'GP=1'
EMIS_IN(114) = 'C2H6,$sVOC_GER;NMHCtra,$sVOC_GER' ,   'import_grid','ROAD_GER_C2H6',    'GP=1'
EMIS_IN(115) = 'C3H6,$sVOC_GER;NMHCtra,$sVOC_GER' ,   'import_grid','ROAD_GER_C3H6',    'GP=1'
EMIS_IN(116) = 'C3H8,$sVOC_GER;NMHCtra,$sVOC_GER' ,   'import_grid','ROAD_GER_C3H8',    'GP=1'
EMIS_IN(117) = 'NC4H10,$sVOC_GER;NMHCtra,$sVOC_GER' , 'import_grid','ROAD_GER_NC4H10',  'GP=1'
!EMIS_IN(118) = 'CH3CHO' ,                            'import_grid','ROAD_GER_CH3CHO',  'GP=1'
EMIS_IN(119) = 'CH3COCH3,$sVOC_GER;NMHCtra,$sVOC_GER','import_grid','ROAD_GER_CH3COCH3','GP=1'
!EMIS_IN(120) = 'CH3CO2H',                            'import_grid','ROAD_GER_CH3CO2H', 'GP=1'
EMIS_IN(121) = 'CH3OH,$sVOC_GER;NMHCtra,$sVOC_GER' ,  'import_grid','ROAD_GER_CH3OH',   'GP=1'
EMIS_IN(122) = 'HCHO,$sVOC_GER;NMHCtra,$sVOC_GER' ,   'import_grid','ROAD_GER_HCHO',    'GP=1'
!EMIS_IN(123) = 'HCOOH' ,                             'import_grid','ROAD_GER_HCOOH',   'GP=1'
EMIS_IN(124) = 'MEK,$sVOC_GER;NMHCtra,$sVOC_GER' ,    'import_grid','ROAD_GER_MEK',     'GP=1'
EMIS_IN(125) = 'NH3' ,                                'import_grid','ROAD_GER_NH3',     'GP=1'
```

A detailed description of the namelist structure and the file import in MESSy can be found in Kerkweg et al. (2006b) and Kerkweg and Jöckel (2015).

A.7. List of EMAC simulations for LUT of TransClim

Table A.3 presents a list of all EMAC simulations used in this thesis to create the LUT of TransClim. The emission scaling factors are indicated.

Em. region	Emission Scaling			Em. region	Emission Scaling		
	NO_x	VOC	CO		NO_x	VOC	CO
Reference	1	1	1	West. Europe	0	0	0
Germany	0	0	0		0	0	1
	0	0	1		0	1	0
	0	1	0		0	1	1
	0	1	1		0	1	2
	0	1	2		0	2	1
	0	2	1		1	0	0
	1	0	0		1	0	1
	1	0	1		1	0	2
	1	0	2		1	1	0
	1	1	0		1	1	2
	1	1	2		1	2	0
	1	1	3		1	2	0
	1	2	0		1	2	1
	1	2	1		1	2	2
	1	2	2		2	0	1
	1	3	1		2	1	0
	2	0	1		2	1	1
	2	1	0		2	1	2
	2	1	1		2	2	1
	2	1	2				
	2	2	1				
	3	1	1				
North. Europe	0	0	0	South. Europe	0	0	0
	0	0	1		0	1	1
	0	1	1		0	2	1
	1	0	1		1	0	1
	1	1	0		1	1	0
	1	1	2		1	1	2

Continued on next page

Table A.3 – *Continued from previous page*

Em. region	**Emission Scaling**			**Em. region**	**Emission Scaling**		
	NO_x	**VOC**	**CO**		**NO_x**	**VOC**	**CO**
	1	2	1		1	2	1
	2	1	1		2	1	1
East. Europe	0	0	0	North America	-	-	-
	0	1	1	Asia	-	-	-
	1	0	1				
	1	1	0				
	1	1	2				
	1	2	1				
	2	1	1				

Table A.3: List of emission variation simulations performed with EMAC and used as LUT for TransClim.

A.8. Evaluation of TransClim

Fig. A.6 shows the relative frequency distribution for all grid boxes in the Northern Hemisphere. The relative errors of O_3, CH4loss and flxn(O_3) are very small. The relative errors of O_3^{tra}, CH4losstra and flxn(O_3^{tra}) are larger. Few grid boxes deviate by more than 100 %. In general, TransClim underestimates the values. Table A.4 indicates the global mean values of selected variables. The deviations are all below 1 %.

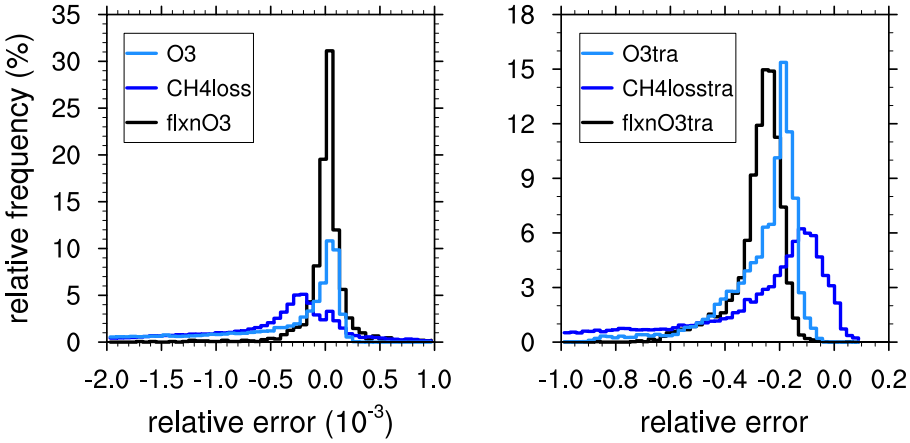

Figure A.6: Relative frequency distribution only for the Northern Hemisphere.

Variable	TransClim	EMAC	Difference (%)
Tropospheric O_3 (DU)	38.1371	38.1375	-0.001
Tropospheric O_3^{tra} (DU)	2.1392	2.1542	-0.70
τ_{CH4} (yr)	7.7159	7.7158	0.001
τ_{CH4}^{tra} (yr)	95.0336	94.4696	0.60
flxn O_3 (Wm^{-2})	-0.8051	-0.8051	0.0
flxn O_3^{tra} (Wm^{-2})	0.0804	0.0812	-0.89

Table A.4: Global means derived by TransClim and EMAC for the emission scaling indicated in table 5.4.

Bibliography

Ackerman, A. S., Toon, O. B., Stevens, D. E., Heymsfield, A. J., Ramanathan, V., and Welton, E. J. Reduction of Tropical Cloudiness by Soot. *Science*, 288 (5468):1042–1047, 2000. ISSN 0036-8075. URL http://science.sciencemag.org/content/288/5468/1042.

Ainsworth, E. A., Yendrek, C. R., Sitch, S., Collins, W. J., and Emberson, L. D. The Effects of Tropospheric Ozone on Net Primary Productivity and Implications for Climate Change. *Annual Review of Plant Biology*, 63(1):637–661, 2012. URL https://doi.org/10.1146/annurev-arplant-042110-103829. PMID: 22404461.

Albrecht, B. Aerosols, cloud microphysics, and fractional cloudiness. *Science*, 245 (4923):1227–1230, 1989. ISSN 0036-8075.

Albritton, D., Meira Filho, L., Cubasch, U., Dai, X., Ding, Y., Griggs, D., Hewitson, B., Houghton, J., Isaksen, I., Karl, T., McFarland, M., Meleshko, V., Mitchell, J., Noguer, M., Nyenzi, B., Oppenheimer, M., Penner, J., Pollonais, S., Stocker, T., and Trenberth, K. Technical Summary. In Houghton, J., Ding, Y., Griggs, D., Noguer, M., van der Linden, P., Dai, X., Maskell, K., and Johnson, C., editors, *Climate Change 2001: The Scientific Basis. Contribution of Working Group 1 to the Third Assessment Report of the Intergovernmental Panel on Climate Change*, page 21pp. Cambridge University Press, Cambridge, United Kingdom and New York, NY, USA, 2001.

Amann, M., Bertok, I., Cofala, J., Gyarfas, F., Heyes, C., Klimont, Z., Schoepp, W., and Winiwarter, W. Baseline Scenarios for the Clean Air for Europe (CAFE) Programme. Technical report, European Commission Directorate General for Environment, Directorate C – Environment and Health, 2004. URL http://pure.iiasa.ac.at/7328/.

Amato, F., Cassee, F. R., van der Gon, H. A. D., Gehrig, R., Gustafsson, M., Hafner, W., Harrison, R. M., Jozwicka, M., Kelly, F. J., Moreno, T., Prevot, A. S., Schaap, M., Sunyer, J., and Querol, X. Urban air quality: The challenge of traffic non-exhaust emissions. *Journal of Hazardous Materials*, 275:31 – 36, 2014. ISSN 0304-3894. URL http://www.sciencedirect.com/science/article/pii/S030438941400315X.

Ångström, A. Atmospheric turbidity, global illumination and planetary albedo of the earth. *Tellus*, 14(4):435–450, 1962. ISSN 2153-3490. URL http://dx.doi.org/10.1111/j.2153-3490.1962.tb01356.x.

Balkanski, Y., Myhre, G., Gauss, M., Rädel, G., Highwood, E. J., and Shine, K. P. Direct radiative effect of aerosols emitted by transport: from road, shipping and aviation. *Atmospheric Chemistry and Physics*, 10(10):4477–4489, 2010. URL https://www.atmos-chem-phys.net/10/4477/2010/.

Baumgaertner, A. J. G., Jöckel, P., Aylward, A. D., and Harris, M. J. Simulation of Particle Precipitation Effects on the Atmosphere with the MESSy Model System. In Lübken, F.-J., editor, *Climate and Weather of the Sun-Earth System (CAWSES): Highlights from a Priority Program*, pages 301–316, Dordrecht, 2013. Springer Netherlands. ISBN 978-94-007-4348-9. URL https://doi.org/10.1007/978-94-007-4348-9_17.

Bell, M., Peng, R., and Dominici, F. The exposure-response curve for ozone and risk of mortality and the adequacy of current ozone regulations. *Environmental Health Perspectives*, 114(4):532–536, 4 2006. ISSN 0091-6765.

Berntsen, T., Fuglestvedt, J., Joshi, M., Shine, K., Stuber, N., Ponater, M., Sausen, R., Hauglustaine, D., and Li, L. Response of climate to regional emissions of ozone precursors: sensitivities and warming potentials. *Tellus*, 57B:283–304, 2005.

Berntsen, T. K., Isaksen, I. S. A., Myhre, G., Fuglestvedt, J. S., Stordal, F., Larsen, T. A., Freckleton, R. S., and Shine, K. P. Effects of anthropogenic emissions on tropospheric ozone and its radiative forcing. *Journal of Geophysical Research-Atmospheres*, 102(D23):28101–28126, 1997. ISSN 0747-7309. URL <GotoISI>://WOS:000071162700010.

Borken-Kleefeld, J., Steller, H., Meretei, T., and Vanhove, F. Global and Country Inventory of Road Passenger and Freight Transportation: Fuel Consumption and Emissions of Air Pollutants in Year 2000. *Transportation Research Record*, 2011, 01 2007.

Bowman, K. W., Shindell, D. T., Worden, H. M., Lamarque, J. F., Young, P. J., Stevenson, D. S., Qu, Z., de la Torre, M., Bergmann, D., Cameron-Smith, P. J., Collins, W. J., Doherty, R., Dalsøren, S. B., Faluvegi, G., Folberth, G., Horowitz, L. W., Josse, B. M., Lee, Y. H., MacKenzie, I. A., Myhre, G., Nagashima, T., Naik, V., Plummer, D. A., Rumbold, S. T., Skeie, R. B., Strode, S. A., Sudo, K., Szopa, S., Voulgarakis, A., Zeng, G., Kulawik, S. S., Aghedo, A. M., and Worden, J. R. Evaluation of ACCMIP outgoing longwave radiation from tropospheric ozone using TES satellite observations. *Atmos. Chem. Phys.*, 13(8): 4057–4072, 2013. ISSN 1680-7324. URL http://www.atmos-chem-phys.net/13/4057/2013/.

Breuer, N., Hauber, T., Schaller, J. K., Schernewski, R., Stein, S., and Wirth, R. Abgasnachbehandlung für Dieselmotoren. In Reif, K., editor, *Abgastechnik für Verbrennungsmotoren*, pages 59–78, Wiesbaden, 2015. Springer Fachmedien Wiesbaden. ISBN 978-3-658-09522-2. URL https://doi.org/10.1007/978-3-658-09522-2_3.

Bringezu, S., Schütz, H., O'Brien, M., Kauppi, L., Howarth, R. W., and McNeely, J. Towards Sustainable Production and Use of Resources: Assessing Biofuels. Technical report, United Nations Environment Programme, 2009.

Butler, T., Lawrence, M., Taraborrelli, D., and Lelieveld, J. Multi-day ozone production potential of volatile organic compounds calculated with a tagging approach. *Atmospheric Environment*, 45(24):4082 – 4090, 2011. ISSN 1352-2310. URL http://www.sciencedirect.com/science/article/pii/S1352231011003001.

Cess, R. D., Potter, G. L., Blanchet, J. P., Boer, G. J., Del Genio, A. D., Déqué, M., Dymnikov, V., Galin, V., Gates, W., Ghan, S. J., Kiehl, J. T., Lacis, A. A., Le Treut, H., Li, Z.-X., Liang, X.-Z., McAvaney, B. J., Meleshko, V. P., Mitchell, J. F. B., Morcrette, J.-J., Randall, D. A., Rikus, L., Roeckner, E., Royer, J. F., Schlese, U., Sheinin, D. A., Slingo, A., Sokolov, A. P., Taylor, K. E., Washington, W. M., Wetherald, R. T., Yagai, . I, and Zhang, M.-H. Intercomparison and Interpretation of Climate Feedbacks Processes in 19 Atmospheric General Circulation Models. *J. Geophys. Res.*, 95(D10):16,601–16,615, 1990.

Chen, T.-M., Kuschner, W. G., Gokhale, J., and Shofer, S. Outdoor Air Pollution: Nitrogen Dioxide, Sulfur Dioxide, and Carbon Monoxide Health Effects. *The American Journal of the Medical Sciences*, 333(4):249 – 256, 2007. ISSN 0002-9629. URL http://www.sciencedirect.com/science/article/pii/S0002962915325933.

Chester, M. V. and Horvath, A. Environmental assessment of passenger transportation should include infrastructure and supply chains. *Environmental Research Letters*, 4(2):024008, 2009. URL http://stacks.iop.org/1748-9326/4/i=2/a=024008.

Ciais, P., Sabine, C., Bala, G., Bopp, L., Brovkin, J., Canadell, V., Chhabra, A., DeFries, R., Galloway, J., Heimann, M., Jones, C., Le Quéré, C., Myneni, R., Piao, S., and Thornton, P. Carbon and Other Biogeochemical Cycles. In Stocker, T., Qin, D., Plattner, G.-K., Tignor, M., Allen, S., Boschung, J., Nauels, A., Xia, Y., Bex, V., and Midgley, P., editors, *Climate Change 2013: The Physical Science Basis. Contribution of Working Group I to the Fifth Assessment Report of the Intergovernmental Panel on Climate Change*, 2013.

Clappier, A., Belis, C. A., Pernigotti, D., and Thunis, P. Source apportionment and sensitivity analysis: two methodologies with two different purposes. *Geoscientific Model Development*, 10(11):4245–4256, 2017. URL https://www.geosci-model-dev.net/10/4245/2017/.

Coates, J. and Butler, T. M. A comparison of chemical mechanisms using tagged ozone production potential (TOPP) analysis. *Atmospheric Chemistry and Physics*, 15(15):8795–8808, 2015. URL https://www.atmos-chem-phys.net/15/8795/2015/.

Council, N. R. *Rethinking the Ozone Problem in Urban and Regional Air Pollution*. The National Academies Press, Washington, DC,

1991. ISBN 978-0-309-04631-2. URL https://www.nap.edu/catalog/1889/rethinking-the-ozone-problem-in-urban-and-regional-air-pollution.

Crippa, M., Janssens-Maenhout, G., Dentener, F., Guizzardi, D., Sindelarova, K., Muntean, M., Van Dingenen, R., and Granier, C. Forty years of improvements in European air quality: regional policy-industry interactions with global impacts. *Atmospheric Chemistry and Physics*, 16(6):3825–3841, 2016. URL https://www.atmos-chem-phys.net/16/3825/2016/.

Crutzen, P. J. and Schmailzl, U. Chemical budgets of the stratosphere. *Planetary and Space Science*, 31:1009–1032, 1983.

Dahlmann, K., Grewe, V., Frömming, C., and Burkhardt, U. Can we reliably assess climate mitigation options for air traffic scenarios despite large uncertainties in atmospheric processes? *Transportation Research Part D: Transport and Environment*, 46(Supplement C):40 – 55, 2016. ISSN 1361-9209. URL http://www.sciencedirect.com/science/article/pii/S1361920916000353.

DeAngelo, B., Beach, R., Rose, S., Salas, W., Li, C., DelGrosso, S., and Sulser, T. International Agriculture: Estimates of Non-CO_2 and Soil Carbon Marginal Mitigation Costs. In Global Mitigation of Non-CO_2 Greenhouse Gases. *U.S. Environmental Protection Agency, Office of Atmospheric Programs*, EPA Report 430-R-06-005, 2006.

Deckert, R., Jöckel, P., Grewe, V., Gottschaldt, K.-D., and Hoor, P. A quasi chemistry-transport model mode for EMAC. *Geoscientific Model Development*, 4 (1):195–206, 2011. URL http://www.geosci-model-dev.net/4/195/2011/.

Dentener, F. J. and Crutzen, P. J. Reaction of N_2O_5 on tropospheric aerosols: Impact on the global distributions of NO_x, O_3, and OH. *Journal of Geophysical Research: Atmospheres*, 98(D4):7149–7163, 1993. ISSN 2156-2202. URL http://dx.doi.org/10.1029/92JD02979.

Despiau, S. and Croci, D. Concentrations and size distributions of fine aerosol particles measured at roof level in urban zone. *Journal of Geophysical Research*, 112:D09212, 05 2007.

Dietmüller, S., Jöckel, P., Tost, H., Kunze, M., Gellhorn, C., Brinkop, S., Frömming, C., Ponater, M., Steil, B., Lauer, A., and Hendricks, J. A new radiation infrastructure for the Modular Earth Submodel System (MESSy, based on version 2.51). *Geoscientific Model Development*, 9(6):2209–2222, 2016. URL https://www.geosci-model-dev.net/9/2209/2016/.

Dodge, M. Combined use of modeling techniques and smog chamber data to derive ozoneprecursor relationships. In Dimitriades, B., editor, *International Conference on Photochemical Oxidant Pollution and its Control: Proceedings*, volume Vol. II., pages 881–889. U.S. Environmental Protection Agency, Environmental Sciences Research Laboratory, Research Triangle Park, N.C., 1977. EPA/600/3-77-001b.

Dunker, A. M., Yarwood, G., Ortmann, J. P., and Wilson, G. M. Comparison of Source Apportionment and Source Sensitivity of Ozone in a Three-Dimensional Air Quality Model. *Environmental Science & Technology*, 36(13):2953–2964, 2002. URL http://dx.doi.org/10.1021/es011418f. PMID: 12144273.

Emmons, L. K., Hess, P. G., Lamarque, J.-F., and Pfister, G. G. Tagged ozone mechanism for MOZART-4, CAM-chem and other chemical transport models. *Geoscientific Model Development*, 5(6):1531–1542, 2012. URL https://www.geosci-model-dev.net/5/1531/2012/.

Eyring, V., Isaksen, I. S., Berntsen, T., Collins, W. J., Corbett, J. J., Endresen, O., Grainger, R. G., Moldanova, J., Schlager, H., and Stevenson, D. S. Transport impacts on atmosphere and climate: Shipping. *Atmospheric Environment*, 44 (37):4735 – 4771, 2010. ISSN 1352-2310. URL http://www.sciencedirect.com/science/article/pii/S1352231009003379. Transport Impacts on Atmosphere and Climate: The ATTICA Assessment Report.

Fang, Y., Naik, V., Horowitz, L. W., and Mauzerall, D. L. Air pollution and associated human mortality: the role of air pollutant emissions, climate change and methane concentration increases from the preindustrial period to present. *Atmospheric Chemistry and Physics*, 13(3):1377–1394, 2013. URL https://www.atmos-chem-phys.net/13/1377/2013/.

Finkelstein, M., Jerrett, M., and Sears, M. Traffic Air Pollution and Mortality Rate Advancement Periods. *American journal of epidemiology*, 160:173–7, 08 2004.

Fouquart, Y. and Bonnel, B. Computations of solar heating of the Earth's atmosphere: A new parameterization. *Beitr. Phys. Atmos.*, 53:35–62, 1980.

Fowler, D., Amann, M., Anderson, R., Ashmore, M., Cox, P., Depledge, M., Derwent, D., Grennfelt, P., Hewitt, N., Jenkin, M., Kelly, F., Liss, P., Pilling, M., Pyle, J., Slingo, J., and Stevenson, D. *Ground-level ozone in the 21st century: future trends, impacts and policy implications*. Science Policy, The Royal Society, 2008.

Frömming, C., Ponater, M., Dahlmann, K., Grewe, V., Lee, D. S., and Sausen, R. Aviation-induced radiative forcing and surface temperature change in dependency of the emission altitude. *Journal of Geophysical Research: Atmospheres*, 117(D19):n/a–n/a, 2012. ISSN 2156-2202. URL http://dx.doi.org/10.1029/2012JD018204. D19104.

Fuglestvedt, J., Berntsen, T., Myhre, G., Rypdal, K., and Skeie, R. B. Climate forcing from the transport sectors. *Proceedings of the National Academy of Sciences*, 105(2):454–458, 2008. ISSN 0027-8424. URL http://www.pnas.org/content/105/2/454.

Gaffney, J. S. and Marley, N. A. The impacts of combustion emissions on air quality and climate – From coal to biofuels and beyond. *Atmospheric Environment*, 43(1): 23 – 36, 2009. ISSN 1352-2310. URL http://www.sciencedirect.com/science/

article/pii/S1352231008009175. Atmospheric Environment - Fifty Years of Endeavour.

Gan, W., Tamburic, L., Davies, H., A Demers, P., Koehoorn, M., and Brauer, M. Changes in Residential Proximity to Road Traffic and the Risk of Death From Coronary Heart Disease. *Epidemiology (Cambridge, Mass.)*, 21:642–9, 09 2010.

Giorgetta, M. A. and Bengtsson, L. Potential role of the quasi-biennial oscillation in the stratosphere-troposphere exchange as found in water vapor in general circulation model experiments. *Journal of Geophysical Research: Atmospheres*, 104(D6):6003–6019, 1999. ISSN 2156-2202. URL http://dx.doi.org/10.1029/1998JD200112.

Gottschaldt, K., Voigt, C., Jöckel, P., Righi, M., Deckert, R., and Dietmüller, S. Global sensitivity of aviation NO_x effects to the HNO_3-forming channel of the HO_2 + NO reaction. *Atmospheric Chemistry and Physics*, 13(6):3003–3025, 2013. URL https://www.atmos-chem-phys.net/13/3003/2013/.

Granier, C., Bessagnet, B., Bond, T., D'Angiola, A., Denier van der Gon, H., Frost, G. J., Heil, A., Kaiser, J. W., Kinne, S., Klimont, Z., Kloster, S., Lamarque, J.-F., Liousse, C., Masui, T., Meleux, F., Mieville, A., Ohara, T., Raut, J.-C., Riahi, K., Schultz, M. G., Smith, S. J., Thompson, A., van Aardenne, J., van der Werf, G. R., and van Vuuren, D. P. Evolution of anthropogenic and biomass burning emissions of air pollutants at global and regional scales during the 1980–2010 period. *Climatic Change*, 109(1):163, Aug 2011. ISSN 1573-1480. URL https://doi.org/10.1007/s10584-011-0154-1.

Granier, C. and Brasseur, G. P. The impact of road traffic on global tropospheric ozone. *Geophysical Research Letters*, 30(2):n/a–n/a, 2003. ISSN 1944-8007. URL http://dx.doi.org/10.1029/2002GL015972. 1086.

Granier, C., Müller, J., Pétron, G., and Brasseur, G. A three-dimensional study of the global CO budget. *Chemosphere - Global Change Science*, 1(1):255 – 261, 1999. ISSN 1465-9972. URL http://www.sciencedirect.com/science/article/pii/S1465997299000070.

Grewe, V. Technical Note: A diagnostic for ozone contributions of various NO_x emissions in multi-decadal chemistry-climate model simulations. *Atmospheric Chemistry and Physics*, 4(3):729–736, 2004. URL https://www.atmos-chem-phys.net/4/729/2004/.

Grewe, V. A generalized tagging method. *Geoscientific Model Development*, 6(1):247–253, 2013. URL https://www.geosci-model-dev.net/6/247/2013/.

Grewe, V., Brunner, D., Dameris, M., Grenfell, J., Hein, R., Shindell, D., and Staehelin, J. Origin and variability of upper tropospheric nitrogen oxides and ozone at northern mid-latitudes. *Atmospheric Environment*, 35(20):3421 – 3433, 2001. ISSN 1352-2310. URL http://www.sciencedirect.com/science/article/pii/S1352231001001340.

Grewe, V., Champougny, T., Matthes, S., Frömming, C., Brinkop, S., Søvde, O. A., Irvine, E. A., and Halscheidt, L. Reduction of the air traffic's contribution to climate change: A REACT4C case study. *Atmospheric Environment*, 94:616 – 625, 2014. ISSN 1352-2310. URL http://www.sciencedirect.com/science/article/pii/S1352231014004063.

Grewe, V., Dahlmann, K., Matthes, S., and Steinbrecht, W. Attributing ozone to NO_x emissions: Implications for climate mitigation measures. *Atmospheric Environment*, 59:102 – 107, 2012. ISSN 1352-2310. URL http://www.sciencedirect.com/science/article/pii/S1352231012004335.

Grewe, V. and Stenke, A. AirClim: an efficient tool for climate evaluation of aircraft technology. *Atmospheric Chemistry and Physics*, 8(16):4621–4639, 2008. URL https://www.atmos-chem-phys.net/8/4621/2008/.

Grewe, V., Tsati, E., and Hoor, P. On the attribution of contributions of atmospheric trace gases to emissions in atmospheric model applications. *Geoscientific Model Development*, 3(2):487–499, 2010. URL http://www.geosci-model-dev.net/3/487/2010/.

Grewe, V., Tsati, E., Mertens, M., Frömming, C., and Jöckel, P. Contribution of emissions to concentrations: the TAGGING 1.0 submodel based on the Modular Earth Submodel System (MESSy 2.52). *Geoscientific Model Development*, 10(7): 2615–2633, 2017. URL https://www.geosci-model-dev.net/10/2615/2017/.

Gromov, S., Jöckel, P., Sander, R., and Brenninkmeijer, C. A. M. A kinetic chemistry tagging technique and its application to modelling the stable isotopic composition of atmospheric trace gases. *Geoscientific Model Development*, 3(2):337–364, 2010. URL https://www.geosci-model-dev.net/3/337/2010/.

Gryparis, A., Forsberg, B., Katsouyanni, K., Analitis, A., Touloumi, G., Schwartz, J., Samoli, E., Medina, S., Anderson, H., Niciu, E., Wichmann, H., Kriz, B., Kosnik, M., Skorkovsky, J., Vonk, J., and Dortbudak, Z. Acute effects of ozone on mortality from the "Air pollution and health: A European approach" project. *American Journal of Respiratory and Critical Care Medicine*, 170(10):1080–1087, 11 2004. ISSN 1073-449X.

Guenther, A., Hewitt, C. N., Erickson, D., Fall, R., Geron, C., Graedel, T., Harley, P., Klinger, L., Lerdau, M., Mckay, W. A., Pierce, T., Scholes, B., Steinbrecher, R., Tallamraju, R., Taylor, J., and Zimmerman, P. A global model of natural volatile organic compound emissions. *Journal of Geophysical Research: Atmospheres*, 100(D5):8873–8892, 1995. ISSN 2156-2202. URL http://dx.doi.org/10.1029/94JD02950.

Günthardt-Goerg, M. and Vollenweider, P. Linking stress with macroscopic and microscopic leaf response in trees: New diagnostic perspectives. *Environmental pollution (Barking, Essex : 1987)*, 147:467–88, 07 2007.

Hanke-Bourgeois, M. *Grundlagen der Numerischen Mathematik und des Wissenschaftlichen Rechnens*, chapter Nichtlineare Gleichungen, pages 149–198. Vieweg+Teubner, Wiesbaden, 2009. ISBN 978-3-8348-9309-3. URL https://doi.org/10.1007/978-3-8348-9309-3_5.

Hansen, J., Sato, M., and Ruedy, R. Radiative forcing and climate response. *J. Geophys. Res.*, 102:6831–6864, 1997.

Heard, D. E. and Pilling, M. J. Measurement of OH and HO_2 in the Troposphere. *Chemical Reviews*, 103(12):5163–5198, 2003. URL http://dx.doi.org/10.1021/cr020522s. PMID: 14664647.

Hein, R., Dameris, M., Schnadt, C., Land, C., Grewe, V., Köhler, I., Ponater, M., Sausen, R., B. Steil, B., Landgraf, J., and Brühl, C. Results of an interactively coupled atmospheric chemistry – general circulation model: Comparison with observations. *Annales Geophysicae*, 19(4):435–457, 2001. URL https://www.ann-geophys.net/19/435/2001/.

Hendricks, J., Righi, M., and Aquila, V. Global Atmospheric Aerosol Modeling. In Schumann, U., editor, *Atmospheric Physics: Background – Methods – Trends*, pages 561–576, Berlin, Heidelberg, 2012. Springer Berlin Heidelberg. ISBN 978-3-642-30183-4. URL https://doi.org/10.1007/978-3-642-30183-4_34.

Hendricks, J., Righi, M., Dahlmann, K., Gottschaldt, K.-D., Grewe, V., Ponater, M., Sausen, R., Heinrichs, D., Winkler, C., Wolfermann, A., Kampffmeyer, T., Friedrich, R., Klötzke, M., and Kugler, U. Quantifying the climate impact of emissions from land-based transport in Germany. *Transportation Research Part D: Transport and Environment*, 2017. ISSN 1361-9209. URL http://www.sciencedirect.com/science/article/pii/S1361920916303820.

Henning, A., Plohr, M., Özdemir, E., Hepting, M., Keimel, H., Sanok, S., Sausen, R., Pregger, T., Seum, S., Heinrichs, M., Müller, S., Winkler, C., Neumann, T., Seeback, O., V., M., and B., V. The DLR Transport and the Environment Project – Building competency for a sustainable mobility future. In Sausen, R., Unterstrasser, S., and Blum, A., editors, *Proceedings of the 4th International Conference on Transport, Atmosphere and Climate (TAC-4)*, pages 192–198. Deutsches Zentrum für Luft- und Raumfahrt, Institut für Physik der Atmosphäre, Oberpfaffenhofen, 2015.

Hoor, P., Borken-Kleefeld, J., Caro, D., Dessens, O., Endresen, O., Gauss, M., Grewe, V., Hauglustaine, D., Isaksen, I. S. A., Jöckel, P., Lelieveld, J., Myhre, G., Meijer, E., Olivie, D., Prather, M., Poberaj, C. S., Shine, K., Staehelin, J., Tang, Q., van Aardenne, J., van Velthoven, P., and Sausen, R. The impact of traffic emissions on atmospheric ozone and OH: results from QUANTIFY. *Atmospheric Chemistry and Physics*, 9(9):3113–3136, 2009. URL http://centaur.reading.ac.uk/17096/.

Horowitz, L. W. and Jacob, D. J. Global impact of fossil fuel combustion on atmospheric NO_x. *Journal of Geophysical Research: Atmospheres*, 104(D19):

23823–23840, 1999. ISSN 2156-2202. URL http://dx.doi.org/10.1029/1999JD900205.

IPCC. *Climate Change 2013: The Physical Science Basis. Working Group I Contribution to the Fifth Assessment report of the Intergovernmental Panel on Climate Change*. Stocker, T.F., Qin, D., Plattner, G.-K., Tignor, M., Allen, S.K., Boschung, J., Nauels, A., Xia, Y., Bex, V. and Midgley, P.M. (eds.). Cambridge University Press, Cambridge, United Kingdom and New York, NY, USA, 2013. 1535 pp.

IPCC/TEAP. *Safeguarding the Ozone Layer and the Global Climate System: Issues Related to Hydrofluorocarbons and Perfluorocarbons (SROC)*. Bert Metz, Lambert Kuijpers, Susan Solomon, Stephen O. Andersen, Ogunlade Davidson, José Pons, David de Jager, Tahl Kestin, Martin Manning, and Leo Meyer (Eds) Cambridge University Press, UK, 2005. pp 478.

Janssens-Maenhout, G., Crippa, M., Guizzardi, D., Muntean, M., Schaaf, E., Dentener, F., Bergamaschi, P., Pagliari, V., Olivier, J. G. J., Peters, J. A. H. W., van Aardenne, J. A., Monni, S., Doering, U., and Petrescu, A. M. R. EDGAR v4.3.2 Global Atlas of the three major Greenhouse Gas Emissions for the period 1970–2012. *Earth System Science Data Discussions*, 2017:1–55, 2017. URL https://www.earth-syst-sci-data-discuss.net/essd-2017-79/.

Jedynska, A., Tromp, P. C., Houtzager, M. M., and Kooter, I. M. Chemical characterization of biofuel exhaust emissions. *Atmospheric Environment*, 116:172 – 182, 2015. ISSN 1352-2310. URL http://www.sciencedirect.com/science/article/pii/S135223101530176X.

Jöckel, P., Kerkweg, A., Buchholz-Dietsch, J., Tost, H., Sander, R., and Pozzer, A. Technical Note: Coupling of chemical processes with the Modular Earth Submodel System (MESSy) submodel TRACER. *Atmospheric Chemistry and Physics*, 8(6): 1677–1687, 2008. URL https://www.atmos-chem-phys.net/8/1677/2008/.

Jöckel, P., Kerkweg, A., Pozzer, A., Sander, R., Tost, H., Riede, H., Baumgaertner, A., Gromov, S., and Kern, B. Development cycle 2 of the Modular Earth Submodel System (MESSy2). *Geoscientific Model Development*, 3(2):717–752, 2010. URL http://www.geosci-model-dev.net/3/717/2010/.

Jöckel, P., Sander, R., Kerkweg, A., Tost, H., and Lelieveld, J. Technical Note: The Modular Earth Submodel System (MESSy) - a new approach towards Earth System Modeling. *Atmospheric Chemistry and Physics*, 5(2):433–444, 2005. URL https://www.atmos-chem-phys.net/5/433/2005/.

Jöckel, P., Tost, H., Pozzer, A., Brühl, C., Buchholz, J., Ganzeveld, L., Hoor, P., Kerkweg, A., Lawrence, M. G., Sander, R., Steil, B., Stiller, G., Tanarhte, M., Taraborrelli, D., van Aardenne, J., and Lelieveld, J. The atmospheric chemistry general circulation model ECHAM5/MESSy1: consistent simulation of ozone from the surface to the mesosphere. *Atmospheric Chemistry and Physics*, 6(12):5067–5104, 2006. URL https://www.atmos-chem-phys.net/6/5067/2006/.

Jöckel, P., Tost, H., Pozzer, A., Kunze, M., Kirner, O., Brenninkmeijer, C. A. M., Brinkop, S., Cai, D. S., Dyroff, C., Eckstein, J., Frank, F., Garny, H., Gottschaldt, K.-D., Graf, P., Grewe, V., Kerkweg, A., Kern, B., Matthes, S., Mertens, M., Meul, S., Neumaier, M., Nützel, M., Oberländer-Hayn, S., Ruhnke, R., Runde, T., Sander, R., Scharffe, D., and Zahn, A. Earth System Chemistry integrated Modelling (ESCiMo) with the Modular Earth Submodel System (MESSy) version 2.51. *Geoscientific Model Development*, 9(3):1153–1200, 2016. URL https://www.geosci-model-dev.net/9/1153/2016/.

Joumard, R. The stakes of air pollution in the transport sector, from the French case. *Atmospheric Environment*, 39(13):2491 – 2497, 2005. ISSN 1352-2310. URL http://www.sciencedirect.com/science/article/pii/S1352231005000865. 12th International Symposium, Transport and Air Pollution.

Karavalakis, G., Durbin, T. D., Shrivastava, M., Zheng, Z., Villela, M., and Jung, H. Impacts of ethanol fuel level on emissions of regulated and unregulated pollutants from a fleet of gasoline light-duty vehicles. *Fuel*, 93:549 – 558, 2012. ISSN 0016-2361. URL http://www.sciencedirect.com/science/article/pii/S0016236111005710.

Karavalakis, G., Stournas, S., and Bakeas, E. Light vehicle regulated and unregulated emissions from different biodiesels. *Science of The Total Environment*, 407 (10):3338 – 3346, 2009. ISSN 0048-9697. URL http://www.sciencedirect.com/science/article/pii/S0048969709000035.

Kerkweg, A., Buchholz, J., Ganzeveld, L., Pozzer, A., Tost, H., and Jöckel, P. Technical Note: An implementation of the dry removal processes DRY DEPosition and SEDImentation in the Modular Earth Submodel System (MESSy). *Atmospheric Chemistry and Physics*, 6(12):4617–4632, 2006a. URL https://www.atmos-chem-phys.net/6/4617/2006/.

Kerkweg, A. and Jöckel, P. The 1-way on-line coupled atmospheric chemistry model system MECO(n) – Part 1: Description of the limited-area atmospheric chemistry model COSMO/MESSy. *Geoscientific Model Development*, 5(1):87–110, 2012a. URL https://www.geosci-model-dev.net/5/87/2012/.

Kerkweg, A. and Jöckel, P. The 1-way on-line coupled atmospheric chemistry model system MECO(n) – Part 2: On-line coupling with the Multi-Model-Driver (MMD). *Geoscientific Model Development*, 5(1):111–128, 2012b. URL https://www.geosci-model-dev.net/5/111/2012/.

Kerkweg, A. and Jöckel, P. The infrastructure MESSy submodels GRID (v1.0) and IMPORT (v1.0). *Geoscientific Model Development Discussions*, 8:8607–8633, 2015. URL https://www.geosci-model-dev-discuss.net/8/8607/2015/.

Kerkweg, A., Sander, R., Tost, H., and Jöckel, P. Technical note: Implementation of prescribed (OFFLEM), calculated (ONLEM), and pseudo-emissions (TNUDGE)

of chemical species in the Modular Earth Submodel System (MESSy). *Atmospheric Chemistry and Physics*, 6(11):3603–3609, 2006b. URL http://www.atmos-chem-phys.net/6/3603/2006/.

Köhler, I., Dameris, M., Ackermann, I., and Hass, H. Contribution of road traffic emissions to the atmospheric black carbon burden in the mid-1990s. *Journal of Geophysical Research: Atmospheres*, 106(D16):17997–18014, 2001. ISSN 2156-2202. URL http://dx.doi.org/10.1029/2001JD900212.

Krol, M., Houweling, S., Bregman, B., van den Broek, M., Segers, A., van Velthoven, P., Peters, W., Dentener, F., and Bergamaschi, P. The two-way nested global chemistry-transport zoom model TM5: algorithm and applications. *Atmospheric Chemistry and Physics*, 5(2):417–432, 2005. URL https://www.atmos-chem-phys.net/5/417/2005/.

Krzyzanowski, M., Kuna-Dibbert, B., and Schneider, J. E. Health Effects of Transport-related Air Pollution. Technical report, WHO Regional Office for Europe, Copenhagen, 2005.

Kvalevåg, M. M. and Myhre, G. Human Impact on Direct and Diffuse Solar Radiation during the Industrial Era. *Journal of Climate*, 20(19):4874–4883, 2007. URL https://doi.org/10.1175/JCLI4277.1.

Lacis, A., Wuebbles, D., and Logan, J. Radiative forcing of climate by changes in the vertical-distribution of ozone. *J. Geophys. Res.*, 95:9971–9981, 1990.

Lamarque, J.-F., Bond, T. C., Eyring, V., Granier, C., Heil, A., Klimont, Z., Lee, D., Liousse, C., Mieville, A., Owen, B., Schultz, M. G., Shindell, D., Smith, S. J., Stehfest, E., Van Aardenne, J., Cooper, O. R., Kainuma, M., Mahowald, N., McConnell, J. R., Naik, V., Riahi, K., and van Vuuren, D. P. Historical (1850–2000) gridded anthropogenic and biomass burning emissions of reactive gases and aerosols: methodology and application. *Atmospheric Chemistry and Physics*, 10(15):7017–7039, 2010. URL https://www.atmos-chem-phys.net/10/7017/2010/.

Lauer, A., Eyring, V., Hendricks, J., Jöckel, P., and Lohmann, U. Global model simulations of the impact of ocean-going ships on aerosols, clouds, and the radiation budget. *Atmospheric Chemistry and Physics*, 7(19):5061–5079, 2007. URL https://www.atmos-chem-phys.net/7/5061/2007/.

Lawrence, M. G., Jöckel, P., and von Kuhlmann, R. What does the global mean OH concentration tell us? *Atmospheric Chemistry and Physics*, 1(1):37–49, 2001. URL https://www.atmos-chem-phys.net/1/37/2001/.

Lawrence, M. G., Rasch, P. J., von Kuhlmann, R., Williams, J., Fischer, H., de Reus, M., Lelieveld, J., Crutzen, P. J., Schultz, M., Stier, P., Huntrieser, H., Heland, J., Stohl, A., Forster, C., Elbern, H., Jakobs, H., and Dickerson, R. R. Global chemical weather forecasts for field campaign planning: predictions and observations of large-scale features during MINOS, CONTRACE,

and INDOEX. *Atmospheric Chemistry and Physics*, 3(1):267–289, 2003. URL https://www.atmos-chem-phys.net/3/267/2003/.

Lee, D. S., Fahey, D. W., Forster, P. M., Newton, P. J., Wit, R. C., Lim, L. L., Owen, B., and Sausen, R. Aviation and global climate change in the 21st century. *Atmospheric Environment*, 43(22):3520 – 3537, 2009. ISSN 1352-2310. URL http://www.sciencedirect.com/science/article/pii/S1352231009003574.

Leitão, J., Van Dingenen, R., and Rao, S. DELIVERABLE No D4.2 Report on spatial emissions downscaling and concentrations for health impacts assessment. Technical report, LIMITS - Low climate IMpact scenarios and the Implications of required Tight emission control Strategies Project No 282846, 2013.

Lelieveld, J. and Dentener, F. J. What controls tropospheric ozone? *Journal of Geophysical Research: Atmospheres*, 105(D3):3531–3551, 2000. ISSN 2156-2202. URL http://dx.doi.org/10.1029/1999JD901011.

Lelieveld, J., Dentener, F. J., Peters, W., and Krol, M. C. On the role of hydroxyl radicals in the self-cleansing capacity of the troposphere. *Atmospheric Chemistry and Physics*, 4(9/10):2337–2344, 2004. URL https://www.atmos-chem-phys.net/4/2337/2004/.

Lelieveld, J., Peters, W., Dentener, F. J., and Krol, M. C. Stability of tropospheric hydroxyl chemistry. *Journal of Geophysical Research: Atmospheres*, 107(D23): ACH 17–1–ACH 17–11, 2002. ISSN 2156-2202. URL http://dx.doi.org/10.1029/2002JD002272. 4715.

Leon Bluhm, G., Berglind, N., Nordling, E., and Rosenlund, M. Road traffic noise and hypertension. *Occupational and Environmental Medicine*, 64(2):122–126, 2007. ISSN 1351-0711. URL http://oem.bmj.com/content/64/2/122.

Liang, Q., Chipperfield, M. P., Fleming, E. L., Abraham, N. L., Braesicke, P., Burkholder, J. B., Daniel, J. S., Dhomse, S., Fraser, P. J., Hardiman, S. C., Jackman, C. H., Kinnison, D. E., Krummel, P. B., Montzka, S. A., Morgenstern, O., McCulloch, A., Mühle, J., Newman, P. A., Orkin, V. L., Pitari, G., Prinn, R. G., Rigby, M., Rozanov, E., Stenke, A., Tummon, F., Velders, G. J. M., Visioni, D., and Weiss, R. F. Deriving Global OH Abundance and Atmospheric Lifetimes for Long-Lived Gases: A Search for CH_3CCl_3 Alternatives. *Journal of Geophysical Research: Atmospheres*, 122(21):11,914–11,933, 2017. ISSN 2169-8996. URL http://dx.doi.org/10.1002/2017JD026926. 2017JD026926.

Lim, L., Lee, D. S., Sausen, R., and Ponater, M. Quantifying the effects of aviation on radiative forcing and temperature with a climate response model. In *Proceedings of the TAC-Conference*, pages 202–208, 01 2007. ISBN 92-79-04583-0.

Lohmann, U. and Feichter, J. Global indirect aerosol effects: a review. *Atmospheric Chemistry and Physics*, 5(3):715–737, 2005. URL https://www.atmos-chem-phys.net/5/715/2005/.

Manoli, E., Voutsa, D., and Samara, C. Chemical characterization and source identification/apportionment of fine and coarse air particles in Thessaloniki, Greece. *Atmospheric Environment*, 36(6):949 – 961, 2002. ISSN 1352-2310. URL http://www.sciencedirect.com/science/article/pii/S1352231001004861.

Matthes, S. *Globale Auswirkung des Straßenverkehrs auf die chemische Zusammensetzung der Atmosphäre.* PhD thesis, Ludwig-Maximilians-Universität München, DLR-Forschungsbericht 2011-19, Deutschen Zentrum für Luft- und Raumfahrt, Juli 2003. URL http://nbn-resolving.de/urn:nbn:de:bvb:19-15130.

Matthes, S., Grewe, V., Sausen, R., and Roelofs, G.-J. Global impact of road traffic emissions on tropospheric ozone. *Atmospheric Chemistry and Physics*, 7 (7):1707–1718, 2007. URL https://www.atmos-chem-phys.net/7/1707/2007/.

Meinshausen, M., Smith, S. J., Calvin, K., Daniel, J. S., Kainuma, M. L. T., Lamarque, J.-F., Matsumoto, K., Montzka, S. A., Raper, S. C. B., Riahi, K., Thomson, A., Velders, G. J. M., and van Vuuren, D. P. The RCP greenhouse gas concentrations and their extensions from 1765 to 2300. *Climatic Change*, 109(1):213, Aug 2011. ISSN 1573-1480. URL https://doi.org/10.1007/s10584-011-0156-z.

Mertens, M., Grewe, V., Rieger, V. S., and Jöckel, P. Revisiting the contribution of land transport and shipping emissions to tropospheric ozone. *Atmospheric Chemistry and Physics*, 18(8):5567–5588, 2018. URL https://www.atmos-chem-phys.net/18/5567/2018/.

Mills, G., Buse, A., Gimeno, B., Bermejo, V., Holland, M., Emberson, L., and Pleijel, H. A synthesis of AOT40-based response functions and critical levels of ozone for agricultural and horticultural crops. *Atmospheric Environment*, 41(12): 2630 – 2643, 2007. ISSN 1352-2310. URL http://www.sciencedirect.com/science/article/pii/S1352231006011356.

Milt, A., Milano, A., Garivait, S., and Kamens, R. Effects of 10% biofuel substitution on ground level ozone formation in Bangkok, Thailand. *Atmospheric Environment*, 43(37):5962 – 5970, 2009. ISSN 1352-2310. URL http://www.sciencedirect.com/science/article/pii/S1352231009006815.

Mlawer, E. J., Taubman, S. J., Brown, P. D., Iacono, M. J., and Clough, S. A. Radiative transfer for inhomogeneous atmospheres: RRTM, a validated correlated-k model for the longwave. *Journal of Geophysical Research: Atmospheres*, 102 (D14):16663–16682, 1997. ISSN 2156-2202. URL http://dx.doi.org/10.1029/97JD00237.

Monks, P., Archibald, A., Colette, A., Cooper, O., Coyle, M., Derwent, R., Fowler, D., Granier, C., Law, K., Mills, G., Stevenson, D., Tarasova, O., Thouret, V., von Schneidemesser, E., Sommariva, R., Wild, O., and Williams, M. Tropospheric ozone and its precursors from the urban to the global scale from air quality to short-lived climate forcer. *Atmospheric Chemistry and Physics*, 15(15):8889–8973,

8 2015. ISSN 1680-7316. © Author(s) 2015. This work is distributed under the Creative Commons Attribution 3.0 License.

Monks, P. S. Gas-phase radical chemistry in the troposphere. *Chem. Soc. Rev.*, 34: 376–395, 2005. URL http://dx.doi.org/10.1039/B307982C.

Mudway, I. and Kelly, F. Ozone and the lung: a sensitive issue. *Molecular Aspects of Medicine*, 21(1):1 – 48, 2000. ISSN 0098-2997. URL http://www.sciencedirect.com/science/article/pii/S0098299700000030.

Myhre, G., Shindell, D., Bréon, F.-M., Collins, W., Fuglestvedt, J., Huang, J., Koch, D., Lamarque, J.-F., Lee, D., Mendoza, B., Nakajima, T., Robock, A., Stephens, G., Takemura, T., and Zhan, H. Anthropogenic and Natural Radiative Forcing. In Stocker, T., Qin, D., Plattner, G.-K., Tignor, M., Allen, S., Boschung, J., Nauels, A., Xia, Y., Bex, V., and Midgley, P., editors, *Climate Change 2013: The Physical Science Basis. Contribution of Working Group I to the Fifth Assessment Report of the Intergovernmental Panel on Climate Change*. Cambridge University Press, Cambridge, United Kingdom and New York, NY, USA, 2013.

Myhre, G., Shine, K., Rädel, G., Gauss, M., Isaksen, I., Tang, Q., Prather, M., Williams, J., van Velthoven, P., Dessens, O., Koffi, B., Szopa, S., Hoor, P., Grewe, V., Borken-Kleefeld, J., Berntsen, T., and Fuglestvedt, J. Radiative forcing due to changes in ozone and methane caused by the transport sector. *Atmospheric Environment*, 45(2):387 – 394, 2011. ISSN 1352-2310. URL http://www.sciencedirect.com/science/article/pii/S1352231010008629.

Naik, V., Voulgarakis, A., Fiore, A. M., Horowitz, L. W., Lamarque, J.-F., Lin, M., Prather, M. J., Young, P. J., Bergmann, D., Cameron-Smith, P. J., Cionni, I., Collins, W. J., Dalsøren, S. B., Doherty, R., Eyring, V., Faluvegi, G., Folberth, G. A., Josse, B., Lee, Y. H., MacKenzie, I. A., Nagashima, T., van Noije, T. P. C., Plummer, D. A., Righi, M., Rumbold, S. T., Skeie, R., Shindell, D. T., Stevenson, D. S., Strode, S., Sudo, K., Szopa, S., and Zeng, G. Preindustrial to present-day changes in tropospheric hydroxyl radical and methane lifetime from the Atmospheric Chemistry and Climate Model Intercomparison Project (ACCMIP). *Atmospheric Chemistry and Physics*, 13(10):5277–5298, 2013. URL https://www.atmos-chem-phys.net/13/5277/2013/.

Nam, E. K., Jensen, T. E., and Wallington, T. J. Methane Emissions from Vehicles. *Environmental Science & Technology*, 38(7):2005–2010, 2004. URL http://dx.doi.org/10.1021/es034837g. PMID: 15112800.

Niemeier, U., Granier, C., Kornblueh, L., Walters, S., and Brasseur, G. P. Global impact of road traffic on atmospheric chemical composition and on ozone climate forcing. *Journal of Geophysical Research: Atmospheres*, 111(D9):n/a–n/a, 2006. ISSN 2156-2202. URL http://dx.doi.org/10.1029/2005JD006407. D09301.

Nissen, K. M., Matthes, K., Langematz, U., and Mayer, B. Towards a better representation of the solar cycle in general circulation models. *Atmospheric Chemistry*

and Physics, 7(20):5391–5400, 2007. URL https://www.atmos-chem-phys.net/7/5391/2007/.

Nyberg, F., Bellander, T., Pershagen, G., and Gustavsson, P. Urban Air Pollution and Lung Cancer in Stockholm. *Epidemiology*, 12:591–592, 09 2001.

Pfister, G., Pétron, G., Emmons, L. K., Gille, J. C., Edwards, D. P., Lamarque, J.-F., Attie, J.-L., Granier, C., and Novelli, P. C. Evaluation of CO simulations and the analysis of the CO budget for Europe. *Journal of Geophysical Research: Atmospheres*, 109(D19):n/a–n/a, 2004. ISSN 2156-2202. URL http://dx.doi.org/10.1029/2004JD004691. D19304.

Pfister, G. G., Avise, J., Wiedinmyer, C., Edwards, D. P., Emmons, L. K., Diskin, G. D., Podolske, J., and Wisthaler, A. CO source contribution analysis for California during ARCTAS-CARB. *Atmospheric Chemistry and Physics*, 11(15):7515–7532, 2011. URL https://www.atmos-chem-phys.net/11/7515/2011/.

Ponater, M., Dietmüller, S., and Sausen, R. Greenhouse Effect, Radiative Forcing and Climate Sensitivity. In Schuhmann, U., editor, *Atmospheric Physics*, pages 85–100. Springer-Verlag Berlin Heidelberg, 2012.

Pozzer, A., Jöckel, P., Sander, R., Williams, J., Ganzeveld, L., and Lelieveld, J. Technical Note: The MESSy-submodel AIRSEA calculating the air-sea exchange of chemical species. *Atmospheric Chemistry and Physics*, 6(12):5435–5444, 2006. URL https://www.atmos-chem-phys.net/6/5435/2006/.

Prather, M. J. Time scales in atmospheric chemistry: Theory, GWPs for CH4 and CO, and runaway growth. *Geophysical Research Letters*, 23(19):2597–2600, 1996. ISSN 1944-8007. URL http://dx.doi.org/10.1029/96GL02371.

Prather, M. J., Holmes, C. D., and Hsu, J. Reactive greenhouse gas scenarios: Systematic exploration of uncertainties and the role of atmospheric chemistry. *Geophysical Research Letters*, 39(9):n/a–n/a, 2012. ISSN 1944-8007. URL http://dx.doi.org/10.1029/2012GL051440. L09803.

Prinn, R. G., Huang, J., Weiss, R. F., Cunnold, D. M., Fraser, P. J., Simmonds, P. G., McCulloch, A., Harth, C., Reimann, S., Salameh, P., O'Doherty, S., Wang, R. H. J., Porter, L. W., Miller, B. R., and Krummel, P. B. Evidence for variability of atmospheric hydroxyl radicals over the past quarter century. *Geophysical Research Letters*, 32(7):n/a–n/a, 2005. ISSN 1944-8007. URL http://dx.doi.org/10.1029/2004GL022228. L07809.

Pucher, E., Brandt, S., Siemund, S., Stiebels, S., Dahle, U., Bergmann, A., Scherm, P., Beutel, T., Mayer, A. C. R., Kasper, M., Burtscher, H., and Punke, A. Abgasemissionen. In van Basshuysen, R. and Schäfer, F., editors, *Handbuch Verbrennungsmotor: Grundlagen, Komponenten, Systeme, Perspektiven*, pages 817–891, Wiesbaden, 2015. Springer Fachmedien Wiesbaden. ISBN 978-3-658-04678-1. URL https://doi.org/10.1007/978-3-658-04678-1_21.

Ramaswamy, V., Boucher, O., Haigh, J., Hauglustaine, D., Haywood, J., Myhre, G., Nakajima, T., Shi, G., and Solomon, S. Radiative Forcing of Climate Change. In Houghton, J., Ding, Y., Griggs, D., Noguer, M., van der Linden, P., Dai, X., Maskell, K., and Johnson, C., editors, *Climate Change 2001: The Scientific Basis. Contribution of Working Group 1 to the Third Assessment Report of the Intergovernmental Panel on Climate Change*, page 349pp. Cambridge University Press, Cambridge, United Kingdom and New York, NY, USA, 2001.

Reich, P. B. and Amundson, R. G. Ambient Levels of Ozone Reduce Net Photosynthesis in Tree and Crop Species. *Science*, 230(4725):566–570, 1985. ISSN 0036-8075. URL `http://science.sciencemag.org/content/230/4725/566`.

Reis, S., Simpson, D., Friedrich, R., Jonson, J., Unger, S., and Obermeier, A. Road traffic emissions – predictions of future contributions to regional ozone levels in Europe. *Atmospheric Environment*, 34(27):4701 – 4710, 2000. ISSN 1352-2310. URL `http://www.sciencedirect.com/science/article/pii/S1352231000002028`.

Riahi, K., Grübler, A., and Nakicenovic, N. Scenarios of long-term socio-economic and environmental development under climate stabilization. *Technological Forecasting and Social Change*, 74(7):887 – 935, 2007. ISSN 0040-1625. URL `http://www.sciencedirect.com/science/article/pii/S0040162506001387`. Greenhouse Gases - Integrated Assessment.

Righi, M., Eyring, V., Gottschaldt, K.-D., Klinger, C., Frank, F., Jöckel, P., and Cionni, I. Quantitative evaluation of ozone and selected climate parameters in a set of EMAC simulations. *Geoscientific Model Development*, 8(3):733–768, 2015. URL `https://www.geosci-model-dev.net/8/733/2015/`.

Righi, M., Hendricks, J., and Sausen, R. The global impact of the transport sectors on atmospheric aerosol: simulations for year 2000 emissions. *Atmospheric Chemistry and Physics*, 13(19):9939–9970, 2013. URL `https://www.atmos-chem-phys.net/13/9939/2013/`.

Roberts, J. M. PAN and related compounds. In Koopmann, R., editor, *Volatile Organic Compounds in the Atmosphere*, pages 221–268. Blackwell Publishing Ltd, 2007.

Rodriguez, S., Van Dingenen, R., Putaud, J.-P., A, A., Pey, J., Querol, X., Alastuey, A., Chenery, S., Ho, K. F., Harrison, R., Tardivo, R., Scarnato, B., and V, G. A study on the relationship between mass concentrations, chemistry and number size distribution of urban fine aerosols in Milan, Barcelona and London. *Atmospheric Chemistry and Physics Discussions*, 7, 01 2007.

Roeckner, E., Bäuml, G., Bonaventura, L., Brokopf, R., Esch, M., Giorgetta, M., Hagemann, S., Kirchner, I., Kornblueh, L., Manzini, E., Rhodin, A., Schlese, U., Schulzweida, U., and Tompkins, A. The atmospheric general circulation model ECHAM 5. PART I: Model description. Technical Report MPI-Report No.

349, Max Planck Institut für Meteorologie, Hamburg, 2003. URL https://www.mpimet.mpg.de/fileadmin/publikationen/Reports/max_scirep_349.pdf.

Roeckner, E., Bengtsson, L., Feichter, J., Lelieveld, J., and Rodhe, H. Transient Climate Change Simulations with a Coupled Atmosphere-Ocean GCM Including the Tropospheric Sulfur Cycle. *J. Climate*, 12:3004–3032, 1999.

Roeckner, E., Brokopf, R., Esch, M., Giorgetta, M., Hagemann, S., Kornblueh, L., Manzini, E., Schlese, U., and Schulzweida, U. Sensitivity of Simulated Climate to Horizontal and Vertical Resolution in the ECHAM5 Atmosphere Model. *Journal of Climate*, 19(16):3771–3791, 2006. URL http://dx.doi.org/10.1175/JCLI3824.1.

Samaras, C. and Meisterling, K. Life Cycle Assessment of Greenhouse Gas Emissions from Plug-in Hybrid Vehicles: Implications for Policy. *Environmental Science & Technology*, 42(9):3170–3176, 2008. URL http://dx.doi.org/10.1021/es702178s. PMID: 18522090.

Sander, R., Baumgaertner, A., Gromov, S., Harder, H., Jöckel, P., Kerkweg, A., Kubistin, D., Regelin, E., Riede, H., Sandu, A., Taraborrelli, D., Tost, H., and Xie, Z.-Q. The atmospheric chemistry box model CAABA/MECCA-3.0. *Geoscientific Model Development*, 4(2):373–380, 2011. URL https://www.geosci-model-dev.net/4/373/2011/.

Sander, R., Jöckel, P., Kirner, O., Kunert, A. T., Landgraf, J., and Pozzer, A. The photolysis module JVAL-14, compatible with the MESSy standard, and the JVal PreProcessor (JVPP). *Geoscientific Model Development*, 7(6):2653–2662, 2014. URL https://www.geosci-model-dev.net/7/2653/2014/.

Sausen, R., Gierens, K., Eyring, V., Hendricks, J., and Righi, M. Climate Impact of Transport. In Schumann, U., editor, *Atmospheric Physics: Background – Methods – Trends*, pages 711–725, Berlin, Heidelberg, 2012. Springer Berlin Heidelberg. ISBN 978-3-642-30183-4. URL https://doi.org/10.1007/978-3-642-30183-4_43.

Schiermeier, Q. The science behind the Volkswagen emissions scandal. Technical report, Nature News, 2015. doi:10.1038/nature.2015.18426.

Seinfeld, J. H. and Pandis, S. N. *Atmospheric Chemistry and Physics: From Air Pollution to Climate Change*. JOHN WILEY & SONS, INC., 2006.

Selander, J., Nilsson, M. E., Bluhm, G., Rosenlund, M., Lindqvist, M., Nise, G., and Pershagen, G. Long-Term Exposure to Road Traffic Noise and Myocardial Infarction. *Epidemiology*, 20:272–279, 2009.

Seum, S., Goletz, M., and Kuhnimhof, T. Verkehrssystemforschung am DLR - Mobil in Deutschland 2040. Teil 1: Der methodische Szenario-Ansatz im Projekt Verkehrsentwicklung und Umwelt. In *Internationales Verkehrswesen*, volume 69, 02 2017a.

Seum, S., Kuhnimhof, T., and Goletz, M. Verkehrssystemforschung am DLR - Mobil in Deutschland 2040. Teil 2: Die Szenarien des VEU-Projekts. In *Internationales Verkehrswesen*, volume 69, 04 2017b.

Shindell, D. T., Faluvegi, G., Koch, D. M., Schmidt, G. A., Unger, N., and Bauer, S. E. Improved Attribution of Climate Forcing to Emissions. *Science*, 326 (5953):716–718, 2009. ISSN 0036-8075. URL http://science.sciencemag.org/content/326/5953/716.

Simmons, A. J., Burridge, D. M., Jarraud, M., Girard, C., and Wergen, W. The ECMWF medium-range prediction models development of the numerical formulations and the impact of increased resolution. *Meteorology and Atmospheric Physics*, 40(1):28–60, Mar 1989. ISSN 1436-5065. URL https://doi.org/10.1007/BF01027467.

Sims, R., Schaeffer, R., Creutzig, F., Cruz-Núñez, X., D'Agosto, M., Dimitriu, D., Meza, M. J. F., Fulton, L., Kobayashi, S., Lah, O., McKinnon, A., Newman, P., Ouyang, M., Schauer, J. J., Sperling, D., and Tiwari, G. Transport. In Edenhofer, O., Pichs-Madruga, R., Sokona, Y., Farahani, E., Kadner, S., Seyboth, K., Adler, A., Baum, I., Brunner, S., Eickemeier, P., Kriemann, B., Savolainen, J., Schlömer, S., von Stechow, C., Zwickel, T., and (eds.), J. M., editors, *Climate Change 2014: Mitigation of Climate Change. Contribution of Working Group III to the Fifth Assessment Report of the Intergovernmental Panel on Climate Change*, Cambridge University Press, Cambridge, United Kingdom and New York, NY, USA, 2014.

Sitch, S., Cox, P. M., Collins, W. J., and Huntingford, C. Indirect radiative forcing of climate change through ozone effects on the land-carbon sink. *Nature*, 448: 791–794, Aug. 2007.

Soden, B. J. and Held, I. M. An assessment of climate feedbacks in coupled ocean-atmosphere models. *J. Climate*, 19:3354–3360, 2006.

Sørensen, M., Hvidberg, M., Andersen, Z. J., Nordsborg, R. B., Lillelund, K. G., Jakobsen, J., Tjønneland, A., Overvad, K., and Raaschou-Nielsen, O. Road traffic noise and stroke: a prospective cohort study. *European Heart Journal*, 32(6):737–744, 2011. URL +http://dx.doi.org/10.1093/eurheartj/ehq466.

Stenke, A., Deckert, R., and Gottschaldt, K.-D. Methane Modeling: From Process Modeling to Global Climate Models. In Schumann, U., editor, *Atmospheric Physics: Background – Methods – Trends*, pages 781–797, Berlin, Heidelberg, 2012. Springer Berlin Heidelberg. ISBN 978-3-642-30183-4. URL https://doi.org/10.1007/978-3-642-30183-4_47.

Stevenson, D. S., Dentener, F. J., Schultz, M. G., Ellingsen, K., van Noije, T. P. C., Wild, O., Zeng, G., Amann, M., Atherton, C. S., Bell, N., Bergmann, D. J., Bey, I., Butler, T., Cofala, J., Collins, W. J., Derwent, R. G., Doherty, R. M., Drevet, J., Eskes, H. J., Fiore, A. M., Gauss, M., Hauglustaine, D. A., Horowitz, L. W.,

Isaksen, I. S. A., Krol, M. C., Lamarque, J.-F., Lawrence, M. G., Montanaro, V., Müller, J.-F., Pitari, G., Prather, M. J., Pyle, J. A., Rast, S., Rodriguez, J. M., Sanderson, M. G., Savage, N. H., Shindell, D. T., Strahan, S. E., Sudo, K., and Szopa, S. Multimodel ensemble simulations of present-day and near-future tropospheric ozone. *Journal of Geophysical Research: Atmospheres*, 111(D8):n/a–n/a, 2006. ISSN 2156-2202. URL http://dx.doi.org/10.1029/2005JD006338. D08301.

Stuber, N., Ponater, M., and Sausen, R. Why radiative forcing might fail as a predictor of climate change. *Climate Dyn.*, 24:497–510, 2005.

Stuber, N., Sausen, R., and Ponater, M. Stratosphere adjusted radiative forcing calculations in a comprehensive climate model. *Theor. Appl. Climatol.*, 68:125–135, 2001.

Suarez-Bertoa, R., Zardini, A., Keuken, H., and Astorga, C. Impact of ethanol containing gasoline blends on emissions from a flex-fuel vehicle tested over the Worldwide Harmonized Light duty Test Cycle (WLTC). *Fuel*, 143:173 – 182, 2015. ISSN 0016-2361. URL http://www.sciencedirect.com/science/article/pii/S0016236114010710.

Tagaris, E., Sotiropoulou, R.-E. P., Gounaris, N., Andronopoulos, S., and Vlachogiannis, D. The effect of the Standard Nomenclature for Air Pollution (SNAP) categories on ozone and PM2.5 concentrations over Europe. In *EGU General Assembly Conference Abstracts*, volume 17 of *EGU General Assembly Conference Abstracts*, page 4576, Apr. 2015.

Tanaka, K., Lund, M. T., Aamaas, B., and Berntsen, T. Climate effects of non-compliant Volkswagen diesel cars. *Environmental Research Letters*, 13(4):044020, 2018. URL http://stacks.iop.org/1748-9326/13/i=4/a=044020.

Tost, H., Jöckel, P., Kerkweg, A., Sander, R., and Lelieveld, J. Technical note: A new comprehensive SCAVenging submodel for global atmospheric chemistry modelling. *Atmospheric Chemistry and Physics*, 6(3):565–574, 2006a. URL https://www.atmos-chem-phys.net/6/565/2006/.

Tost, H., Jöckel, P., and Lelieveld, J. Influence of different convection parameterisations in a GCM. *Atmospheric Chemistry and Physics*, 6(12):5475–5493, 2006b. URL https://www.atmos-chem-phys.net/6/5475/2006/.

Tost, H., Jöckel, P., and Lelieveld, J. Lightning and convection parameterisations – uncertainties in global modelling. *Atmospheric Chemistry and Physics*, 7(17):4553–4568, 2007. URL https://www.atmos-chem-phys.net/7/4553/2007/.

Tost, H., Lawrence, M. G., Brühl, C., Jöckel, P., Team, T. G., and Team, T. S.-O.-D. Uncertainties in atmospheric chemistry modelling due to convection parameterisations and subsequent scavenging. *Atmospheric Chemistry and Physics*, 10(4):1931–1951, 2010. URL https://www.atmos-chem-phys.net/10/1931/2010/.

Tsati, E. E. *Investigation of the impacts of emissions on the trace gas budgets in the troposphere by using global climate chemistry model simulations*. PhD thesis, Ludwig-Maximilians-Universität München, 2014. URL https://edoc.ub.uni-muenchen.de/17524/.

Twomey, S. The Influence of Pollution on the Shortwave Albedo of Clouds. *Journal of the Atmospheric Sciences*, 34(7):1149–1152, 1977. URL https://doi.org/10.1175/1520-0469(1977)034<1149:TIOPOT>2.0.CO;2.

Uherek, E., Halenka, T., Borken-Kleefeld, J., Balkanski, Y., Berntsen, T., Borrego, C., Gauss, M., Hoor, P., Juda-Rezler, K., Lelieveld, J., Melas, D., Rypdal, K., and Schmid, S. Transport impacts on atmosphere and climate: Land transport. *Atmospheric Environment*, 44(37):4772 – 4816, 2010. ISSN 1352-2310. URL http://www.sciencedirect.com/science/article/pii/S1352231010000099. Transport Impacts on Atmosphere and Climate: The ATTICA Assessment Report.

Unger, N., Shindell, D. T., Koch, D. M., Amann, M., Cofala, J., and Streets, D. G. Influences of man-made emissions and climate changes on tropospheric ozone, methane, and sulfate at 2030 from a broad range of possible futures. *Journal of Geophysical Research: Atmospheres*, 111(D12):n/a–n/a, 2006. ISSN 2156-2202. URL http://dx.doi.org/10.1029/2005JD006518.

van Kempen, E., Kruize, H., Boshuizen, H., Ameling, C., Staatsen, B., and E M de Hollander, A. The Association Between Noise Exposure and Blood Pressure and Ischemic Heart Disease: a Meta-Analysis. *Environmental health perspectives*, 110: 307–17, 04 2002.

van Vuuren, D. P., Edmonds, J., Kainuma, M., Riahi, K., Thomson, A., Hibbard, K., Hurtt, G. C., Kram, T., Krey, V., Lamarque, J.-F., Masui, T., Meinshausen, M., Nakicenovic, N., Smith, S. J., and Rose, S. K. The representative concentration pathways: an overview. *Climatic Change*, 109(1):5, Aug 2011. ISSN 1573-1480. URL https://doi.org/10.1007/s10584-011-0148-z.

Vial, J., Dufresne, J.-L., and Bony, S. On the interpretation of the inter-model spread in CMIP5 climate sensitivity estimates. *Climate Dyn.*, 41:3339–3362, 2013.

Voulgarakis, A., Naik, V., Lamarque, J.-F., Shindell, D. T., Young, P. J., Prather, M. J., Wild, O., Field, R. D., Bergmann, D., Cameron-Smith, P., Cionni, I., Collins, W. J., Dalsøren, S. B., Doherty, R. M., Eyring, V., Faluvegi, G., Folberth, G. A., Horowitz, L. W., Josse, B., MacKenzie, I. A., Nagashima, T., Plummer, D. A., Righi, M., Rumbold, S. T., Stevenson, D. S., Strode, S. A., Sudo, K., Szopa, S., and Zeng, G. Analysis of present day and future OH and methane lifetime in the ACCMIP simulations. *Atmospheric Chemistry and Physics*, 13(5): 2563–2587, 2013. URL https://www.atmos-chem-phys.net/13/2563/2013/.

Wallace, J. M. and Hobbs, P. V. *Atmospheric Science - An Introductory Survey*. Elsevier, 2006.

Wang, Z. S., Chien, C.-J., and Tonnesen, G. S. Development of a tagged species source apportionment algorithm to characterize three-dimensional transport and transformation of precursors and secondary pollutants. *Journal of Geophysical Research: Atmospheres*, 114(D21):n/a–n/a, 2009. ISSN 2156-2202. URL http://dx.doi.org/10.1029/2008JD010846. D21206.

WHO. Air quality guidelines. Global update 2005. Particulate matter, ozone, nitrogen dioxide and sulfur dioxide. Technical report, World Health Organization Regional Office for Europe, Copenhagen, 2006a.

WHO. Health risks of particulate matter from long-range transboundary air pollution. Technical report, World Health Organization Regional Office for Europe, Copenhagen, 2006b.

WHO. Health risk assessment of air pollution - general principles. Technical report, World Health Organization Regional Office for Europe, Copenhagen, 2016.

WHO. Evolution of WHO air quality guidelines: past, present and future. Technical report, World Health Organization Regional Office for Europe, Copenhagen, 2017.

Wild, O. and Prather, M. J. Excitation of the primary tropospheric chemical mode in a global three-dimensional model. *Journal of Geophysical Research: Atmospheres*, 105(D20):24647–24660, 2000. ISSN 2156-2202. URL http://dx.doi.org/10.1029/2000JD900399.

Wild, O., Prather, M. J., and Akimoto, H. Indirect long-term global radiative cooling from NO_x Emissions. *Geophysical Research Letters*, 28(9):1719–1722, 2001. ISSN 1944-8007. URL http://dx.doi.org/10.1029/2000GL012573.

Williams, J. and Koppmann, R. Volatile Organic Compounds in the Atmosphere: An Overview. In Koppmann, R., editor, *Volatile Organic Compounds in the Atmosphere*, pages 1–32. Blackwell Publishing Ltd, 2007.

Winkler, K., Müller, W., and Reif, K. Abgasnachbehandlung für Ottomotoren. In Reif, K., editor, *Abgastechnik für Verbrennungsmotoren*, pages 79–110, Wiesbaden, 2015. Springer Fachmedien Wiesbaden. ISBN 978-3-658-09522-2. URL https://doi.org/10.1007/978-3-658-09522-2_4.

Worden, H., Bowman, K., Worden, J., Eldering, A., and Beer, R. Satellite measurements of the clear-sky greenhouse effect from tropospheric ozone. *Nature Geoscience*, 1:305–308, 2008. ISSN 1752-0894.

Wrobel, A., Rokita, E., and Maenhaut, W. Transport of Traffic-Related Aerosols in Urban Areas. *The Science of the total environment*, 257:199–211, 08 2000.

Wu, S., Duncan, B. N., Jacob, D. J., Fiore, A. M., and Wild, O. Chemical nonlinearities in relating intercontinental ozone pollution to anthropogenic emissions. *Geophysical Research Letters*, 36(5):n/a–n/a, 2009. ISSN 1944-8007. URL http://dx.doi.org/10.1029/2008GL036607. L05806.

Yienger, J. J. and Levy, H. Empirical model of global soil-biogenic NO_x emissions. *Journal of Geophysical Research: Atmospheres*, 100(D6):11447–11464, 1995. ISSN 2156-2202. URL http://dx.doi.org/10.1029/95JD00370.

Young, P. J., Archibald, A. T., Bowman, K. W., Lamarque, J.-F., Naik, V., Stevenson, D. S., Tilmes, S., Voulgarakis, A., Wild, O., Bergmann, D., Cameron-Smith, P., Cionni, I., Collins, W. J., Dalsøren, S. B., Doherty, R. M., Eyring, V., Faluvegi, G., Horowitz, L. W., Josse, B., Lee, Y. H., MacKenzie, I. A., Nagashima, T., Plummer, D. A., Righi, M., Rumbold, S. T., Skeie, R. B., Shindell, D. T., Strode, S. A., Sudo, K., Szopa, S., and Zeng, G. Pre-industrial to end 21st century projections of tropospheric ozone from the Atmospheric Chemistry and Climate Model Intercomparison Project (ACCMIP). *Atmospheric Chemistry and Physics*, 13(4): 2063–2090, 2013. URL https://www.atmos-chem-phys.net/13/2063/2013/.

Zdunkowski, W., Trautmann, T., and Bott, A. *Radiation in the Atmosphere - A course in Theoretical Meteorology*. Cambridge University Press, 2007. pp. 2.

Zeldovich, J. The oxidation of nitrogen in combustion and explosions. *European Physical Journal A. Hadrons and Nuclei*, 21:577–628, 1946.

Acknowledgements

I wish to thank, first and foremost, my supervisor and promotor Prof. Dr. Volker Grewe for his extraordinary support in this thesis. Thank you very much for all your good advices, helpful discussions, the trust and the freedom you gave me in my work. I share the credit of my work with Prof. Dr. Robert Sausen who enabled me to work at the Institute of Atmospheric Physics at DLR.

I am grateful to Prof. Dr. Dick G. Simons for making it possible to become a PhD student at TU Delft. I am indebted to Lisette Vollmer helping me with organisational issues at TU Delft. I also would like to thank Thijs Bouwhuis for translating the summary into Dutch.

I am grateful to Dr. Johannes Hendricks, Dr. Mattia Righi, Dr. Katrin Dahlmann and Dr. Klaus-Dirk Gottschaldt for supporting me greatly in evaluating TransClim. I also would like to thank Dr. Patrick Jöckel who always helped me with EMAC. Special thanks go to Dr. Henrike Wilms, Dr. Matthias Nützel and Dr. Mariano Mertens for the fruitful discussions about TransClim, about the tagging method and about anything else. I also thank Dr. Helmut Ziereis for being my mentor and the interesting conversations in the kitchen.

Last but not least, I want to thank my colleagues for the great working atmosphere. Special thanks go to the current and former colleagues of my office who made it always a joy to come to work.

Curriculum Vitæ

Vanessa Simone RIEGER

25/03/1988	Born in Munich, Germany.

Education

1994–1998	Grammar School, Baldham, Germany
1998–2007	Gymnasium Vaterstetten, Germany
2008–2011	Bachelor of Science in Physics
	Ludwig-Maximilians-Universität, Munich, Germany
2011–2014	Master of Science in Physics
	Ludwig-Maximilians-Universität, Munich, Germany
	University of Maryland, USA (02/2012–07/2012)
	Université Paul Sabatier, Toulouse France (09/2012–01/2013)
2014–2018	PhD student at German Aerospace Center (DLR),
	Oberpfaffenhofen, Germany
	Thesis: A new method to assess the climate effect of mitigation strategies for road traffic – The fast climate-chemistry response model TransClim
	Promotor: Prof. Dr. rer. nat. V. Grewe

Awards

2007	Membership in "Deutschen Physikalischen Gesellschaft"
2007	Honour of course work "Distance measurement in astronomy"
2014	Poster Award of the European Meteorological Society ("Can feedback analysis be used to understand efficacy differences between radiative forcings?" by *Michael Ponater, Vanessa Rieger and Simone Dietmüller*)

List of Publications

1. K. Schmid, **V. Rieger**, A. Manhard, Comparison of hydrogen retention in W and W/Ta alloys, Journal of Nuclear Materials, 426 (2012) 247 - 253.

2. **Rieger, V.S.**, Dietmüller, S., Ponater M., Can feedback analysis be used to uncover the physical origin of climate sensitivity and efficacy differences?, Clim Dyn (2017) 49: 2831. https://doi.org/10.1007/s00382-016-3476-x.

3. Mertens, M., Grewe, V., **Rieger, V. S.**, and Jöckel, P.: Revisiting the contribution of land transport and shipping emissions to tropospheric ozone, Atmos. Chem. Phys., 18, 5567-5588, https://doi.org/10.5194/acp-18-5567-2018, 2018.

4. **Rieger, V. S.**, Mertens, M., and Grewe, V.: An advanced method of contributing emissions to short-lived chemical species (OH and HO_2): The TAGGING 1.1 submodel based on the Modular Earth Submodel System (MESSy 2.53), Geosci. Model Dev., 11, 2049-2066, https://doi.org/10.5194/gmd-11-2049-2018, 2018.